Decorated Cellulose Surfaces - Opportunities For Novel, Sustainable Ingredients For Formulated Products And Tissue Engineering Scaffolds

Courtenay, James

Award date:
2019

Awarding institution:
University of Bath

Decorated cellulose surfaces – opportunities for novel, sustainable ingredients for formulated products and tissue engineering scaffolds

James C. Courtenay

PhD thesis

Supervisor: Prof. Janet L. Scott

Co-supervisors: Dr Ram Sharma & Prof. Karen Edler

University of Bath

Department of Chemistry

Centre for Sustainable Chemical Technologies

Oct 2018

Centre for Sustainable Chemical Technologies

UNIVERSITY OF BATH

Abstract

Current demand for donor organs and tissues for transplantation vastly surpasses availability. To address this, tissue engineering is a rapidly advancing field, with much research directed towards the production of new biomaterial scaffolds, from sustainable and economically viable sources, with tailored properties to generate functional tissue for specific applications. Herein, a family of diverse cellulose scaffolds, with novel decorated surfaces, were developed through simple, robust and scalable chemical modifications, with the aim to facilitate cellular attachment and further tune, or regulate, cell response in tissue culture applications.

Two-component systems (cell and scaffold) were achieved using 2D cellulose films derivitised with glycidyl trimethylammonium chloride, introducing a positive surface charge, which facilitated cellular attachment comparable to tissue culture plastic, without the addition of foetal bovine serum or other ligands. Surface properties were characterised and scaffold-cell interactions revealed that initial attachment was governed by electrostatic interactions between cellulose bearing a positive charge and the negatively charge phospholipid bilayer of the cell membrane. Micropatterned surfaces with cationic cellulose 'islands' were produced using reactive inkjet printing and cells shown to preferentially attach to these islands, thus demonstrating *directed* cell attachment. Crosslinking with glyoxal had the dual effect of enhancing cellular response, by increasing the cell microenvironment stiffness, and scaffold robustness, enabling more complex 3D structures to be produced.

Applying this chemical modification to cellulose fibres resulted in dispersible cationic cellulose nanofibrils (CCNF), which led to the formation of hydrogels. The fundamental form and dimensions of the CCNF were probed and interfibrillar interactions, leading to gelation, investigated. Directionally freezing these hydrogels, followed by lyophilisation, produced 3D porous foams. Internal architectures were produced ranging from aligned smooth walled micro-channels, mimicking vascularised tissue, to pumice-like wall textures, reminiscent of porous bone. These exquisitely structured, yet robust foams, could provide biomaterial scaffolds suitable for industrial applications that require 3D cell culturing.

Acknowledgements

Firstly, I would like to thank my supervisors Prof. Janet Scott, Dr Ram Sharma and Prof. Karen Edler. I have learnt a great deal from them and their guidance throughout my PhD has helped me develop as a researcher. Working with Janet has been a real pleasure; she has an incredible breadth and depth of knowledge and always encouraged me to be critical of my own work. Ram's knowledge of cell biology was crucial for developing my understanding of tissue engineering. Karen's expertise in soft matter helped me gain the technical skills required to study the fundamental structure of my scaffold materials.

Collaboration has been a core feature of my PhD and I have been very fortunate to work with experts from around the world, thanks to EPSRC and Global Innovation Initiative funding. I would like to thank Prof. Munir Skaf at UNICAMP, Dr Christoph Deneke at LNnano, Prof. Aurora Pérez Gramatges at PUC Rio for hosting me in their laboratories for three months during my PhD. Research carried out at LNnano using their scanning probe microscopy facilities features in the 2nd and 3rd paper in this thesis. In my final year I was awarded a Santander Postgraduate mobility award which allowed me to visit Assistant Prof. Yongho Bae's laboratory in SUNY at Buffalo, USA, for two months and use atomic force microscopy which features in the 3rd paper. I thoroughly enjoyed the experiences and gained a lot from the research visits. I am grateful for all their assistance and generosity whilst working in their laboratories. Thanks must also go to Prof. Yaroslav Khimyak and Dr Susana Ramalhete at the University of East Anglia for the use of their NMR facilities and expertise during our collaborative project that features in the 5th paper. Thanks are due to Dr Eduardo Ribeiro de Azevedo for his expertise in NMR relaxometry, enabling further studies into the 3D scaffold pore structure in the 6th paper.

There are many people that I would like to thank closer to home: the Centre for Sustainable Chemical Technologies; the Scott Group; the Edler Group; and the Ellis Group, but honourable mentions to Dr Marcus Johns and Dr James Coombs Obrien for showing me the ropes at the start of my PhD and their continued help and discussion with regards to cellulose; Dr Julien Schmitt for his assistance with neutron studies; Jaspreet Kular for help with cell experiments; and fellow members of Cohort 2014. Finally, I must thank my family for all their help throughout my University career.

Publications

molecules

MDPI

Review

Recent Advances in Modified Cellulose for Tissue Culture Applications

James C. Courtenay [1,2,*], Ram I. Sharma [1,3] and Janet L. Scott [1,2]

1 Centre for Sustainable Chemical Technologies, University of Bath, Bath BA2 7AY, UK; R.Sharma@bath.ac.uk (R.I.S.); J.L.Scott@bath.ac.uk (J.L.S.)
2 Department of Chemistry, University of Bath, Bath BA2 7AY, UK
3 Department of Chemical Engineering, University of Bath, Bath BA2 7AY, UK
* Correspondence: J.Courtenay@bath.ac.uk; Tel.: +44-(0)1225-386073

Received: 29 January 2018; Accepted: 12 March 2018; Published: 14 March 2018

Abstract: Tissue engineering is a rapidly advancing field in regenerative medicine, with much research directed towards the production of new biomaterial scaffolds with tailored properties to generate functional tissue for specific applications. Recently, principles of sustainability, eco-efficiency and green chemistry have begun to guide the development of a new generation of materials, such as cellulose, as an alternative to conventional polymers based on conversion of fossil carbon (e.g., oil) and finding technologies to reduce the use of animal and human derived biomolecules (e.g., foetal bovine serum). Much of this focus on cellulose is due to it possessing the necessary properties for tissue engineering scaffolds, including biocompatibility, and the relative ease with which its characteristics can be tuned through chemical modification to adjust mechanical properties and to introduce various surface modifications. In addition, the sustainability of producing and manufacturing materials from cellulose, as well as its modest cost, makes cellulose an economically viable feedstock. This review focusses specifically on the use of modified cellulose materials for tissue culturing applications. We will investigate recent techniques used to promote scaffold function through physical, biochemical and chemical scaffold modifications, and describe how these have been utilised to reduce reliance on the addition of matrix ligands such as foetal bovine serum.

Keywords: tissue engineering; sustainable chemistry; cellulose; biomaterials; surface modifications; cell culturing; regenerative medicine

1. Introduction

Organ failure is one of the most frequent, devastating and costly problems in human healthcare. Tissue engineering is an interdisciplinary field, enlisting expertise from engineering and life sciences towards the development of new biological substituents, through the regeneration of human cells, tissues or organs, in order to repair or replace and restore function to damaged tissue or organs [1,2]. This desire to heal those ill or wounded is a concept recounted in literature and religion throughout history [3], and pioneering practical research is now making tissue engineering a reality [4].

The first attempts to repair damaged organs often relied upon primitive biomaterials, such as ceramics, wood and metals used as implants or prosthetics [5]. Modern surgery and the scientific understanding of germ theory, sterilisation and anaesthesia, catalysed technical advancements leading to the introduction of skin grafts and reconstructive surgery founded in an understanding of cellular biology [3,4].

By the 20th century advances in science and medical practices made whole organ transplants feasible and the first human heart transplantation was conducted in 1967 by the South African surgeon Christian Bernard. Receiving much media interest at the time, it also sparked controversy over the

Cellulose (2017) 24:253–267
DOI 10.1007/s10570-016-1111-y

ORIGINAL PAPER

Surface modified cellulose scaffolds for tissue engineering

James C. Courtenay · Marcus A. Johns · Fernando Galembeck · Christoph Deneke · Evandro M. Lanzoni · Carlos A. Costa · Janet L. Scott · Ram I. Sharma

Received: 11 August 2016 / Accepted: 25 October 2016 / Published online: 9 November 2016

Abstract We report the ability of cellulose to support cells without the use of matrix ligands on the surface of the material, thus creating a two-component system for tissue engineering of cells and materials. Sheets of bacterial cellulose, grown from a culture medium containing *Acetobacter* organism were chemically modified with glycidyltrimethylammonium chloride or by oxidation with sodium hypochlorite in the presence of sodium bromide and 2,2,6,6-tetramethylpipiridine 1-oxyl radical to introduce a positive, or negative, charge, respectively. This modification process did not degrade the mechanical properties of the bulk material, but grafting of a positively charged moiety to the cellulose surface (cationic cellulose) increased cell attachment by 70% compared to unmodified cellulose, while negatively charged, oxidised cellulose films (anionic cellulose), showed low levels of cell attachment comparable to those seen for unmodified cellulose. Only a minimal level of cationic surface derivitisation (ca 3% degree of substitution) was required for increased cell attachment and *no* mediating proteins were required. Cell adhesion studies exhibited the same trends as the attachment studies, while the mean cell area and aspect ratio was highest on the cationic surfaces. Overall, we demonstrated the utility of positively charged bacterial cellulose in tissue engineering in the absence of proteins for cell attachment.

Keywords Bacterial cellulose · Surface modification · Cell adhesion · Tissue engineering scaffolds

Electronic supplementary material The online version of this article (doi:10.1007/s10570-016-1111-y) contains supplementary material, which is available to authorized users.

J. C. Courtenay · M. A. Johns · J. L. Scott · R. I. Sharma
Centre for Sustainable Chemical Technologies, University of Bath, Claverton Down, Bath BA2 7AY, UK

M. A. Johns · R. I. Sharma (✉)
Department of Chemical Engineering, University of Bath, Claverton Down, Bath BA2 7AY, UK
e-mail: r.sharma@bath.ac.uk

F. Galembeck · C. Deneke · E. M. Lanzoni · C. A. Costa
National Nanotechnology Laboratory, Centre for National Research in Energy and Materials, Campinas, São Paulo, Brazil

Present Address:
F. Galembeck
Department of Chemistry, University of Campinas, Campinas, Brazil

J. L. Scott (✉)
Department of Chemistry, University of Bath, Claverton Down, Bath BA2 7AY, UK
e-mail: j.l.scott@bath.ac.uk

Cellulose (2018) 25:925–940
https://doi.org/10.1007/s10570-017-1612-3

ORIGINAL PAPER

Modulating cell response on cellulose surfaces; tunable attachment and scaffold mechanics

James C. Courtenay · Christoph Deneke · Evandro M. Lanzoni · Carlos A. Costa · Yongho Bae · Janet L. Scott · Ram I. Sharma

Received: 19 October 2017 / Accepted: 11 December 2017 / Published online: 19 December 2017

Abstract Combining surface chemical modification of cellulose to introduce positively charged trimethylammonium groups by reaction with glycidyltrimethylammonium chloride (GTMAC) allowed for direct attachment of mammalian MG-63 cells, without addition of protein modifiers, or ligands. Very small increases in the surface charge resulted in significant increases in cell attachment: at a degree of substitution (DS) of only 1.4%, MG-63 cell attachment was > 90% compared to tissue culture plastic, whereas minimal attachment occurred on unmodified cellulose. Cell attachment plateaued above DS of ca. 1.85% reflecting a similar trend in surface charge, as determined from ζ-potential measurements and capacitance coupling (electric force microscopy). Cellulose film stiffness was modulated by cross linking with glyoxal (0.3–2.6% degree of crosslinking) to produce a range of materials with surface shear moduli from 76 to 448 kPa (measured using atomic force microscopy). Cell morphology on these materials could be regulated by tuning the stiffness of the scaffolds. Thus, we report tailored functionalised biomaterials based on cationic cellulose that can be tuned through surface reaction and glyoxal crosslinkin+g, to influence the attachment and morphology of cells. These scaffolds are the first steps towards materials designed to support cells and to regulate cell morphology on implanted biomaterials using only scaffold and cells, i.e. without added adhesion promoters.

Electronic supplementary material The online version of this article (https://doi.org/10.1007/s10570-017-1612-3) contains supplementary material, which is available to authorized users.

J. C. Courtenay · J. L. Scott (✉) · R. I. Sharma (✉)
Centre for Sustainable Chemical Technologies, University of Bath, Bath BA2 7AY, UK
e-mail: j.l.scott@bath.ac.uk

R. I. Sharma
e-mail: r.sharma@bath.ac.uk

J. C. Courtenay · J. L. Scott
Department of Chemistry, University of Bath, Bath BA2 7AY, UK

R. I. Sharma
Department of Chemical Engineering, University of Bath, Bath BA2 7AY, UK

C. Deneke · E. M. Lanzoni · C. A. Costa
National Nanotechnology Laboratory, Centre for National Research in Energy and Materials, Campinas, São Paulo, Brazil

Y. Bae
Department of Pathology and Anatomical Sciences, Jacobs School of Medicine and Biomedical Sciences, University at Buffalo, The State University of New York, Buffalo, NY 14214, USA

Soft Matter

PAPER

View Article Online
View Journal | View Issue

Cite this: Soft Matter, 2018, 14, 255

Unravelling cationic cellulose nanofibril hydrogel structure: NMR spectroscopy and small angle neutron scattering analyses†‡

James C. Courtenay,[ab] Susana M. Ramalhete,[c] William J. Skuze,[b] Rhea Soni,[c] Yaroslav Z. Khimyak,[c] Karen J. Edler[ab] and Janet L. Scott*[ab]

Received 26th October 2017,
Accepted 7th December 2017

DOI: 10.1039/c7sm02113e

rsc.li/soft-matter-journal

Stiff, elastic, viscous shear thinning aqueous gels are formed upon dispersion of low weight percent concentrations of cationically modified cellulose nanofibrils (CCNF) in water. CCNF hydrogels produced from cellulose modified with glycidyltrimethylammonium chloride, with degree of substitution (DS) in the range 10.6(3)–23.0(9)%, were characterised using NMR spectroscopy, rheology and small angle neutron scattering (SANS) to probe the fundamental form and dimensions of the CCNF and to reveal interfibrillar interactions leading to gelation. As DS increased CCNF became more rigid as evidenced by longer Kuhn lengths, 18–30 nm, derived from fitting of SANS data to an elliptical cross-section, cylinder model. Furthermore, apparent changes in CCNF cross-section dimensions suggested an "unravelling" of initially twisted fibrils into more flattened ribbon-like forms. Increases in elastic modulus (7.9–62.5 Pa) were detected with increased DS and ^{1}H solution-state NMR T_1 relaxation times of the introduced surface $-N^+(CH_3)_3$ groups were found to be longer in hydrogels with lower DS, reflecting the greater flexibility of the low DS CCNF. This is the first time that such correlation between DS and fibrillar form and stiffness has been reported for these potentially useful rheology modifiers derived from renewable cellulose.

Introduction

Cellulose fibres can be processed into an array of nanoparticles including nanocrystals, nanowhiskers, and micro- and nanofibrils.[1] An array of mechanical nanofibrillation methods, enzymatic pretreatments and chemical modifications have been applied to yield so-called 'nanofibrillated' cellulose, as summarised in the comprehensive review by Kalia *et al.*[2] First described by Rånby in 1951,[3] cellulose nanocrystals and nanowhiskers are usually prepared by strong acid hydrolysis of cellulose fibres to yield stiff rod-like, crystalline cellulose nanoparticles with diameters ranging from 2 to 20 nm.[4–6] These nanoparticles have an axial elastic modulus greater than that of Kevlar, and thus are of interest in the composite materials industry,[7] however, up to 80% of the cellulose mass is lost during the hydrolysis process. As an alternative method to produce nanoparticulate cellulose Saito *et al.* demonstrated that oxidation, followed by relatively gentle shear, led to aqueous dispersions of oxidised cellulose nanofibrils with a cross-section of 3–5 nm.[8,9] This method results in conversion of between 80 and 90% of the input cellulose into the product nanofibrils.

Well dispersed cellulose nanocrystals and nanofibrils have been widely used to form hydrogels,[10,11] which are cross-linked by physical interactions (van der Waals forces), chain entanglement, hydrogen bonds, and hydrophobic and electrostatic interactions. In addition to the significantly enhanced yields of cellulose nanofibrils (CNF) achieved by dispersion following chemical modification, such as oxidation, hydrogels can be formed by dispersion of small quantities of CNF in water. As the nanofibrils have a very large aspect ratio and retain a degree of fibril flexibility, these can be induced to form gels at low weight percent inclusion.[12] Many reports have appeared of chemical modification of hydroxyl groups exposed on the surface of cellulose materials, leading to new applications for cellulose as a biomaterial,[13] drug delivery vehicle[14] or water purifying agent[15] and there is a wide array of chemistry that can be applied to derivatisation of exposed hydroxyl groups including: oxidation,[16] grafting of cationic tetralkylammonium groups,[17] sulfonation,[18] silylation,[19] acylation,[20] grafting of a range of substituents through ester linkages[21] (generated by reaction

[a] Centre for Sustainable Chemical Technologies, University of Bath, Bath BA2 7AY, UK. E-mail: j.l.scott@bath.ac.uk
[b] Department of Chemistry, University of Bath, Bath BA2 7AY, UK
[c] School of Pharmacy, University of East Anglia, Norwich Research Park, Norwich, NR4 7TG, UK

† Experimental work was conducted by JCC (CCNF synthesis and characterisation; conductometry, NMR, SANS and TEM) with the support of WJS (conductometry and rheology). SMR lead the NMR studies with the support of RS and JCC.

‡ Electronic supplementary information (ESI) available: Material characterisation, SANS fitting parameter information and NMR analyses. See DOI: 10.1039/c7sm02113e

Available online at www.sciencedirect.com

ScienceDirect

Current Opinion in Green and Sustainable Chemistry

Pickering emulsions stabilized by naturally derived or biodegradable particles

Vincenzo Calabrese, James C. Courtenay, Karen J. Edler and Janet L. Scott

Emulsions are used widely in formulated consumer products, paints and coatings, foods, and pharmaceutical preparations to name just a few examples. Frequently surfactants are employed as emulsifiers, but the use of particles, including nanoparticles, can offer advantages. Naturally derived, or synthetic, particles that are biodegradable can reduce end-of-life environmental impact, while offering advantages such as lack of irritancy in use (*e.g.*, on skin) and, in some cases, the use of particle supported Pickering emulsions may provide more environmentally friendly processes (*e.g.*, biphasic catalysis mitigating use of solvents) or environmental cleanup solutions (*e.g.*, oil spill dispersion). Here we review four classes of (nano)particles that can be employed as Pickering emulsion stabilizers: minerals, polysaccharides, synthetic polymers and proteins.

Addresses
Centre for Sustainable Chemical Technologies and Department of Chemistry, University of Bath, Claverton Down, Bath BA2 7AY, UK

Corresponding authors: Edler, Karen J. (k.edler@bath.ac.uk); Scott, Janet L. (j.l.scott@bath.ac.uk)

Current Opinion in Green and Sustainable Chemistry 2018, **12**:83–90

This review comes from a themed issue on **Green Nanotechnology 2018**

Edited by **Karen Edler, Janet Scott** and **Davide Mattia**

https://doi.org/10.1016/j.cogsc.2018.07.002

Introduction

Since the first reports of Ramsden [1] in 1903 and Pickering [2] in 1907, describing emulsions solely stabilized by particles adsorbed to the oil/water interface, nanoparticles have been widely used as "Pickering emulsion" stabilizers [3,4]. Unlike conventional surfactant stabilized emulsions, nanoparticles allow the formation of stable emulsions not by decreasing surface tension, but by providing a physical barrier at the interface —particles may vary widely in shape, aspect ratio and morphology, with fibrils, spheres or globules and platelets all serving as "Pickering particles" (Figure 1).

Many inorganic particles have been reported and well-known consumer products, such as sunscreens, may contain nanomaterials, *e.g.* nanoparticulate titania [5], which acts as an effective UV filter, reducing the incidence of skin cancers [6]. However, concerns about deleterious effects of "hard" nanoparticles have led to regulations pertaining to their use in some applications, such as in cosmetic preparations [7]. The potential health risks associated with many so-called "hard" nanoparticles have been elucidated, and form the basis for the emerging field of "nanotoxicology" [8]. Given these potential risks we will largely confine this discussion to naturally derived particles and potentially greener applications thereof, with a focus on: natural mineral, polysaccharide, biodegradable polymer, and protein nanoparticles.

Minerals

The ability of natural clay particles to stabilize emulsions has been noted as an occasional frustrating factor in oil extraction, but can be exploited to prepare more environmentally friendly drilling fluids [9]. In addition to avoiding environmental release of surfactants or polymeric stabilizers, Pickering emulsions can be less prone to "down-well" destabilization at elevated temperatures. Cloisite clay nanoparticles hydrophobised with dimethyl dehydrogenated tallow quaternary ammonium ions (Cloisite® 20A) were shown to yield stable water in oil (W/O) emulsions, even at temperatures >200 °C, for lengthy periods [10]. Combining such natural clay particles, modified with bioderived surface treatment agents, with biodiesel based drilling fluids [11] could offer opportunities for mitigating environmental contamination during drilling operations.

Oil spills will remain an unfortunate consequence of failure of controls during oil extraction for as long fossil oil is extracted. Replacing chemical surfactant dispersants with particle based dispersants can produce oil in water (O/W) Pickering stabilized emulsions that allow the oil droplets to sink into the water column where they are more effectively dispersed, while avoiding the secondary contamination that may result from the use of chemical dispersants [12]. Thus modified kaolinite [12] and halloysite clay nanotubes combined with food grade surfactants [13] have been reported as promising oil-in-seawater dispersants with projected low toxicity to marine life. These particulate dispersants, when combined with oil degrading bacteria, such as modified *Bacillus cereus* S-1 [14] (also reported previously as a

Journal of Materials Chemistry B

ARTICLE

Mechanically robust cationic cellulose nanofibril 3D scaffolds with tuneable biomimetic porosity for cell culture

Received 00th January 20xx,
Accepted 00th January 20xx

DOI: 10.1039/x0xx00000x

www.rsc.org/

James C. Courtenay[a,b], Jefferson G. Filgueris[d], Eduardo Riberio de Azevêdo[d], Yun Jin[b,e], Karen J. Edler[a,b], Ram I. Sharma[a,c] and Janet L. Scott[a,b,*]

3D foam scaffolds were produced in a "bottom up" approach from lyophilised cationic cellulose nanofibril (CCNF) dispersions and emulsions (CCNF degree of substitution 23.0 ±0.9 %), using a directional freezing /lyophilisation approach, producing internal architectures ranging from aligned smooth walled micro channels, mimicking vascularised tissue, to pumice-like wall textures, reminiscent of porous bone. The open, highly porous architecture of these biomimetic scaffolds included mesopores within the walls of the channels. A combination of SEM and NMR cryoporometry and relaxometry was used to determine the porosity at different length scales: CCNF foams with aligned channels had an average macropore (channel) size of 35 ±9 µm and a mesopore (wall) diameter of 26 ±2 nm, while CCNF foams produced from directional freezing and lyophilisation of Pickering emulsions had mesoporous walls (5 ±3 µm) in addition to channels (54 ±20 µm). Glyoxal crosslinking both enhanced robustness and stiffness, giving Young's moduli of 0.45 to 50.75 MPa for CCNF foams with degrees of crosslinking 0 to 3.05 mol. %. Porosity and channels are critical scaffold design elements for transport of nutrients and waste products, as well as O_2 / CO_2 exchange. The viability of MG-63 cells was enhanced on crosslinked, mechanically stiff scaffolds, indicating that these exquisitely structured yet robust foams could provide biomaterial scaffolds suitable for industrial applications requiring 3D cell culturing.

Introduction

Current demand for donor organs and tissues for transplantation vastly surpasses availability. For example, more than 100,000 US patients wait on the organ donor list in 2018 and, on average, 22 will die per day.[1] The goal of tissue engineering is to develop new cell constructs that can be implanted into a patient to restore function to the damaged organs.[2] This process requires a biocompatible scaffold to support the cells, often by mimicking the extracellular matrix (ECM), as these proliferate and grow into tissues.[3] Traditionally, adherent cells are cultured on a two-dimensional (2D) scaffold *in vitro*. Cells growing on 2D scaffolds tend to only be attached to the substrate at their periphery, which forces the cells into a monolayer culture, rather than promoting layering as would be found *in vivo*, as well as limiting the size of the cell population produced.[4] Once the cell layer has reached 100 % confluence (all available surface is covered), cell viability can decrease, and cell death can occur as mass transfer of nutrients and oxygen diffusion is limited to depths of 100-200 µm,[5] and, to retain cell viability beyond this depth, a vascularised network is required.[6,7,8] Furthermore, if primary keratinocytes are grown to 100 % confluence, the phenomenon of "terminal differentiation" can arise: cells receiving insufficient nutrients die and those that remain alive become senescent, limiting the size of the cell construct that can be grown on a 2D scaffold.

On the other hand, 3D scaffolds require internal porosity to mimic the vascular morphology of native tissue, facilitating transfer of nutrients and gases and allowing larger tissue fragments to be grown. Ideally, the scaffolds should be resorbed and replaced, over time, by the newly regenerated tissue at the site of implant.[9] A 3D arrangement of cells enables more complex cell-cell and cell-ECM interactions as cells are surrounded by ECM or scaffold, due to the greater surface area available for adhesion. Thus, cells cultured in a 3D scaffold more accurately mimic the response and behaviour of cells *in vivo*, beneficial for applications in both cell culturing for tissue engineering and as model tissues for drug development.[10]

Interconnecting porous networks can be used to promote cell growth, migration and mass transfer of nutrients.[11] Generally, a larger pore size is considered to be beneficial for improving both cell migration and nutrient flow, however, this decreases the specific surface area of the scaffold, in turn reducing the matrix ligand density available for cell binding.

[a] Centre for Sustainable Chemical Technologies, University of Bath, Bath, BA2 7AY, UK
[b] Department of Chemistry, University of Bath, Bath, BA2 7AY, UK
[c] Department of Chemical Engineering, University of Bath, Bath, BA2 7AY, UK
[d] São Carlos Institute of Physics, University of São Paulo, 13566-590, Brazil
[e] Current address, FiberLean® Technologies Ltd, Par Moor Centre, Par Moor Rd, Par PL24 2SQ, UK
*Email - j.l.scott@bath.ac.uk

Electronic Supplementary Information (ESI) available: Further experimental details for material preparation, modification and characterisation. See DOI:10.1039/x0xx00000x

Contents

Figures

Tables

Nomenclature

2D – two dimension

3D – three dimension

AC/DC – alternating current / direct current

AFM – atomic force microscopy

AGU - anhydroglucose unit

ANOVA - a one-way analysis of variance

ASC – adipose-derived stem cells

ATR – Attenuated total reflection

BC - bacterial cellulose

BNC – Bacterial nanocellulose

CAD – computer aided design

CBM3 – carbohydrate-binding module

CC – cationic cellulose

CCNF – cationically modified cellulose nanofibrils

CMC – carboxymethyl cellulose

CNC – cellulose nanocrystals

CNF - cellulose nanofibrils

CP/MAS – cross-polarisation magic angle spinning

CPMG – Carr−Purcell Meiboom−Gill

DAC – dialdehyde cellulose

DAPI - 6-diamidino-2-phenylindole

dC/dz – capacitance gradient

DMA – Dynamic Materials Analyser

DMAc – N,N-dimethylacetamide

DMEM – Dulbecco's Modified Eagle Medium

DMSO - dimethyl sulfoxide

DO degree of oxidation

DP – degree of polymerisation

DS – degree of substitution

DXL – degree of crosslinking

E – Young's modulus

ECM - extracellular matrix

EFM – electric force microscopy

EHEC – Ethyl hydroxyethyl cellulose

EMIM Ac – 1-ethyl-3-methylimidazolium acetate

FAK – focal adhesion kinase

FBS – foetal bovine serum

FESEM – Field Emission Scanning Electron Microscopy

FITC – fluorescein isothiocyanate

FTIR – Fourier transform infrared

G' – elastic storage modulus

G'' – loss modulus

GDA – glutaraldehyde

GTMAC – glycidyltrimethylammonium chloride

HMDS – hexamethyldisilazane

hMSCs – human mesenchymal stem cells

HPC – Hydroxypropyl cellulose

HPLC – High-performance liquid chromatography

HR-MAS – High-resolution magic angle spinning

IFT – interfacial tension

IKVAV – Ile-Lys-Val-Ala-Val

IL - Ionic liquids

ITL – Inverse Laplace Transform

MAS – magic angle spinning

MCC - microcrystalline cellulose

MFC - microfibrillated cellulose

MSC – mesenchymal stem cell

MTT – methylthiazolyldiphenyl-tetrazolium bromide

MWCO – molecular weight cut-off

NaPyr – sodium pyruvate

NCC – nanocrystaline cellulose

NEAA - non-essential amino acid

NHS - National health service

NMR – nuclear magnetic resonance

OCNF – oxidised cellulose nanofibrils

PBS - phosphate buffer solution

PDA – polydopamine

PDO – polydioxanne

PE – Pickering emulsion

PEG – poly(ethylene glycol)

PenStep –penicillin streptomycin

Phalloidin-FITC - phalloidin, fluorescein isothiocyanate labelled

PLA – poly (lactic acid)

PLGA - poly(lactic-co-glycolic acid)

PLGA – poly(lactic-co-glycolic acid)

PTFE – Polytetrafluoroethylene

RGD – arginyl-glycyl-aspartic acid

rhBMP-2 – human recombinant bone morphogenetic protein-2

RISM - reference interaction site model

ROCK - RHO-associated protein kinase

SANS – small angle neutron scattering

SEM – scanning electron microscopy

SLD – scattering length density

T_1 – longitudinal relaxation times

T_2 – spin-spin relaxation

TCP – tissue culture plastic

TEM – Transmission electron microscope

TEMPO - 2,2,6,6-tetramethylpipiridine 1-oxyl radical

T_g – glass transition temperature

TGA – thermo gravimetric analysis

TMS – tetramethylsilane

UC – unmodified cellulose

VEGF – vascular endothelial growth factor

XL – crosslinked

η' – dynamic viscosiy

PhD Aims & Objectives

Overarching aims and objectives are presented to provide context for the published work which follows as chapters.

Aim

In this PhD project the aim was to use simple, robust and scalable chemical modifications to develop novel decorated cellulose surfaces, which could be utilised to produce functional scaffolds. Functionality would include facilitation of cellular attachment and further tuning, or regulation of, cell response in tissue culture applications. This aim would be achieved through research reported in the following chapters. Each focused on a specific objective from fundamental understanding of cationic cellulose surface chemistry and nanofibril structure to the production of three dimensional (3D) materials for application as a sustainably sourced material for tissue engineering scaffolds. This thesis is formed from a portfolio of research publications which follow the narrative established by the PhD objectives and will each be preceded by a commentary to critique and link the papers.

Objectives

Chapter 1: In this chapter the objectives were, to: introduce the field of tissue engineering, outlining the key principles of used to culture cells and tissue; define the important properties needed for a suitable scaffold; survey types of biomaterials currently used; introduce cellulose as a sustainably sourced material and state the case for its use in tissue engineering; identify potential limiting properties of cellulose materials which need to be addressed and to review of the recent literature in modified cellulose scaffold for tissue engineering applications.

Chapter 2: The objectives of the work described in this chapter were, to: identify a cell-scaffold two-component system for tissue engineering, i.e. not requiring immobilised matrix proteins, through surface modification to change scaffold surface charge; test the hypothesis of ionic charge facilitated cell attachment, bacterial cellulose membranes would be modified to introduce a positive or negative charge to the surface; develop methods for identifying and quantifying the presence of charged groups on the scaffolds and to characterise how modifications affects scaffold properties and cellular response to the scaffold.

Chapter 3: In this chapter the objectives were, to: investigate the response of MG-63 cells on the modified scaffolds, to understand how the presence of quaternary ammonium moieties influenced cell response (attachment, adhesion strength, morphology and proliferation); explore whether cell morphology can be further tuned, or regulated, by changing the elastic moduli of the scaffolds through crosslinking chemistry ; determine the minimum levels of cationisation required to facilitate cell attachment in a protein free system and to develop a methodology to quantify the crosslinking modification and characterise effect on both surface and bulk properties.

Chapter 4: The objectives of the work described in this chapter were, to: develop and optimise a process that enabled controlled and directed cell attachment on cellulose scaffolds; utilise reactive inkjet printing to deposit micro-droplets of reagents (e.g. GTMAC) onto cellulose film surfaces to form micro-patterns of <100 µm in diameter; develop protocols to image and characterise the cationic cellulose features present on the scaffold surface; investigate whether MG-63 cells preferentially attached to the positively charged micro-patterns and to determine whether the cell spreading was confined only to the micro-patterns and if this influences cellular alignment.

Chapter 5: In this chapter the objectives were, to: prepare cationic cellulose nanofibrils (CCNF), characterise fibril structure and behaviour of dispersed CCNF suspensions; utilise a combination of small angle neutron scattering, NMR spectroscopy and rheology to probe the fundamental form and dimensions of the CCNF and to reveal interfibrillar interactions leading to gelation and to investigate the relationship between degree of modification with fibrillar form and stiffness.

Chapter 6: The objectives of the work described in this chapter were, to: develop 3D scaffolds from cationic cellulose hydrogels with a range of structures including variable form, internal architecture and robustness via a “bottom-up approach; determine whether fabrication procedure influenced scaffold internal structure and porosity using scanning electron microscopy, NMR cryoporometry and NMR relaxometry; develop a method to increase the robustness of the 3D scaffold and characterise the mechanical properties and to monitor cell activity on the scaffold using a metabolic assay and investigate whether scaffold properties can be tuned to enhance cell metabolism.

Chapter 1

1 Paper 1: Recent Advances in Modified Cellulose for Tissue Culture Applications

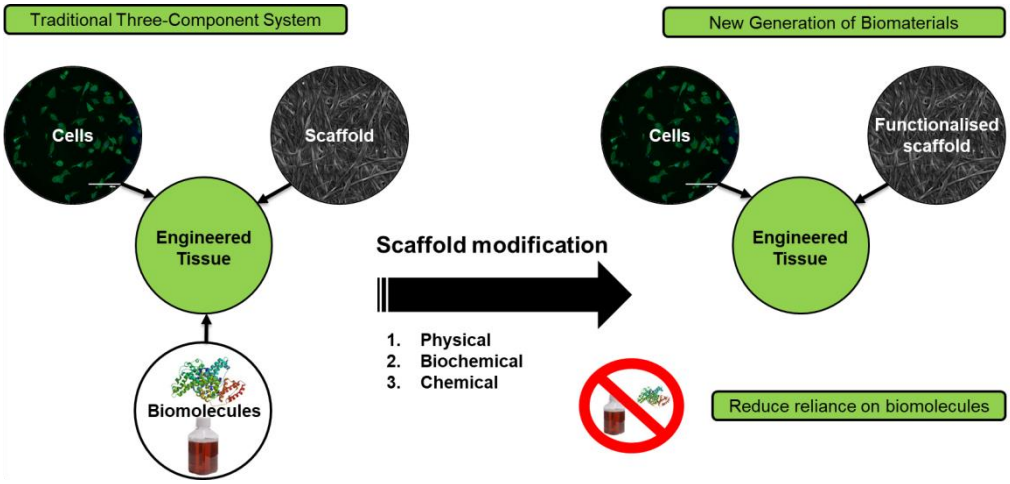

1.0 Publication Commentary

Humankind has always been plagued by illness and injury. The fundamental desire to overcome this to live a fulfilled and healthy life through regeneration is deeply embedded in cultures across the world and has been expressed throughout history.

There are examples of this in mythology and literature: from the torment of Prometheus in Greek mythology, to the creation of Eve in Genesis and the gothic tale of Frankenstein.[1,2] It is clearly evident that these themes of creating and restoring life have passed through the ages and are still rooted in human culture. Not until the development of scientific understanding of germ theory and human biology over the last century, could this be translated into reality.[3]

Currently the practice with medical treatments, when it is not possible to repair a damaged organ, is to seek a healthy donor replacement. However, with an ever growing and aging population, we face a global organ shortage. In the UK alone in 2017 over 6,000 people required an organ transplant, however less than half of these were treated with donor organs. This shortage arises from the source of donor organs, which, in most cases, comes from deceased donors. With demand exceeding supply, there are now lengthy waiting lists and the UK National Health Service (NHS) estimates that three people will die a day whilst waiting for donors.[4]

Is there an alternative to relying on donor organs? Can we generate new tissue or even functioning organs from cell cultures using existing technology?

Tissue engineering strives to answer this question. One of the best descriptions of tissue engineering is by two pioneering scientists in the field, Langer and Vacanti, who in 1993 described it as:

"An interdisciplinary field that applies the principles of engineering and life science toward the development of biological substitutes that restore, maintain, or improve the function of tissue or a whole organ."[5]

This definition highlights how tissue engineering requires many different disciplines to achieve the goals. The principle components of tissue engineering can be divided into three sections: cell source, biomolecules and scaffold. Therefore, aspects of biology, chemistry, material science and engineering are frequently used to develop new engineered tissue. More recently, given the use of tissue engineering as a

therapy in regenerative medicine, its scope has been broadened to incorporate the regenerative aspect of the discipline by Mason & Dunnill, 2008 who defined it as:

"The process of replacing or regenerating human cells, tissues or organs to restore or establish normal function."[6]

The main difference between tissue engineering and regenerative medicine relates to the cell type used. Tissue engineering describes the culturing of cells into tissue from a wide range of cell types, whereas regenerative medicine focuses mainly on the use of a patient's own cells, commonly stem cells or progenitor cells, to regenerate their tissue.

Along with engineering new tissue for regenerative medicine, tissue engineering is also applied to create cell culture for in vitro drug screening and modelling. In these cases the cell types used are commonly from animal sources, such as mouse cells.

Another interesting application of tissue engineering technology, which is not used for biomedical applications, is the newly emergent field of cellular agriculture. In 1931 Winston Churchill predicted:

"Fifty years hence, we shall escape the absurdity of growing a whole chicken in order to eat the breast or wing by growing these parts separately under a suitable medium"[7]

This area, which has arisen in the last 10 years, focuses on the production of agricultural products from cell culture, obviates the need to slaughter the animal, *i.e.* culturing beef from bovine muscle cells, pork from porcine muscle cells and chicken from chicken muscle cells for consumption as food.[8] In addition, milk and eggs can be produced from fermentation-based cellular agriculture.[8] This field is growing rapidly and could revolutionise the supply chain of animal products providing affordable and sustainable food, with a lower environmental impact, to an ever increasing population.

The purpose of the first chapter is to provide an introduction to the field of tissue engineering and outline the principles required to generate new tissue from cell culture. The role of the scaffold is described and properties beneficial for enhancing cell attachment and growth on scaffolds are identified. Specifically, this chapter will present the case for cellulose as a suitable material for the production of sustainable

scaffolds for tissue engineering and review the use of modified cellulose scaffolds for cell culture applications. As will be discussed in detail in the paper, cellulose is a polysaccharide which offers many beneficial properties for tissue engineering, including biocompatibility, tuneable chemical and physical properties and abundance as a renewable material. Although there is a plethora of chemical modifications which could be performed on cellulose, commonly to the primary OH group exposed on its surface, the introduced chemical groups must not pose toxicity issues to the cells if it is to remain a biocompatible material.

A point of consideration addressed in this chapter is that the enzyme cellulase, which degrades cellulose, is not present in the human body. Thus cellulose scaffolds will not biodegrade in vivo in the same way that they do enzymatically in the environment. However, this can be overcome through suitable chemical modifications to render the scaffolds bioresorbable. Furthermore, for cell culturing applications in vitro, this is not an issue.

Thus, the development and application of cellulose in tissue engineering could have significant impact in tackling global healthcare challenges including: providing platforms for high throughput drug screening, offering clinical tissue models to mitigate vivisection, leading to new regenerative treatments and providing the means for sustainable food production.

1.1 Statement of Authorship

<table>
<tr><th colspan="10">This declaration concerns the article entitled:</th></tr>
<tr><td colspan="10">Recent Advances in Modified Cellulose for Tissue Culture Applications</td></tr>
<tr><td colspan="10">Publication status</td></tr>
<tr><td>Draft manuscript</td><td></td><td>Submitted</td><td></td><td>In review</td><td></td><td>Accepted</td><td></td><td>Published</td><td>✓</td></tr>
<tr><td>Publication details</td><td colspan="9">Courtenay, J., Sharma, R., & Scott, J. (2018). Recent Advances in Modified Cellulose for Tissue Culture Applications. Molecules, 23(3), 1-20. [654]. DOI: 10.3390/molecules23030654</td></tr>
<tr><td>Candidate's contribution to the paper</td><td colspan="9">JCC was responsible for carrying out a thorough literature review on how cellulose biomaterials can be modified for use in tissue culture applications. The purpose of this review was to establish an overview of current literature to introduce the main body of the thesis research. The manuscript was initially written by JCC with editorial feedback from supervisors. JCC was the corresponding author.

Formulation of ideas:
Scope of review was proposed by JCC and discussed with JLS and RIS for editorial advice (90 % JCC contribution)

Design of methodology:
The structure of the review was delivered by JCC (100 % JCC contribution)

Experimental work:
The literature search and review written by JCC (98 % JCC contribution) – edited by JLS and RIS.

Presentation of data in journal format:
All of the figures and tables were prepared by JCC (100 % JCC contribution)</td></tr>
<tr><td>Statement from candidate</td><td colspan="9">This paper is a review of the literature I conducted during the period of my Higher Degree by Research candidature</td></tr>
<tr><td>Signed</td><td colspan="6"></td><td>Date</td><td colspan="2"></td></tr>
</table>

1.2 Abstract

Tissue engineering is a rapidly advancing field in regenerative medicine, with much research directed towards the production of new biomaterial scaffolds with tailored properties to generate functional tissue for specific applications. Recently, principles of sustainability, eco-efficiency and green chemistry have begun to guide the development of a new generation of materials, such as cellulose, as an alternative to conventional polymers based on conversion of fossil carbon (e.g., oil) and finding technologies to reduce the use of animal and human derived biomolecules (e.g., foetal bovine serum). Much of this focus on cellulose is due to it possessing the necessary properties for tissue engineering scaffolds, including biocompatibility, and the relative ease with which its characteristics can be tuned through chemical modification to adjust mechanical properties and to introduce various surface modifications. In addition, the sustainability of producing and manufacturing materials from cellulose, as well as its modest cost, makes cellulose an economically viable feedstock. This review focuses specifically on the use of modified cellulose materials for tissue culturing applications. We will investigate recent techniques used to promote scaffold function through physical, biochemical and chemical scaffold modifications, and describe how these have been utilised to reduce reliance on the addition of matrix ligands such as foetal bovine serum.

1.3 Introduction

Organ failure is one of the most frequent, devastating and costly problems in human healthcare. Tissue engineering is an interdisciplinary field, enlisting expertise from engineering and life sciences towards the development of new biological substituents, through the regeneration of human cells, tissues or organs, in order to repair or replace and restore function to damaged tissue or organs [6,9]**.** This desire to heal those ill or wounded is a concept recounted in literature and religion throughout history [1], and pioneering practical research is now making tissue engineering a reality [3].

The first attempts to repair damaged organs often relied upon primitive biomaterials, such as ceramics, wood and metals used as implants or prosthetics [10]. Modern surgery and the scientific understanding of germ theory, sterilisation and anaesthesia, catalysed technical advancements leading to the introduction of skin grafts and reconstructive surgery founded in an understanding of cellular biology [1,3].

By the 20th century advances in science and medical practices made whole organ transplants feasible and the first human heart transplantation was conducted in 1967 by the South African surgeon Christian Bernard. Receiving much media interest at the time, it also sparked controversy over the ethical issues of transplantation. One major concern is that the host immune system might reject the transplant, thus voiding the purpose of the procedure [3].

Pioneering research by Green in 1977 investigated seeding a chondrocyte culture onto bone scaffolds and implanting these into mice to generate new cartilage [2,11]. Despite being unsuccessful, this work identified the process of culturing tissue by seeding cells onto an appropriate scaffold. Building on this, Burke and Constant, in 1982, attempted to generate a tissue engineered skin substitute using a collagen matrix to support the growth of dermal fibroblasts [12]. Others used sheets of keratinocytes to treat burn patents [13] and developed scaffolds from a collagen gel [14].

Limitations of using naturally sourced biomaterials (such as collagen) include their limited range of physical and chemical properties as well as source variability. To overcome these limitations, researchers turned to synthetic polymeric scaffold materials. The first synthetically produced polymeric scaffolds were used by Vacanti and Langer in 1993, who generated new tissue that could be implanted back into the

body [5]. Their findings catapulted tissue engineering into the forefront of the public awareness after they published the image showing the now infamous "Auriculosaurus"—a mouse with a human ear. This demonstrated that tissue constructs could be further grown in vivo [5].

The first human to receive a tissue engineered implant was a young patient with Poland Syndrome in 1991. The implant was composed of a synthetic PLGA polymer scaffold seeded with chondrocytes and was intended to replace the patients absent sternum [2]. In 2008, the first transplantation of a tissue engineered trachea was conducted. This novel procedure used a decellularised trachea, from a human donor, which was seeded with cartilage cells derived from the patient's own stem cells, as well as epithelial cells taken from a healthy part of their trachea [15]. Whether the scaffold functioned largely as a support for the airways, or actually induced regeneration of the epithelial lining within the tracheal implant, has been debated [16]. In 2014, to treat a patient with a severed spinal cord, surgeons seeded cells taken from the patient's olfactory bulb onto strips of nerve fibres from the patient's ankle, to form a bridge for the cells to grow across [17].

1.4 Principles of Tissue Engineering

The basic principles of cell culture for tissue engineering commonly involve the use of living cells to repair or regrow tissue or an organ damaged by disease, or trauma, as described below and illustrated in Figure 1.1. The steps involved may include:

1. Desired cells are extracted from the patient;
2. The isolated cells are cultured and expanded in vitro on a 2D scaffold;
3. The cell culture is seeded into a 3D scaffold support and additional biomolecules, such as matrix ligands, are added to promote growth;
4. A bioreactor is often used to develop the cell/scaffold construct into functioning tissue; and
5. Once the functional tissue graft is generated, this is implanted onto the damaged site where it becomes integrated into the surrounding tissue, restoring tissue function [9,18].

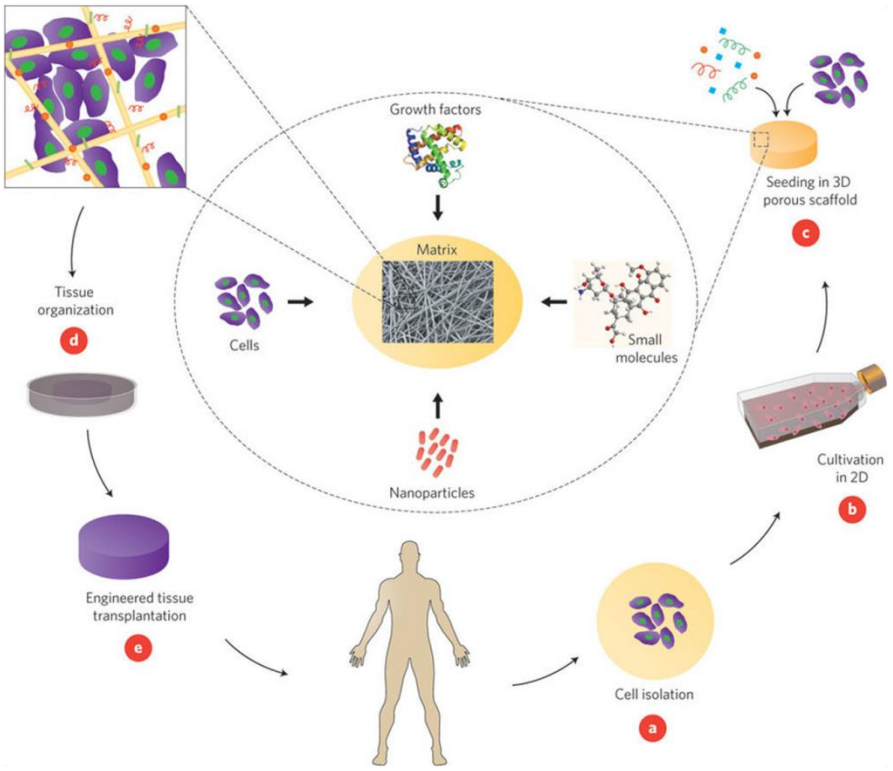

Figure 1.1 The key steps of tissue engineering: (a) cell isolation, (b) cultivation in 2D, (c) seeding in 3D porous scaffold, (d) tissue organisation and (e) engineering tissue transplantation. Figure reproduced from Dvir et al., 2011, Copyright © 2010, Springer Nature [19].

To engineer tissue, there are traditionally three components: Cells, biomolecules, and a scaffold. Different cell lines can be used depending on where they are isolated from and the end application. Both allogenic and autologous cells can be used, but the later are obtained from the patient itself and therefore do not elicit an immune response from the recipient, thus mitigating the risk of implant rejection [18]. Stem cells may also be used as these can differentiate into various cell lines. Stem cells isolated from adult or embryonic tissues are the main types of human stem cells used for tissue engineering. Embryonic stem cells are pluripotent in nature, i.e., show unlimited proliferative capacity and potentially differentiate into all body cells, which is beneficial for culturing new tissue [20,21]. However, there are some ethical concerns associated with the use of embryonic stem cells, which are harvested from "excess" human embryos created for implantation following in vitro fertilisation. Adult stem cells are becoming more commonly used and are harvested from umbilical cord blood, bone marrow and even discarded fat tissue from liposuction procedures, which will reduce the need to use embryonic stem cells. However, the major limitations of adult stem cells are: (i) that they are multipotent, not pluripotent (there are fewer cell types that can be differentiated from adult stem

cells than from embryonic stem cells) [22] and (ii) fewer population doublings occur in adult stem cells with fewer numbers of cell passages possible, leading to a slower doubling rate [23].

Biological molecules, including proteins, matrix ligands and growth factors, are often added to cell cultures to facilitate adhesion and enhance cell proliferation and differentiation, thus promoting tissue formation [18]. Growth factors are large biomolecules that consist of smaller proteins that act as signalling molecules for the cell. A common reagent used in cell culture is foetal bovine serum (FBS) derived from the blood of bovine foetuses, which contains bovine serum albumin, numerous adhesion proteins and a cocktail of other components [24]. However, despite its widespread use, there are serious concerns about the use of FBS in clinical applications, due to its high cost, batch reproducibility and issues associated with animal welfare. Therefore, there is currently a drive to reduce the reliance on FBS in tissue engineering through achieving the effect of FBS via scaffold modifications or serum substitutes, Figure 1.2 [25].

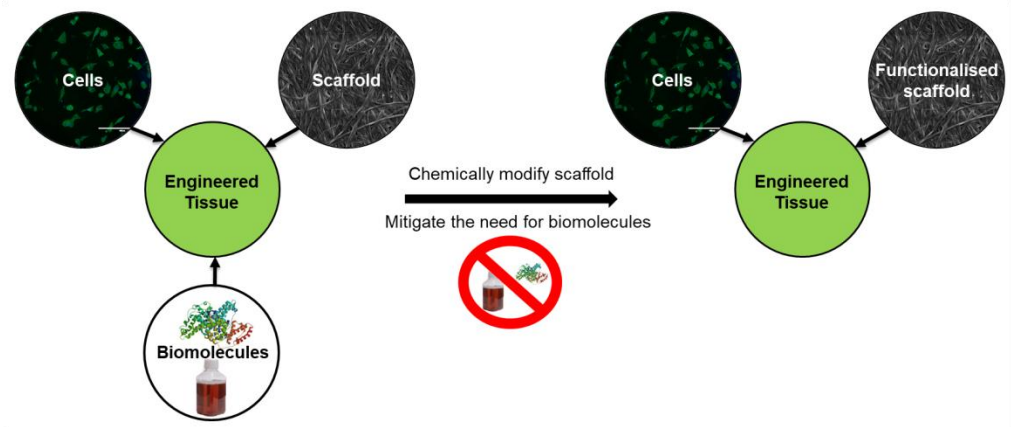

Figure 1.2 The traditional three-component system of tissue engineering vs. a two-component system, whereby the scaffolds have been functionalised to reduce the reliance on additional biomolecules such as FBS.

Scaffolds provide the 3D framework and support for seeded cells to attach, spread, proliferate and eventually form into tissue [26]. The porous nature of the scaffold allows for high mass transfer and waste removal [19]. A wide range of scaffolds have been produced from synthetic materials, such as polymers and composites, as well as naturally sourced materials and decellularised human/animal tissue [27,28]. Scaffolds fabricated from natural biomaterials possess the chemical structures that can mimic native tissue, aiding biocompatibility, and can be recognised by the body, however

they often lack the requisite mechanical strength and their origin can lead to complications such as premature scaffold degradation, particularly production in large quantities at a commercial scale from limitations due to raw material availability or lot-to-lot (or batch-to-batch) variations [29,30]. In contrast, synthetic materials have well-defined chemical compositions which allows for precise control over mechanical properties and degradation rates, as well as production in almost unlimited quantities [31]. However, these may require addition of growth factors to initiate cell adhesion and may have issues around biocompatibility as they often lack the necessary binding site for cell recognition [32,33]. Hence, the type of scaffold used in culturing tissue is not only paramount for the successful generation of tissue, but can also govern the applications accessible.

Recent advances in cell culture include applications other than regenerative medicine, such as "cellular agriculture", whereby cells are cultured in a scaffold to form meat fit for human consumption—an alternative to livestock meat production [34]. This emerging application of tissue engineering has potentially beneficial environmental implications, as a more efficient, non-methane producing means to produce meat [35]. Another application of tissue culture is the production of functional tissue analogues used in the pharmaceutical industry for drug screening to reduce this industry's reliance on vivisection (particularly early in the drug screening process) [36].

1.5 Cellulose as a Sustainable Scaffold for Tissue Engineering

Recently, principles of sustainability, eco-efficiency and green chemistry have begun to guide the development of a new generation of materials as an alternative to conventional polymers based on conversion of fossil carbon (e.g., oil) [37,38]. There are a wide range of biomaterials currently used in tissue engineering such as proteins, polysaccharides and biodegradable polymers. Protein and polysaccharide based biomaterials have been reviewed previously as nanoparticle scaffolds for tissue engineering [39]. Biodegradable and biocompatible polymer scaffolds have been reviewed [40] and an overview of hydrogels based on natural polymers and their various applications in the field of tissue engineering was published in 2011 [41]. For completeness, the reader is also referred to the review of decellularised whole-organ scaffolds by Peloso et al. [29], although, as such scaffolds are derived from

(deceased) human donors, supply is limited and some of the concerns associated with animal derived scaffolds apply.

The most common natural biomaterials are polymeric in nature and either protein-based, such as collagen, elastin, gelatin and silk, or polysaccharide-based, such as chitosan, alginate, hyaluronic acid and cellulose [42]. One of the most promising of these natural biomaterials, which has received much attention, is the polysaccharide cellulose. Much of this focus on cellulose is due to it possessing the necessary scaffold properties for tissue engineering, such as its biocompatibility, and relative readiness to be tuned through chemical modification to adjust mechanical properties and introduce various surface modifications. In addition, the sustainability of producing and manufacturing materials from cellulose, as well as its modest cost, makes cellulose an economically viable feedstock [43–47]. Cellulose can be sourced from a range of natural materials, most commonly from the cell wall of plants, where it is the major component. Other sources include tunicates and cellulose synthesised by bacteria, such as *Gluconacetobacter xylinum* (Figure 1.3). As the most abundant biopolymer on the planet [48], cellulose is considered an almost inexhaustible source of raw sustainable material, with an estimated 28.2 billion tonnes produced via biomass annually [43].

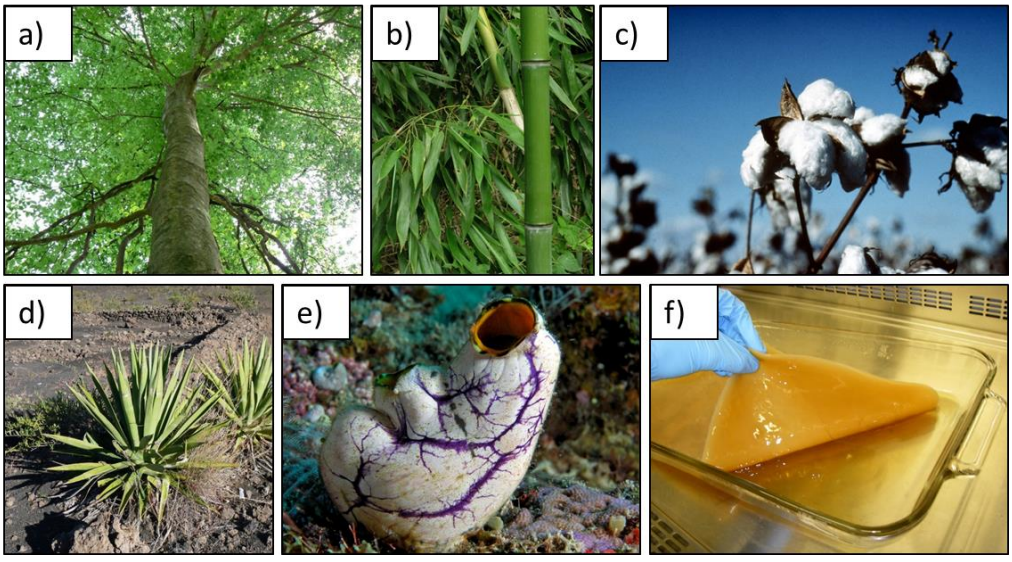

Figure 1.3 Cellulose can be obtained from various sources: (a) beech tree; (b) bamboo; (c) cotton; (d) sisal; (e) tunicine; and (f) *Gluconacetobacter xylinus*.

Regardless of origin, the chemical structure of cellulose is the same: Anhydroglucose units connected by β-1,4 glycosidic bonds between the C1 and C4 positions [42]. Unlike its monomer, glucose, cellulose is insoluble in water and many organic solvents. The

lack of solubility arises due to the presence of intramolecular bonding and strong hydrogen-bonding between cellulose polymer chains, which extend to interfibril interactions. This lack of solubility makes solution processing challenging and, as cellulose is not a thermoplastic material (it does not melt), it cannot be formed using typical melt extrusion techniques. This can result in processing challenges, but recently it has been demonstrated that cellulose dissolved in ionic liquid solutions may be processed into the desired structure and form by: Electrospinning, casting or moulding, before being regenerated in an anti-solvent, such as water and ethanol [49]. The degree of polymerisation (number of monomeric units in the polymer chain, DP) of the cellulose backbone is dependent on where it is sourced from, as well as how it is processed, which, in turn, affects its material properties. For example, bacterial cellulose has a DP of 800–10,000 repeat units, whilst the DP of cellulose from wood pulp is only 300–1700 [43]. Differences in the DP can affect the viscosity of cellulose solutions, as well as the mechanical properties of the final processed product.

There are many different types of cellulose particles that can be obtained (summarised in Table 1.1), including bacterial cellulose (BNC), microfibrillated cellulose (MFC), nanocrystalline cellulose (NCC), regenerated cellulose and decellularised plant tissue [50]. These have been widely investigated as potential materials for tissue engineering, due to their biocompatibility, biodegradability, and low cytotoxicity as well as tuneable chemical and physical properties [51,52]. Bacterial cellulose is formed as the *Acetobacter* bacterium extrudes pellicles of very pure cellulose fibrils and can be produced sustainably on scale using bioreactors [53]. When growing bacterial cellulose, the pellicles rise to the surface of the reactor and agglomerate, forming a membrane. Due to the high purity of cellulose these can be used as dense hydrogels, processed into nanofibrils, or solubilised or dispersed for further processing into formed materials. Membranes of bacterial cellulose are already used clinically as dressings to treat burn wounds as they have a high water content, do not adhere to healing skin and can be sterilised [54].

Table 1.1 A summary of the different types of nanocellulose, origin, formation and sizes. The table was reproduced from Klemm et al., 2011 [55]. Copyright © 2011 WILEY-VCH Verlag GmbH & Co. KGaA, Weinheim.

Type of Nanocellulose	Selected References and Synonyms	Typical Sources	Formation and Average Size
Microfibrillated cellulose (MFC)	Microfibrillated cellulose [56], nanofibrils and microfibrils [38], nanofibrillated cellulose [57]	Wood, sugar beet, potato tuber, hemp, flax delamination	Delamination of wood pulp by mechanical pressure before and/or after chemical or enzymatic treatment Diameter: 5–60 nm Length: several micrometres
Nanocrystalline cellulose (NCC)	Cellulose nanocrystals, crystallites [58], whiskers [59], rod-like cellulose microcrystals[60]	Wood, cotton, hemp, flax, wheat straw, mulberry bark, ramie, Avicel, tunicin, cellulose from algae and bacteria	Acid hydrolysis of cellulose from many sources Diameter: 5–70 nm Length: 100–250 nm (from plant celluloses); 100 nm to several micrometres (from celluloses of tunicates, algae, bacteria)
Bacterial nanocellulose (BNC)	Bacterial cellulose [43], microbial cellulose [52], biocellulose [61]	Low-molecular-weight sugars and alcohols	Bacterial synthesis Diameter: 20–100 nm; different types of nanofiber networks

Other forms of cellulose nanofibres include MFC fibres, mainly sourced from wood pulp [56]. The wood pulp is delaminated by mechanical pressure before being treated

chemically, or enzymatically, to produce nanofibres 5–60 nm wide and several microns long. NCC is produced by treating wood pulp (or other cellulose sources) with concentrated sulfuric acid, to dissolve the non-crystalline domains of the fibres, followed by high pressure homogenisation to fully disintegrate the nanoparticles [62]. These nanocrystals are the smallest type of cellulose particle, have a cross-sectional diameter as low as 5 nm and are 100s of nm in length, whereas MFC and BNC are several microns in length [50]. Although cellulose is considered to be a highly sustainable material it is important to note that the mechanical disintegration of the wood pulp fibres can be very energy intensive at scale [63]. However, a more environmentally friendly process to produce cellulose nanofibrils (CNF) has been identified. This relies on an oxidative chemical modification using 2,2,6,6-tetramethylpiperidine-1-oxyl (TEMPO) and an oxidant after the acid hydrolysis step, which significantly reduces the energy requirement of the homogenisation process from 20,000—30,000 kWh/tonne to 1000 kWh/tonne [64].

Another key advantage with using cellulose is that it can be processed into an array of materials. Cellulose nanocrystals can be dispersed to form delicate hydrogels [65], cellulose solutions can be electrospun into nanofibres [66] or regenerated as films [47] as well as formed into porous 3D structures [67]. Each of these has different mechanical and physical properties beneficial for specific tissue culture applications. Complex tissue formation requires a level of vascularity in scaffolds to allow mass transfer of nutrients and waste. Some plant tissue has vascular structures similar to human tissue and scaffolds can be prepared by decellularising the plant tissue [68]. This process is a convenient way to obtain complex structures without the need for multiple processing stages [69].

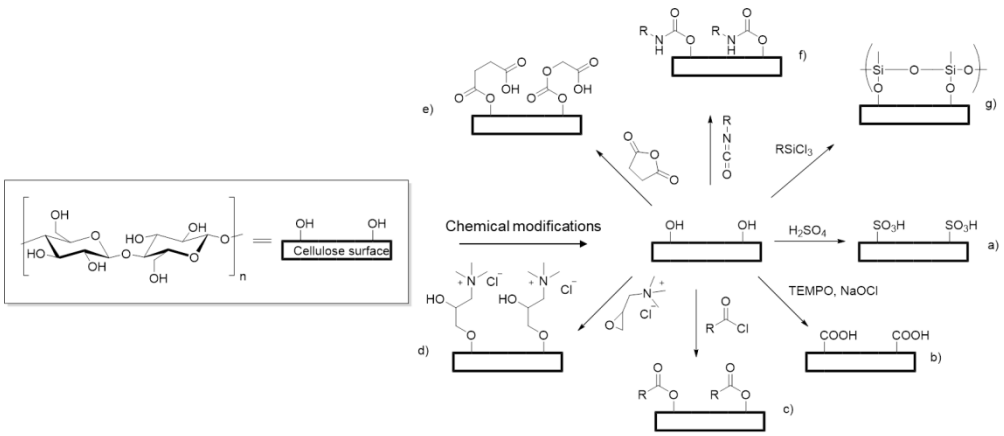

Scheme 1.1 The chemical structure of the anhydroglucose unit in cellulose and examples of some chemical modifications possible by reaction of the hydroxyl groups exposed on the surface of CNF: (a) sulfonation; (b) 2,2,6,6-tetramethylpiperidine-1-oxyl (TEMPO) mediated oxidation; (c) ester formation by reaction with acid chlorides; (d) grafting of tetra-alkylammonium groups by reaction with glycidyltrimethylammonium chloride (GTMAC); (e) grafting via ester linkages generated by reaction with acid anhydrides; (f) formation of urethanes by reaction with isocyanates; and (g) silylation. Reproduced with permission from Courtenay et al., 2018, published by The Royal Society of Chemistry [70].

Not only does cellulose have tuneable mechanical and structural properties, but it also can be readily functionalised due to the exposed hydroxyl groups on the surface of the fibrils, summarised in Scheme 1.1. Common modifications include the TEMPO oxidation of the hydroxyl group to a carboxylic acid [71], cationisation by grafting of glycidyl trimethylammonium chloride to the surface to introduce a positive charge [70], sulfuric acid hydrolysis leading to sulfate half esters [72] and derivitisation to produce a range of cellulose esters and ethers [73]. Although different modifications of cellulose materials have been widely reviewed [48,74,75] and exploited for other applications such as water purification [76], drug delivery [77] and rheology modification [78], reports of use in tissue engineering applications are more recent. This review focuses specifically on the use of modified cellulose materials for tissue culturing applications, including modifications and tissue culture applications summarised in Table 1.2.

Table 1.2 A summary of the recent literature on modified cellulose for tissue culture applications.

Cellulose Type	Modification	Scaffold Form	Tissue Culture Application
Bacterial Cellulose	Mannosylated	Membranes	Enhanced fibroblast growth [79]
	Cationisation and oxidation	Membranes	Protein free cell attachment [79]
	Silanisation	Lyophilised membranes	Wound dressing [80]
	TEMPO-mediated oxidation	Hydrogel with hydroxyapatite and crosslinked by glutaraldehyde	Bone tissue [81]
	RGD and xyloglucan-peptide grafting	Membranes	Engineering blood vessels [82]
	Modified with heparin	3D porous scaffold loaded with vascular endothelial growth factor (VEGF)	Tissue regeneration [83]
	Peptides fused to a carbohydrate-binding module (CBM3)	Membranes	Promoting neuronal and mesenchymal stem cell (MSC) adhesion [84]
	Tri-calcium phosphate and hydroxyapatite blend	Hydrogel	Bone tissue implants [85]
	Collagen and hydroxyapatite blend	Hydrogel crosslinked by procyanidins	Bone tissue [86]
	Hydroxyapatite and glycosaminoglycan blends	Layered scaffolds	Repair of osteochondral defects [87]
	Alginate blend	Porous scaffold crosslinked with Ca^{2+}	Biocompatibility and porous [88]
Nanocrystalline Cellulose	Dialdehyde cellulose crosslinked with collagen	3D porous scaffold	Dielectric behaviour relevant to neural tissue engineering [89]
	Acetate esterification	Interconnected highly porous scaffold	Hydrophobic and lipophilic scaffolds [90]
	Phosphorylation	Thin films	In vitro cell culture and in vivo tissue regeneration [91]

	Oxidised cellulose grafted with soybean protein isolate	Scaffold soaked in doubly concentrated simulated body fluid	Biomimetic calcium phosphate mineralisation [92]
	Copolymer dispersed with cellulose nanocrystals	3D nanocomposites	Biomedical and tissue engineering applications [93]
	CNC and reduced graphene oxide blended in PLA matrix	Nanocomposite film	Antibacterial activity [94]
	Nanocellulose blended with nanochitin	CAD generated porous structure	Biomimetic tissue engineering [67]
Microfibrillated Cellulose	Cationisation and glyoxalation	Regenerated modified cellulose films	Tailoring scaffold properties to regulate cell response [95]
	Cellulose-chitosan infusions	Hydrogels	Cell attachment [96]
	Oxidation followed by sulfonation	Electrospun fibre meshes	Bone tissue [97]
	Decellularisation followed by glutaraldehyde crosslinking	3D cellulose scaffolds	In vitro culture of mammalian cells in a 3D environment [69]
	Dopamine coated	Electrospun PLA/CNF composite nanofibres	Enhance cell biocompatibility [98]
	Polyurethane coated in a CNF dispersion	Electrospun nanofibres	Tissue engineering [99]
Cellulose Derivatives	Hydroxypropyl cellulose (HPC) crosslinked by methyl acrylate	Biocompatible and hydrolytically degradable scaffold	Long term cell culture [100]
	Ethyl hydroxyethyl cellulose (EHEC) crosslinked with citric acid	Electrospun nanofibres	Drug delivery and as scaffolds in tissue engineering [101]
	HPC modified with methacrylic anhydride	3D hydrogel constructed with interconnecting pores	Adipose tissue [102]
	Crosslinked gelatin/carboxymethyl cellulose (CMC) blend	Hydrogel with perfusable vascular networks	Engineering vascularised and cell-dense 3D tissues and organs [103]

CMC/MFC/pectin blend	Lyophilised hydrogels	Biocompatible composite scaffolds [104]
Cellulose acetate with polymer graft and polydopamine (PDA) coating	Electrospun nanofibre mats	Antifouling surface [105]
Cellulose acetate blended with PLA or PDO	Electrospun nanofibre mats	Biomineralisation [106]

1.6 Methods of Scaffold Modification

Modifications applied to cellulose materials to be used as tissue scaffolds can be divided into three main categories following trends in the recent literature:

1. Physical modifications—composites and blends;
2. Biochemical modifications—grafting of biomolecules onto the surface;
3. Chemical modifications—introducing new functional groups.

1.6.1 Physical Modifications

Composite scaffolds can be prepared through blending a cellulose powder, dispersion or solution which another material, often a polymer or an inorganic component. The benefits of blending cellulose with other materials are the ability to modulate or introduce new properties beneficial to the application in question, for instance introducing a charge [67], altering topography [107], or varying the mechanical properties [108,109]. This allows the creation of a family of cellulose composites.

Bacterial cellulose offers certain advantages for tissue engineering as it possesses high purity and an ultrafine fibrous network structure with variable porosity. Furthermore, it can be produced into different shapes and moulded into 3D structures during in vitro cultures [110]. Hydroxyapatite is commonly added to cellulose scaffolds as it is biocompatible, increases the tensile properties and promotes calcium phosphate mineralisation, which is valuable for bone tissue generation [111]. Scaffolds with pores in the micrometre and nanometre range have been prepared by blending bacterial cellulose with tri-calcium phosphate and hydroxyapatite and such scaffolds could be used to form implants for bone tissue

engineering as mineralisation occurs on the hydroxyapatite [85]. By forming layers of bacterial cellulose, harvested from the floating pellicles at the air-liquid interface, with hydroxyapatite or glycosaminoglycans, a nanocomposite scaffold could be fabricated that was biocompatible and mimicked the nanoscale fibrous structure of bone and cartilage ECM, respectively, resulting in tissue constructs that could regenerate osteochondral defects when implanted into the body [87]. Furthermore, hydrogels have been formed by gelation of bacterial cellulose nanofibres, stabilised by procyanidins, and blended with collagen and hydroxyapatite. Once lyophilised, these scaffolds supported the growth of human bone marrow stromal cells and osteoblastic differentiation was observed after 10 days by detecting the level of alkaline phosphatase expressed [86]. Compared with pure bacterial cellulose, the addition of both gelatin and hydroxyapatite improved the osteoinductivity of the scaffolds, vital for application for the culturing of bone tissue.

Cellulose can also be blended with other polysaccharides such as chitin, chitosan and alginate, to produce novel biomaterials. Chitin and chitosan are similar in structure to cellulose, being comprised of anhydroglucosamine units—*N*-acetylated in the case of chitin. Chitosan is not as robust as cellulose, as it is solubilised in weak acidic solutions, however it does exhibit a slightly positive charge when protonated and will absorb to cellulose surfaces, which are weakly negatively charged in aqueous media [112]. Chitosan-cellulose scaffolds have been developed by regenerating cellulose in an anti-solvent solution of chitosan and used to support MG-63 cell attachment and spreading [96].

Complex 3D scaffolds made from a gel composed of nanocellulose and nanochitin were fabricated using sacrificial templating of a methacrylate and acrylamide resin. Computer aided design enabled a 3D template to be printed with features of ~50 µm, which was filled with the nanocellulose-nanochitin gel. The scaffold template was removed in an alkaline solution leaving a highly porous interconnected biomimetic scaffold, which provided a stiff microenvironment necessary to facilitate the differentiation of human mesenchymal stem cells (hMSCs) [67]. Alginate, in comparison, is an anionic polysaccharide and can be easily fabricated by crosslinking with Ca^{2+} ions [88]. Scaffolds have been produced by mixing bacterial cellulose with alginate hydrogels and directionally freeze-drying to create a composite material with an open porous structure that supports the growth of L929 mouse fibroblast

cells [88]. The advantage of blending chitin, chitosan or alginate into the scaffolds is they are all degradable in vivo [113], whereas cellulosic materials are biodurable and are absorbed into the tissue, but can be degraded into glucose in the presence of added cellulase enzymes in vivo [114].

Cellulose is often used as a matrix to support other materials beneficial for cell culture. Pectin is used in tissue engineering as cells can be embedded into the structure, however, it has poor mechanical properties. To overcome this, pectin has been blended with a water soluble cellulose derivative, Carboxymethyl cellulose (CMC) and further reinforced with MFC. Lyophilised CMC/MFC/pectin composite hydrogels have been shown to support viable cells of the NIH3T3 fibroblast cell line [104]. The solubility of CMC in water means that it can be easily mixed with gelatin to form hydrogels. To improve the stability, hydrazide-modified gelatin and aldehyde-modified CMC, which readily crosslink to form stronger hydrogels, have been used. The fabrication of micro-channels in the hydrogel mimic the vascular networks in healthy tissue and cells can be embedded within these channels as a step towards engineering vascularised and cell-dense 3D tissues [103].

Other popular scaffolds produced from cellulose include electrospun nanofibres. This is a relatively simple technique to produce mats of entangled nanofibres with a high surface area, open porous structure and high tensile strength. This method requires the dissolution of cellulose and it is often first converted to cellulose acetate via a mercerisation-acetylation method, to improve its electrospinnability [106]. Once in solution other polymer additives are commonly added; for example poly(lactic acid) (PLA) and poly(dioxanone) (PDO) are both biodegradable polymers which will influence mechanics and degradation rate of the scaffold in vivo [106]. The electrospun mats formed supported L929 mouse fibroblast proliferation and cell infiltration into the scaffold, as well as biomineralisation of nano-hydroxyapatite deposits on the fibres [106].

Cellulose nanocrystals have been added to polymer solutions to reinforce the resultant extruded fibres. A copolymer of maleic anhydride modified poly(butylene adipate-co-terephthalate) was dispersed with cellulose nanocrystals by extruding the copolymer solution into the cellulose dispersion [93]. The addition of cellulose nanocrystals increased the elastic modulus and tensile strength of the fibres, as well as improving the low thermal stability and raising the glass transition temperature,

T_g, of the composite. As little as 9% cellulose nanocrystals in the composite significantly enhanced L929 mouse fibroblast cell adhesion [93]. Nanocrystal cellulose has been used as a nanofiller additive, along with reduced graphene oxide, to make thin films of PLA [94]. The presence of cellulose nanocrystals significantly increased the tensile strength of the film up to 23% and improved the ductile properties. The nanocomposite films produced by this method showed antibacterial activity and in vitro cell based cytotoxicity assays confirmed biocompatibility with the fibroblast cell line NIH-3T3.

Fabricating composite scaffolds from blends of cellulose nanofibres can be considered more environmentally friendly than scaffolds made from regenerated cellulose because this removes the need for using ionic liquids in manufacturing. Solubilising cellulose in ionic liquids can add to the processing costs and ionic liquids can be toxic to cells if left in the material, so rigorous cleaning procedures need to be included to ensure that no ionic liquid remains [115]. Nonetheless, ionic liquid aided processing facilitates formation of a range of materials by solution casting and phase inversion methods [116] and use of a range of co-solvents can facilitate co-dissolution of other components [117,118]. Variation of anti-solvents in phase inversion directly impacts on the porous nature of the materials [119].

1.6.2 Biochemical Modifications

Despite having many beneficial properties for a tissue scaffold, one potential limitation of using cellulose is its hydrophilic nature and low non-specific protein binding affinity, which means that mammalian cells do not readily absorb onto cellulose surfaces [120–122]. This can be overcome by the introduction of biomolecules, such as matrix ligands, growth factors, or FBS either contained in the cell growth media, or functionalised onto the scaffold surface, to facilitate initial cell attachment [123].

RGD (Arg-Gly-Asp) is commonly used to facilitate cellular adhesion onto scaffolds as it is the minimal fragment of the active site of cell adhesive proteins such as fibronectin [124]. Bacterial cellulose hydrogels have been modified with xyloglucan-RGD conjugates to enhance the attachment and proliferation of human endothelial cells [82]. Carbohydrate-binding modules (CBM) are protein domains present in cellulose-degrading enzymes and have an affinity to cellulose surfaces. These have

been used as intermediaries to attach biological molecules, which would not readily bind to native cellulose, onto cellulose surfaces [119]. The recombinant protein IKVAV (Ile-Lys-Val-Ala-Val), is another cell adhesion motif found in the ECM which has been attached onto the surface of a bacterial cellulose scaffold using CBM3, resulting in an appropriate environment for promoting neural and MSC adhesion [84].

To direct the development of vascularised structures, angiogenesis, growth factors such as VEGF are required. However, it is necessary to incorporate VEGF into the scaffold matrix as it has a short half-life and can readily diffuse into the media in vivo [125]. 3D porous scaffolds from bacterial cellulose/gelatin composites were surface modified with heparin, via a condensation reaction, in order to bind VEGF onto the surface through electrostatic interactions between negatively charged *N*- and *O*-sulfated groups of heparin and the basic lysine and arginine residues of VEGF. By fixing VEGF onto the scaffold surfaces, the sustained delivery of VEGF, required to facilitate the production of new blood vessels in the tissue construct, was enabled [83].

The addition of biological molecules onto the scaffold surface can also enhance the biocompatibility of the biomaterial. Biomimetic scaffolds have been produced from electrospun PLA/CNF composite nanofibres coated in a dopamine solution, to form a layer of poly(dopamine) (PDA) on the surface [98]. The addition of PDA onto the surface of the scaffold increases the adhesion of hMSCs, due to the large amount of amine and hydroxyl groups present. CNF have also been electrospun with poly(2-methacryloyloxyethyl phosphorylcholine) before being coated with PDA [105]. This formed a zwitterionic polymer coating, limiting the fouling on the nanofibre membranes necessary for biomaterials for wound healing or tissue engineering, where antibacterial scaffolds are required. However, a disadvantage to the technique is the deposition of dopamine, which is a very time-consuming process, taking up to several days [98].

Along with animal based proteins, there are several types of proteins derived from plants that can be used to enhance the biomimetic nature of the scaffold [126]. In particular, soy protein isolates (SPI) have been grafted onto oxidised cellulose in order to absorb growth factors necessary for in vitro biomineralisation. When the scaffolds were soaked in a doubly concentrated simulated body fluid solution, biomimetic calcium phosphate mineralisation was initiated, producing

hydroxyapatite rod-like nanocrystals, a perquisite for bone tissue engineering [92]. However, a disadvantage of using SPI is its solubility in acidic or basic media.

1.6.3 Chemical Modifications

The three primary alcohol groups present in the anhydroglucose unit makes cellulose very amenable to functionalisation as these are exposed at surfaces, e.g., of nanofibrils, sheets, or nanocrystals. This enables new chemical and physical scaffold properties to be introduced or further tuned. Oxidation of CNF is an attractive modification method as it changes the behaviour of the nanofibrils, rendering these readily dispersible in water. This allows for cellulose to be processed in a viscous liquid form without requiring ionic liquid solvents [78]. Surface hydroxyl groups on bacterial CNF were oxidised by TEMPO to carboxylic acid groups and used to disperse hydroxyapatite nanoparticles. Upon addition of gelatin, a hydrogel was formed and crosslinked by glutaraldehyde, producing a scaffold which showed potential for engineering bone tissue [81]. Oxidation using acidified sodium periodate forms dialdehyde cellulose (DAC) and scaffolds have been fabricated by blending DAC with collagen, followed by crosslinking to form a 3D porous sponge that demonstrated dielectric behaviour, indicating a material that could be suitable for neural tissue engineering focused on the regeneration of the nervous system [89].

Cellulose nanocrystals can also be modified to become water dispersible (often described as “water-soluble”, although clearly the crystals are not dissolved). Scaffolds of highly esterified acetate cellulose nanocrystals (ACNC) were prepared through an environmental friendly single step esterification method resulting in materials with a degree of substitution of 2.18, making these hydrophobic, oleophilic and lipophilic. Ice-templating and freeze drying yielded interconnected, highly porous scaffolds, creating a microenvironment suitable for tissue engineering [90].

Furthermore, the chemical modification of microcrystalline cellulose by phosphorylation, using a molten phosphorous acid-urea reaction mixture, resulted in a water soluble material which could be cast into pellets. Normal human dermal fibroblast were viable on the phosphorylated surface, which was said to mimic the glucosaminoglycans of in vivo cartilage tissue [91]. Cellulose phosphate is more

hydrophilic than native cellulose, but it is beneficial for bone tissue generation as calcium can easily be mineralised [127].

Electrospun scaffolds are often used due to their good tensile mechanical strength and as mimics of the fibrous structure of the ECM. However, native cellulose is a poor candidate for electrospinning due to its poor solubility on most organic solvents. Cellulose is often converted to cellulose acetate to be electrospun into fibres. Further modifications have been applied to the nanofibres including oxidation followed by sulfonation to form water-stable sulfated cellulose [97]. These fibrous meshes have demonstrated potential for bone tissue engineering as the sulfate groups are able to retain the osteogenic growth factor, human recombinant bone morphogenetic protein-2 (rhBMP-2), which supports the growth of bone marrow stromal cells on a bone tissue scaffold [97].

Attempts have been made to utilise the existing structure of plants for tissue engineering. Given that cellulose is a major component of the plant cell wall, plant tissues can be decellularised and used as scaffolds. The mechanical structure of cellulose can be modified using chemical cross-linkers such as glyoxal or glutaraldehyde to stiffen the scaffold [128]. Scaffolds derived from apple hypanthium tissue were decellularised, coated with collagen and crosslinked with glutaraldehyde to stiffen the material [69]. Apple tissue was used as a promising candidate for in vitro culture of mammalian cells in a 3D environment because its internal structure consists of connected pores and air pockets needed to transfer nutrients and waste produced in 3D tissue [69]. These scaffolds supported a range of cell lines as well as being easily produced, inexpensive and originating from a renewable, sustainable source.

It has been reported that the contractility of fibroblast cells on a native bacterial cellulose scaffold surface is much lower than between other fibroblast cells [129]. This is detrimental for cell attachment and proliferation on these scaffolds, as the seeded cells would tend to round up instead of elongate [129]. Bacterial cellulose has been functionalised with organosilanes, by grafting methyl terminated octadecyltrichlorosilane or amine terminated 3-aminopropyltriethoxysilane [80]. These modifications increased both hydrophobic and electrostatic interactions with fibroblast cells, beneficial to promote cell growth for wound dressing applications [80]. The growth of fibroblast cells was enhanced on the mannosylated surface of

bacterial cellulose membranes, achieved by grafting aryl monosaccharides into succinylated bacterial cellulose [79]. The covalent attachment of carbohydrates onto the surface was made viable through the succinic crosslink and was reported to be beneficial to the stimulation of fibroblast growth, as it is a monosaccharide motif used in cellular recognition. Furthermore, the cells have a higher affinity for the succinylated bacterial cellulose due to a higher charge on the carboxylated surface.

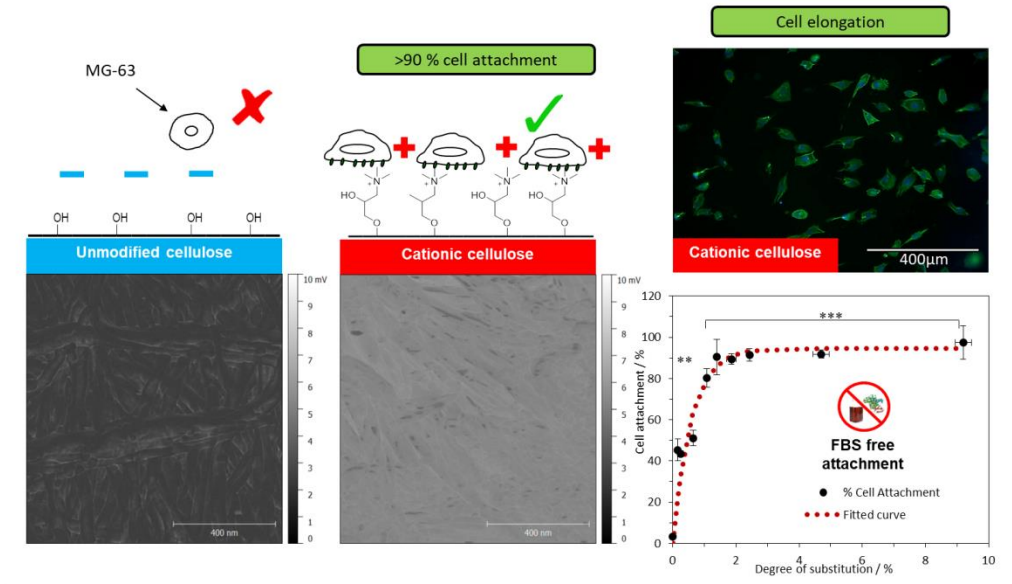

Figure 1.4 Cationisation of cellulose film by GTMAC introduced a positive charge to the surface facilitating MG-63 cell attachment, in a matrix ligand free system, whereas only minimal attachment was observed on unmodified cellulose surfaces. Electric force microscopy revealed the cationic cellulose had a positive surface charge compared to the negatively charged native cellulose. Interestingly only a low level of ~1.4% degree of substitution was required to induce this effect. After 24 h incubation at 37 °C in 5% CO_2 greater cell elongation occurred in on the cationic scaffolds compared to the unmodified cellulose. Reproduced with permission from Courtenay et al., 2017 [95], Copyright © 2016, Springer Nature.

Cellulose surfaces bear a slight negative charge in aqueous media [112] and, to overcome this, the epoxide, glycidyltrimethylammonium chloride (GTMAC), has been used to introduce a positive charge onto the surface via introduction of quaternary ammonium moieties. Unlike chitosan, these cationised CNF have a permanent charge and can be dispersed in water to form stable hydrogels if the degree of GTMAC substitution along the nanofibril is high enough to charge stabilise the dispersed particles [70]. Bacterial cellulose films were chemically modified with GTMAC facilitating the attachment of MG-63 osteoblast cells through electrostatic interactions between the phosphate-lipid bilayer of the cell membrane and the positively charged quaternary ammonium group (Figure 1.4 [25]). Importantly, this was

achieved in the absence of matrix ligands needed for cell attachment—no FBS was present in the culture medium during attachment. Reducing the reliance on growth factors, or proteins, for cell culture is important for industrial application as these are very costly, can exhibit batch variability and are derived from animals or humans. In addition to modification of the surface charge, the structural properties of the scaffolds could be tuned by crosslinking with glyoxal to increase stiffness and further regulate cellular response [95]. These modifications use simple yet robust chemistries that can be applied to any form of cellulose and are amenable to scaling up for industrial applications.

Other derivatives of cellulose have been chemically modified to produce novel scaffolds and are often used as biomaterials due to their solubility in water and most organic solvents, low cost and commercial availability in a range of molecular weights [102]. HPC was photo crosslinked with methyl methacrylate to form a photo-patterned and biodegradable hybrid paper substrate which could be used for cell culture. Using lithographic techniques enables patterns of modified cellulose to be produced, which could be used to form arrays of discrete cell clusters for cell assays such as toxicity or population dynamics [100]. EHEC and hydrophobically modified EHEC were blended with PVA and electrospun into fibres. These fibres were cross-linked with citric acid and supported the growth of L929 mouse fibroblast cells, showing potential for cell culture applications [101]. Soft, interconnected microporous scaffolds were prepared by modifying HPC with methacrylic anhydride, improving the biodegradability [102]. These 3D hydrogel scaffolds were used to culture human adipose-derived stem cells (ASCs) due to the interconnecting pores aiding nutrient transfer [102].

1.6.4 Cellulose Bioresorbability and Biodegradability In Vivo

An important factor when considering cellulose as a scaffold material for tissue engineering applications is its biodegradation in vivo. Cellulose is commonly referred to as biodegradable, as it is degraded by microorganisms, however the resorption of cellulose in vivo does not occur as animals and humans do not synthesise cellulases [77]. A long-term study by Martson et al. [130], described cellulose-based implants as biodurable as cellulose sponge scaffolds only underwent very slow degradation in rat subcutaneous tissue after 60 days [130]. Whilst this may be a potential limitation

for the success of cellulose scaffolds to be used for in vivo tissue engineering; it is not the case for in vitro culture or cellular agriculture applications.

Regenerated cellulose fibres when treated with N_2O_4 to produce oxidised cellulose have been shown to bioresorb in vivo [131,132]. Several Johnson and Johnson Medical Inc. patents exist, covering the preparation and use of oxidised cellulose for use as surgical haemostats and gauzes (SURGICEL®) to prevent post-operative adhesions [133,134]. Periodate oxidation to introduce aldehyde groups on the cellulose chain has been shown to promote degradation of the cellulose at physiological pH [45,77,135]. However limited advancements have been made since. Another more recent approach involved dosing cellulosic scaffolds with cellulase prior to implantation to stimulate in vivo degradation [45,114]. Moreover, including hyaluronic acid into cellulose structures introduces area of the scaffold that are enzyme degradable [45]. Sannino et al. demonstrated that carbodiimide could be used as a crosslinker between hyaluronic acid and cellulose derivatives [136]. This process introduces ester bonds amongst the cellulose networks, which can be digested via hydrolysis [45,136]. Furthermore, cellulose can be functionalised with several biomolecules, through carbodiimide crosslinking, such as cell function promoting polypeptides [137,138]. Despite limited progress in the last decade to make cellulose degrade in vivo, this has not deterred the breadth of recent literature investigating modified cellulose scaffolds for cell culture.

1.7 Conclusions

It is clearly apparent that there is much potential for cellulose based materials as scaffolds in tissue engineering. These are attractive from both a sustainability point of view as well as industrial applications as there are a range of readily accessed fabrication methods possible. Cellulose is a cost effective and sustainably source biomaterial amenable to an array of modifications that unlock new properties and applications. Whilst there are a vast range of chemistries at hand that can be applied to cellulose, only those that are robust, scalable and amenable to manufacturing are likely to have longevity in tissue engineering beyond the laboratory.

It is very beneficial for the scaffold modifications, either chemical or biochemical, to reduce the reliance of matrix ligands for cell attachment, which is important as currently the majority of matrix ligands are provided by foetal bovine serum, which is not a sustainable source for industrial scale due to high cost, batch variation and

ethical considerations arising from to its origin. Moreover, developing scaffolds with complex vascular-like structural features will be important for transitioning cell culture from simple constructs to functional tissues. Sourcing cellulose from decellularised plant tissue can reduce the cost and complexity of processing of the scaffold whilst introducing vascularity onto the scaffold. Furthermore, there are many opportunities to blend cellulose with other biomaterials to obtain a scaffold with the desired properties for specific applications.

Thus, modified cellulose meets the demand for a new biomaterial with suitable properties for tissue engineering: Derived from a sustainable source and requiring minimal chemical processing, or added growth factors, to culture cells for industrial applications.

1.8 Acknowledgements

J.C.C. acknowledges funding support from the EPSRC Centre for Doctoral Training in Sustainable Chemical Technology (EP/L016354/1).

1.9 References

1. R. Lanza, R. Langer, and J. Vacanti, *Principles of tissue engineering*, Academic press, 3rd editio., 2011.

2. C. Vacanti, *J. Cell. Mol. Med.*, 2006, **1**, 569–576.

3. U. Meyer, T. Meyer, J. Handschel, and H. P. Wiesmann, *The History of Tissue Engineering and Regenerative Medicine in Perspective*, Springer, Berlin, 2009.

4. NHS Blood and Transplant, *Organ Donation and Transplantation Activity Report 2017/18*, 2018.

5. R. Langer and J. P. Vacanti, *Science (80-.).*, 1993, **260**, 920–926.

6. C. Mason and P. Dunnill, *Regen. Med.*, 2008, **3**, 1–5.

7. W. S. Churchill, *The U-boat War. Thoughts and Adventures*, Thorton Butterworth, London, 1932.

8. N. Stephens, L. Di, I. Dunsford, M. Ellis, A. Glencross, and A. Sexton, *Trends Food Sci. Technol.*, 2018, **78**, 155–166.

9. A. J. Salgado, J. M. Oliveira, A. Martins, F. G. Teixeira, N. A. Silva, N. M. Neves, N. Sousa, and R. L. Reis, *Int. Rev. Neurobiol.*, 2013, **108**, 1–33.

10. P. Murail and L. Girard, *Nature*, 1998, **391**, 7–8.

11. W. T. J. Green, *Clin. Orthop. Relat. Res.*, 1977, 237–250.

12. E. Constant and J. F. Burke, *Plast. Reconstr. Surg.*, 1982, **70**, 784.

13. T. J. Phillips, O. Kehinde, H. Green, and B. A. Gilchrest, *J. Am. Acad. Dermatol.*, 1989, **21**, 191–199.

14. B. Coulomb, L. Friteau, J. Baruch, J. Guilbaud, B. Chretien-Marquet, J. Glicenstein, C. Lebreton-Decoster, E. Bell, and L. Dubertret, *Plast. Reconstr. Surg.*, 1998, **101**, 1891–1903.

15. A. Gonfiotti, M. O. Jaus, D. Barale, S. Baiguera, C. Comin, F. Lavorini, G. Fontana, O. Sibila, G. Rombolà, P. Jungebluth, and P. Macchiarini, *Lancet*, 2014, **383**, 238–44.

16. P. R. Delaere and D. Van Raemdonck, *J. Thorac. Cardiovasc. Surg.*, 2014, **147**, 1128–1132.

17. B. Quinn, Paralysed man Darek Fidyka walks again after pioneering surgery, http://www.theguardian.com/science/2014/oct/21/paralysed-darek-fidyka-pioneering-surgery, (accessed2014.

18. C. M. Agrawal, J. L. Ong, M. R. Appleford, and G. Mani, in *Introduction to Biomaterials - Basic Theory with Engineering Applications*, eds. M. W. Saltzman and S. Chien, Cambridge University Press, 2014, pp. 341–374.

19. T. Dvir, B. P. Timko, D. S. Kohane, and R. Langer, *Nat. Nanotechnol.*, 2011, **6**, 13–22.

20. G. Keller, *Genes Dev.*, 2005, **19**, 1129–1155.

21. C. A. Heath, *Trends Biotechnol.*, 2000, **18**, 17–19.

22. R. Gupta, T. Enver, and A. Medvinsky, Cord blood stem cells: current uses and future challenges, http://www.eurostemcell.org/factsheet/cord-blood-stem-cells-current-uses-and-future-challenges, (accessed2012.

23. R. Hass, C. Kasper, S. Böhm, and R. Jacobs, *Cell Commun. Signal.*, 2011, **9**, 12.

24. J. van der Valk, *ALTEX*, 2017, **35**, 99–118.

25. J. C. Courtenay, M. A. Johns, F. Galembeck, C. Deneke, E. M. Lanzoni, C. A. Costa, J. L. Scott, and R. I. Sharma, *Cellulose*, 2017, **24**, 253–267.

26. J. K. Kular, S. Basu, and R. I. Sharma, *J. Tissue Eng.*, 2014, **5**, 1–17.

27. S. J. Hollister, R. D. Maddox, and J. M. Taboas, *Biomaterials*, 2002, **23**, 4095–4103.

28. R. B. Agrawal, C. M. and Ray, *J. Biomed. Mater. Res. - Part A*, 2001, **55**, 141–150.

29. A. Peloso, A. Dhal, J. P. Zambon, P. Li, G. Orlando, A. Atala, and S. Soker, *Stem Cell Res. Ther.*, 2015, **6**, 107.

30. G. M. Abouna, *Transplant. Proc.*, 2008, **40**, 34–38.

31. M. Okamoto and B. John, *Prog. Polym. Sci.*, 2013, **38**, 1487–1503.

32. J. Patterson, M. M. Martino, and J. A. Hubbell, *Mater. Today*, 2010, **13**, 14–22.

33. D. S. W. Benoit and K. S. Anseth, *Acta Biomater.*, 2005, **1**, 461–470.

34. M. J. Post, *Meat Sci.*, 2012, **92**, 297–301.

35. H. L. Tuomisto and M. J. Teixeira De Mattos, *Environ. Sci. Technol.*, 2011, **45**, 6117–6123.

36. F. Pampaloni, E. G. Reynaud, and E. H. K. Stelzer, *Nat. Rev. Mol. Cell Biol.*, 2007, **8**, 839–845.

37. W. R. Lustri, H. Gomes de Oliveira Barud, H. Da Silva Barud, M. F. S. Peres, J. Gutierrez, A. Tercjak, O. Batista de Oliveira Junior, and S. José Lima Ribeiro, in *Cellulose - Fundamental Aspects and Current Trends*, ed. D. M. Poletto, INTECH Open Access Publisher, 2015.

38. D. C. Potulski, G. I. B. De Muniz, U. Klock, and A. S. De Andrade, *Sci. For. Sci.*, 2014, **40**, 345–351.

39. S. K. Nitta and K. Numata, *Int. J. Mol. Sci.*, 2013, **14**, 1629–1654.

40. I. Armentano, M. Dottori, E. Fortunati, S. Mattioli, and J. M. Kenny, *Polym. Degrad. Stab.*, 2010, **95**, 2126–2146.

41. S. Van Vlierberghe, P. Dubruel, and E. Schacht, *Biomacromolecules*, 2011, **12**,

1387–1408.

42. C. M. Agrawal, J. L. Ong, M. R. Appleford, and G. Mani, in *Introduction to Biomaterials - Basic Theory with Engineering Applications*, Cambrigde University Press, Cambridge, 2014, pp. 198–232.

43. D. Klemm, B. Heublein, H.-P. P. Fink, and A. Bohn, *Angew. Chemie - Int. Ed.*, 2005, **44**, 3358–3393.

44. D. J. Modulevsky, C. M. Cuerrier, and A. E. Pelling, *PLoS One*, 2016, **11**, 1–19.

45. A. Sannino, C. Demitri, and M. Madaghiele, *Materials (Basel).*, 2009, **2**, 353–373.

46. A. Svensson, E. Nicklasson, T. Harrah, B. Panilaitis, D. L. Kaplan, M. Brittberg, and P. Gatenholm, *Biomaterials*, 2005, **26**, 419–31.

47. F. G. Torres, S. Commeaux, and O. P. Troncoso, *J. Funct. Biomater.*, 2012, **3**, 864–78.

48. S. Eyley and W. Thielemans, *Nanoscale*, 2014, **6**, 7764–7779.

49. K. Jedvert and T. Heinze, *J. Polym. Eng.*, 2017, **37**, 845–860.

50. R. J. Moon, A. Martini, J. Nairn, J. Simonsen, and J. Youngblood, *Chem Soc Rev*, 2011, **40**, 3941–3994.

51. M. Jorfi and E. J. Foster, *J. Appl. Polym. Sci.*, 2015, **132**, 1–19.

52. W. K. Czaja, D. J. Young, M. Kawecki, and R. M. Brown, *Biomacromolecules*, 2007, **8**, 1–12.

53. Y. Chao, T. Ishida, Y. Sugano, and M. Shoda, *Biotechnol. Bioeng.*, 2000, **68**, 345–352.

54. L. Fu, J. Zhang, and G. Yang, *Carbohydr. Polym.*, 2013, **92**, 1432–1442.

55. D. Klemm, F. Kramer, S. Moritz, T. Lindström, M. Ankerfors, D. Gray, and A. Dorris, *Angew. Chemie - Int. Ed.*, 2011, **50**, 5438–5466.

56. I. Siró and D. Plackett, *Cellulose*, 2010, **17**, 459–494.

57. M. Henriksson, L. A. Berglund, P. Isaksson, T. Lindstro, and T. Nishino, *Biomacromolecules*, 2008, **9**, 1579–1585.

58. Y. Habibi, L. A. Lucia, and O. J. Rojas, *Chem. Rev.*, 2010, **110**, 3479–3500.

59. M. A. S. A. Samir, F. Alloin, J. Y. Sanchez, and A. Dufresne, *Macromolecules*, 2004, **37**, 4839–4844.

60. M. M. de Souza Lima and R. Borsali, *Macromolecules*, 2004, **25**, 771–787.

61. A. Sani and Y. Dahman, *J. Chem. Technol. Biotechnol.*, 2010, **85**, 151–164.

62. H. P. S. Abdul Khalil, Y. Davoudpour, M. Nazrul Islam, A. Mustapha, K. Sudesh, R. Dungania, and M. Jawaid, *Carbohydr. Polym.*, 2014, **99**, 649–655.

63. S. Afewerki, R. Alimohammadzadeh, S. H. Osong, C.-W. Tai, P. Engstrand, A. Córdova, S. Afewerki, R. Alimohammadzadeh, A. Córdova, S. H. Osong, P. Engstrand, and C. Tai, *Glob. challenges*, 2017, **1**, 1–6.

64. Q. Li, S. McGinnis, C. Sydnor, A. Wong, and S. Renneckar, *ACS Sustain. Chem. Eng.*, 2013, **1**, 919–928.

65. M. Bhattacharya, M. M. Malinen, P. Lauren, Y.-R. Lou, S. W. Kuisma, L. Kanninen, M. Lille, A. Corlu, C. GuGuen-Guillouzo, O. Ikkala, A. Laukkanen, A. Urtti, and M. Yliperttula, *J. Control. Release*, 2012, **164**, 291–298.

66. Z. Ma and S. Ramakrishna, *J. Memb. Sci.*, 2008, **319**, 23–28.

67. J. G. Torres-Rendon, T. Femmer, L. De Laporte, T. Tigges, K. Rahimi, F. Gremse, S. Zafarnia, W. Lederle, S. Ifuku, M. Wessling, J. G. Hardy, and A. Walther, *Adv. Mater.*, 2015, **27**, 2989–2995.

68. J. R. Gershlak, S. Hernandez, G. Fontana, L. R. Perreault, K. J. Hansen, S. A. Larson, B. Y. K. Binder, D. M. Dolivo, T. Yang, T. Dominko, M. W. Rolle, P. J. Weathers, F. Medina-Bolivar, C. L. Cramer, W. L. Murphy, and G. R. Gaudette, *Biomaterials*, 2017, **125**, 13–22.

69. D. J. Modulevsky, C. Lefebvre, K. Haase, Z. Al-Rekabi, and A. E. Pelling, *PLoS One*, 2014, **9**, e97835.

70. J. C. Courtenay, S. M. Ramalhete, W. J. Skuze, R. Soni, Y. Z. Khimyak, K. J. Edler, and J. L. Scott, *Soft Matter*, 2018.

71. A. Isogai, T. Saito, and H. Fukuzumi, *Nanoscale*, 2011, **3**, 71–85.

72. I. Capron and B. Cathala, *Biomacromolecules*, 2013, **14**, 291–296.

73. B. Braun and J. R. Dorgan, *Biomacromolecules*, 2009, **10**, 334–341.

74. K. Missoum, M. N. Belgacem, and J. Bras, *Materials (Basel).*, 2013, **6**, 1745–1766.

75. Y. Habibi, *Chem. Soc. Rev.*, 2014, **43**, 1519–1542.

76. H. Kono, K. Ogasawara, R. Kusumoto, K. Oshima, H. Hashimoto, and Y. Shimizu, *Carbohydr. Polym.*, 2016, **152**, 170–180.

77. E. Lam, K. B. Male, J. H. Chong, A. C. W. Leung, and J. H. T. Luong, *Trends Biotechnol.*, 2012, **30**, 283–290.

78. R. J. Crawford, K. J. Edler, S. Lindhoud, J. L. Scott, and G. Unali, *Green Chem.*, 2012, **14**, 300–303.

79. S. Birkheur, P. C. de S. Faria-Tischer, C. A. Tischer, E. F. Pimentel, M. Fronza, D. C. Endringer, A. P. Butera, and R. M. Ribeiro-Viana, *Mater. Sci. Eng. C*, 2017, **77**, 672–679.

80. S. Taokaew, M. Phisalaphong, and B. min Z. Newby, *Cellulose*, 2015, **22**, 2311–2324.

81. M. Park, D. Lee, S. Shin, and J. Hyun, *Colloids Surfaces B Biointerfaces*, 2015,

130, 222–228.

82. A. Bodin, L. Ahrenstedt, H. Fink, H. Brumer, B. Risberg, and P. Gatenholm, *Biomacromolecules*, 2007, **8**, 3697–3704.

83. B. Wang, X. Lv, S. Chen, Z. Li, J. Yao, X. Peng, C. Feng, Y. Xu, and H. Wang, *Carbohydr. Polym.*, 2018, **181**, 948–956.

84. R. Pertile, S. Moreira, F. Andrade, L. Domingues, and M. Gama, *Biotechnol. Prog.*, 2012, **28**, 526–532.

85. P. Basu, N. Saha, S. Bandyopadhyay, and P. Saha, *AIP Conf. Proc.*, 2017, **1843**, 0–7.

86. Y. Huang, J. Wang, F. Yang, Y. Shao, X. Zhang, and K. Dai, *Mater. Sci. Eng. C*, 2017, **75**, 1034–1041.

87. J. V. Kumbhar, S. H. Jadhav, D. S. Bodas, A. Barhanpurkar-Naik, M. R. Wani, K. M. Paknikar, and J. M. Rrajwade, *Int. J. Nanomedicine*, 2017, **12**, 6437–6459.

88. S. Kirdponpattara, A. Khamkeaw, N. Sanchavanakit, P. Pavasant, and M. Phisalaphong, *Carbohydr. Polym.*, 2015, **132**, 146–155.

89. K. Pietrucha, E. Marzec, and M. Kudzin, *Int. J. Biol. Macromol.*, 2016, **92**, 1298–1306.

90. E. Abraham, D. E. Weber, S. Sharon, S. Lapidot, and O. Shoseyov, *ACS Appl. Mater. Interfaces*, 2017, **9**, 2010–2015.

91. T. Petreus, B. A. Stoica, O. Petreus, A. Goriuc, C. E. Cotrutz, I. V. Antoniac, and L. Barbu-Tudoran, *J. Mater. Sci. Mater. Med.*, 2014, **25**, 1115–1127.

92. A. Salama, N. Shukry, A. El-Gendy, and M. El-Sakhawy, *Ind. Crops Prod.*, 2017, **95**, 170–174.

93. S. Kashani Rahimi, R. Aeinehvand, K. Kim, and J. U. Otaigbe, *Biomacromolecules*, 2017, **18**, 2179–2194.

94. N. Pal, P. Dubey, P. Gopinath, and K. Pal, *Int. J. Biol. Macromol.*, 2017, **95**, 94–105.

95. J. C. Courtenay, C. Deneke, E. M. Lanzoni, C. A. Costa, Y. Bae, J. L. Scott, and R. I. Sharma, *Cellulose*, 2017, 1–16.

96. M. A. Johns, Y. Bae, F. E. G. Guimarães, E. M. Lanzoni, C. A. R. Costa, P. M. Murray, C. Deneke, F. Galembeck, J. L. Scott, and R. I. Sharma, *ACS Omega*, 2018, **3**, 937–945.

97. T. M. Filion, A. Kutikov, and J. Song, *Bioorganic Med. Chem. Lett.*, 2011, **21**, 5067–5070.

98. Z. Yang, J. Si, Z. Cui, J. Ye, X. Wang, Q. Wang, K. Peng, W. Chen, and S. C. Chen, *Carbohydr. Polym.*, 2017, **174**, 750–759.

99. J. Ye, J. Si, Z. Cui, Q. Wang, K. Peng, W. Chen, X. Peng, and S.-C. Chen, *Macromol. Mater. Eng.*, 2017, **302**, 1–9.

100. A. Qi, S. P. Hoo, J. Friend, L. Yeo, Z. Yue, and P. P. Y. Chan, *Adv. Healthc. Mater.*, 2014, **3**, 543–554.

101. A. Wali, Y. Zhang, P. Sengupta, Y. Higaki, A. Takahara, and M. V. Badiger, *Carbohydr. Polym.*, 2018, **181**, 175–182.

102. S. P. Hoo, Q. L. Loh, Z. Yue, J. Fu, T. T. Y. Tan, C. Choong, and P. P. Y. Chan, *J. Mater. Chem. B*, 2013, **1**, 3107.

103. T. Kageyama, T. Osaki, J. Enomoto, D. Myasnikova, T. Nittami, T. Hozumi, T. Ito, and J. Fukuda, *ACS Biomater. Sci. Eng.*, 2016, **2**, 1059–1066.

104. N. Ninan, M. Muthiah, I. K. Park, A. Elain, S. Thomas, and Y. Grohens, *Carbohydr. Polym.*, 2013, **98**, 877–885.

105. K. W. Kolewe, K. M. Dobosz, K. A. Rieger, C. C. Chang, T. Emrick, and J. D. Schiffman, *ACS Appl. Mater. Interfaces*, 2016, **8**, 27585–27593.

106. H. Ramphul, A. Bhaw-Luximon, and D. Jhurry, *Carbohydr. Polym.*, 2017, **178**, 238–250.

107. D. Han and P. I. Gouma, *Nanomedicine Nanotechnology, Biol. Med.*, 2006, **2**, 37–41.

108. M. Chau, K. J. De France, B. Kopera, V. R. Machado, S. Rosenfeldt, L. Reyes, K. J. W. Chan, S. Förster, E. D. Cranston, T. Hoare, and E. Kumacheva, *Chem. Mater.*, 2016, **28**, 3406–3415.

109. A. Kumar, K. M. Rao, and S. S. Han, *Chem. Eng. J.*, 2017, **317**, 119–131.

110. T. R. Stumpf, X. Yang, J. Zhang, and X. Cao, *Mater. Sci. Eng. C*, 2016, **82**, 372–383.

111. S. Saska, H. S. Barud, A. M. M. Gaspar, R. Marchetto, S. J. L. Ribeiro, and Y. Messaddeq, *Int. J. Biomater.*, 2011, **2011**, 1–8.

112. H. Orelma, I. Filpponen, L. S. Johansson, J. Laine, and O. J. Rojas, *Biomacromolecules*, 2011, **12**, 4311–4318.

113. K. Tomihata and Y. Ikada, *Biomaterials*, 1997, **18**, 567–575.

114. E. Entcheva, H. Bien, L. Yin, C.-Y. Chung, M. Farrell, and Y. Kostov, *Biomaterials*, 2004, **25**, 5753–62.

115. G. Laus, G. Bentivoglio, H. Schottenberger, V. Kahlenberg, H. Kopacha, T. Röder, and H. Sixta, *Lenzinger Berichte*, 2005, **84**, 71–85.

116. J. Coombs Obrien, L. Torrente-Murciano, D. Mattia, and J. L. Scott, *ACS Sustain. Chem. Eng.*, 2017, **5**, 5931–5939.

117. E. Gale, R. H. Wirawan, R. L. Silveira, C. S. Pereira, M. A. Johns, M. S. Skaf, and J. L. Scott, *ACS Sustain. Chem. Eng.*, 2016, **4**, 6200–6207.

118. E. M. Gale, M. A. Johns, R. H. Wirawan, and J. L. Scott, *Phys. Chem. Chem. Phys.*, 2017, **19**, 17805–17815.

119. M. A. Johns, A. Bernardes, E. R. De Azevêdo, F. E. G. Guimarães, J. P. Lowe, E. M. Gale, I. Polikarpov, J. L. Scott, and R. I. Sharma, *J. Mater. Chem. B*, 2017, **5**, 3879–3887.

120. H. Zou, Q. Luo, and D. Zhou, *J. Biochem. Biophys. Methods*, 2001, **49**, 199–240.

121. R. Pelton, *Trends Anal. Chem.*, 2009, **28**, 925–942.

122. J. L. Brash and P. Ten Hove, *J. Biomater. Sci. Polym. Ed.*, 1993, **4**, 591–599.

123. K. Watanabe, Y. Eto, S. Takano, S. Nakamori, H. Shibai, and S. Yamanaka, *Cytotechnology*, 1993, **13**, 107–114.

124. U. Hersel, C. Dahmen, and H. Kessler, *Biomaterials*, 2003, **24**, 4385–4415.

125. A. Perets, Y. Baruch, F. Weisbuch, G. Shoshany, G. Neufeld, and S. Cohen, *J. Biomed. Mater. Res.*, 2003, **65A**, 489–497.

126. C. Merle, S. Perret, T. Lacour, V. Jonval, S. Hudaverdian, R. Garrone, F. Ruggiero, and M. Theisen, *FEBS Lett.*, 2002, **515**, 114–118.

127. P. L. Granja, B. De Jéso, R. Bareille, F. Rouais, C. Baquey, and M. A. Barbosa, *React. Funct. Polym.*, 2006, **66**, 728–739.

128. F. Quero, M. Nogi, K. Y. Lee, G. Vanden Poel, A. Bismarck, A. Mantalaris, H. Yano, and S. J. Eichhorn, *ACS Appl. Mater. Interfaces*, 2011, **3**, 490–499.

129. N. Sanchavanakit, W. Sangrungraungroj, R. Kaomongkolgit, T. Banaprasert, P. Pavasant, and M. Phisalaphong, *Biotechnol. Prog.*, 2006, **22**, 1194–9.

130. M. Märtson, J. Viljanto, T. Hurme, P. Laippala, and P. Saukko, *Biomaterials*, 1999, **20**, 1989–1995.

131. W. H. Ashton and C. E. Moser, 1968.

132. J. D. Petty, J. N. Huckins, and A. David, 2007.

133. C. B. Linsky and T. J. Cunningham, US5002551A, 1985.

134. C. H. Broadnax Jr., US4626253A, 1984.

135. R. M. A. Domingues, M. E. Gomes, and R. L. Reis, *Biomacromolecules*, 2014, **15**, 2327–2346.

136. A. Sannino, S. Pappadà, M. Madaghiele, A. Maffezzoli, L. Ambrosio, and L. Nicolais, *Polymer (Guildf).*, 2005, **46**, 11206–11212.

137. N. Nakajima and Y. Ikada, *Bioconjug. Chem.*, 1995, **6**, 123–130.

138. L. H. H. Olde Damink, P. J. Dijkstra, M. J. A. Van Luyn, P. B. Van Wachem, P. Nieuwenhuis, and J. Feijen, *Biomaterials*, 1996, **17**, 765–773.

Chapter 2

2 Paper 2: Surface Modified Cellulose Scaffolds for Tissue Engineering

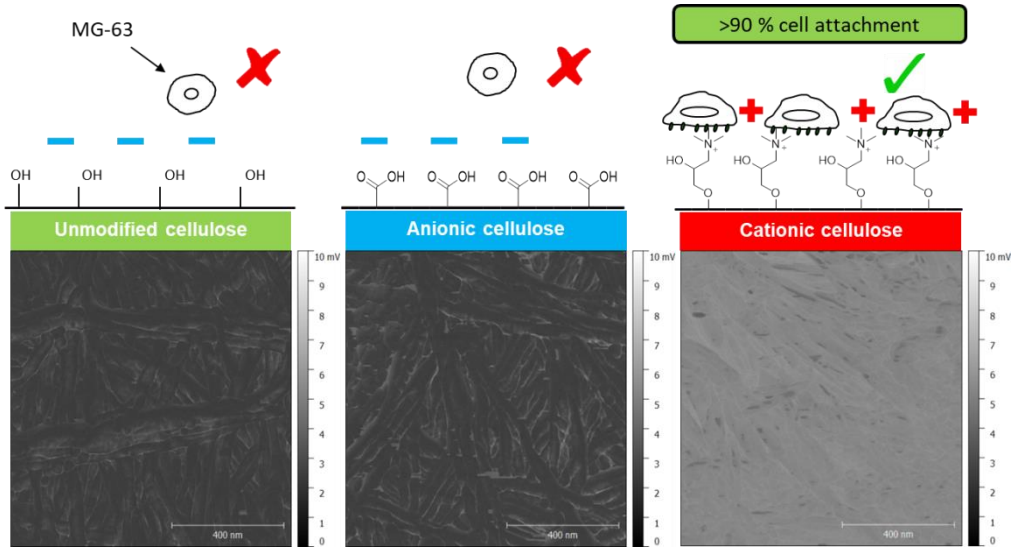

2.0 Publication Commentary

Despite being an economically viable, sustainable and biocompatible scaffold material, with many beneficial properties, cellulose has a major drawback that needs to be tackled to convert it into a suitable material for tissue culture. The surface of cellulose materials have inherently low non-specific protein absorption and lack the binding sites necessary for enabling mammalian cells to attach. This can be improved by coating scaffolds with serum such as foetal bovine serum (FBS) or matrix ligands such as the peptide Arg-Gly-Asp (RGD), fibronectin or collagen. However, these components can be costly, and in the case of FBS, can have ethical implications and increase risk of contamination due to its origin. The literature review, presented in the previous chapter, outlines a range of chemical and biochemical modifications that have been developed to facilitate cell attachment.

The membranes of mammalian cells comprise of a phospholipid bilayer which possesses an overall negative surface charge. Cellulose also bears a slightly negative surface charge which could also be a factor hindering initial cell attachment. It was hypothesised that introducing a positive surface charge to the cellulose scaffold would facilitate cellular attachment through electrostatic interactions, without the need for pre-treatment of the scaffolds with FBS.

In this paper we used MG-63 cells, which are a mammalian cancer osteosarcoma cell line, in all cell studies. The rational for using this cell line was its reliability, suitable doubling rate and robustness for cell culturing. Given that the aim of the research reported in this paper was to investigate cell-scaffold interaction, it would not have been appropriate to use a primary cell lines such as rat skeletal muscle cells (RSkMC), human vascular smooth muscle cells (VSMCs), mouse myoblast cells (C2C12) or stem cells, which are commonly used in cell studies for specific applications. These cells can be very delicate, require a cocktail of growth factors to culture and are prone to senescence if left to 100 % confluence.

Bacterial cellulose scaffolds were prepared by culturing *Acetobacter xylinum*, which produces cellulose of high purity, requiring minimal processing, as pellicles of cellulose are extruded by the bacteria to form flat membranes. These can be used directly as 2D scaffolds thus negating the need to dissolve cellulose, for example in ionic liquids, and to form films by casting and antisolvent regeneration. Although regeneration of cellulose solutions enables much finer control of the film

membranes obtained compared to bacterial cellulose, allowing tuning effectors such as thickness and cellulose content, it introduces added processing steps as the ionic liquids used for dissolution must be fully removed to avoid contamination of the scaffolds to the growing cells.

In this paper a preliminary study to test this hypothesis is reported. Scaffolds were to be chemically modified to introduce a surface charge and the modification investigated is the nucleophilic substitution of GTMAC onto primary OH groups to introduce a positive charge. This chemistry was chosen following indications that chitosan-cellulose composites supported cell attachment. Unlike chitosan, which bears a primary amine group and thus a positively charge ammonium group at pH below 6.3, the quaternary ammonium group has a permanent charge which is independent of pH. The TEMPO-mediated oxidation of the cellulose primary OH groups to a carboxylic acid was also investigated to allow testing of the hypothesis of charge induced attachment. The carboxylate groups on the oxidised cellulose will have a negative charge at the pH and thus potentially yield minimal cell attachment. One of the main aims of this paper was to develop a FBS free two-component (cell and scaffold) system for tissue engineering, thus cell growth media were prepared with and without FBS present, which was a novel undertaking, to determine whether charge alone is facilitating attachment. Furthermore, the absorption of RGD onto the charged scaffolds will be investigated as a means of further enhancing attachment.

In this chapter several methodologies for identifying and quantifying the presence of charged groups on the cellulose surface will be described and characterisation of how the modifications affect the scaffold properties and cellular response through attachment, adhesion and morphology studies assessed.

2.1 Statement of Authorship

<table>
<tr><th colspan="10">This declaration concerns the article entitled:</th></tr>
<tr><td colspan="10">Surface modified cellulose scaffolds for tissue engineering</td></tr>
<tr><td colspan="10">Publication status</td></tr>
<tr><td>Draft manuscript</td><td></td><td>Submitted</td><td></td><td>In review</td><td></td><td>Accepted</td><td></td><td>Published</td><td>✓</td></tr>
<tr><td>Publication details</td><td colspan="9">Courtenay, J. C., Johns, M. A., Galembeck, F., Deneke, C., Lanzoni, E. M., Costa, C. A., Scott, J. L., Sharma, R. I. (2017). Surface modified cellulose scaffolds for tissue engineering. Cellulose, 24(1), 253-267. DOI: 10.1007/s10570-016-1111-y</td></tr>
<tr><td>Candidate's contribution to the paper</td><td colspan="9">Formulation of ideas:
Initial ideas were discussed and planned by JLS, RIS and JCC. (JCC contribution 60%) The manuscript was prepared by JCC and reviewed by supervisors for feedback.

Design of methodology:
Experiments were planned by JCC and discussed with JLS and RIS. (JCC contribution 90%)

Experimental work:
Experimental work was conducted and analysed by the candidate (JCC contribution 90%)

Figure 4, 5 & 7; scanning probe microscopy measurements were carried out at the Brazilian Nanotechnology National Laboratory (LNNano) by RIS as part of our collaboration. The data from these studies were analysed by JCC and formed the basis for a future research visit by JCC to the laboratories at LNNano, to learn how to use the instruments and carry out further analysis, which contributed to another publication.

Presentation of data in journal format:
All figures were prepared by JCC (JCC contribution 100%)</td></tr>
<tr><td>Statement from candidate</td><td colspan="9">This paper reports on original research I conducted during the period of my Higher Degree by Research candidature</td></tr>
<tr><td>Signed</td><td colspan="6"></td><td>Date</td><td colspan="2"></td></tr>
</table>

2.2 Abstract

We report the ability of cellulose to support cells without the use of matrix ligands on the surface of the material, thus creating a two-component system for tissue engineering of cells and materials. Sheets of bacterial cellulose, grown from a culture medium containing *Acetobacter* organism were chemically modified with glycidyltrimethylammonium chloride or by oxidation with sodium hypochlorite in the presence of sodium bromide and 2,2,6,6-tetramethylpipiridine 1-oxyl (TEMPO) to introduce a positive, or negative, charge, respectively. This modification process did not degrade the mechanical properties of the bulk material, but grafting of a positively charged moiety to the cellulose surface (cationic cellulose) increased cell attachment by 70 % compared to unmodified cellulose, while negatively charged, oxidised cellulose films (anionic cellulose), showed low levels of cell attachment comparable to those seen for unmodified cellulose. Only a minimal level of cationic surface derivitisation (*ca* 3 % degree of substitution) was required for increased cell attachment and *no* mediating proteins were required. Cell adhesion studies exhibited the same trends as the attachment studies, while the mean cell area and aspect ratio was highest on the cationic surfaces. Overall, we demonstrated the utility of positively charged bacterial cellulose in tissue engineering in the absence of proteins for cell attachment.

2.3 Introduction

Damaged tissues and organs are a costly problem in healthcare, which, in some cases, cannot be addressed using traditional medical intervention.[1] Tissue engineering approaches to rectify damaged tissue and organs are proving to be a viable alternative to transplantation, prosthetics, and surgical intervention. These approaches entail culturing cells on scaffolds that are placed into the injury site.[2] The scaffold serves as a support for the cells and provides a 3D framework for the cells to proliferate, produce extracellular matrix and generate tissue.[3] . Scaffolds can be constructed from synthetic or natural biomaterials, but should be biocompatible, promote cell attachment and growth, and degrade over time.[4,5]

Scaffolds derived from synthetic polymeric materials may offer advantages over natural biomaterials, such as reproducibility; their well-defined chemical composition can allow for precise control over mechanical properties and degradation rates.[6] However, synthetic biomaterials suffer from a major disadvantage as they often lack sites for cell adhesion, therefore, many need to be modified to introduce the cell attachment cues, such as matrix ligands, for adhesion [7]. The addition of ligands or peptides may be achieved by passive adsorption (simplest method)[8], or more complex routes such as incorporation into the polymer backbone,[9] at the ends of the polymer chains,[10] or functionalised on the material surfaces [11]. In general, these approaches involve complex chemistries, or costly crosslinking reagents that are unstable after a short period of time, adding cost and complexity to production. Furthermore, some are poorly biocompatible and may cause inflammation or immune responses when implanted or upon degradation *in vivo* (the degradation products can also be deleterious).[12] Natural scaffolds are often biocompatible with the implant tissue [13,14], but the origin of the scaffold material can be lead to complications: many are from animal sources, which may offend some religious sensitivities and personal beliefs. In addition, concerns may arise pertaining to transmission of pathogens, such as including prions.

Common synthetic polymers used in tissue engineering include poly(lactic-co-glycolic acid), PLGA, and poly(ethylene glycol), PEG. PLGA is a biocompatible, polyester copolymer of lactic and glycolic acid, which degrades *in vivo*. Due to its tuneable mechanical properties, it has been used to prepare biodegradable scaffolds for a range of applications including: bone grafts;[15] to generate adipose tissue for

reconstructive surgery,[16] and spun into fibres for seeding cells.[17] However, when PLGA degrades *in vivo* the acidic metabolites can have a detrimental effect on the local pH of the extracellular matrix (ECM), which can cause inflammation and an immune response, or even cell and tissue necrosis.[12,18] Hydrogels prepared from PEG are able to resist protein adsorption due to the non-ionic hydrophilic nature of the polymer[19] and have been used to engineer a wide range of tissue from bone[20] and cartilage[21] to nerve tissue.[22] However, like PGLA, PEG scaffolds often need to be functionalised with matrix ligands or peptides to facilitate cell attachment.

In spite of the potential variability in composition of natural biomaterials, protein derived scaffold materials, such as collagen, fibrin and glycosaminoglycan[23] often possess the chemical structures that can mimic native tissue, thereby aiding biocompatibility.[5] For example, collagen type I (a key component of the ECM), can be reconstructed into a fibrillar matrix beneficial for cell attachment and has been formed into hydrogel sponges used for bone and tissue repair.[24] Decellularised tissue and organs have also been used in a variety of tissue engineering applications.[1,25] However, the risk of immunogenicity and disease transmission can remain after treatment. Cells are removed from donor tissue to prevent recognition by the host, avoiding an inflammatory response, or an immune-mediated rejection of the tissue.[26] The remaining tissue is a complete ECM, which can closely match the damaged tissue.[27] However, as the source of material is a deceased donor (for most organs), this is not a sustainable supply. Aging of donor tissue leading to biochemical and mechanical changes [28] and variation in properties with origin as well as alteration in the decellularisation process, may also render this scaffold type less useful.[26]

There is a need for a new biomaterial with suitable properties for tissue engineering, derived from a sustainable source, and which requires minimal processing to achieve cell viability for industrial application. Cellulose has the potential to fulfil these requirements, as it is: the most abundant biopolymer on earth, found in plant cell walls and produced by certain bacteria such as *Acetobacter*[29]; chemically homogeneous, being constructed from anhydroglucose units connected by β-1,4 glycosidic bonds[5]; biocompatible[30]; has tuneable tensile strength [31]; and can be readily functionalised as it bears three accessible OH groups per repeat unit, which are available for a vast range of modifications.[5,32–34]

Scaffolds prepared from cellulose have been considered previously for tissue engineering. However, as cellulose is a hydrophilic material with low non-specific protein adsorption (which is why mammalian cells do not readily adsorb to cellulose surfaces)[35–38], these scaffolds required the addition of a matrix ligands, to facilitate cell attachment to their surfaces.[39–42] In 1993 Watanabe *et al.* demonstrated by introducing an ionic charge to cellulose membranes collagen could be adsorbed to the membrane surface to promote cellular adhesion.[43]

Here we investigate whether the introduction of a surface charge on cellulose films, through simple chemical derivitisation, will increase cell attachment, without the use of matrix ligands. To introduce a positive charge the epoxide glycidyltrimethylammonium chloride (GTMAC) was grafted onto cellulose through the nucleophilic addition to the alkali-activated cellulose hydroxyl groups.[44] The radical 2,2,6,6-tetramethylpipiridine 1-oxyl (TEMPO) was used to mediate the oxidation of the primary alcohols to introduce a negative charge.[32] This methodology identified novel application of using surface modified cellulose films by derivitisation.

2.4 Experimental Procedures

2.4.1 Materials and methods

To produce bacterial cellulose the *Acetobacter* organism was sourced from Happy Kombucha (UK). Glucose, yeast extract, peptone, anhydrous disodium phosphate and citric acid monohydride were all purchased from Sigma-Aldrich (UK) and used as received.

For surface modifications, sodium hydroxide pellets (≥98 %), glycidyltrimethylammonium chloride (GTMAC) (≥90 %), 0.1 *M* $AgNO_3$ aqueous solution (≥95 %), 2,2,6,6-tetramethylpipiridine 1-oxyl radical (TEMPO) powder, NaBr powder, NaOCl 5.00 vol. % solution, HCl (reagent grade) were purchased from Sigma-Aldrich. Aqueous solutions of $AgNO_3$, NaOH and HCl were made up to the required concentrations with deionised (DI) water.

For cell investigations Dulbecco's Modified Eagle Medium (DMEM) (GlutaMAX™), non-essential amino acids (NEAA), sodium pyruvate (NaPyr), trypsin (0.05 %) and trypan blue (0.4 %) were purchased from Gibco® and stored at 4 °C. Foetal bovine serum (FBS) (non-USA origin), MG-63 cells, RGD-peptide and formaldehyde (37 % in 10-15 % methanol H_2O solution) were purchased from Sigma-Aldrich®. Phosphate buffer solution (PBS) was purchased from HyClone® (0.1 µm sterile filtered), 6-diamidino-2-phenylindole (DAPI), phalloidin-FITC and penicillin streptomycin (PenStrep) from Life Technologies. Norland optical adhesive 63 was purchased from Norland Products. All materials were used as received.

Polystyrene latex beads (0.3 µm) were purchased from Sigma-Aldrich and used as tracer particles for zeta-potential measurements.

2.4.2 Preparation of Bacterial cellulose films

Sheets of bacterial cellulose (30 cm x 50 cm) were produced under culture conditions following ref 45.[45] The cellulose sheets were sterilised (and bleached) by treatment for 2 h in 2 L of 5 % sodium hypochlorite in DI water, followed by thorough washing in 2 L aliquots of DI water. The cleaned sheets were stored in 2 L of 20 % methanol in DI water solution to prevent fungal growth. Cellulose sheets were cut into 5 cm^2 squares, placed on glass petri dishes and dried under vacuum at 50 °C for 24 h (yielding <2 % of the original wet mass). The remaining moisture

content was determined by thermogravimetric analysis and dried cellulose sheets were stored in sealed polyethylene bags.

2.4.3 Surface modification by derivitisation and oxidation

Cationic-cellulose: following the semi dry procedure described by Zaman et al. 2012. 5 wt. % NaOH (relative to corrected film mass) dissolved in 5 mL of DI water, was added to the cellulose films contained in polyethylene bags. Accurately weighed GTMAC (0.60-1.05 g) in molar ratios of 0.5 – 3.0, relative to anhydroglucose units (AGUs) of the weighed cellulose, was added drop wise and the sample kneaded to achieve homogenisation, prior to reaction at 65 ^{o}C (water bath) for 75 min. Modified cellulose films were washed thoroughly in DI water before being dried under vacuum at 50 ^{o}C for 24 h. These GTMAC modified films will be referred to as "cationic–cellulose" in this paper.

The degree of substitution was determined by conductometric titration of chloride ions (trimethylammonium chloride groups) with $AgNO_{3(aq)}$. Squares of film (2 x 2 cm, 10-50 mg) were accurately weighed and immersed in 20 mL of DI water for 5 min. Titrant (0.837 m*M* $AgNO_3$) was added in 0.50 mL aliquots and the conductivity was monitored using a SevenMulti Mettler Toledo conductivity probe. The degree of substitution is calculated using Eq. 1:

$$Degree\ of\ Substitution\ \% = \left[\frac{162.15\times(C\times V)}{w-(151.63\times C\times V)}\right]100 \qquad \textbf{(Eq. 1)}$$

Where C is the concentration of $AgNO_3$ solution (*M*), V is the volume of $AgNO_3$ solution (in dm^3), and w is the weight of the dried cationic cellulose sample (g), 162.15 is the M_w of the AGU and 151.63 is the difference in M_w between the AGU and cationised AGU with trimethylammonium chloride group. Triplicate samples were analysed for each material and an average reported.

Anionic-cellulose: TEMPO (0.016 g, 0.1 mmol) and NaBr (0.1 g, 1.0 mmol) was added to 200 mL DI water in an ice bath. Accurately weighed dry bacterial cellulose films (1-2 g) were submerged in the solution for 10 min. The pH of 5 vol. % NaOCl solution was adjusted to 10 with 0.1 *M* HCl and a quantity equivalent to 0.05 – 0.30 mole equivalents, relative to AGU, added drop wise to the film containing solution, under constant stirring, the pH was maintained at 10 by drop wise addition of 0.5 *M* NaOH $_{(aq)}$ when required. Ethanol (10 mL) was added to quench the reaction and the films

were washed thoroughly in DI water and dried. These modified films will be referred to as “anionic–cellulose” in this paper.

The carboxylate content of the anionic-cellulose films was determined by conductometric titration; 50 mg anionic cellulose samples (accurately weighed) were immersed in 15 mL of 10.00 m*M* HCl standard solution for 10 min. Titrant (10.00 m*M* NaOH) of was added in 0.50 mL aliquots and conductivity monitored using a SevenMulti Mettler Toledo conductivity probe. The degree of oxidation is calculated using Equation 2:

$$Degree\ of\ Oxidation\ \% = \left[\frac{162.15 \times C \times (V_2 - V_1)}{w - (35.97 \times C \times (V_2 - V_1))}\right] 100 \qquad \textbf{(Eq. 2)}$$

Where C is the concentration of NaOH solution (*M*), V is the volume of NaOH solution (in dm^3), w is the weight of the dried anionic cellulose sample (g), 162.15 is the M_w of the AGU and 35.97 is the difference in M_w of AGU and sodium salt of the glucoronic acid group (Zaman et al. 2012). Triplicate samples were analysed for each material and an average reported.

Characterisation: ^{1}H-^{13}C CP/MAS NMR was performed on unmodified, cationic (DS = 3.0 ±0.0 %) and anionic (DO = 7.6± 1.0 %) cellulose powders (freeze dried). Spectra were acquired at 25 ^{o}C, an MAS rate of 10 kHz and a contact time of 2000 µs. FTIR spectra for unmodified, cationic (DS = 3.0 ±0.0 %) and anionic (DO = 7.6± 1.0 %) cellulose powders were obtained on a Perkin Elmer Spectrum 100 with a universal ATR sampling accessory; 10 scans were acquired in the range 4000 – 600 cm^{-1}.

The presence of quaternary ammonium, or carboxylic acid, functional groups was confirmed by both FTIR and solid-state ^{13}C NMR measurements. FTIR: prominent bands at 1440 cm^{-3} and 1483 cm^{-3} were attributed to the CH_2 bending mode and methyl groups of the cationic cellulose substituents in accordance with data published by Zaman et al. 2012)^{13}C solid-state NMR: signals between 66 ppm and 105 ppm referred to the anhydroglucose, while a signal at 175 ppm appeared upon oxidation, due to the carboxylic acid group,[46] and a signal at 56 ppm due to the methyl groups on the quaternary ammonium was detected in the cationic cellulose sample[47] (Figure A.1 & 2, Appendix A).

2.4.4 Scaffold characterisation

Zeta potential measurements: The surface ζ-potentials of unmodified, cationic and anionic bacterial cellulose films were measured at 25 ^{o}C using a Malvern Zetasizer Surface ζ-Potential Cell. Films were cut into 4 x 4 mm squares, adhered to the sample plate and placed between the electrodes of the measurement cell. The position of the sample plate was aligned to the laser height. An aqueous suspension of 0.3 µm polystyrene latex tracer particles was prepared and 1.50 mL added to a 3 mL cuvette. The measurement cell was inserted into the cuvette ensuring no air bubble was trapped underneath the film. The application of an electric field via the electrodes initiated electrophoresis of the particles and electro-osmosis close to the surface.

The measured electrophoretic mobility of the tracer particles will vary as a function of distance from the sample surface. By plotting the reported mobility (ζ-potential) as a function of displacement from the surface, the relationship can be extrapolated back to the intercept (zero displacement). Therefore, the surface ζ-potential can be defined by Equation 3.

$$\zeta film\ surface = -intercept + \zeta particle \qquad \textbf{(Eq. 3)}$$

Triplicate samples were analysed for each material, the measurement repeated fifteen times per sample, and an average reported.

Scanning probe microscopy: Topography and capacitance gradient (dC/dz) images of unmodified, cationic and anionic cellulose films were obtained using a Park NX-10 Atomic Force Microscope (Gouveia et al. 2009; Ferreira et al. 2015). PPP-EFM probes (NanoWorld) with spring constant of 2.8 N m^{-1} and resonance frequency within 75 kHz were used for measurements. Topography and electrical images were acquired in air by single pass scanning at room temperature and humidity between 74.5-75.5 %. Topography was measured using intermittent contact mode setup, slightly below the frequency of resonance. Kelvin force and capacitance coupling measurements were conducted in parallel by applying an electric AC signal at 17 kHz to the metal-coated cantilever. The electric potential of the sample is deduced by the DC potential applied to the cantilever to nullify the AC signal at 17 kHz. Furthermore, the second harmonic of the AC signal (34 kHz), which is shown to be proportional to the capacitance gradient (dC/dz), or capacitance coupling, of the tip to the sample,

was monitored. Analysis and processing of the AFM images were carried out with Gwyddion (Necas et al. 2012). The capacitance coupling signal distribution was calculated using the 1D height analysis function of the programme.

Mechanical testing: The Young's modulus and tensile strength of the scaffolds were determined using an Instron 3343 electromechanical test machine. The samples used were unmodified, cationic (3.6±0.3 % degree of substitution) and anionic (6.7±0.6 % degree of oxidation) cellulose films. The films were cut into strips ≥1.50 cm in length by 0.30 or 0.50 cm width and the thickness recorded with a steel digital vernier micrometer calliper. The film strips were glued onto card mounts and the adhesive was allowed to set, which prevented damage to the films prior to characterisation. The mounts were gripped between the vices and a 1000 N cell was used to deliver strain to the films until deformation or failure. Five samples were tested for each film and an average reported.

2.4.5 Cell adhesion

Preparation of scaffolds: Films (unmodified or modified) were cut to a size that fit into a well plate and washed with DI water. The films were placed into a well plate (Costar®, Tissue culture-treated well plates, which were used as the control substrate throughout) and sterilised in a Hoefer UVC 500 cross linker for 15 min. After this time the films were turned over with sterilised tweezers and the sterilised side adhered to well plate with a single drop of Norland optical adhesive 63. The well plate and contents were resterilised (15 min irradiation), PBS (1 mL) was added to each well and the plate stored at 4 °C.

Under sterile conditions, the PBS was removed from the films and 300 µL of DMEM medium either alone or with pure FBS, or RGD solution (10 µL / mL), as appropriate was added to the wells and left to hydrate for 24 h at 4 °C prior to cell attachment studies.

Cell attachment: once the films had been hydrated with the relevant medium for 24 h, the medium was removed under sterile conditions and the scaffolds were seeded at a seeding density of 20,000 cells / cm^2 from a suspension of MG-63 cell culture of a known concentration. An empty well plate was seeded as a control. Growth medium (500 µL) was added to each well, which was then sealed and placed in a CO_2 incubator for 1 h. The samples were tested in triplicate.

Cell fixation and DAPI staining: the medium (and unattached cells) was aspirated from the cells and scaffolds and cells fixed: 2 x wash with 1 mL PBS; treatment with 1-2 mL of 3.7 % formalin (1 mL formaldehyde solution diluted to 9 mL with PBS) for 15 min at RT; followed by 2 x wash with 1 mL PBS; then stained under low light level conditions: 2 x wash with 1 mL PBS; 15 min staining with DAPI solution (300 µL of DAPI in PBS, 1 µL in 50 mL); 2 x wash with 1 mL PBS. A final 1 mL PBS was added to the scaffold, the plate wrapped in aluminium foil and stored at 4 °C.

Analysis of cell attachment: under low light levels, the films were removed from the well plate and placed cell side down on glass microscope slides for viewing with an EVOS optical microscope using blue light. Six independent images of the film surface were obtained using a 10x objective and cells counted using the "cell count" function in ImageJ, normalised to the area of field of view. The average count from the six images was used to determine the percentage cell attachment, using Eq. 4.

$$\%\ \text{cell attachment} = \frac{\text{No.of cells on scaffold}}{\text{Seeding density}} \times 100 \qquad \textbf{(Eq. 4)}$$

Cell Adhesion: Scaffolds were prepared as described for cell attachment experiments. After 1 h incubation the seeded scaffolds were centrifuged at 200 rpm (8 *g*) for 10 min, following which the cells were fixed and stained with DAPI. Attachment was determined as described above.

Cell Morphology: PBS was removed from hydrated films, which were seeded at 2,500 cells / cm^2 in serum free medium and incubated for 1 h. Following which the medium was removed and replaced with FBS containing medium (performed gently with a pipette, ensuring the attached cells were not disturbed during the process). Cells were fixed, permeabilised, and stained with 200 µL of dilute Phalloidin-FITC solution (100 µL in 10 mL PBS) for 40 min at RT, followed by washing with two 1 mL aliquots of PBS solution. A final 1 mL PBS was added to the scaffold, the plate wrapped in aluminium foil and stored at 4°C. Cells were visualised as above, with the exception that Phalloidin-FITC stains the polymeric F actin in the cell membranes, thus providing an image of the outline of the cell. The degree of cell spreading was inferred from measurement of area and aspect ratio. Six independent images of the film surface were taken at 10x objective and the average value reported.

Images were analysed using ImageJ following the method described by Fardin et al. 2010.[51] Projected cell area and aspect ratio were used in combination to quantify changes in cell morphology over 24 h.

2.4.6 Statistical analysis

Triplicate data were analysed using IBM SPSS Statistics Data Editor. A one-way analysis of variance (ANOVA) was used to determine whether there were any statistical differences between the means of two or more independent measurements, assuming equal variance. The differences were considered significant at the level of $p < 0.001$ (***), $p < 0.01$ (**) and $p < 0.05$(*).

2.5 Results

2.5.1 Surface modification and characterisation

Cellulose surfaces were rendered positively charged by nucleophilic substitution of alkali activated 1° alcohol groups with an epoxide bearing a quaternary ammonium group (GTMAC), or negatively charged by controlled oxidation using the well-studied TEMPO/NaOCl/NaBr system, (Scheme 2.1).

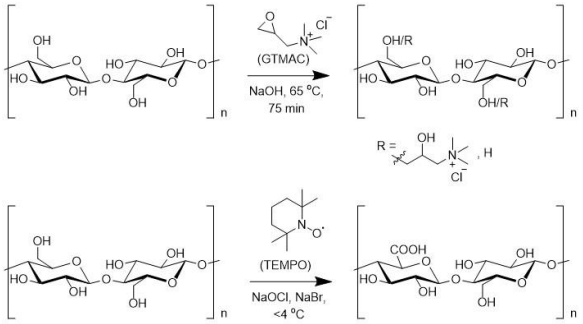

Scheme 2.1 Cationisation of cellulose films with GTMAC following activation of cellulose alcohol functionality by treatment with NaOH (top). Oxidation of C6 1° alcohol groups to C6 carboxylate groups pH 10-11 (bottom). In both cases the reaction is primarily with primary OH groups accessible on the film surface and the degree of substitution, or oxidation, is controlled by modulating the quantity of reagent (GTMAC) or oxidant (NaOCl) added.

The degree of surface modification was controlled by modulating the quantity of reagent (GTMAC), or oxidant (NaOCl), and the degree of substitution (DS), or oxidation (DO), of cellulose films assessed using conductometric titration (Figure A3). While, in both cases, the extent of introduction of charged groups increased with increased molar ratio of reagent, or oxidant, to AGU (Figure 2.1), it is clear that the oxidation reaction is significantly more efficient than the derivatisation. The former yielded oxidation levels between 3 and 4 % at an NaOCl:AGU ratio <0.1, while a ratio of 3:1 GTMAC:AGU was required to achieve a similar level of substitution.

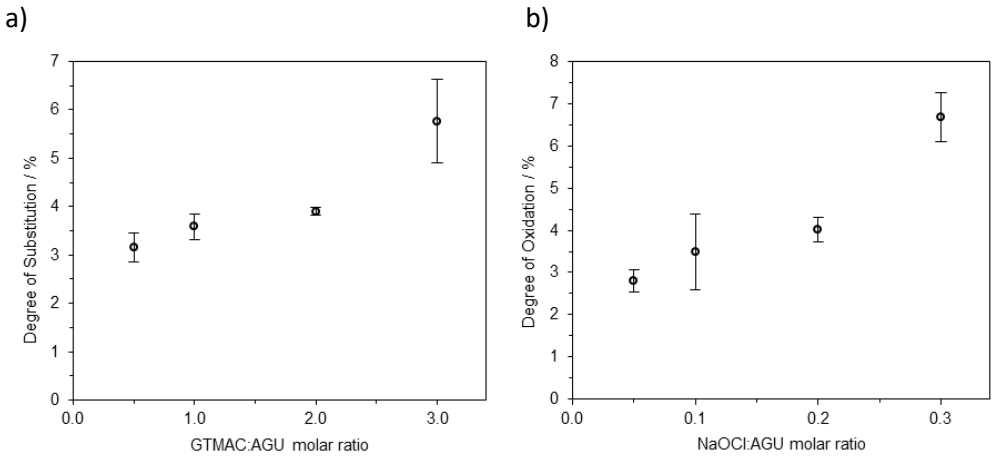

Figure 2.1 a) DS and b) DO per anhydrous glucose repeat unit for the modified bacterial cellulose films determined by conductometric titration. The average of three values was reported with the standard deviation shown as error bars.

GTMAC was successfully grafted onto the surface hydroxyl groups of α-cellulose producing cationic cellulose. The cellulose films were functionalised with a DS value between 3.2 – 5.8 % and a DO of 2.7 – 6.7 %. This showed that the degree of modification on the surface could be controlled.

2.5.2 Mechanical properties

Bulk mechanical properties of the unmodified and modified bacterial cellulose films were compared to discern if modification of surface chemistry was likely to compromise the integrity of the films. It is known that oxidation of fibrous cellulose leads to some loss of material (presumably by dissolution) and individualisation of fibrils, thus a film of relatively high DO was selected for comparison.[52]

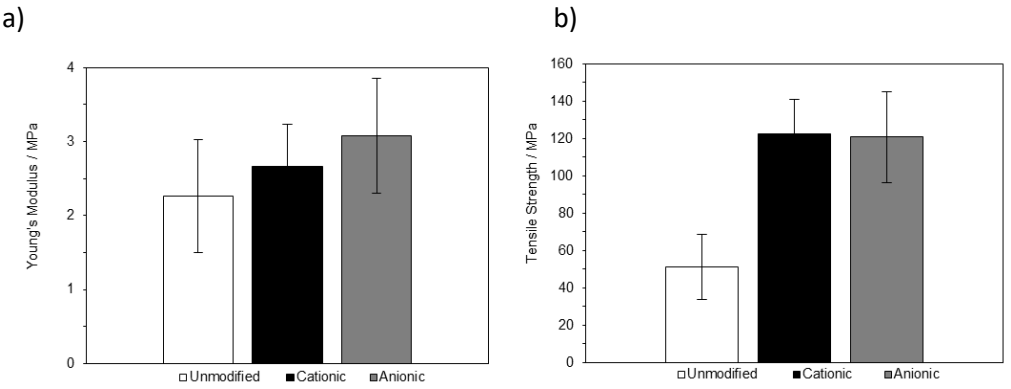

Figure 2.2 a) Young's modulus and b) tensile strength of unmodified, cationic (3.6 ±0.3 % DS) and anionic (6.7 ±0.6 % DO) cellulose films, n=5. The average of five values was reported with the standard deviation shown as error bars.

The Young's modulus for the unmodified cellulose films was 2 ± 0.8 MPa (comparable with previously reported value of 1.6 MPa [53]) and did not change significantly upon modification (Figure 2.2a). Tensile strength appeared to increase significantly upon modification (Figure 2.2b), providing confidence that, even at the highest DS and DO values tested, film strength was not compromised. It was postulated that the strengthening of the modified films was due to increased density of packed fibrils within the films, as the modified films exhibited thickness of only 60 – 80 % that of unmodified films, reflecting previous reports that films made from modified cellulose fibrils possess higher tensile strengths than native cellulose.[54]

2.5.3 Surface ζ-potential and capacitance

To discern the effect of modification on surface charge, the surface ζ-potential was measured for each of the modified films (Figure 2.3).

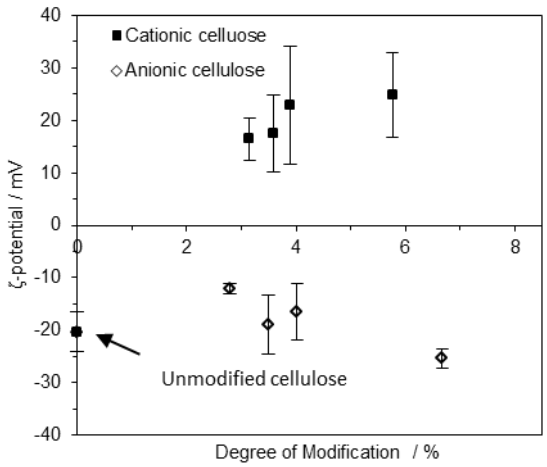

Figure 2.3 The ζ-potential measurements on modified cellulose films confirmed that the cationic surfaces were indeed positive and anionic negative, n=3. The average of three values was reported with the standard error shown as error bars.

The measured ζ-potential for unmodified cellulose films was -20 ±4 mV, indicating that, prior to alteration of surface chemistry, the cellulose films bear some surface functionality that imparts anionic character to the materials (in agreement with previous reports, where a value of -8 mV was reported [55]). When derivatised with GTMAC, the ζ-potential increased to 25 ±9 mV due to the introduction of the positively charged trimethylammonium groups. Oxidised cellulose exhibited a negative value, as expected, but this was not significantly different from underivatised cellulose.

To compare films, both with respect to surface charge and charge distribution (homogeneity), electric force microscopy was employed to characterise changes in capacitive coupling (proportionally to the mobility of charge) of the tip to the film surface, *dC/dz* (Figure 2.4). Clearly, unmodified and anionic cellulose surfaces exhibit similar capacitance coupling (mirroring the ζ-potential measurements), while the cationic material exhibits a significantly greater capacitive coupling, *dC/dz*, across the entire sample. This is reflected in Figure 2.5 showing distribution of capacitive coupling over a larger area: both unmodified and oxidised surfaces exhibit similar surface capacitance coupling values of 2.6 arbitrary units (AU), while that of the cationised surface is 5.9 AU.

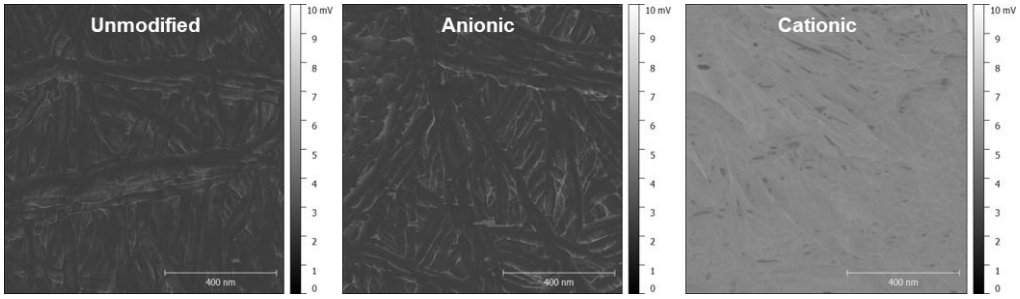

Figure 2.4 Capacitance gradient (*dC/dz*) images of unmodified, cationic and anionic cellulose films were obtained over a 1 µm^2 sample. The capacitance coupling of the tip to the sample was measured and determined by the capacitance of the probed sample volume. The scale is in mV as a signal is generated that is linearly proportional to *dC/dz*. The black/white scale indicates the magnitude of *dC/dz* signal of the sample, whereby black = 0 & white = 10 mV. The cationic cellulose surface is a lighter shade which reflects a higher capacitive coupling *dC/dz*.

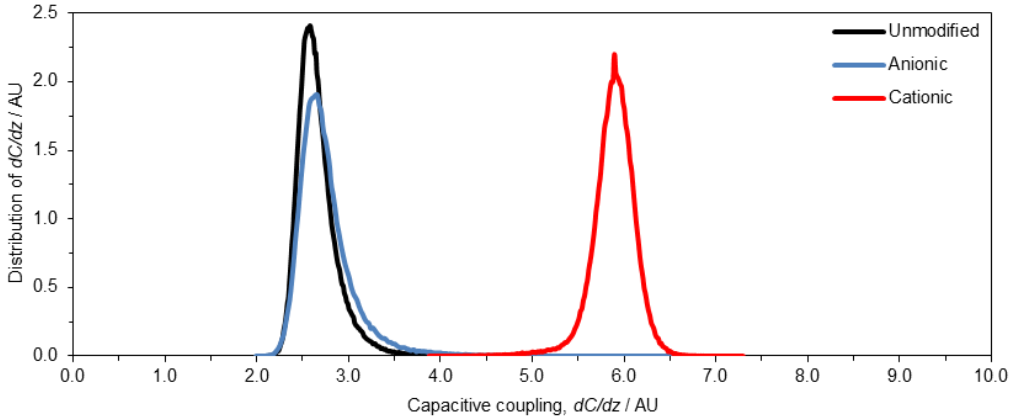

Figure 2.5 The capacitive coupling distribution between the tip and surface was generated by a 1D statistical analysis of images depicted in Figure 2.4, for the unmodified, anionic and cationic cellulose films. Capacitance coupling was measured across a 10 µm^2 sample surface area. The peak at 5.9 AU indicates that the cationic cellulose has a higher capacitive coupling, *dC/dz*.

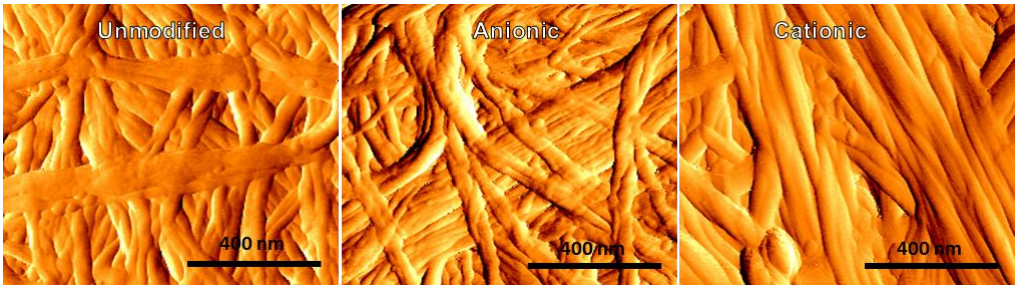

Figure 2.6 Tip amplitude image (error image) of the topography obtained of the surface over a 1 μm^2 sample for unmodified, anionic and cationic cellulose films. The fibril network does not appear to have been degraded by the surface modification. Scale bar is 400 nm in length.

The surface topography of the samples is reflected in the tip amplitude image of each film surface (Figure 2.6) and only very minor differences noted. Unmodified films show the typical overlapping fibrillar structure of bacterial cellulose and this is reflected in both modified films; there is no significant change in the fibril dimensions.

2.5.4 Cell attachment

Human osteoblast cancer cells, MG-63, were selected for their fibroblast phenotype and cell adhesion was tested in both the presence and absence of FBS and RGD to discern whether cell attachment could proceed without the need for added growth factors or matrix ligands. A two component scaffold system reduces the cost of processing scaffolds and mitigates the implications of using animal derived ligands. After one hour there was significantly greater cell attachment on the positively charged surfaces of cationic cellulose compared to the unmodified and anionic surfaces (Figure 2.7). This difference was clearest in the *absence* of any added proteins and this is the first instance that direct cell attachment has been reported for modified cellulose scaffolds without mediation of FBS or RGD.

In the absence of mediating proteins, FBS and RGD, cell attachment to anionic cellulose was negligible, but some adhesion was recovered when scaffolds were pre-incubated with FBS, suggesting that surface charge is not the only important factor and surface chemistry may play a role in cell adhesion. Remarkably, the degree of substitution did not appear to have a significant affect with similar levels of cell attachment detected for all cationic cellulose films, regardless of DS (Figure 2.8).

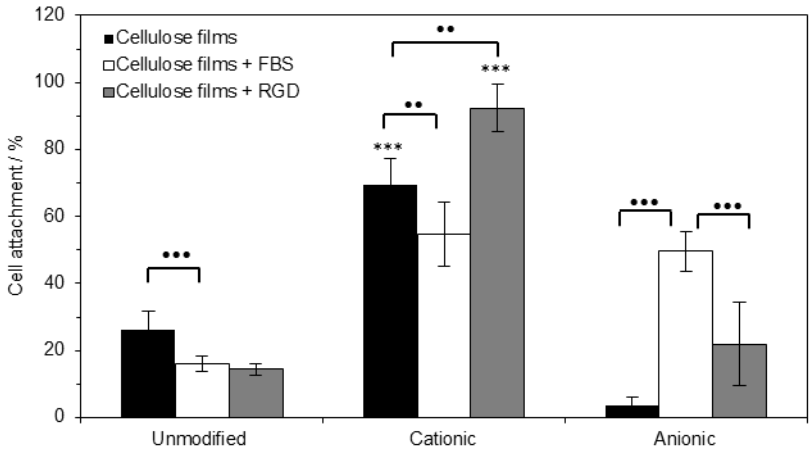

Figure 2.7 MG-63 cell attachment on cellulose films after 1 h incubation at 37 ^{o}C under 5 % CO_2, n=3 & error bars show standard error. Films were immersed for 24 h prior to seeding in DMEM medium alone or DMEM medium containing FBS or RGD as appropriate. Significant cell attachment on cationic cellulose films was achieved without the need for FBS or RGD growth factors. Values significantly different from unmodified cellulose films were indicated by the confidence values * $p < 0.05$, ** $p < 0.01$ and *** $p < 0.001$. To indicate significant differences between two values the symbol $^{\bullet}$ was used to refer to the p value.

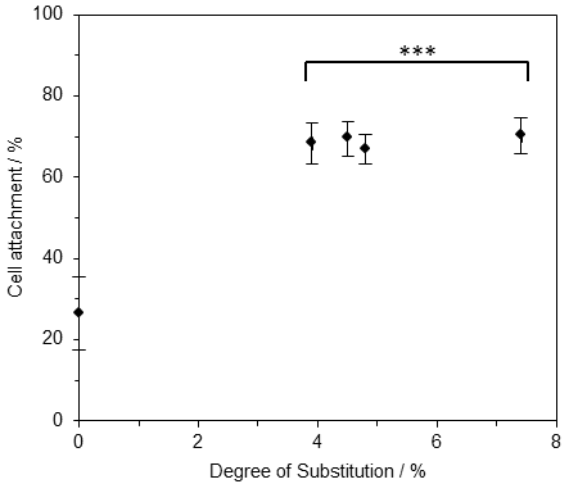

Figure 2.8 Influence of degree of substitution on MG-63 cell attachment on cationic cellulose films after 1 h incubation at 37 ^{o}C in 5 % CO_2, n=3 and error bars show standard error. Films were immersed for 24 h in DMEM medium, prior to seeding. Only a minimal level of modification with GTMAC was required for significant enhancement of cell attachment on cationic cellulose surface *versus* unmodified cellulose. Values significantly different from unmodified cellulose films were indicated by the confidence values * $p < 0.05$, ** $p < 0.01$ and *** $p < 0.001$.

Cell adhesion strength was assessed by counting the percentage of cells remaining after centrifugation with and without FBS in the media (Figure. 2.9).

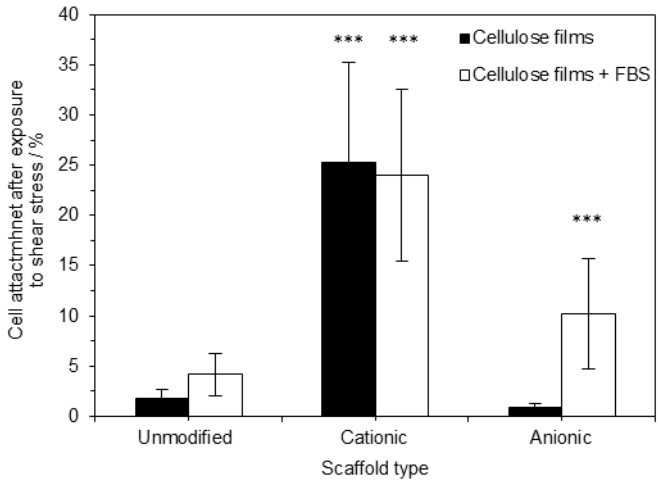

Figure 2.9 The percent of MG-63 cells attached on cellulose films after exposure to shear stress (centrifugation at 8 *g*), n=3 & error bars show standard error. Films were seeded in DMEM medium alone or DMEM medium containing FBS. Values significantly different from unmodified cellulose films were indicated by the confidence values * $p < 0.05$, ** $p < 0.01$ and *** $p < 0.001$.

To determine the cells response to the substrate, the degree of cell spreading and morphology was characterised by the change in projected cell area and aspect ratio after 24 h incubation, (Figure 2.10). An increase in cell aspect ratio, through elongation, and cell area was noted on cationic cellulose, but minimal spreading was observed on the native and anionic cellulose scaffolds.

a) Cell area

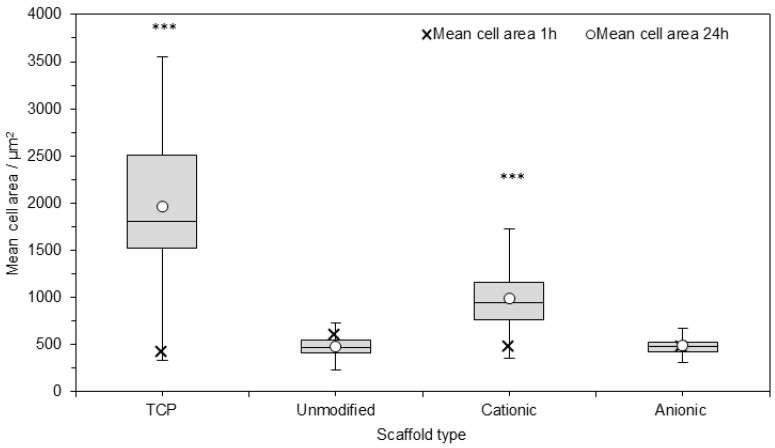

b) Cell aspect ratio

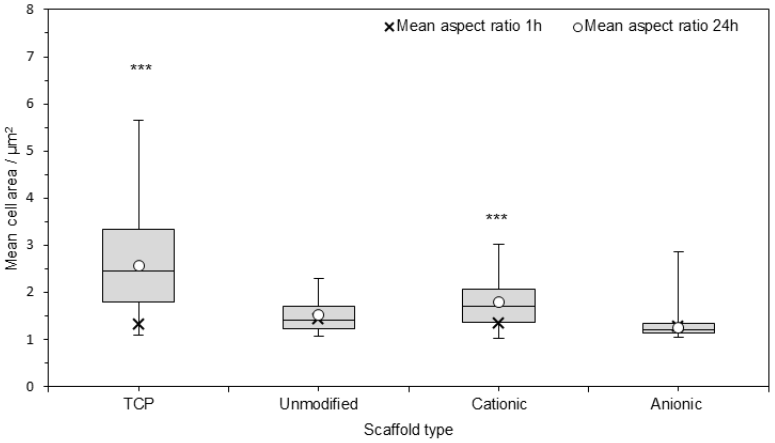

Figure 2.10 Change in MG-63 cell morphology; cell area and aspect ratio on cationic, anionic and unmodified bacterial cellulose scaffolds after 1 and 24 h incubation at 37 ^{o}C in 5 % CO_2, n = 17 - 53 cells measured and error bars show standard error. Cell images were analysed using ImageJ to calculate the average cell aspect ratio and area. The control was tissue culture plastic (TCP). Values significantly different from unmodified cellulose films were indicated by the confidence values * $p < 0.05$, ** $p < 0.01$ and *** $p < 0.001$.

2.6 Discussion

This is the first report of modulation of cell attachment on cellulose scaffolds induced by simple changes in surface chemistry of the cellulose scaffolds *without* mediation by added proteins. Cellulose in its natural form only permits minimal cell attachment, but when modified to have a positive charge, cell attachment increases to levels comparable to tissue culture plastic. Thus, we have established a minimally processed material for tissue engineering. The oxidation and derivatisation reactions employed are well known and thus easy to implement, offering opportunities to enhance, or indeed reduce, cell attachment simply by very minor alterations to (largely) the primary C6 hydroxyl groups exposed on the surface of cellulose scaffolds. Measurement of Young's modulus and tensile strength suggest that these chemical modifications do not compromise the mechanical strength, or integrity, of the cellulose scaffold material and analysis by electrostatic force microscopy reveals that alteration of surface charge is reasonably homogeneous across the surface and that no significant changes in fibrillar morphology result. Together, these results suggest that oxidation, or derivatisation with GTMAC, at the low levels used here, result in modification of surface, rather than bulk, chemistry of the materials. While demonstrated here for bacterial cellulose, the chemistry of cellulose (a linear homopolymer of glucose with β 1-4 glycosidic linkages) is invariable between cellulose sources and this methodology would be expected to be extendable to a wide range of cellulose scaffolds.

Importantly, measurement of cell attachment values indicates that pre-treatment of the scaffolds ligands, in this case FBS (a protein serum supplement), prior to cell seeding, was not necessary for cell attachment to occur on the cationic cellulose scaffolds. (While attachment did occur in the presence of FBS, the results were somewhat more variable and no significant *improvement* in attachment was noted.) In a three-component system (cell, biomolecule, materials), containing FBS, matrix ligands will be dominant in mediating cell attachment, as their presence facilitates integrin binding and focal adhesion formation. FBS contains a cocktail of growth factors and proteins that will adsorb both to cationic and anionic cellulose surfaces. The influence of RGD, a simple peptide often used to enhance cell attachment, was also minimal. There are few *direct* studies of the influence of surface charge on cell attachment in the absence of, or without pre-treatment with, matrix ligands.[56,57] Thus, for the first time, we demonstrate that simply modifying the surface charge of

a cellulose scaffold, by derivatisation using chemistry developed for the cloth dying industry, promotes attachment of cells (70 % increase over unmodified cellulose scaffolds). This is significant as it reduces the cost of processing and preparing scaffolds and the implications of using animal derived proteins or synthetic peptides. This methodology allows a move away from the traditional three component tissue engineering approach of scaffold / biomolecule attachment mediators / cells to a simpler, two component system of only the scaffold plus cells. As the chemical modification can be conducted immediately after scaffold fabrication, this provides longer shelf life and simplifies the process at point of use (tissue culture), facilitating scale-up and potentially reducing cost.

The proposed mechanism for cell attachment is suggested to be through ionic interactions between the quaternary ammonium functional groups on the surface and oppositely charged phosphate groups present in the phospholipid bilayer of the cell membrane.[58,59] The lack of cell attachment on the negatively charged anionic cellulose films supports the suggestion that ionic interactions between scaffold and phospholipid bilayer is an important factor in cell attachment. On cationic cellulose, cells appeared to be homogenously distributed across the surface with evidence of significant spreading, demonstrating cell viability on the films, while minimal spreading was observed on the unmodified and anionic cellulose films (reflecting attachment data). Furthermore, trends in cell attachment, after exposure to centrifugal force were the same as that observed in attachment studies: cells bound to cationic cellulose were least affected by centrifugation, whereas minimal cells remained attached on unmodified and anionic cellulose. In the case of anionic cellulose, the presence of FBS was required to retain even 20 % cell attachment.

The Young's modulus (E) defines the elongation stiffness of an elastic material and is the ratio of stress to strain. In tissue engineering it is important that the scaffold has a similar E to the surrounding tissue so that it can cope with mechanical wear and also to guide stem cell differentiation.[60] The value of $E \approx 2$ MPa measured for these cationic cellulose films suggests potential for application in scaffolds for soft tissues or non-weight bearing bone. [53]

2.7 Conclusion

Cationic bacterial cellulose films, prepared by grafting with GTMAC, showed significantly increased cell attachment and spreading compared to either unmodified, or oxidised (anionic), bacterial cellulose films. An increase of 70% cell attachment occurred even in the absence of any surface-presented proteins. The modification did not degrade the mechanical properties of the films and only a minimal degree of modification and processing was required to improve cell attachment, which is beneficial, reducing processing steps at the point of tissue culture and obviating the use of animal derived products such as FBS. This novel application of using cationically surface functionalised cellulose for tissue engineering provides a range of opportunities in the development of new scaffolds. While we have focussed on films, as 2D scaffolds, useful for rapid cell viability screening and, by extension for measuring cell kinetics, proliferation and morphology, the methodology would be readily applied to 3D scaffolds and will enhance the application of new technology for forming cellulose structures, e.g. by advanced 3D printing techniques.

2.8 Acknowledgments

Materials characterisation facilities were provided by Dr Sameer Rahatekar at the University of Bristol with the assistance of Sheril Rizal Vincent. Use of Park NX10 atomic force microscope was provided by LLNano Brazilian Nanotechnology National Laboratory. Dr Darrell Patterson, University of Bath, kindly provided access to a surface zeta potential cell. We thank Prof Yaroslav Khimyak at the University of East Anglia and Susana Ramalhete, University of East Anglia for solid-state ^{13}C NMR measurements. This research was partly supported by funding from the EPSRC Centre for Doctoral Training in Sustainable Chemical Technology (EP/G03768X/1 and EP/L016354/1), in the form of a PhD studentship for JCC, and research visits to Brazil were facilitated by a Global Innovation Initiative grant from the British Council and the UK Department for Business, Innovation and Skills, the University of Bath International Research Mobility Scheme and a University of Bath-FAPESP Exchange Scheme.

2.9 References

1. J. J. Song and H. C. Ott, *Trends Mol. Med.*, 2011, **17**, 424–432.

2. A. J. Salgado, J. M. Oliveira, A. Martins, F. G. Teixeira, N. A. Silva, N. M. Neves, N. Sousa, and R. L. Reis, *Int. Rev. Neurobiol.*, 2013, **108**, 1–33.

3. C. M. Agrawal, J. L. Ong, M. R. Appleford, and G. Mani, in *Introduction to Biomaterials - Basic Theory with Engineering Applications*, eds. M. W. Saltzman and S. Chien, Cambridge University Press, 2014, pp. 341–374.

4. S. J. Hollister, R. D. Maddox, and J. M. Taboas, *Biomaterials*, 2002, **23**, 4095–4103.

5. C. M. Agrawal, J. L. Ong, M. R. Appleford, and G. Mani, in *Introduction to Biomaterials - Basic Theory with Engineering Applications*, Cambrigde University Press, Cambridge, 2014, pp. 198–232.

6. M. Okamoto and B. John, *Prog. Polym. Sci.*, 2013, **38**, 1487–1503.

7. F. O'Brien, *Mater. Today*, 2011, **14**, 88–95.

8. S. M. Cutler and A. J. García, *Biomaterials*, 2003, **24**, 1759–1770.

9. R. H. Schmedlen, K. S. Masters, and J. L. West, *Biomaterials*, 2002, **23**, 4325–4332.

10. U. Hersel, C. Dahmen, and H. Kessler, *Biomaterials*, 2003, **24**, 4385–4415.

11. Y. Wan, X. Qu, J. Lu, C. Zhu, L. Wan, J. Yang, J. Bei, and S. Wang, *Biomaterials*, 2004, **25**, 4777–4783.

12. S. M. Willerth and S. E. Sakiyama-Elbert, *Combining stem cells and biomaterial scaffolds for constructing tissues and cell delivery*, Harvard Stem Cell Institute, Cambridge (MA), 2008.

13. A. Peloso, A. Dhal, J. P. Zambon, P. Li, G. Orlando, A. Atala, and S. Soker, *Stem Cell Res. Ther.*, 2015, **6**, 107.

14. G. M. Abouna, *Transplant. Proc.*, 2008, **40**, 34–38.

15. C. M. Agrawal, J. L. Ong, M. R. Appleford, and G. Mani, in *Introduction to Biomaterials - Basic Theory with Engineering Applications*, Cambridge University Press, Cambridge, 2014, pp. 134–164.

16. M. Neubauer, M. Haxker, P. Bauer-Kreisel, B. Weiser, C. Fischbach, M. Schulz, A. Goepferich, and T. Blunk, *Tissue Eng.*, 2005, **11**, 1840–1851.

17. Y. D. Teng, E. B. Lavik, X. Qu, K. I. Park, J. Ourednik, D. Zurakowski, and R. Langer, *Proc. Natl. Acad. Sci.*, 2002, **99**, 3024–3029.

18. H. Liu, E. B. Slamovich, and T. J. Webster, *Int. J. Nanomedicine*, 2006, **1**, 541–5.

19. K. Knop, R. Hoogenboom, D. Fischer, and U. S. Schubert, *Angew. Chemie - Int. Ed.*, 2010, **49**, 6288–6308.

20. Y. K. Luu, K. Kim, B. S. Hsiao, B. Chu, and M. Hadjiargyrou, *J. Control. release*, 2003, **89**, 341–353.

21. S. J. Bryant and K. S. Anseth, *J. Biomed. Mater. Res. A*, 2003, **64**, 70–79.

22. Z. Cai and J. Kim, *Cellulose*, 2010, **17**, 83–91.

23. J. Patterson, M. M. Martino, and J. A. Hubbell, *Mater. Today*, 2010, **13**, 14–22.

24. J. Glowacki and S. Mizuno, *Biopolymers*, 2008, **89**, 338–344.

25. M. T. Provencher, A. Mazzocca, and A. a. Romeo, *Tech. Orthop.*, 2007, **22**, 43–54.

26. T. W. Gilbert, T. L. Sellaro, and S. F. Badylak, *Biomaterials*, 2006, **27**, 3675–3683.

27. P. M. Crapo, T. W. Gilbert, and S. F. Badylak, *Biomaterials*, 2011, **32**, 3233–3243.

28. F. T. Blevins, A. T. Hecker, G. T. Bigler, A. L. Boland, and W. C. Hayes, *Am. J. Sports Med.*, 1991, **22**, 328–333.

29. S. Eyley and W. Thielemans, *Nanoscale*, 2014, **6**, 7764–7779.

30. D. Klemm, B. Heublein, H.-P. P. Fink, and A. Bohn, *Angew. Chemie - Int. Ed.*, 2005, **44**, 3358–3393.

31. K. Syverud, S. R. Pettersen, K. Draget, and G. Chinga-Carrasco, *Cellulose*, 2015, **22**, 473–481.

32. A. Isogai, T. Saito, and H. Fukuzumi, *Nanoscale*, 2011, **3**, 71–85.

33. B. L. Peng, N. Dhar, H. L. Liu, and K. C. Tam, *Can. J. Chem. Eng.*, 2011, **89**, 1191–1206.

34. Z. Ma and S. Ramakrishna, *J. Memb. Sci.*, 2008, **319**, 23–28.

35. C.-Y. Wu, S.-Y. Suen, S.-C. Chen, and J.-H. Tzeng, *J. Chromatogr. A*, 2003, **996**, 53–70.

36. H. Zou, Q. Luo, and D. Zhou, *J. Biochem. Biophys. Methods*, 2001, **49**, 199–240.

37. R. Pelton, *Trends Anal. Chem.*, 2009, **28**, 925–942.

38. J. L. Brash and P. Ten Hove, *J. Biomater. Sci. Polym. Ed.*, 1993, **4**, 591–599.

39. N. Singh, S. S. Rahatekar, K. K. K. Koziol, T. H. S. Ng, A. J. Patil, S. Mann, A. P. Hollander, and W. Ka, *Biomaterials*, 2013, **14**, 1287–1298.

40. D. J. Modulevsky, C. Lefebvre, K. Haase, Z. Al-Rekabi, and A. E. Pelling, *PLoS One*, 2014, **9**, e97835.

41. J. G. Torres-Rendon, T. Femmer, L. De Laporte, T. Tigges, K. Rahimi, F. Gremse, S. Zafarnia, W. Lederle, S. Ifuku, M. Wessling, J. G. Hardy, and A.

Walther, *Adv. Mater.*, 2015, **27**, 2989–2995.

42. E. Feldmann, M. M. Pleumeekers, L. Nimeskern, W. Kuo, W. C. De Jong, S. Schwarz, R. Müller, J. Hendriks, N. Rotter, G. J. V. M. Van Osch, K. S. Stok, and P. Gatenholm, *Biomaterials*, 2015, **44**, 122–133.

43. K. Watanabe, Y. Eto, S. Takano, S. Nakamori, H. Shibai, and S. Yamanaka, *Cytotechnology*, 1993, **13**, 107–114.

44. M. Zaman, H. Xiao, F. Chibante, and Y. Ni, *Carbohydr. Polym.*, 2012, **89**, 163–70.

45. A. Dufresne, *Nanocellulose: from nature to high performance tailored materials*, Walter de Gruyter, 2012.

46. T. Saito, I. Shibata, A. Isogai, N. Suguri, and N. Sumikawa, *Carbohydr. Polym.*, 2005, **61**, 414–419.

47. A. Chaker and S. Boufi, *Carbohydr. Polym.*, 2015, **131**, 224–232.

48. R. F. Gouveia and F. Galembeck, *J. Am. Chem. Soc.*, 2009, **131**, 11381–11386.

49. E. S. Ferreira, E. M. Lanzoni, C. A. R. Costa, C. Deneke, J. S. Bernardes, and F. Galembeck, *ACS Appl. Mater. Interfaces*, 2015, **7**, 18750–18758.

50. D. Necas and P. Klapetek, *Cent. Eur. J. Physic*, 2012, **10**, 18–188.

51. M. A. Fardin, O. M. Rossier, P. Rangamani, P. D. Avigan, N. C. Gauthier, W. Vonngut, M. A., J. Hone, R. Iyengar, and M. P. Sheetz, *Soft Matter*, 2010, **6**, 4788–4799.

52. Y. Jin, K. J. Edler, F. Marken, and J. L. Scott, *Green Chem.*, 2014, **16**, 3322.

53. M. Zaborowska, A. Bodin, H. Bäckdahl, J. Popp, A. Goldstein, and P. Gatenholm, *Acta Biomater.*, 2010, **6**, 2540–2547.

54. R. Tanaka, T. Saito, T. Hänninen, Y. Ono, M. Hakalahti, T. Tammelin, and A. Isogai, *Biomacromolecules*, 2016, **17**, 2104–2111.

55. K. Lee, F. Quero, J. J. Blacker, C. A. S. Hill, S. J. Eichhorn, and A. Bismark, *Cellulose*, 2011, **18**, 595–605.

56. M. Hamdan, L. Blanco, A. Khraisat, and I. F. Tresguerres, *Clin. Implant Dent. Relat. Res.*, 2006, **8**, 32–38.

57. C. Fotia, G. M. L. Messina, G. Marletta, N. Baldini, and G. Ciapetti, *Eur. Cells Mater.*, 2013, **26**, 133–149.

58. L. Li, X. Shi, X. Guo, H. Li, and C. Xu, *Trends Biochem. Sci.*, 2014, **39**, 130–140.

59. F. Schweizer, *Eur. J. Pharmacol.*, 2009, **625**, 190–194.

60. A. J. Engler, S. Sen, H. L. Sweeney, and D. E. Discher, *Cell*, 2006, **126**, 677–689.

Chapter 3

3 Paper 3: Modulating cell response on cellulose surfaces; tunable attachment and scaffold mechanics

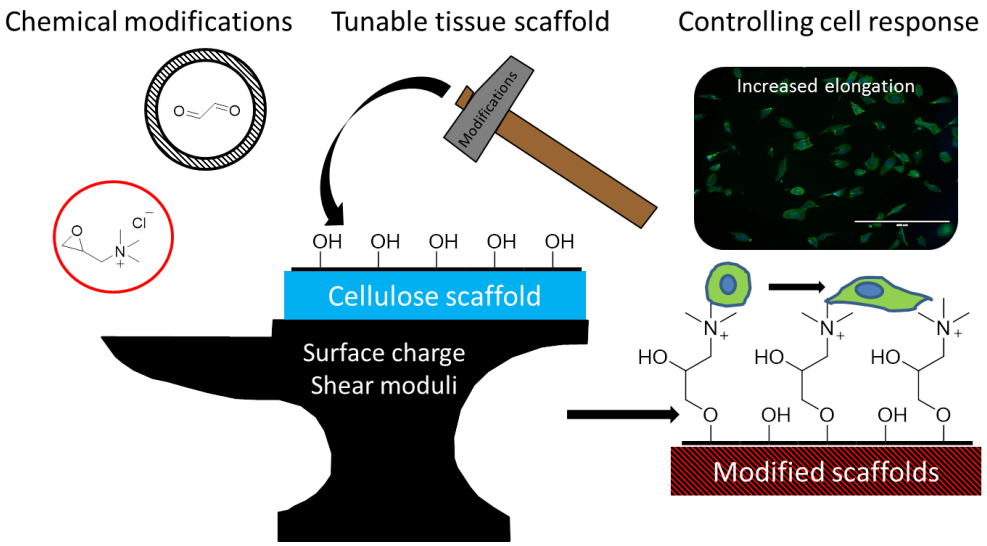

3.0 Publication Commentary

In the previous chapter it was demonstrated that cationic modification of cellulose with GTMAC introduced a positive surface charge, thus facilitating cell attachment even in the absence of FBS. In this next chapter scaffold properties are more deeply probed providing insight about how these can be tuned through further chemical modifications.

The main focus of this chapter is to combine cationisation (for cell attachment) with glyoxalisation to modulate scaffold stiffness. The mechanical properties the cells experience can influence behaviour, such as cell proliferation, by up-regulating the cell cycle. The crosslinker glyoxal was used to increase the scaffold stiffness, as it forms acetal and hemiacetal groups between the OH groups on the cellulose. The effect of modifications on both surface and bulk properties were investigated using a combination of atomic and electric force microscopy techniques, along with mechanical testing of the scaffolds. It was considered important to determine the extent these modifications change the scaffold properties and whether these can be used to further regulate cell behaviour. Potential applications of this investigation are to provide a method to produce scaffolds with the same mechanical properties as the desired tissue, such as stiff bone-like substances or softer muscle-like tissue. Furthermore it could unlock a way to direct the differentiation of stem cells through scaffold microenvironment cues, rather that biochemical cues.

A challenge that presented itself in the previous paper was the visualisation of stained cells on the bacterial cellulose membranes using a transmitted light microscope. This proved difficult for two reasons: i) the membranes were translucent but not transparent, which reduced the amount of light that could pass through the scaffold and ii) cellulose auto-fluoresces at the specific wavelengths needed to visualise the stains, thus making it hard to distinguish the cell outline from background. The membranes used in this paper were derived from cellulose dialysis tubing which has same chemical structure to bacterial cellulose (indeed all cellulose materials have the same chemical structure, but different bulk physical structures) but is much thinner (<100 μm), transparent and very uniform, thus allowing much clearer fluorescent images to be obtained. Also, homogeneity of the films meant that changes in scaffold properties could be attributed to the modification and not to variations in film thickness, for example.

Interestingly, the surface charge of the dialysis tubing was much more negative than anticipated particularly in comparison with bacterial cellulose. Initial studies were first conducted using the scanning probe microscope at LNnano in Brazil, to measure the surface capacitance coupling, dC/dz. These values for unmodified cellulose were very similar to that of cationic cellulose with a high DS. This surface charge arises from the production method for cellulose dialysis tubing, which is either regenerated cellulose acetate or via a xanathate method. When compared with zeta potential data it was apparent that dC/dz represents the extent of surface charge, *i.e.* |z|, but not whether it is positive or negative and when combined with zeta potential data, reveals how increasing the number of quaternary ammonium groups gradually makes the surface positively charged.

One of the important aims in this work was to determine the lowest degree of substitution required to facilitate cell adhesion in FBS free systems. When producing larger quantities of cationic cellulose it is beneficial to use the minimum amount of GTMAC required from an economical and waste reduction point of view. This also reduces the potential for compromising mechanical properties, given that cationisation enhances fibrillar dispersion.

3.1 Statement of Authorship

<table>
<tr><th colspan="10">This declaration concerns the article entitled:</th></tr>
<tr><td colspan="10">Modulating cell response on cellulose surfaces; tunable attachment and scaffold mechanics</td></tr>
<tr><td colspan="10">Publication status (tick one)</td></tr>
<tr><td>Draft manuscript</td><td></td><td>Submitted</td><td></td><td>In review</td><td></td><td>Accepted</td><td></td><td>Published</td><td>✓</td></tr>
<tr><td>Publication details</td><td colspan="9">Courtenay, J. C., Deneke, C., Lanzoni, E. M., Costa, C. A., Bae, Y., Scott, J. L., & Sharma, R. I. (2018). Modulating cell response on cellulose surfaces; tunable attachment and scaffold mechanics. Cellulose, 25, 925-940. DOI: 10.1007/s10570-017-1612-3</td></tr>
<tr><td>Candidate's contribution to the paper</td><td colspan="9">Formulation of ideas:
Ideas were discussed and planned with supervisor and collaborators. (JCC contribution 70%) The manuscript draft prepared by JCC with input from supervisors during the editing stage.

Design of methodology:
Experiments were discussed and planned with JLS and RIS (JCC contribution 90%)

Experimental work:
The experimental work was conducted and analysed by JCC. Technical support for EFM studies was provided by instrument scientists at LNnano. (JCC contribution 90%)

Figure 4.a; atomic force microscopy measurements were conducted at Penn State University by our collaborator YB. This analysis enabled surface mechanics to be probed. This collaboration developed into a two month research internship for JCC at State University of New York, (SUNY) at Buffalo to work in YB research group using their AFM instrument and carry out molecular cell biology studies on JCC scaffold materials.

Presentation of data in journal format:
All figures were prepared by JCC. (JCC contribution 100%))</td></tr>
<tr><td>Statement from candidate</td><td colspan="9">This paper reports on original research I conducted during the period of my Higher Degree by Research candidature</td></tr>
<tr><td>Signed</td><td colspan="6"></td><td>Date</td><td colspan="2"></td></tr>
</table>

3.2 Abstract

Combining surface chemical modification of cellulose to introduce positively charged trimethylammonium groups by reaction with glycidyltrimethylammonium chloride (GTMAC) allowed for direct attachment of mammalian MG-63 cells, without addition of protein modifiers, or ligands. Very small increases in the surface charge resulted in significant increases in cell attachment: at a degree of substitution (DS) of only 1.4%, MG-63 cell attachment was > 90% compared to tissue culture plastic, whereas minimal attachment occurred on unmodified cellulose. Cell attachment plateaued above DS of ca. 1.85% reflecting a similar trend in surface charge, as determined from ζ-potential measurements and capacitance coupling (electric force microscopy). Cellulose film stiffness was modulated by cross linking with glyoxal (0.3–2.6% degree of crosslinking) to produce a range of materials with surface shear moduli from 76 to 448 kPa (measured using atomic force microscopy). Cell morphology on these materials could be regulated by tuning the stiffness of the scaffolds. Thus, we report tailored functionalised biomaterials based on cationic cellulose that can be tuned through surface reaction and glyoxal crosslinking, to influence the attachment and morphology of cells. These scaffolds are the first steps towards materials designed to support cells and to regulate cell morphology on implanted biomaterials using only scaffold and cells, i.e. without added adhesion promoters.

3.3 Introduction

The development of functional substitutes for damaged tissue and organs is an aim of tissue engineering.[1] This approach involves isolating healthy cells from the patient and expanding them in vitro, to increase their numbers.[2] Traditionally, the cultured cells are seeded onto a ligand-functionalised scaffold, with the ligands facilitating cell attachment.[3] Scaffolds provide a 3D support, often mimicking the natural extracellular matrix (ECM) of the cell, thus influencing cell behaviour and encouraging cell proliferation, differentiation and migration.[4] The ECM is a structural support network that provides the 'glue' to bind cells together in tissue and consists of diverse proteins, sugars and other components.

Whether scaffolds are constructed from synthetic, or natural, biomaterials, they should be biocompatible, promote cell attachment and specialised cell functions, and, if to be implanted, be bioresorbable.[5,6] Furthermore, a key challenge of tissue engineering is to design scaffolds that direct cells to attach or perform their phenotypic functions, which promotes tissue functionality. Cellular responses to the substratum (attachment, proliferation and differentiation) are influenced by many factors including: surface charge,[7–9] surface roughness,[10–12] topology,[13,14] the presence of matrix proteins,[15–17] and porosity,[18–20] as well as the mechanical properties of the scaffold, such as Young's modulus.[21–23]

Cell affinity to a biomaterial is governed by cell/matrix interactions, which result from specific recognition among cell surface adhesion receptors, *i.e.* integrins, and extracellular matrix (ECM) proteins (*e.g.* fibronectin, vitronectin, and collagen) that have a cell-binding domain containing the Arg-Gly-Asp (RGD), or similar, sequence.[24] A traditional technique used to improve and regulate the degree of cell attachment to a synthetic scaffold, lacking such binding sites, is to coat with cell adhesive proteins, such as collagen and fibronectin.[25–27] However, this method of modification has potential disadvantages, such as control over isolation and purification - components of the modifying medium may elicit an inflammatory response and the proteins degrade over time.[17] Synthetic peptides have been developed to replace cell-binding proteins and the most commonly used peptide is RGD, which promotes integrin-cell adhesion on synthetic surfaces.[17] This can be a very effective way to facilitate cell attachment to synthetic surfaces; however, stable linking of RGD peptides to the surface is essential. In addition to proteins/peptides on surfaces, the

mechanical properties of the scaffold surface govern cell-scaffold interactions. Thus, while the properties of the bulk scaffold material define the mechanical integrity of the scaffold, the mechanical properties of the material surface, to a depth of less than 1 nm, influence cell response.[28] Surface modifications of the biomaterial allow tailoring of surface properties without impact on bulk material properties. Thus, through surface modification, the native surfaces of biomaterials can be physically, or chemically, transformed with the primary goal of engineering desired surface chemistry,[29] topology,[30] reactivity,[31] biocompatibility,[32] hydrophilicity,[24] and/or charge.[7]

Cell function on the scaffold can be directly influenced by: cell and ECM interactions modulated via transmembrane receptors,[33] soluble growth factors,[34] and the mechanical properties of the biomaterial.[35] At the cellular level, once attached to the scaffold cells probe its elasticity as they anchor and pull on their surroundings, receiving mechanical feedback from the ECM or substrate.[36] This process is known by the term mechanotransduction and is one of the mechanism by which cells convert bio-mechanical stimuli from the scaffolds to chemical cues which direct cell responses.[37] Thus, when constructing a scaffold for tissue engineering, the mechanical properties of the biomaterial are critical in regulating and guiding cell response. This has important implications in clinical application, for example, directing the differentiation of mesenchymal stem cell (MSCs) to generate specific tissue using scaffolds with elasticity matching that of the desired tissue type.[38]

Cellulose has previously been investigated as a potential scaffold material for tissue engineering as it is biocompatible and has tunable chemical and mechanical properties.[39–42] Furthermore, cellulose nanocrystals have been incorporated into a range of composite materials as reinforcements to produce hybrid scaffolds with stiffer mechanical properties.[43–45] While native cellulose requires the presence of matrix ligands to facilitate cell attachment due to the lack of integrin binding sites on the substrate,[46–48] chemical modification may be employed to alter surface chemistry, allowing cell attachment.[7] Scaffolds produced from cellulose can range from hard composites blended with hydroxyapatite,[49] to soft hydrogels,[50] as well as variably cross-linked materials: oxidised cellulose crosslinked with diamines,[51] or other crosslinking such as glyoxal, glutaraldehyde or diisocyanates.[52,53] It is hypothesised that changing the elastic modulus of cellulose scaffolds can influence

how cells respond and spread on the surface through mechanotransduction. This can be achieved through chemical crosslinking to increase the elastic modulus.[51]

Herein we describe the modulation and regulation of cellular responses through a dual approach of tuning both the chemical and mechanical properties of the scaffolds. Previously, we have demonstrated that surface modification, to introduce a positive surface charge to cellulose (Scheme 3.1), allows cell attachment in the *absence* of matrix ligands.[7] Here we demonstrate the minimal level of surface modification required and combine this with modulation of the mechanical properties of the scaffold material, achieved by cross-linking with glyoxal,[54] which results in formation of acetal and hemeacetal linkages upon curing (Scheme 3.2),[55] yielding films with increased elastic moduli depending on degree of cross-linking.[52]

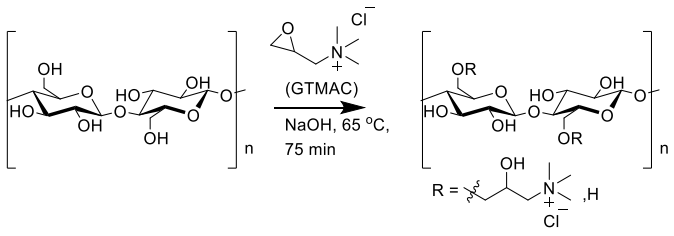

Scheme 3.1 Surface derivatisation of cellulose films *via* the cationisation of primary OH groups accessible on the film surface by GTMAC. Cationisation results in a positive surface charge on the films.

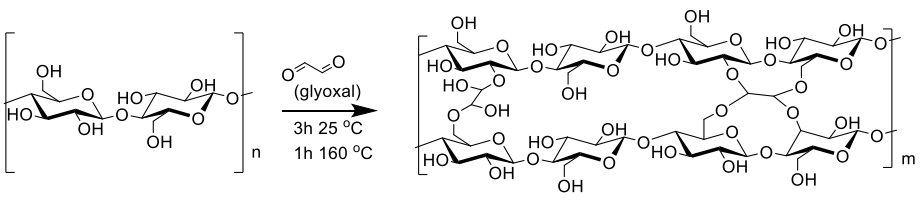

Scheme 3.2 Structural modification of cellulose films through acetal, or hemiacetal, linkages formed by reaction of glyoxal with the hydroxyl groups of the cellulose, leading to increased film stiffness.

Scaffold surfaces are probed using capacitance coupling and ζ-potential measurements to provide a sound basis for the proposed mechanism of enhanced cell attachment through complementary ionic interactions. Furthermore, changes in elastic modulus upon cross-linking are characterized for both the bulk material and the scaffold surface and the effect of the latter on cell morphology ascertained. Key surface and structural properties: surface charge and *surface* shear modulus are demonstrated to modulate cell attachment and cell spreading respectively, thus, enhancing understanding of the influence of scaffold surface properties on cell responses.

3.4 Experimental Procedures

3.4.1 Materials and methods

Cellulose dialysis tubing (regenerated cellulose, MWCO 12400 Da) from Sigma Aldrich was used a scaffold substrate for cell studies. For surface modifications, sodium hydroxide pellets (≥98 %), glycidyltrimethylammonium chloride (GTMAC) (≥90 %), 0.1 M $AgNO_3$ aqueous solution (≥95 %), indigo carmine powder (≥98 %), and 5(6)-carboxyfluorescein (≥95 %) were purchased from Sigma-Aldrich and used as received. For crosslinking modifications, glyoxal 40 % w/w aqueous solution was purchased from Alfa Aesar and made up to required concentrations with deionised (DI) water. Aqueous solutions of $AgNO_3$, NaOH and HCl, purchased from Sigma-Aldrich, were made up to the required concentrations with deionised (DI) water. Polystyrene latex beads (0.3 μm) were purchased from Sigma-Aldrich for use as tracer particles in ζ-potential measurements.

For cell studies Dulbecco's Modified Eagle Medium (DMEM, GlutaMAX™), non-essential amino acids, sodium pyruvate, trypsin (0.05 %) and trypan blue (0.4 %) were purchased from Gibco and stored at 4 °C. Foetal bovine serum (FBS, non-USA origin), MG-63 cells, Pluronic F127 and formaldehyde (37 % in 10-15 % methanol in H_2O solution) were purchased from Sigma-Aldrich. Phosphate buffer solution (PBS, 0.1 μm sterile filtered) was purchased from HyClone, and 6-diamidino-2-phenylindole (DAPI), phalloidin-FITC and penicillin streptomycin from Life Technologies. Norland optical adhesive 63 was purchased from Norland Products. All materials were used as received.

3.4.2 Surface modification by derivitisation

Following the semi dry procedure described for modification of cellulose powder by Zaman et al.,[56] cellulose films were cationically modified with GTMAC. These GTMAC modified films are referred to as "cationic–cellulose".

Fourier Transform Infrared spectroscopy (FTIR), Perkin Elmer Spectrum 100 FTIR spectrometer, was used to confirm the presence of quaternary ammonium functional groups on cationic cellulose films, FTIR measurements were previously substantiated by ^{1}H-^{13}C cross polarization / magic angle spinning NMR spectroscopy[7] (Figure B.1 – B.2, Appendix B). The degree of substitution (DS) was determined by

conductometric titration (Figure B.3) against $AgNO_3$(aq) solutions, conducted in triplicate.

3.4.3 Structural modification by crosslinking

Cellulose dialysis membrane films, ~1 g, were washed thoroughly in DI water and soaked in 50 mL glyoxal solution (0.5, 1, 3, 6, or 12 wt. % as required) for 3 h. The still-wet films were heated at 160 °C for 1 h and washed with copious quantities of DI water. Following this reaction, the films were cationised using the same method as previously reported[7] with a GTMAC:anhydroglucose unit (AGU) ratio of 2:1 and the resultant degree of substitution determined as above.

The degree of crosslinking (DXL) was determined by HPLC analysis following a method adapted from Schramm et al.[55] Briefly, dry crosslinked cellulose films (0.2 – 0.4 g), accurately weighed, in 20 mL 4 M NaOH were heated at 100 °C for 15 min to hydrolyse crosslinks, generating glycolic acid. The resultant solutions were filtered (PTFE, 0.45 µm disposable filter) and the concentration of glycolic acid in each solution was determined by HPLC analysis: aminex organic acid analysis column (HPX-87H, 300 mm × 7.8 mm, 50 °C), mobile phase 0.01 M H_2SO_4 (0.6 mL/min), and UV detector λ = 210 nm (Figure B.4 & B.5.).

Once the mass of glyoxal present in the cross linked films was determined (using a calibration curve, Figure B.4-6) the degree of crosslinking (DXL) was calculated using the following equation:

$$Degree\ of\ Crosslinking\ \% = \left[\frac{162.15 \times Mol_{glyoxal}}{w - (58.04 \times Mol_{cellulose})}\right] 100 \qquad \text{(Eqn. 1)}$$

Where $Mol_{glyoxal}$ is the amount of glyoxal detected by HPCL (mol), $Mol_{cellulose}$ is the amount of crosslinked cellulose present (mol) and *w* is the weight of the dried crosslinked cellulose sample (g), 162.15 is the M_w of the AGU and 58.04 is the difference in M_w between the AGU and crosslinked AGU bearing a glyoxal group. Triplicate samples were analysed for each material and an average reported.

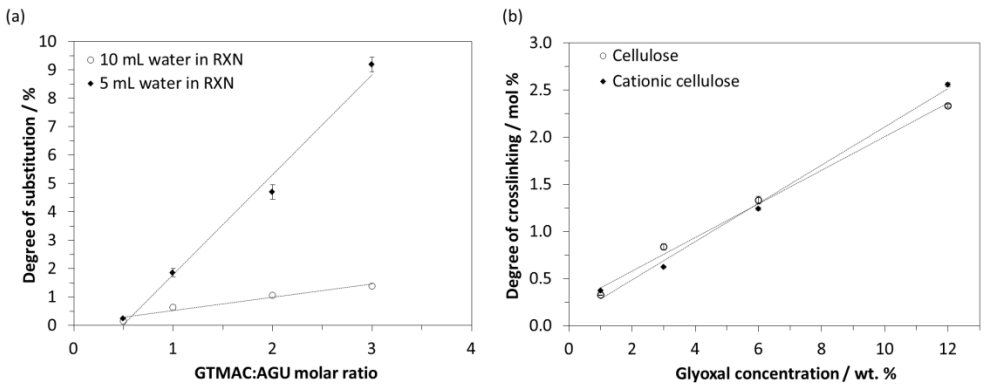

Figure 3.1 a) DS per anhydroglucose repeat unit for the modified cellulose films determined by conductometric titration. Varying DS is achieved by using different GTMAC molar ratios and volume of water in reaction (n=3; error bars show standard error). 3.1 b) Degree of crosslinking (mol. %) in unmodified (R^2 = 0.994) and cationic cellulose (R^2 = 0.994) films determined by HPLC. (n = 3, error bars show standard error)

3.4.4 Scaffold surface characterisation

Zeta potential measurements The surface ζ-potentials of unmodified and cationic cellulose films were measured at 25 ^{o}C using a Malvern Zetasizer surface ζ-potential cell. Samples were cut to the appropriate size, mounted onto the sample plate and aligned with the laser. The measured electrophoretic mobility of 300 nm tracer particles in dispersion was recorded at varying distances from the sample surface to determine the surface ζ-potentials. Triplicate film samples were analysed for each material, the measurement repeated fifteen times per sample and an average reported.

Scanning probe microscopy Scanning probe microscopy was employed to obtain topography and capacitance gradient (*dC/dz*) images of unmodified, and cationic, cellulose films using a Park NX-10 Atomic Force Microscope.[57,58] Kelvin force and capacitance coupling measurements were conducted in parallel by applying an electric AC signal at 17 kHz to the metal-coated cantilever - the DC potential was applied to the cantilever to nullify the AC signal at 17 kHz to determine the electric potential of the sample. The capacitance gradient (*dC/dz*), or capacitance coupling, of the tip to the sample was proportional to the second harmonic of the AC signal (34 kHz). The AFM images were processed and analysed using Gwyddion software[59] and the "1D height analysis" function of the programme used to calculate the capacitance coupling signal distribution on the film.

Confocal microscopy: The degree of penetration of the GTMAC reagent solution and hence the depth of penetration of modification into the bulk cellulose was evaluated by confocal florescence microscopy. Cationic films with DS of 0.6, 2.4, 4.7 and 9.2% were cut into 0.5 x 1 cm strips, washed and hydrated in 100 mL DI H_2O, then stained by immersion in a 100 µM solution of 5(6)-carboxyfluorescein for 30 s, followed by thorough washing in DI H_2O to remove excess dye. The films were secured to a glass slide and viewed using a LSM 510 META confocal laser scanning microscope with an EC-Plan-Neofluor 20x/0.5 PH2M27 lens. An argon laser, λ = 488 nm, was used to excite the dyed films. Multiple images acquired at 0.5 µm steps in depth were combined in a *z*-stack to determine the depth of dye penetration into the bulk of the film.

3.4.5 Scaffold Structural Characterisation

Mechanical properties: The bulk elastic modulus of the scaffolds was determined using a Dynamic Materials Analyser (DMA1 STAR^e System, Mettler Toledo). The samples used were unmodified and cationic (DS = 4.7 ±0.3 %) cellulose films, with a range of cross-linking in both sets (DXL = 0 – 2.6 %). The films (dried at 50 ^oC for 24 h) were cut into strips ≥1.50 cm in length by 0.50 cm width and the thickness recorded with a steel digital vernier micrometer calliper. The film strips were gripped between titanium tension clamp sample holders and a preload force of 1 N was applied to the sample. An offset of 10 µm was set at a frequency of 1 Hz and the elastic moduli were recorded over 5 min. To replicate "hydrated" conditions the relative humidity was set to 80 % using a humidity chamber (MHG, modular humidity generator) and samples equilibrated for 10 mins. Five samples were tested for each film and an average reported.

Atomic force microscopy (AFM) was used to characterise the surface shear moduli of films as previously described by Bae et al.[60,61] In brief, to measure shear modulus, films were first pre-soaked in PBS overnight at room temperature. After removing PBS, cyanoacrylate adhesive was applied to glue each end of the films to the 35 mm tissue culture dish and the films re-immersed in PBS. Shear modulus was measured in force mode using a Bruker DAFM-2X BioScope AFM system. A silicon nitride probe (spring constant, 0.06 N m^{-1}) with a conical tip (40 nm in diameter) was used to indent the films with 15 measurements of each film were collected per sample. To calculate the shear modulus, the first 600 nm of tip deflection from the horizontal

was fit with the Hertz model for a cone for each measurement.[62] The data were analyzed utilizing custom MATLAB scripts kindly provided by Professor Paul Janmey.

3.4.6 Cell response

Cellulose films, modified as described above, were cut into square shapes to fit a Costar® tissue culture well plate, washed, and placed into wells. Loaded plates were sterilised in a Hoefer UVC 500 cross linker for 15 min, a drop of Norland optical adhesive placed atop the sterilised films, and the films inverted and re-sterilised. Films were hydrated by adding PBS and stored at 4 ^{o}C before cell experiments.

To measure cell attachment, films were incubated with the appropriate cell culture medium for 24 h at 4 ^{o}C, the medium was removed, films seeded with MG-63 cells at a density of 10000 cells cm^{-2} and incubated for 1 h at 37 ^{o}C. As a positive control, cells were seeded in empty tissue culture wells. At the 1 h time point, the medium was removed; cells were washed with two aliquots of PBS to remove unattached cells; remaining cells were fixed with 3.7% formaldehyde for 15 min at room temperature; washed twice with PBS; stained with DAPI for 15 min at room temperature (DAPI stains the nuclei enabling cell counts); washed with PBS and stored in PBS at 4 ^{o}C prior to image acquisition.

Cellulose films were removed from the well plate and inverted on glass microscope slides. Six independent, non-overlapping, fluorescence images of each film were acquired with a 10X objective on an EVOS optical microscope. Cell numbers were counted using ImageJ software and normalised to the area of the image. Average cell counts from the images were used to determine cell attachment by normalising to the initial seeding density, Equation 2:

$$\%\ \text{cell attachment} = \frac{\text{No.of cells on scaffold}}{\text{Seeding density}} \times 100 \qquad \text{(Eqn. 2)}$$

To measure cell adhesion, seeded scaffolds incubated for 1 h were centrifuged at 200 rpm (8 g) for 10 min, cells were fixed, stained with DAPI and attachment determined as described above.

To measure cell morphology, films were seeded with MG-63 cells at 2500 cells cm^{-2} in serum free DMEM for 1 h to allow cells to attach without the aid of serum-containing cues. A low cell density was used to reduce cell aggregates on the surface so that individual cell morphologies could be analysed. Control experiments were

performed by incubating cells in empty tissue culture well plates. The medium was then removed and replaced with serum containing medium, which is necessary for cell survival. After 24 h, cells were washed twice with PBS, fixed with formaldehyde for 15 min at room temperature, washed, permeabilised by treatment with 0.1% Triton-X for 15 min at room temperature, and washed again with PBS. Cells were stained with FITC-phalloidin (diluted 1:100) by incubating for 40 min at room temperature, washed with PBS, then stored in PBS at 4 ^{o}C prior to image acquisition. Images were acquired on as described above and analysis to quantify cell area and aspect ratio was conducted using ImageJ software, as described by Fardin.[63]

3.4.7 Statistical analysis

An IBM SPSS Statistics Data Editor was used to perform a one-way analysis of variance (ANOVA) on data sets to determine statistically significant differences between samples at confidence levels of $p < 0.001$ (***), $p < 0.01$ (**) and $p < 0.05$ (*). Cell morphology data was presented as a box and whisker plot to convey the wide spread of cell aspect ratio and cell area.

3.5 Results and Discussion

Working towards the development of easily manufactured tissue engineering scaffold materials that are tunable to specific applications, we have demonstrated that chemical surface modification of cellulose materials, to impart positive surface charge, yielded scaffold materials that allowed ligand free attachment of cells.[7] Here we examine the minimum level of modification required to promote cell attachment and describe the influence of scaffold surface chemistry and mechanics on the adhesion and growth of a human osteosarcoma cancer cell line, MG-63. A dual approach, utilizing two easily applied chemical modifications was used to modulate the scaffold properties:

- surface charge was regulated by reaction with GTMAC to produce cationic cellulose scaffolds and
- mechanical properties of the bulk and the surface were varied by cross linking cellulose with glyoxal.

Cellulose films, with DS ranging from 0.2 to 9.2 % (determined by conductometric titration) and DXL ranging from 0.3 to 2.6 % (determined by HPLC analysis), were prepared as 2D scaffolds and MG-63 cell attachment and spreading compared to unmodified films and to tissue culture polystyrene. Understanding how these facilely modified properties influence cell response aids the development of scaffolds that can promote specific, or specialized, cell function needed for proper tissue functionality and morphogenesis.[29]

3.5.1 Influence of chemical modification on cell response - cell adhesion

Modulation of surface charge substantially enhanced cell attachment, while cross-linking had little effect (Figure B.7). Cell attachment increases with increasing DS, reaching a value of 90 % (relative to tissue culture polystyrene) at DS of only *ca.* 1.4 % - a maximum is reached between DS of 1.4 and 2 % and no further enhancement in attachment follows (Figure 3.2a). As expected, cells showed little affinity for unmodified cellulose, yet this very low degree of surface modification led to an amplification of cell attachment by almost *3000 times, even in the absence of any matrix proteins*, such as foetal bovine serum (FBS), added to the medium.

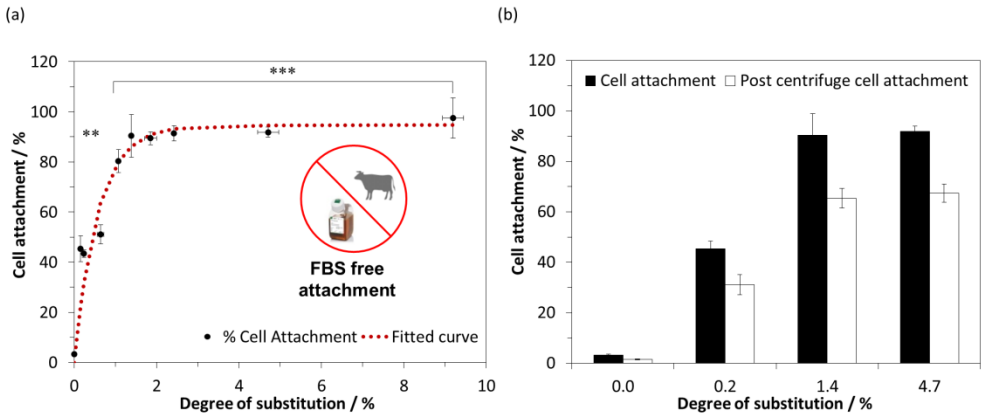

Figure 3.2 a) The effect of varying degree of substitution on MG-63 cell attachment (after 1 h incubation at 37 °C in 5 % CO_2) on cationically modified cellulose films, with no added ligands adsorbed on the surface (n=3; error bars show standard error). Minimal surface chemical modification resulted in significant cell attachment to cationic cellulose. Samples marked *** and ** were significantly different from unmodified cellulose with a $p < 0.001$ and $p < 0.01$ respectively. b) The percentage of MG-63 cells attached to modified cellulose films after centrifugation at 8*g* (n=3 and error bars show standard error). There was no statistical difference between the cell attachment values before and post centrifugation for the modified films. The trend in increasing attachment onto films with up to *ca* 1.4 % DS, followed by a plateau was mirrored after the seeded scaffolds are subjected to shear, indicating good cell adhesion.

To test cell adhesion, seeded scaffolds were subjected to centrifugation after the initial cell attachment (1 h). Centrifugation exposes cells to shear stress, and normalising the cell counts post-centrifugation to the original seeding density yields the percentage of cells remaining (Figure 3.2b). Cell counts post-centrifugation were consistent with cell attachment observations, suggesting that attachment was not an artefact of transient charge/charge interactions, as cells were well adhered to the positively charged cellulose, and that modified scaffolds would support adherent dependent cell behaviour, such as cell spreading and protein secretion.

Previously native cellulose has been described as requiring the addition of growth factors, or matrix ligands, functionalised to the cellulose surface, to facilitate cell attachment,[46–48] however, we demonstrate that a simplified two-component system (cell and biomaterial) can supersede the usual three-component system (cell, biomolecule and material) required for tissue engineering. This reduces the need to use animal, or even human, derived growth factors, potentially enabling scaffold manufacture, transport and storage and obviating some of the concerns that can arise from use of materials derived from mammalian sources, other than the intended recipient of the engineered tissue.

3.5.2 Influence of chemical modification on cell response - cell morphology

Cell spreading (morphology) is an important measure of the cellular response to a given scaffold. In general, changes in cell shape from spherical to a more flattened disc-like form reflects cells encountering a scaffold surface upon which they can thrive.[64]

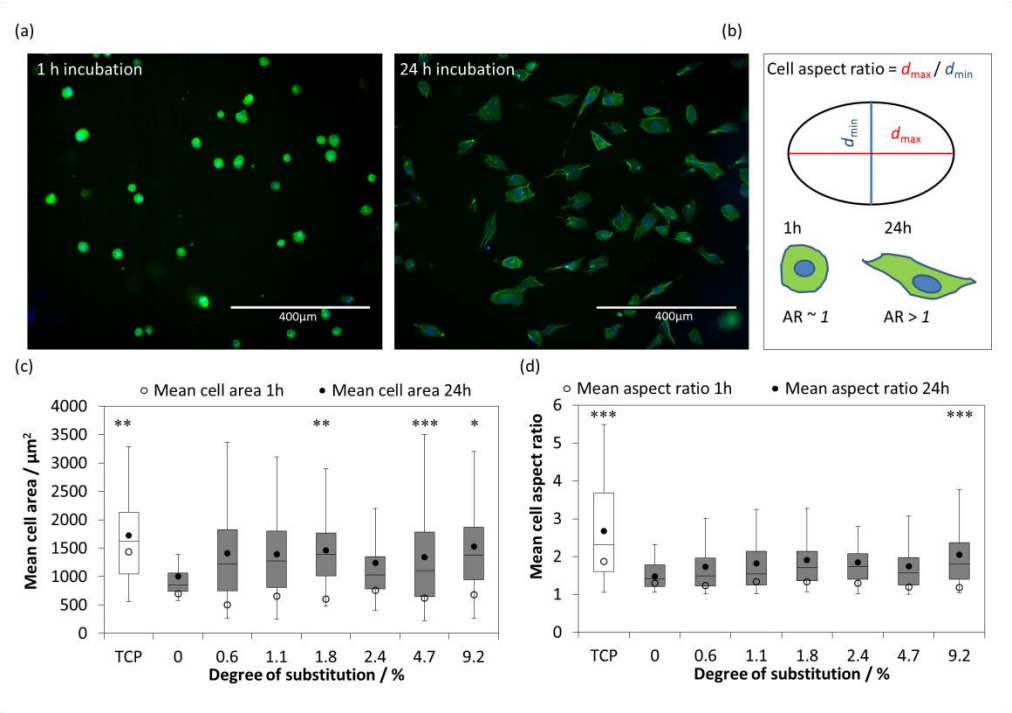

Figure 3.3 a) Optical microscopy images of MG-63 cells spreading on cationic cellulose (9.19 % DS) after incubation at 37 °C in 5 % CO_2 for 1 h (left) and 24 h (right). Attached cells were stained with DAPI (blue) and FITC-phalloidin (green) to highlight the cell nuclei and membranes respectively (scale bar = 400 µm). b) A schematic illustrating the measurements used to determine cell aspect ratio from fluorescence images, using ImageJ software. c-d) The change in cell area and aspect ratio after 24 h incubation at 37 °C in 5 % CO_2, (n= 24 - 435; error bars show standard error) demonstrated spreading and expansion of MG-63 occurred on the cationic cellulose scaffolds. The control scaffold was treated tissue culture plastic and cells on this surface exhibited an average area of 1725 ±129 µm^2 and an aspect ratio of 2.68 ±0.17. Samples marked ***, ** and * are significantly different from unmodified cellulose with $p < 0.001$, $p < 0.01$ and $p < 0.05$ respectively. This data has also been presented in a bar graph in Figure B.13.

Changes in cell spreading were monitored by comparison of the projected cell area and elongation on cationised and unmodified cellulose surfaces, visualized using a fluorescent FITC-phalloidin green stain (Figure 3.3a-b). For all cationised films, a significant increase in cell area (from 505 – 755 µm^2 to 1186 – 1529 µm^2) and aspect ratio (from 1.2 – 1.4 to 1.7 – 2.1) was observed after 24 h incubation at 37 °C in 5 %

CO_2 (Figure 3.3c-d). However, this increase was not statistically different from the cell area and aspect ratio of the very few attached cells on unmodified cellulose. This confirmed that MG-63 cells not only attached to, but also began to spread on, the cationic surface, whereas only a minimal change was observed on the unmodified cellulose scaffolds. After an initial increase in cell area due to cells flattening on the surface, the area will not necessarily increase further as cells spread out (Figure B.12). Therefore, the change in cell aspect ratio was considered to be a more relevant measure of spreading as it reflects the elongation, not the flattening, of attached cells. Interestingly, the level of cationisation of the surface did not appear to influence the cell morphology, suggesting that changes to the structural properties of the scaffold are required to further modulate spreading. This was achieved by crosslinking and we return to this discussion later. Cell area initially increases upon attachment due to the flattening of the cells, however.

3.5.3 Modulation of scaffold properties - cationisation

It is hypothesised that enhanced cell attachment arose, at least in part, from a change in surface charge from negative to positive upon derivatisation and introduction of tetra-alkylammonium groups. To test this hypothesis, and to gain an understanding of the criteria for cell attachment, materials were characterised with respect to surface charge and capacitance using ζ-potential and electric force microscopy measurements. (Changes in bulk elastic modulus and surface roughness had been discounted, as no significant differences were measured between modified and unmodified materials, Figure B9-10).

The measured ζ-potential for unmodified cellulose films was -36 ±4 mV, similar to values reported previously,[56,65] but, upon the addition of quaternary ammonium moieties, the surface ζ-potential became less negative, continuing to increase and becoming positive, 9 ±2 mV, at 1.85 % DS (Figure 3.4a). Further derivatisation led to further increase in positive surface charge measured by ζ-potential, but values plateaued at 23 ±4 mV at only 2.42 % DS (reflecting values reported previously for cellulose nanocrystals [66,67]), suggesting complete saturation of available surface reactive groups. A novel observation here is that this trend is reflected in the affinity of MG-63 cells for the surface, with no further increase in numbers of cells adhered to the scaffold surface above DS of between *ca*. 1.8 and 2.4 %.

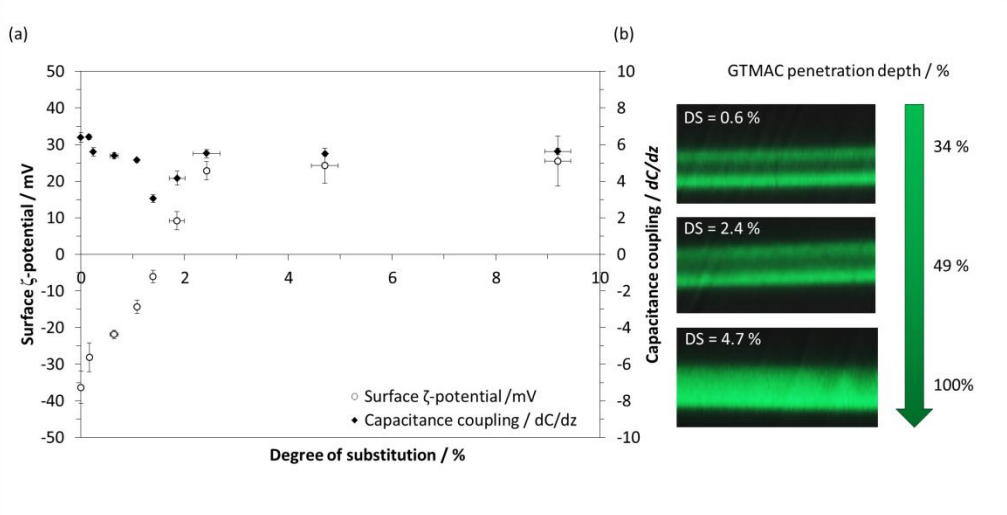

Figure 3.4 a) ζ-potential and capacitance coupling measurements on cationic cellulose films indicated that, initially, increasing DS was correlated to increasing positive charge on the film surface, but a plateau in the surface charge properties was observed after 2.4 % DS. Capacitive coupling between an EFM tip and cationic cellulose surface was generated by a 1D statistical height analysis across a 10 µm2 sample surface area (n=3-5; error bars show standard error). b) The depth of derivitisation by GTMAC was determined by staining the cationic cellulose with 5(6)-carboxyfluorescein. Constructing a z-stack from confocal microscopy images of films with varying DS revealed that the cationic derivatisation penetrates into the bulk of the cellulose after surface saturation is reached.

The change in surface capacitance coupling, *dC/dz*, measured by electric force microscopy, supported the surface ζ-potential findings, reflecting the observed trend. This property, *dC/dz*, is proportional to the electric constant at the surface, however, the value measured by electric force microscopy (EFM) is independent of sign, as the instrument measures the force between the charged tip and the electrical field emanating from the sample. Therefore, surfaces of similar absolute charge density (negative or positive) would yield similar *dC/dz*. Unmodified cellulose has a *dC/dz* of 6.4 ±0.25 AU, which, upon introduction of quaternary ammonium groups, decreases to a minimum of 3.0 ±0.2 AU at 1.39 % DS. ζ-potential shows a charge inversion (from negative to positive), which is reflected in the *dC/dz* values beyond this % DS. With further increased DS measured *dC/dz* rises and ζ-potential continues to increase reaching 5.5 ±0.1 AU and 23 ±2 mV at 2.42 % DS whereafter both values plateau (in agreement with the value of 5.9 AU that we previously measured for cationic bacterial cellulose[7]). Thus, it appears that, once reactive groups on the surface of the films are reacted, i.e. surface saturation is achieved, increases in measured DS reflect penetration of the GTMAC reagent into the film to greater depth, as illustrated in the confocal microscopy images (Figure 3.4b).

It is instructive to consider the mechanism by which MG-63 cells adhere and the evidence suggests that favourable ionic interactions between positively charged scaffolds and the net negatively charged phospholipid groups present in the mammalian cancerous cell membrane [67] are responsible for the initial "attraction" and attachment of cancer cells to the surfaces. Furthermore, using Pluronic F127 as a blocker of non-specific cell/substrate binding interactions had negligible impact on the levels of cell attachment on cationic cellulose, whereas it did reduce it on tissue culture plastic, (Figure B.8). Moreover, MG-63 cells have been reported previously to attach onto chitosan scaffolds, which can be a positively charged polymer at some pHs.[68] This supports the hypothesis that cell attachment on cationic cellulose scaffolds is "surface charge driven".[69,70] Importantly, this response should be general (not restricted cancerous cells or pathological state of the cell), as many cell types exhibit the same net negative charge on their plasma membranes from the phospholipids constituting the plasma membrane, so would be expected to adhere, attaching to the positively charged cellulose substrate. Studies with various cell types and pathological state are currently being investigated to explore this further.

3.5.4 Modulation of scaffold properties - crosslinking

Glyoxal was chosen in this study as a chemical crosslinker due to its low toxicity to mammalian cells and ability to finely regulate the elastic moduli of the scaffolds.[54,71] Both unmodified and cationic cellulose films were cured in glyoxal solutions (1 – 12 wt. %) to achieve films with a range of crosslinking determined by HPLC (Figure B4-6). Quantifying the glyoxylic acid concentration post base hydrolysis enabled the degree of crosslinking (DXL) to be calculated. The DXL ranged from 0.3 – 2.6 % (controlled by initial glyoxal concentration), with minimal difference between the starting cationic or unmodified cellulose films.

Crosslinking of cationic cellulose films increased both bulk elastic modulus and surface shear modulus (Figure 3.5a). The effect on the surface shear modulus was greater, which is significant, as the surface shear modulus more closely reflects the scaffold property defining the micro-environment at the cell-scaffold interface. The mechanical properties of the scaffolds could be tuned to further regulate cell response on the cationic scaffolds (Figure 3.5b).

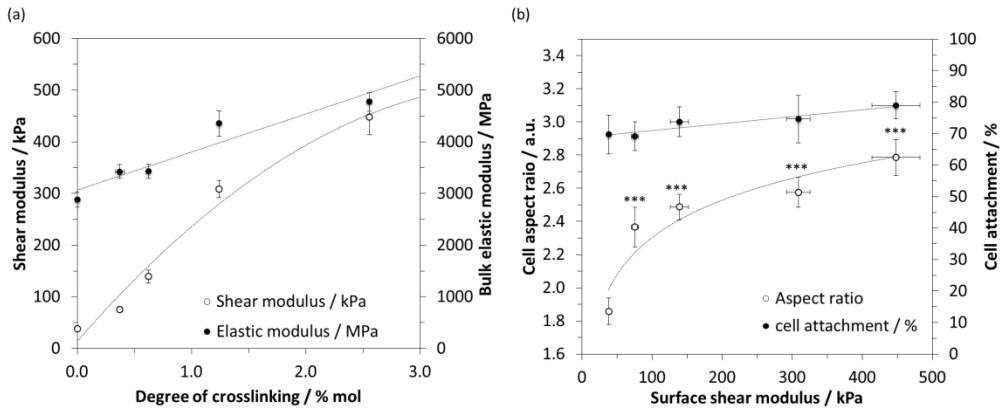

Figure 3.5 a) Crosslinking of cationic (and unmodified) cellulose films lead to an increase in the bulk elastic modulus (measured on samples equilibrated at 80 % relative humidity, n=5, error bars show standard error, cationic cellulose, R^2 = 0.907) and surface shear modulus (n=4; error bars show standard error, cationic cellulose, R^2 = 0.989 for data fitted to a logarithmic expression). b) Modulating the structural properties of the scaffolds through glyoxal crosslinking had minimal effect on cell attachment, but a significant influence on the degree of cell spreading observed after 24 h incubation. Change in MG-63 cell aspect ratio on cationic cellulose scaffolds (DS 4.7 %) with increasing surface shear modulus, after 24 h incubation at 37 ^{o}C in 5 % CO_2 (n= 51 – 116, error bars show standard error). Untreated cellulose scaffolds had an average cell aspect ratio of 1.86 ±0.1, which increased significantly increased upon crosslinking. MG-63 cells, incubated on tissue culture polystyrene, were used as the control: average cell area 1725 ±129 cm^2 and aspect ratio 2.68. Samples marked *** were significantly different from non-crosslinked cationic cellulose with $p < 0.001$.

The bulk elastic modulus for the unmodified cellulose film (Figure B.10) was 2677 ±195 MPa which rose to 4775 ±182 MPa at a DXL of 2.6 mol % (comparable with values of 3917 MPa for cross-linked cellulosic materials previously reported.[72,73] Prior to crosslinking, cationic cellulose films exhibited elastic moduli very similar to that of unmodified cellulose, indicating that the integrity of the bulk films was not compromised by the cationisation reaction. As expected, crosslinking stiffens the cellulose films (and reduces swelling when exposed to moisture [52]), but, notably (and unexpectedly) the influence of crosslinking on the *surface shear moduli* was significantly greater than the effect on the bulk. An almost *tenfold* increase in surface shear modulus occurred upon crosslinking unmodified films (Figure B.11); from 38 ±2 kPa to 332 ±37 kPa and this trend was reflected for cationised films, although the shear modulus values differed at higher degrees of crosslinking, 448 ±35 kPa *vs*. 332 ±37 kPa. It is postulated that the chemical surface modification enhances crosslinking efficiency at the surface, either by more efficient reaction (with the introduced secondary alcohol beta to an ether and quaternary ammonium group), or by enhanced swelling, in the aqueous glyoxal solution, of the modified surface layer.

Cell attachment was not significantly altered upon increase in elastic, or surface shear moduli, thus, surface charge was deemed to have the greatest impact on facilitating cell attachment. However, changes in cell morphology, as measured by aspect ratio were much more dramatic.

3.5.5 Influence of structural modification on cell response - cell morphology

The significantly greater effect of cross-linking than cationisation on cell elongation and thus aspect ratio is illustrated in Figure 3.6a and b. Substrate stiffness has been previously reported, by Bae et al., to activated FAK signalling, stimulating N-cadherin expression and increased cell spreading [74] and the effect of stiff tissue culture plastic on cell spreading is known: normal adherent cells probe elasticity as they anchor and pull on their surrounding and it has been demonstrated that, on stiffer materials, tactile sensing of the substrate by fibroblast cells feeds back on adhesion and cytoskeleton development, resulting in stronger adhesion and cell spreading.[23,38] Therefore, modulating the scaffold mechanics can be used to further regulate cell response. It is recognized that cell response may vary from cell line to cell line, however, in this study MG-63 cells were used to probe the scaffold mechanics as they are robust yet behave in a manner similar to an osteoblast cell phenotype.[75] Furthermore, MG-63 cells have been shown to spread on chitosan scaffolds with similar, or greater, stiffness than the cationic cellulose scaffold [68]. In this case it is possible to regulate cell attachment and spreading through modulating the scaffold surface charge and mechanics. Soft scaffolds do not provide enough resistance to counterbalance the tension generated by anchored MG-63 cells; as a result fewer focal adhesions are formed and cells retain their spherical shape.[23,38] It has been suggested that MG-63 cells form stronger adhesions to stiffer scaffolds due to increased shear stress exerted on the actin fibres as they contract, resulting in a greater degree of spreading and increase cell-ECM interface area.[76]

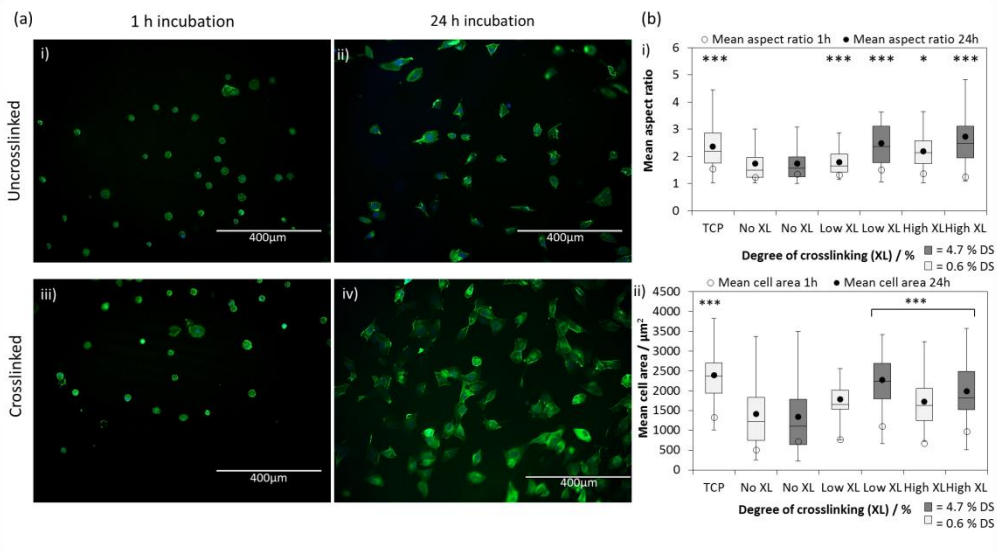

Figure 3.6 a) MG-36 cells appeared to spread out more on the stiffer cationic cellulose scaffolds cross-linked with glyoxal. Optical microscope image of cells adhered to cationic cellulose scaffold after incubation at 37 ^{o}C and 5 % CO_2: i) 1 h cationic cellulose, ii) 24 h cationic cellulose, iii) 1 h cross-linked cationic cellulose and iv) 24 h cross-linked cationic cellulose. The DS used was 4.7 % and DXL was 2.6 %. (The blue coloured structures are the DAPI stained nuclei and green staining, with 5(6)-carboxyfluorescein). Scale bar = 400 µm. b) Influence of DS and DXL on MG-63 morphology; cell area (i) and aspect ratio (ii) on cationic cellulose scaffolds (DS 0.6 and 4.7 %) treated with varying glyoxal concentrations (0, 1, 6 wt. %) after 24 h incubation at 37 ^{o}C in 5 % CO_2, (n= 38 - 193; error bars show standard error). Cell images were analysed by ImageJ to calculate the average cell aspect ratio and area Tissue culture plastic was used as a control, which had an area of 1725 ±129 cm^2 and an aspect ratio of 2.37. Samples marked ***, ** & * were significantly different from uncross-linked cationic cellulose with $p < 0.001$, $p < 0.01$ and $p < 0.05$ respectively. This data has also been presented in a bar graph in Figure B.14.

As no statistically significant effect on cell spreading was observed on moderately cationised cellulose compared to the unmodified cellulose scaffolds, crosslinking was used to stiffen the scaffolds in order to regulate cell spreading. To assess the influence of cross-linking on cell spreading, a cationised cellulose film, with low DS, was used to facilitate the cell attachment only, thus allowing the effect of crosslinking and further cationisation to be determined. The effect of increased scaffold stiffness, particularly at the surface, is important as, once cells have attached to the scaffold, responses such as: migration, proliferation and differentiation (in the case of stem cells) are all initiated by a change in morphology of the attached cell, *i.e.* elongation of the cell through spreading. Thus, the ability to tune the mechanical properties of cationic cellulose scaffolds by glyoxal crosslinking in order to regulate cell response, demonstrated here, could provide advantages in clinical application, complementing approaches such as blending with hard particles [49], or increased fibril density in bacterial cellulose.[77–79]

Thus, we have demonstrated that cellulose can form a promising and simple to modify cell scaffold material and that the combination of chemical surface modification, to introduce positive surface charge, and cross-linking, to modulate scaffold surface stiffness, provides cells with the necessary signaling required for cell attachment and spreading. It has been previously reported that the MG-63 cell line is a representative model of the osteoblast phenotype and can be used to investigate osteoblast function.[75] The values obtained for variously cross-linked cationic cellulose, with surface shear modulus ranging from 40 to 450 kPa, suggests that these scaffolds could mimic myocytes of skeletal muscle and osteogenic environments, which have the potential to be used to generate functional musculoskeletal tissue.[80]

Further, modulated spreading suggests opportunities in differentiation of mesenchymal stem cells (MSCs), given their propensity to differentiate into cell lineage guided by scaffold elasticity - a range of scaffold types could be developed to facilitate the production of different linages, for example, soft hydrogels to rigid composites suitably mimicking brain and musculoskeletal tissue respectively.[38] This offers potential advantages in:

- scaffold production (no sensitive proteinaceous components that can be prone to contamination or requiring special storage);
- scaffold use (mitigation of personal sensitivities, *e.g.* veganism, pertaining to use of animal derived materials); and
- clinical applications: these functionalised scaffolds could be seeded with cells and implanted into the patient without ligand pre-treatment prior to cell seeding. Once cells were adherent to the implant these could begin to produce their own extracellular matrix and would be supported by the *in vivo* environment.

3.6 Conclusion

Tailored functionalised biomaterials based on cationic, crosslinked cellulose have been developed and demonstrated to support cell attachment and spreading, without the use of matrix proteins. Derivatisation of cellulose surfaces with the epoxide GTMAC - to yield positively charged cellulose surfaces - enables both attachment and spreading of cells directly on cellulose scaffolds. No added proteins, or ligands, are required. Modulated cross-linking, with glyoxal, produced materials with variable (and tunable) surface shear moduli that resulted in differential cell

spreading, suggesting a simple, but effective mechanism to control response. The chemical reactions required are easily effected and the degree of both cationisation and cross-linking can be controlled. Cationisation does not compromise the integrity of the bulk material and, while crosslinking renders the bulk stiffer, the effect is greatest at the surface, thus the cell/scaffold interface can be tuned without significantly compromising the mechanical strength of the bulk construct; potentially beneficial in complex 3D scaffold constructs designed to mimic a particular organ or biological component. The elastic moduli of the crosslinked scaffolds mimicked that of myocytes and osteogenic tissue, suggesting the potential to develop such materials into tailored scaffolds to produce musculoskeletal tissue from MSCs.

Cell studies demonstrated that cell response could be further regulated by tuning the surface stiffness of the scaffolds. Thus, combining these approaches, of minimal surface modification to enable ligand-free cell attachment and modulation of mechanical properties by cross-linking, with addition of hard particles to form composites, promises to greatly extend the range of cell environments that could be mimicked.

Finally, tuning properties using cellulose as a base material and requiring only two facile chemical modifications at varying levels, offers potential advantages in production: a range of materials could be “dialed-up” and one production method could produce a range a scaffolds, or even a range of properties within one scaffold making production cost effective and enabling scale up of these two-component systems.

3.7 Acknowledgments

Materials characterisation facilities were provided by the Chemical Characterisation and Analysis Facility (CCAF), University of Bath and we acknowledge the assistance of Dr Rémi Castaing. Access to the Park NX10 atomic force microscope was provided by the Brazilian Nanotechnology National Laboratory (LNNano) and Dr Darrell Patterson, University of Bath, kindly provided access to a surface ζ-potential cell. JCC acknowledges funding support from the EPSRC Centre for Doctoral Training in Sustainable Chemical Technology (EP/L016354/1) and research visits to Brazil were facilitated by a Global Innovation Initiative grant from the British Council and the University of Bath International Research Mobility Scheme and a University of Bath-FAPESP Exchange Scheme

3.8 References

1. T. Dvir, B. P. Timko, D. S. Kohane, and R. Langer, *Nat. Nanotechnol.*, 2011, **6**, 13–22.

2. A. J. Salgado, J. M. Oliveira, A. Martins, F. G. Teixeira, N. A. Silva, N. M. Neves, N. Sousa, and R. L. Reis, *Int. Rev. Neurobiol.*, 2013, **108**, 1–33.

3. C. M. Agrawal, J. L. Ong, M. R. Appleford, and G. Mani, in *Introduction to Biomaterials - Basic Theory with Engineering Applications*, eds. M. W. Saltzman and S. Chien, Cambridge University Press, 2014, pp. 341–374.

4. J. K. Kular, S. Basu, and R. I. Sharma, *J. Tissue Eng.*, 2014, **5**, 1–17.

5. S. J. Hollister, R. D. Maddox, and J. M. Taboas, *Biomaterials*, 2002, **23**, 4095–4103.

6. R. B. Agrawal, C. M. and Ray, *J. Biomed. Mater. Res. - Part A*, 2001, **55**, 141–150.

7. J. C. Courtenay, M. A. Johns, F. Galembeck, C. Deneke, E. M. Lanzoni, C. A. Costa, J. L. Scott, and R. I. Sharma, *Cellulose*, 2017, **24**, 253–267.

8. Y. N. Sergeeva, T. Huang, O. Felix, L. Jung, P. Tropel, S. Viville, and G. Decher, *Biointerphases*, 2016, **11**, 019009.

9. M. Dadsetan, M. Pumberger, M. E. Casper, K. Shogren, M. Giuliani, T. Ruesink, T. E. Hefferan, B. L. Currier, and M. J. Yaszemski, *Acta Biomater.*, 2011, **7**, 2080–2090.

10. E. Biazar, M. Heidari, A. Asefnejad, and N. Montazeri, *Int. J. Nanomedicine*, 2011, **6**, 631–639.

11. C. S. Ranucci and P. V. Moghe, *J. Biomed. Mater. Res.*, 2001, **54**, 149–161.

12. H. Chang and Y. Wang, *Regen. Med. Tissue Eng. - Cells Biomater.*, 2011, **27**, 569–588.

13. F. V. Berti, C. R. Rambo, P. F. Dias, and L. M. Porto, *Mater. Sci. Eng. C*, 2013, **33**, 4684–4691.

14. J. M. Dugan, R. F. Collins, J. E. Gough, and S. J. Eichhorn, *Acta Biomater.*, 2013, **9**, 4707–4715.

15. K. Watanabe, Y. Eto, S. Takano, S. Nakamori, H. Shibai, and S. Yamanaka, *Cytotechnology*, 1993, **13**, 107–114.

16. R. A. Marklein and J. A. Burdick, *Adv. Mater.*, 2010, **22**, 175–189.

17. U. Hersel, C. Dahmen, and H. Kessler, *Biomaterials*, 2003, **24**, 4385–4415.

18. N. Ninan, M. Muthiah, I. K. Park, A. Elain, S. Thomas, and Y. Grohens, *Carbohydr. Polym.*, 2013, **98**, 877–885.

19. M. Gravel, T. Gross, R. Vago, and M. Tabrizian, *Biomaterials*, 2006, **27**, 1899–1906.

20. M. Zaborowska, A. Bodin, H. Bäckdahl, J. Popp, A. Goldstein, and P. Gatenholm, *Acta Biomater.*, 2010, **6**, 2540–2547.

21. Y. Cao, B. H. Lee, H. B. Peled, and S. S. Venkatraman, *J. Biomed. Mater. Res. Part A*, 2016, **104**, 2401–2411.

22. H. Bäckdahl, G. Helenius, A. Bodin, U. Nannmark, B. R. Johansson, B. Risberg, and P. Gatenholm, *Biomaterials*, 2006, **27**, 2141–2149.

23. P. C. Georges and P. a Janmey, *J. Appl. Physiol.*, 2005, **98**, 1547–1553.

24. J. Yang, J. Bei, and S. Wang, *Biomaterials*, 2002, **23**, 2607–2614.

25. Li, J. M., M. J. Menconi, H. B. Wheeler, M. J. Rohrer, V. A. Klassen, J. E. Ansell, and M. C. Appel, *J. Vasc. Surg.*, 1996, **15**, 1010–1017.

26. D. S. W. Benoit and K. S. Anseth, *Acta Biomater.*, 2005, **1**, 461–470.

27. J. Patterson, M. M. Martino, and J. A. Hubbell, *Mater. Today*, 2010, **13**, 14–22.

28. C. M. Agrawal, J. L. . Ong, M. R. Appleford, and G. Mani, in *Introduction to Biomaterials - Basic Theory with Engineering Applications*, ed. M. W. Saltzman and S. Chien, Cambridge University Press, 2014, pp. 233–281.

29. F. S. M. Ismail, R. Rohanizadeh, S. Atwa, R. S. Mason, A. J. Ruys, P. J. Martin, and A. Bendavid, *J. Mater. Sci. Mater. Med.*, 2007, **18**, 705–714.

30. P. Viswanathan, M. G. Ondeck, K. Chirasatitsin, Somyot Nghamkham, G. C. Reilly, A. J. Engler, and G. Battaglia, *Biomaterials*, 2016, **8**, 583–592.

31. P. Ducheyne and Q. Qui, *Biomaterials*, 1999, **20**, 2287–2303.

32. D. Lin, K. Yang, W. Tang, Y. Liu, Y. Yuan, and C. Liu, *Colloids Surfaces B Biointerfaces*, 2015, **131**, 1–11.

33. P. Lu, V. M. Weaver, and Z. Werb, *J. Cell Biol.*, 2012, **196**, 395–406.

34. J. R. Lieberman, A. Daluiski, and T. A. Einhorn, *J. Bone Joint Surg. Am.*, 2002, **84**–**A**, 1032–44.

35. A. Reddi, *Ann. Rheum. Dis.*, 2003, **62**, ii73-ii78.

36. D. E. Discher, P. Janmey, and Y.-L. Wang, *Science*, 2005, **310**, 1139–43.

37. N. Wang, J. P. Butler, and D. E. Ingber, *Science (80-.).*, 1993, **260**, 1124–1127.

38. A. J. Engler, S. Sen, H. L. Sweeney, and D. E. Discher, *Cell*, 2006, **126**, 677–689.

39. D. J. Modulevsky, C. Lefebvre, K. Haase, Z. Al-Rekabi, and A. E. Pelling, *PLoS One*, 2014, **9**, e97835.

40. A. Sannino, C. Demitri, and M. Madaghiele, *Materials (Basel).*, 2009, **2**, 353–373.

41. A. Svensson, E. Nicklasson, T. Harrah, B. Panilaitis, D. L. Kaplan, M. Brittberg, and P. Gatenholm, *Biomaterials*, 2005, **26**, 419–31.

42. F. G. Torres, S. Commeaux, and O. P. Troncoso, *J. Funct. Biomater.*, 2012, **3**, 864–78.

43. A. Kumar, K. M. Rao, and S. S. Han, *Chem. Eng. J.*, 2017, **317**, 119–131.

44. A. Kumar, K. M. Rao, S. E. Kwon, Y. N. Lee, and S. S. Han, *Mater. Lett.*, 2017, **193**, 274–278.

45. A. Kumar, Y. S. Negi, V. Choudhary, and N. K. Bhardwaj, *Cellulose*, 2014, 3409–3426.

46. C.-Y. Wu, S.-Y. Suen, S.-C. Chen, and J.-H. Tzeng, *J. Chromatogr. A*, 2003, **996**, 53–70.

47. H. Zou, Q. Luo, and D. Zhou, *J. Biochem. Biophys. Methods*, 2001, **49**, 199–240.

48. R. Pelton, *Trends Anal. Chem.*, 2009, **28**, 925–942.

49. L. Jiang, Y. Li, X. Wang, L. Zhang, J. Wen, and M. Gong, *Carbohydr. Polym.*, 2008, **74**, 680–684.

50. J. G. Torres-Rendon, T. Femmer, L. De Laporte, T. Tigges, K. Rahimi, F. Gremse, S. Zafarnia, W. Lederle, S. Ifuku, M. Wessling, J. G. Hardy, and A. Walther, *Adv. Mater.*, 2015, **27**, 2989–2995.

51. K. Syverud, S. R. Pettersen, K. Draget, and G. Chinga-Carrasco, *Cellulose*, 2015, **22**, 473–481.

52. F. Quero, M. Nogi, K. Y. Lee, G. Vanden Poel, A. Bismarck, A. Mantalaris, H. Yano, and S. J. Eichhorn, *ACS Appl. Mater. Interfaces*, 2011, **3**, 490–499.

53. T. Puspasari, N. Pradeep, and K.-V. Peinemann, *J. Memb. Sci.*, 2015, **491**, 132–137.

54. E. C. Ramires, J. D. Megiatto Jr., C. Gardrat, A. Castellan, and E. Frollini, *Polímeros*, 2010, **20**, 126–133.

55. C. Schramm and B. Rinderer, *Anal. Chem.*, 2000, **72**, 5829–5833.

56. M. Zaman, H. Xiao, F. Chibante, and Y. Ni, *Carbohydr. Polym.*, 2012, **89**, 163–70.

57. R. F. Gouveia and F. Galembeck, *J. Am. Chem. Soc.*, 2009, **131**, 11381–11386.

58. E. S. Ferreira, E. M. Lanzoni, C. A. R. Costa, C. Deneke, J. S. Bernardes, and F. Galembeck, *ACS Appl. Mater. Interfaces*, 2015, **7**, 18750–18758.

59. D. Necas and P. Klapetek, *Cent. Eur. J. Physic*, 2012, **10**, 18–188.

60. Y. H. Bae, K. L. Mui, B. Y. Hsu, S.-L. Liu, A. Cretu, Z. Razinia, and R. K. Assoian, *Sci. Signal.*, 2014, **7**, ra57.

61. Y. H. Bae, S. Liu, F. J. Byfield, P. A. Janmey, and R. K. Assoian, *J. Vis. Exp.*, 2016, e54630–e54630.

62. J. Domke and M. Radmacher, *Langmuir*, 1998, **14**, 3320–3325.

63. M. A. Fardin, O. M. Rossier, P. Rangamani, P. D. Avigan, N. C. Gauthier, W. Vonngut, M. A., J. Hone, R. Iyengar, and M. P. Sheetz, *Soft Matter*, 2010, **6**, 4788–4799.

64. M. Lotfi, M. Nejib, and M. Naceur, in *Advances in Biomaterials Science and Biomedical Applications*, ed. R. Pignatello, INTECH Open Access Publisher, 2013, pp. 207–240.

65. M. Hasani, E. D. Cranston, G. Westman, and D. G. Gray, *Soft Matter*, 2008, **4**, 2238–2244.

66. M. Hasani, E. D. Cranston, G. Westman, and D. G. Gray, *Soft Matter*, 2008, **4**, 2238–2244.

67. Y. Song, Y. Sun, X. Zhang, J. Zhou, and L. Zhang, *Biomacromolecules*, 2008, **9**, 2259–64.

68. Z. Li, H. R. Ramay, K. D. Hauch, D. Xiao, and M. Zhang, *Biomaterials*, 2005, **26**, 3919–3928.

69. L. Li, X. Shi, X. Guo, H. Li, and C. Xu, *Trends Biochem. Sci.*, 2014, **39**, 130–140.

70. F. Schweizer, *Eur. J. Pharmacol.*, 2009, **625**, 190–194.

71. L. Wang and J. P. Stegemann, *Acta Biomater.*, 2011, **7**, 2410–2417.

72. A. Retegi, N. Gabilondo, C. Pena, R. Zuluaga, C. Castro, P. Ganan, K. de la Caba, and I. Mondragon, *Cellulose*, 2010, **17**, 661–669.

73. H. Qi, J. Cai, L. Zhang, and S. Kuga, *Biomacromolecules*, 2009, **10**, 1597–1602.

74. K. L. Mui, Y. H. Bae, L. Gao, S. L. Liu, T. Xu, G. L. Radice, C. S. Chen, and R. K. Assoian, *Cell Rep.*, 2015, **10**, 1477–1486.

75. J. Clover and M. Gowen, *Bone*, 1994, **15**, 585–591.

76. B. M. Gumbiner, *Cell*, 1996, **84**, 345–357.

77. K. Watanabe and S. Yamanaka, *Biosci. Biotechnol. Biochem.*, 1995, **59**, 65–68.

78. E. L. Hult, S. Yamanaka, M. Ishihara, and J. Sugiyama, *Carbohydr. Polym.*, 2003, **53**, 9–14.

79. A. Bodin, H. Bäckdahl, H. Fink, L. Gustafsson, B. Risberg, and P. Gatenholm, *Biotechnol. Bioeng.*, 2006, **97**, 425–434.

80. P. a Janmey and R. T. Miller, *J. Cell Sci.*, 2011, **124**, 9–18.

Chapter 4

4 Paper 4: Simple to fabricate, micropatterned, 2D cellulose scaffolds for localised cell attachment

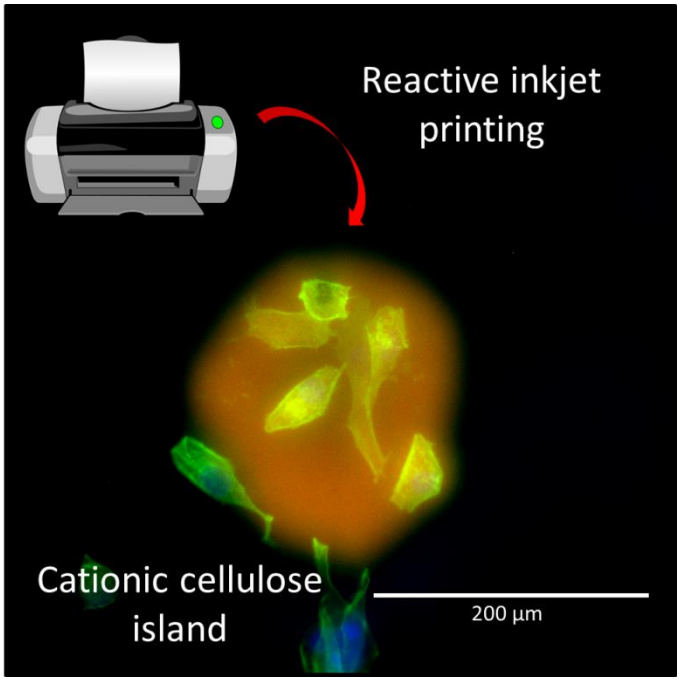

4.0 Publication Commentary

The ability to control where cells attach on a scaffold has many applications in tissue engineering. These include: creating cell-clusters used as in vitro tissue models for the high throughput screening of active ingredients; introducing alignment of cells for development of more complex functional and co-culture of different cell types on one scaffold.

In the previous chapters it has been demonstrated that cationisation of cellulose, to produce positively charged surfaces, enhances cell adhesion. The main focus of this chapter was to develop a methodology to reduce the area of cationic modification from the bulk to <100 µm, as it was proposed that the placement of cell attachment can be controlled and localised to this region. Preliminary studies were carried out using pipettes and syringe needles to deposit GTMAC onto the films of cellulose. These methods could be produce circles and lines, but the resultant patterns were too large to be used, as the thinnest line produced using a syringe needle was 200 µm across. The target size of the patterns was in the order of 10s of microns; given the diameter of MG-63 cells are between 10 – 20 µm.

Thus, the aim was to utilise reactive inkjet printing to deposit micro droplets of "reactive-inks", e.g. GTMAC, onto cellulose film surfaces, to form micro-patterns. First the suitability of GTMAC as a "reactive-ink" needed to be assessed so that GTMAC droplets could be jetted onto the cellulose film surfaces by a piezoelectric head inkjet printer. Viscosity and interfacial surface tension of the ink can influence its ability to jet. Furthermore, protocols needed to be developed to visualise and characterise the cationic cellulose features present on the scaffold surface. Investigations into whether MG-63 cells would preferentially attach to the positively charged micro-patterns and if cell spreading was restricted to within these regions was conducted, as this could be developed to guide cell alignment.

It had been planned to use electric force microscopy (EFM) to map the change in dC/dz across the printed cationic islands. However, due to the closeness in dC/dz values between unmodified and cationic cellulose we were unable to distinguish between the droplet and background using this technique. It was apparent that to print patterns with increasing density of drops to form a gradient in DS across the film, the resolution of the gradient would be limited to ~ 50 µm, *i.e.* the smallest circle that can be printed. Furthermore, this would not be a continuous gradient,

rather areas of high DS surrounded by areas of unmodified cellulose, which would gradually decrease as droplets were printed closer together, until a continual line was formed. There is potential to overcome this issue using laser lithography as an alternative method of patterning the films.

4.1 Statement of Authorship

<table>
<tr><th colspan="10">This declaration concerns the article entitled:</th></tr>
<tr><td colspan="10">Simple to fabricate, micropatterned, 2D cellulose scaffolds for localised cell attachment</td></tr>
<tr><td colspan="10">Publication status</td></tr>
<tr><td>Draft manuscript</td><td>✓</td><td>Submitted</td><td></td><td>In review</td><td></td><td>Accepted</td><td></td><td>Published</td><td></td></tr>
<tr><td>Publication details</td><td colspan="9">Courtenay, J. C., Sharma, R. I. & J. L., Scott, (2018). Simple to fabricate, micropatterned, 2D cellulose scaffolds for localised cell attachment</td></tr>
<tr><td>Candidate's contribution to the paper</td><td colspan="9">Formulation of ideas:
Ideas were discussed and planned with JLS and RIS (JCC contribution 90%). A complete manuscript draft was prepared by JCC and edited by supervisor, JLS + RIS.

Design of methodology:
Experiments were discussed and designed with JLS and RIS (JCC contribution 90%).

Experimental work:
Experimental work was conducted and analysed by the JCC (JCC contribution 100%).

Presentation of data in journal format:
All figures were prepared by JCC (JCC contribution 100%).</td></tr>
<tr><td>Statement from candidate</td><td colspan="9">This paper reports on original research I conducted during the period of my Higher Degree by Research candidature</td></tr>
<tr><td>Signed</td><td colspan="6"></td><td>Date</td><td colspan="2"></td></tr>
</table>

4.2 Abstract

Finely patterned cellulose film based scaffolds were prepared by “reactive inkjet printing” of glycidyltrimethylammonium chloride. MG-63 cells preferentially attached to, and spread on, the resulting islands of “cationic cellulose” of ~47 µm in diameter, demonstrating *directed* cell attachment, important for creating cellular constructs in tissue engineering. The fabrication technology uses established, robust chemistry, to yield reproducible, regularly patterned surfaces and is scalable and cheap, requiring little specialised equipment, thus could be widely applied where control of cell placement is required.

4.3 Introduction

The ability to direct cell attachment to specific parts of a scaffold surface has significant potential to further the construction of complex tissues *ex vivo* by introducing cell alignment, arrangement and orientation organised in a specific manner. Surface patterning of scaffolds with the matrix ligand RGD at <100 µm in scale, has been demonstrated to yield aligned cells, which potentially enables the culture of aligned tissue – especially useful for muscle and nerve cells.[1,2] Furthermore, well controlled directed cell attachment could also lead to the production of cell co-cultures whereby multiple cell types are seeded onto scaffolds. This approach is designed to provide heterogeneous cultured tissues more closely mimicking natural tissues.

Technologies used to control cell attachment through surface patterning of scaffolds include: microcontact printing,[3] spatial control of single cells,[4] photolithography,[5] laser-directed cell-writing,[6] dip-pen nanolithography,[7] and inkjet printing of surface modifiers and/or cells.[8] While all such methods yield patterned surfaces and aid in control of positioning of cells, some are complex to implement, while others require highly specialised materials, or equipment. Many are difficult to scale up, limiting manufacturability. Printing based techniques are attractive, as printers are widely available and can be customised to print surface modifiers, or biomolecules, onto scaffolds to produce the protein arrays [9] and cell patterns.[10]

To ensure that scaffolds developed can be manufactured at scale, with minimal use of animal derived products, the choice of a biocompatible, readily available, natural biopolymer is desirable. Here we select plant cellulose, which has been demonstrated to be processable into a range of tissue scaffold materials with appropriate tensile strength for a given application [11]). This polysaccharide is biocompatible, but matrix ligands are usually required to facilitate cellular attachment, as cellulose lacks integrin binding sites.[12]

We have recently demonstrated that cells may be induced to attach to surface modified cellulose without addition of adhesion proteins.[13] The introduction of positively charged tetra-alkylammonium groups onto cellulose (by reaction with glycidyltrimethylammonium chloride, GTMAC) facilitates cell attachment. Here cell seeding and attachment proceeds in serum free medium, with foetal bovine serum (FBS) added only during the cell expansion phase.

Herein we report the development of surface modified cellulose scaffolds micropatterned with modified, positively charged regions in well-defined arrays, to control cell adhesion and placement. Chemistry that is amenable to scaling-up and rapid printing - grafting of the epoxide GTMAC *via* nucleophilic addition to alkali-activated cellulose hydroxyl groups [14,15] - is combined with inkjet printing using *unmodified* commercial printers, to simply and rapidly decorate cellulose films with micro-patterns, so directing and controlling cell attachment in a manner that is quick, simple, flexible, amenable to scale-up and yields scaffolds that can be stored without degradation, yet requires no specialised equipment, or added adhesion proteins. This has the potential to unlock novel innovation opportunities at both research and industrial level.

4.4 Experimental Procedures

4.4.1 Materials and methods

For surface modifications, sodium hydroxide pellets (≥98 %), glycidyltrimethylammonium chloride (GTMAC) (≥90 %) were purchased from Sigma-Aldrich®. For cell investigations Dulbecco's Modified Eagle Medium (DMEM) (GlutaMAX™), non-essential amino acids (NEAA), sodium pyruvate (NaPyr), trypsin (0.05 %) and trypan blue (0.4 %) were purchased from Gibco® and stored at 4 °C. Foetal bovine serum (FBS) (non-USA origin), MG-63 cells, Triton-X and formaldehyde (37 % in 10-15 % methanol H_2O solution) were purchased from Sigma-Aldrich®. Phosphate buffer solution (PBS) was purchased from HyClone® (0.1 µm sterile filtered), 6-diamidino-2-phenylindole (DAPI), phalloidin-FITC and penicillin streptomycin (PenStrep) from Life Technologies. Norland optical adhesive 63 was purchased from Norland Products. All materials were used as received.

4.4.2 Inkjet printing of reactive inks

Arrays of "islands" of surface modified cellulose were obtained by inkjet printing neat GTMAC (Sigma Aldrich) onto alkali activated, dried cellulose films (cellulose dialysis tubing MWCO 12400, Sigma Aldrich D0530) using a Fujifilm Dimatix printer with DMC 11601 or 11610 print cartridges (16 nozzles at 254 µm spacing, equivalent to 4 drops per mm) delivering droplet volumes of 1 or 10 pL respectively. Piezoelectric print heads were heated to 40 °C and a jetting voltage of 27 mV applied. (Determination of "ink" interfacial tension, optimisation of composition and stability of GTMAC to hydrolysis at elevated temperature, for reactant delivery via jetting from a print head is described in detail in the Appendix C.) Etherification was initiated by heating the micropatterned films to 65 °C for 75 min following which films were washed (DI water) and dried. Micropatterns were stained with 5(6)-carboxyfluoroscein and visualised using an EVOS optical microscope (470 nm light source / 535 nm emission filter), or a LSM 510 META confocal scanning microscope with an EC-Plan_Neofluor 20x/0.5 PH2M27 lens (Ar laser excitation, λ= 488 nm). To determine the thickness of cationic islands, an optical slice of 25 µm was generated by combining 11 x 5 µm slices overlapped by 50 % in the *z*-axis.

4.4.3 Directed cell attachment

Pretreatment of cellulose materials, analysis of the degree of substitution and cell studies followed the protocols previously described by Courtenay et al. 2017 [13]. Briefly, for cell attachment, MG-63 cells were seeded at 100,000 cells cm^{-2} in serum-free Dulbecco's Modified Eagle Medium (DMEM) and incubated for 1 h (37 °C, 5 % CO_2) before medium (and unattached cells) was removed scaffolds washed and cells fixed (formaldehyde, 15 min) and stained with DAPI prior to visualisation (EVOS optical microscope). For cell morphology studies cells were seeded at a density of 2,500 cells cm^{-2} (serum free DMEM). After 1 h incubation, unattached cells/medium were removed as above, serum containing medium added and cells incubated for 24 h, prior to fixing, washing, permeabilisation (0.1 % Triton-X, 15 min), washing, staining (FITC-phalloidin dilution 1:100, 40 min) and analysis to quantify cell area and aspect ratio using imageJ software.

4.5 Results and discussion

4.5.1 Micropatterned surfaces

Having demonstrated previously that bulk modification of the surface of cellulose with GTMAC led to enhanced cell attachment, even at low degrees of substitution [13], the next step was to direct cell attachment to specific regions, at the micron scale, i.e. to prepare micropatterned surfaces to direct cell attachment. This was achieved using an unmodified Dimatix inkjet printer to jet droplets of GTMAC directly onto commercially available smooth cellulose films (Figure 4.1a), which, when reacted under moderate heating (65 °C), resulted in well-defined, discrete islands of modified cellulose (Figure 4.1c and d).

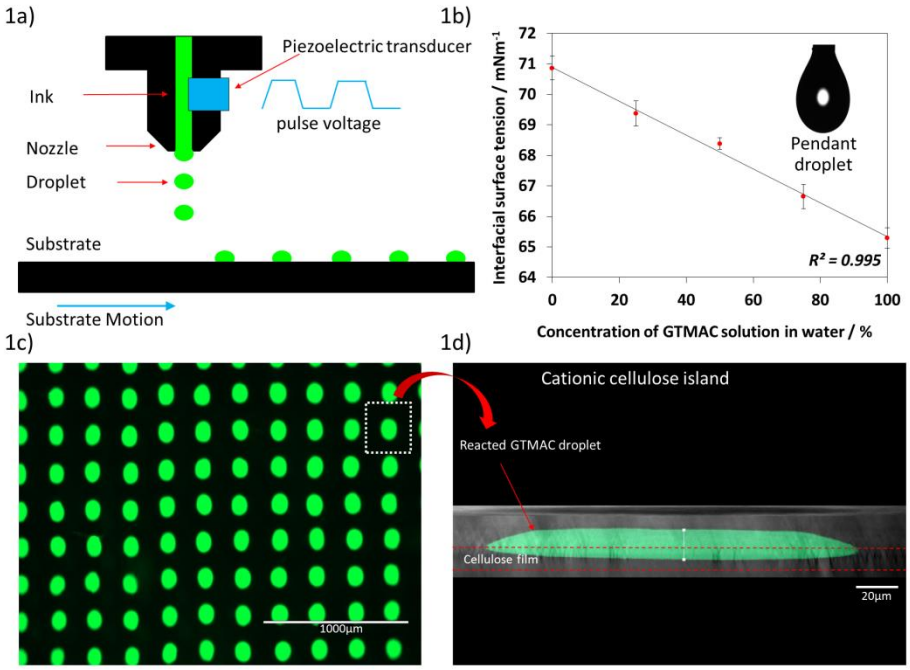

Figure 4.1 a) Schematic illustrating the Dimatix ink jetting process. b) Interfacial surface tension measurements at the air/liquid interface for GTMAC solutions of varying concentrations. c) Cationic islands on cellulose films formed by inkjet printing and reaction of GTMAC (stained with 5(6)-carboxyfluorescein and visualised by confocal fluorescent microscopy); the average droplet diameter is 80 ±4 µm (scale bar = 1000 µm). d) Z-stack of confocal images of one cationic island, showing the lens shaped cross-section; the average lens thickness is 15.7 ±0.4 µm (scale bar = 20 µm).

As high resolution inkjet printing requires "inks" with suitable physical properties to jet effectively, the air-water interfacial tension (IFT) of a range of GTMAC aqueous solutions was determined by pendant droplet measurements. An appropriate IFT for jetting droplets is between 32 – 42 mN m^{-1}; high enough to retain the ink in the

nozzle without dripping, yet low enough to allow droplets to be expelled by piezoelectric activation. Addition of GTMAC to water reduced the IFT, with the lowest value, 65.3 ±0.3 mN m^{-1}, measured for neat reagent (Figure 4.1b). This IFT value still exceeded the optimal range for effective jetting, and prevented the piezoelectric transducer from priming the nozzle when jetting voltages of 20 – 40 mV were applied. While surfactants, or other modifiers, are frequently incorporated into ink formulations to lower the IFT, we preferred to avoid adding extra ink components to reduce possible adverse effects on cell attachment. Instead, the nozzles were heated to 40 ^{o}C, which lowered the IFT sufficiently to enable the jetting mechanism to operate effectively, yet remains a low enough temperature to avoid pre-reaction of GTMAC with, for example, atmospheric moisture, as illustrated by variable temperature NMR studies of hydrolysis of GTMAC (Figure C.1-5).

This methodology was used to produce arrays of uniform GTMAC droplets, arranged at a spacing of four droplets per mm, on cellulose films. Upon reaction, initiated by heating to 65 °C for 75 min, these yielded discrete, well-defined “cationic islands” patterning the surface of the 2D cellulose scaffold. Using neat GTMAC reagent as the ink, with attendant high IFT, resulted in minimal wetting of the cellulose upon droplet settling, thus preventing “bleeding” of the droplets and coalescence - beneficial for retaining the high resolution of the array of printed cationic islands (Figure 4.1c). The smallest cationically surface modified islands produced by this technique had an average diameter of 47 ±2 µm. This scale is suitable for directed cell attachment, as it allows for multiple cells to adhere to each island. Further probing of the derivatised regions with laser scanning confocal microscopy showed that GTMAC derivatisation was homogeneous across the island surface and, in cross-section, the islands appeared as flattened lenses with average thickness of 15.7 ±0.4 µm (Figure 4.1d).

4.5.2 Directed cell attachment

Using this novel approach, it was possible to control attachment of MG-63 cells to the surface (Figure 4.2a, b and c), limiting these to the printed ‘islands’ thus directing cell attachment by patterning the cellulose scaffold surface (Figure 4.2d, e and f).

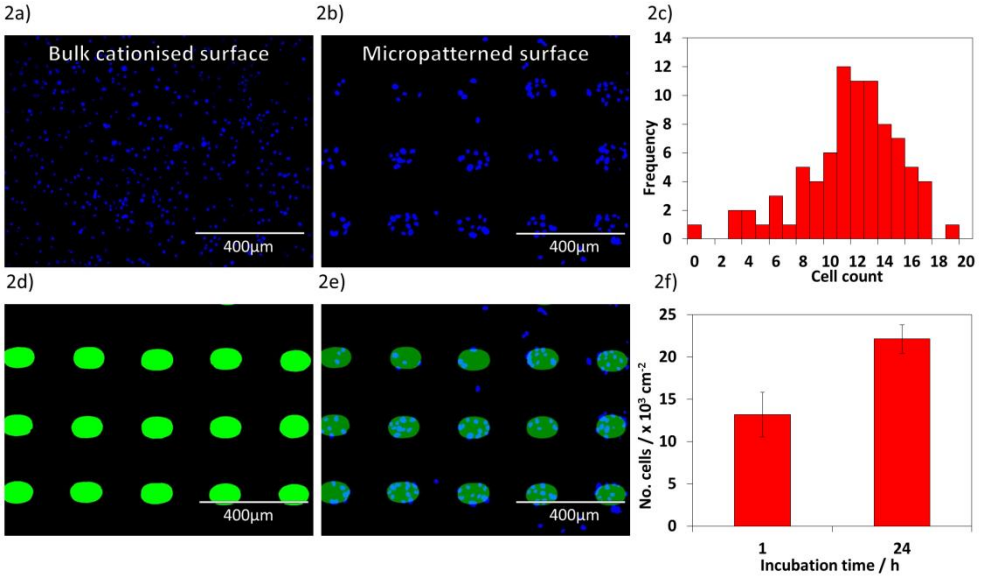

Figure 4.2 Optical microscope images of cells attached to cationised, patterned cellulose scaffolds following seeding at a density of 100,000 cells cm^{-2} and 1 h incubation at 37 ^{o}C and 5 % CO_2 (DAPI stained cell nuclei appear blue, while green fluorescence demarcates the cationised regions on the cellulose film, scale bar = 400 µm). a) MG-63 cells attached to bulk cationised cellulose films (DS 9.2 %). b) MG-63 cells attached to patterned cellulose films. The majority of cells are attached to the modified islands only. c) Histogram indicating distribution of cells attached to the patterned scaffolds. d) Fluorescent image of the cationised regions on the cellulose film. e) Overlay showing cells preferentially attached to the GTMAC derivitised regions of cellulose, indicating directed cell attachment. f) Cell growth after 24 h at 37 ^{o}C and 5 % CO_2 on cationic cellulose islands, seeding density of 10,000 cells cm^{-2}.

The level of cationisation on islands is high, thus it is fortuitous that, as we have reported, cell attachment and adhesion is not sensitive to high degrees of derivatisation, i.e. a plateau in optimum derivatization is reached, not a maximum [13]. This allows for fine control of reagent placement using jetted droplet printing of concentrated GTMAC (Figure 4.2e), which has an appropriate viscosity for printing. It is clearly visible in Figure 4.2e that MG-63 cells preferentially attached to the cationic islands and did not attach to unmodified cellulose. It is postulated that this initial directed attachment results from complementary electrostatic interactions between the cell membranes and quaternary ammonium groups,[16] but here we have also demonstrated that cells spread well on such “cationic cellulose” surfaces as illustrated by the changes in cell morphology (Figure 4.3a and c) and cell spreading (Figure 4.3c and d). Cell attachment on patterned cellulose was 41 ±7 % compared to a tissue culture plastic control, but cell attachment per cationic island (area of 9173 ±14 μm^2), was slightly greater than the initial seeding as the cells became localised to the island.

Reduction in island size was facilely achieved by reduction in inkjet nozzle droplet volume (here 10 and 1 pm droplet volumes yielded islands with diameters 80 and 47 µm), however, there is further scope for refining island size by also formulating inks with properties that minimise wetting. Thus, there is scope to develop this methodology further to produce islands small enough to allow a very small number of cells, or even a single cell only, to attach. As arrays of individualised cells have potential applications as models for studying cell responses to external cues and high throughput screening of pharmaceutical drugs[17] this approach is being further explored.

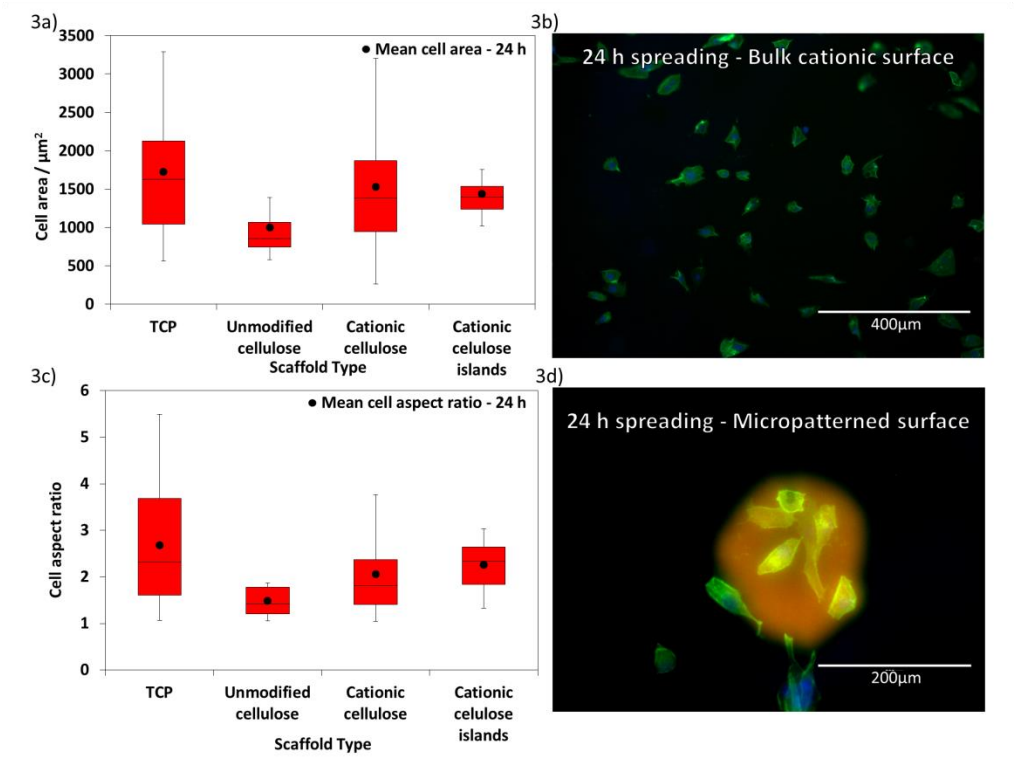

Figure 4.3 a) Cell area and c) cell aspect ratio on tissue culture plastic (control), unmodified cellulose, cationic cellulose and cationic cellulose islands, after 24 h at 37 ^{o}C and 5 % CO_2. Optical images of b) cell spreading on bulk surface cationised cellulose and d) cationic cellulose islands (DAPI stained nuclei appear blue and phalloidin-FITC stained cell membranes, green, while the red stain, 5(6)-carboxyfluorescein, demarcates cationised regions on the cellulose film). Scale bars: b) 400 µm and d) 200 µm.

An increase in cell population and morphological changes after 24 h incubation indicated that MG-63 cells remain viable on the cationic cellulose islands. Cell area expansion (Figure 4.3a) and spreading (Figure 4.3c) was observed on both cationic cellulose and on the cationic islands (Figure 4.3b and d). It has been previously reported that elongated surface micron/submicron patterns resulted in alignment of cells, as elongation could only occur within the modified regions.[2] Interestingly, here the elongation of cells was not only confined within the boundaries of the cationic

regions, with cells appearing to have spread somewhat onto the surrounding unmodified cellulose (Figure 4.3d), suggesting that these islands could be used as seeding sites for developing clusters of cells for further testing, or for development of textured tissues.

Patterns accessible by reactive inkjet printing were not limited to dots, but could be extended to lines (Figure C.6a-d) and gradients (Figure C.7a-f). The range of patterns that can be generated using inkjet printing is vast (although maximum resolution is defined by drop size) and cellulose substrates could be bespoke patterned for particular applications depending on the cell type, or phenomena, in question.

4.6 Conclusion

In summary, reactive printing, using unmodified commercial printers and a commercially available reagent, GTMAC, allowed for rapid and reproducible patterning of cellulose films, providing 2D scaffolds that facilitated directed attachment of cells. Demonstrated here for arrays of dots that reflect individual GTMAC reactant droplets, islands with average diameter of only 47 ±2 µm were achieved. This surface patterning is of dimensions that point to opportunities in cell alignment (cell diameter 10 – 20 µm) *via* surface patterning. Thus, the attachment of cells to selected regions of the scaffold can not only be achieved in protein free media and increased over that achieved for bulk modification, but also directed and, potentially, aligned. This is an important step towards the culture of cells on contained regions of a substrate. Using inkjet printing, other geometries, features, and patterns can be generated using GTMAC, or other reagents, as the ink.

Notably, this chemistry, known for polysaccharides, is directly translatable to any scaffolds bearing surface hydroxyl, or similarly reactive, groups. Additionally, other reactive chemistries could be applied using this methodology. A micropattern produced using multiple ink reagents, resulting in a scaffold with defined regions of variable surface chemistries, could lead to production of cell co-cultures with multiple cell types seeded onto the patterned scaffolds, which better reflects natural tissue and provides for development of tissue functionality.[18] Opportunities extend beyond the production of *ex vivo* tissues for clinical applications – for example, isolation of small groups of cells, or even individual cells, offers opportunities in screening of active agents, such as drugs, and selection of suitable patterning chemistries could lead to co-localisation of muscle and fat cells, of potential utility in synthetic meat production.

4.7 Acknowledgments

Materials characterisation facilities were provided by the Chemical Characterisation and Analysis Facility (CCAF), University of Bath. JCC acknowledges funding support from the EPSRC Centre for Doctoral Training in Sustainable Chemical Technology (EP/L016354/1).

4.8 References

1. A. Agrawal, B. H. Lee, S. A. Irvine, J. An, R. Bhuthalingam, V. Singh, K. Y. Low, C. K. Chua, and S. S. Venkatraman, *Int. J. Biomater.*, 2015, **279**, 27410–27421.

2. Y. Ito, *Biomaterials*, 1999, **20**, 2333–2342.

3. A. Folch, B. H. Jo, O. Hurtado, D. J. Beebe, and M. Toner, *J. Biomed. Mater. Res.*, 2000, **52**, 346–353.

4. S. N. Bhatia, M. L. Yarmush, and M. Toner, *J. Biomed. Mater. Res.*, 1997, **34**, 189–199.

5. V. A. Liu, W. E. Jastromb, and S. N. Bhatia, *J. Biomed. Mater. Res.*, 2002, **60**, 126–134.

6. D. Odde and M. Renn, *Biotechnol. Bioeng.*, 2000, **67**, 312–318.

7. K.-B. Lee, S.-J. Park, C. A. Markin, J. C. Smith, and M. Mrksich, *Science (80-.).*, 2002, **295**, 1702–1705.

8. T. Xu, J. Jin, C. Gregory, J. J. Hickman, and T. Boland, *Biomaterials*, 2005, **26**, 93–99.

9. A. Roda, M. Guardigli, C. Russo, P. Pasini, and M. Baraldini, *Biotechniques*, 2000, **28**, 492–496.

10. E. A. Roth, T. Xu, M. Das, C. Gregory, J. J. Hickman, and T. Boland, *Biomaterials*, 2004, **25**, 3707–3715.

11. K. Syverud, S. R. Pettersen, K. Draget, and G. Chinga-Carrasco, *Cellulose*, 2015, **22**, 473–481.

12. H. Zou, Q. Luo, and D. Zhou, *J. Biochem. Biophys. Methods*, 2001, **49**, 199–240.

13. J. C. Courtenay, M. A. Johns, F. Galembeck, C. Deneke, E. M. Lanzoni, C. A. Costa, J. L. Scott, and R. I. Sharma, *Cellulose*, 2017, **24**, 253–267.

14. M. Hasani, E. D. Cranston, G. Westman, and D. G. Gray, *Soft Matter*, 2008, **4**, 2238–2244.

15. M. Zaman, H. Xiao, F. Chibante, and Y. Ni, *Carbohydr. Polym.*, 2012, **89**, 163–70.

16. Y. Song, Y. Sun, X. Zhang, J. Zhou, and L. Zhang, *Biomacromolecules*, 2008, **9**, 2259–64.

17. P. K. Chattopadhyay, T. M. Gierahn, M. Roederer, and J. C. Love, *Nat. Immunol.*, 2014, **15**, 128–135.

18. J. Hendriks, J. Riesle, and C. A. van Blitterswijk, *J. Tissue Eng. Regen. Med.*, 2010, **4**, 524–531.

Chapter 5

5 Paper 5: Unravelling cationic cellulose nanofibril hydrogel structure: NMR spectroscopy and small angle neutron scattering analyses

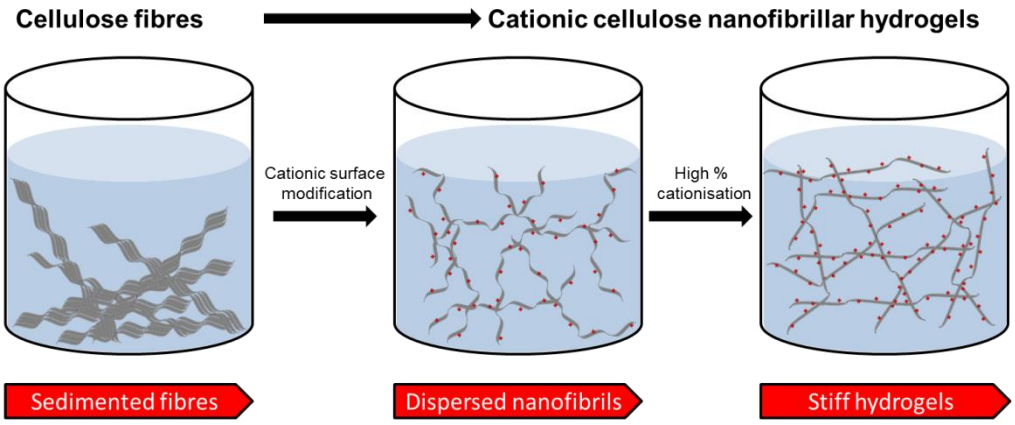

5.0 Publication commentary

So far the cationic cellulose scaffolds produced had been in the form of 2D films. Reasons why 2D scaffolds would be used in cell culture include: relative ease of production, routine cell expansion and the ease probing cell-substrate interactions *e.g.* by microscopic analysis. However, the thickness of a cell construct growing on a 2D surface is limited to ~200μm, due to low mass transfer of nutrients and O_2 into the tissue. Moreover, the environment that cells experience on a 2D film is not representative of 3D tissue and therefore they may respond differently to the scaffold. This is an issue when using cell cultures as a model for in vivo tissue in drug studies, for example.

In order to make 3D cellulose structures, cellulose material needed to be prepared in a form whereby they can be processed. Dissolving cellulose in an ionic liquid, followed by antisolvent regeneration can be used to produce 3D hydrogels. These materials can be lyophilised, resulting in porous aerogels (foams) with the desired porosity for suitable mass transfer.

In this chapter a different approach is adopted. Cellulose nanofibrillar surfaces were modified utilising the same chemistry as described in previous chapters. The cationisation of the cellulose lead to the formation of cationic cellulose nanofibrils (CCNF) which could be dispersed in H_2O forming stable hydrogels due to the charge-charge repulsion between CCNF. These hydrogels could now be further processed into a range of shapes and structures.

As hydrogel structure would be expected to influence aerogel structure this was investigated. The fundamental structure and form of the cationic nanofibrils was probed by small angle neutron scattering (SANS), NMR and transmission electron microscopy. SANS is a very powerful technique commonly used to probe the structure and interactions within soft matter and relies on the scattering length density (SLD) differences between elements, commonly hydrogen and deuterium.

Unlike X-rays which are scattered by interaction with electron density, which increases periodically with atomic number, neutrons interact with the nucleus and the SLD of neutrons varies by element and isotope. It is fortuitous that hydrogen and deuterium nuclei have very different SLDs, as many compounds can be prepared in deuterated forms. Usually, when conducting SANS experiments, several samples are

prepared with different contrast combinations. For example for a CCNF hydrogel: H-CCNF in H_2O; H-CCNF in D_2O; D-CCNF in D_2O and D-CCNF in H_2O. Scattering data is obtained for each of these contrasts and an appropriate model can be used to fit to the data. The more contrasts prepared the more accurate the fit to the model will be. However, in our case it was very difficult and extremely costly to obtain deuterated cellulose thus only the two contrasts could be studied (H-CCNF in H_2O; H-CCNF in D_2O).

Appropriate selection of the model used to fit the scattering data is important for accurate fits of model parameters to data. Various models were tested, beginning with a simple rigid cylinder, but the best fit was found to be a flexible, ellipsoidal cylinder model. This model is of a number of locally stiff, ellipsoidal cross-section rods, defined by the key parameters: cross-section minor radius, r_a; axis ratio, r_b; and Kuhn length, b. SANS data alone were not sufficient to fully describe the structure and interaction of CCNF as the SANS instrument used (SANS2d) could only probe Q-ranges of $0.02 < Q\ nm^{-1} < 20$ (Q representing reciprocal space), which corresponds to real space sizes of 0.25-300 nm. Although CCNF cross-sections are only a few nm, the fibril lengths are >100 µm, much larger than the accessible Q-range could probe. Instead, a combination of techniques was used to provide a complete picture to best understand the structure and molecular interactions between modified nanofibrils.

5.1 Statement of Authorship

<table>
<tr><th colspan="10">This declaration concerns the article entitled:</th></tr>
<tr><td colspan="10">Unravelling cationic cellulose nanofibril hydrogel structure: NMR spectroscopy and small angle neutron scattering analyses</td></tr>
<tr><td colspan="10">Publication status (tick one)</td></tr>
<tr><td>Draft manuscript</td><td></td><td>Submitted</td><td></td><td>In review</td><td></td><td>Accepted</td><td></td><td>Published</td><td>✓</td></tr>
<tr><td>Publication details (reference)</td><td colspan="9">Courtenay, J. C., Ramalhete, S. M., Skuse, W. J., Soni, R., Khimyak, Y. Z., Edler, K. J., & Scott, J. L. (2018). Unravelling cationic cellulose nanofibril hydrogel structure: NMR spectroscopy and small angle neutron scattering analyses. Soft Matter, 14(2), 255-263. DOI: 10.1039/C7SM02113E</td></tr>
<tr><td>Candidate's contribution to the paper (detailed, and also given as a percentage).</td><td colspan="9">Formulation of ideas:
The manuscript was initially prepared by JCC (90%) with technical input for NMR data from colleagues at University of East Anglia (UEA). The manuscript was edited alongside JLS and KJE.

Design of methodology:
SANS data was acquired and fitted by JCC (100%). Analysis of SANS data was discussed with supervisors

Experimental work:
CCNF modifications, small angle neutron scattering and transmission electron microscopy were carried out by JCC (100%). This included sample preparation, data collection and analysis. Rheological studies and conductometric titrations were performed by WJS (an undergraduate project student) under the guidance of the candidate and data were analysed by JCC.

Figure 2, 3, 7, 8, 9; NMR studies were part of a collaborative project between the University of Bath and University of East Anglia. The candidate regularly visited the NMR facilities at UEA to work with SMR to conduct ^{13}C solid state, ^{1}H solution-state, HR-MAS NMR experiments. JCC worked alongside collaborators to analyse NMR data (50%).

Presentation of data in journal format:
100% of figures were prepared by JCC.</td></tr>
<tr><td>Statement from candidate</td><td colspan="9">This paper reports on original research I conducted during the period of my Higher Degree by Research candidature</td></tr>
<tr><td>Signed</td><td colspan="5"></td><td>Date</td><td colspan="3"></td></tr>
</table>

5.2 Abstract

Stiff, elastic, viscous shear thinning aqueous gels are formed upon dispersion of low weight percent concentrations of cationically modified cellulose nanofibrils (CCNF) in water. CCNF hydrogels produced from cellulose modified with glycidyltrimethylammonium chloride, with degree of substitution (DS) in the range 10.6(3) – 23.0(9) %, were characterised using NMR spectroscopy, rheology and small angle neutron scattering (SANS) to probe the fundamental form and dimensions of the CCNF and to reveal interfibrillar interactions leading to gelation. As DS increased CCNF became more rigid as evidenced by longer Kuhn lengths, 18 – 30 nm, derived from fitting of SANS data to an elliptical cross-section, cylinder model. Furthermore, apparent changes in CCNF cross-section dimensions suggested an "unravelling" of initially twisted fibrils into more flattened ribbon-like forms. Increases in elastic modulus (7.9 – 62.5 Pa) were detected with increased DS and ^{1}H solution-state NMR T_1 relaxation times of the introduced surface -$N^{+}(CH_3)_3$ groups were found to be longer in hydrogels with lower DS, reflecting the greater flexibility of the low DS CCNF. This is the first time that such correlation between DS and fibrillar form and stiffness has been reported for these potentially useful rheology modifiers derived from renewable cellulose.

5.3 Introduction

Cellulose fibres can be processed into an array of nanoparticles including nanocrystals, nanowhiskers, and micro- and nanofibrils.[1] An array of mechanical nanofibrillation methods, enzymatic pretreatments and chemical modifications have been applied to yield so-called 'nanofibrillated' cellulose, as summarised in the comprehensive review by Kalia *et al*.[2] First described by Rånby in 1951,[3] cellulose nanocrystals and nanowhiskers are usually prepared by strong acid hydrolysis of cellulose fibres to yield stiff rod-like, crystalline cellulose nanoparticles with diameters ranging from 2 to 20 nm.[4–6] These nanoparticles have an axial elastic modulus greater than that of Kevlar, and thus are of interest in the composite materials industry,[7] however, up to 80 % of the cellulose mass is lost during the hydrolysis process. As an alternative method to produce nanoparticulate cellulose Saito *et al.* demonstrated that oxidation, followed by relatively gentle shear, led to aqueous dispersions of oxidised cellulose nanofibrils with a cross-section of 3 – 5 nm.[8,9] This method results in conversion of between 80 and 90 % of the input cellulose into the product nanofibrils.

Well dispersed cellulose nanocrystals and nanofibrils have been widely used to form hydrogels,[10,11] which are cross-linked by physical interactions (van der Waals forces), chain entanglement, hydrogen bonds, and hydrophobic and electrostatic interactions. In addition to the significantly enhanced yields of cellulose nanofibrils (CNF) achieved by dispersion following chemical modification, such as oxidation, hydrogels can be formed by dispersion of small quantities of CNF in water. As the nanofibrils have a very large aspect ratio and retain a degree of fibril flexibility, these can be induced to form gels at low weight percent inclusion.[12] Many reports have appeared of chemical modification of hydroxyl groups exposed on the surface of cellulose materials, leading to new applications for cellulose as a biomaterial,[13] drug delivery vehicle[14] or water purifying agents[15] and there is a wide array of chemistry that can be applied to derivatisation of exposed hydroxyl groups including: oxidation,[16] grafting of cationic tetralkylammonium groups,[17] sulfonation,[18] silylation,[19] acylation,[20] grafting of a range of substituents through ester linkages[21] (generated by reaction with acid anhydrides,[22] or chlorides[23]), and formation of polyurethane linkages by reaction with isocyanates[24] (Scheme 5.1). Modification of the surface exposed hydroxyl groups leads to disruption of the non-covalent interactions between bundled cellulose fibrils, allowing dispersion of the

individualised CNF in water leading to formation of hydrogels.[25] The driving force for the formation of modified cellulose hydrogels is the molecular self-assembly of nanofibrils through electrostatic repulsion of charged functional groups, hydrophobic interactions and hydrogen bonds.[26]

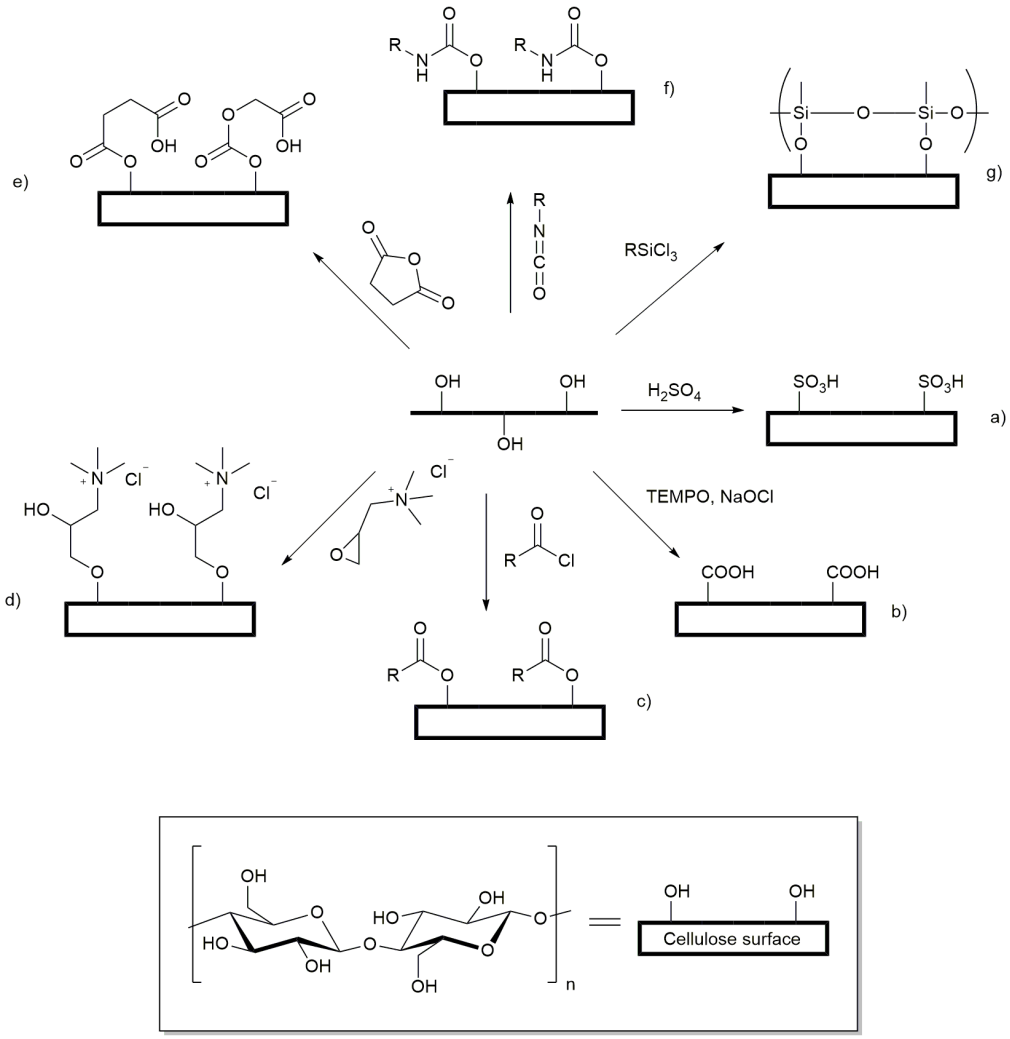

Scheme 5.1 Examples of some chemical modifications possible by reaction of the hydroxyl groups exposed on the surface of cellulose nanofibrils: a) sulfonation; b) (2,2,6,6-tetramethylpiperidin-1-yl)oxyl (TEMPO) mediated oxidation; c) ester formation by reaction with acid chlorides; d) grafting of tetra-alkylammonium groups by reaction with glycidyltrimethylammonium chloride (GTMAC); e) grafting via ester linkages generated by reaction with acid anhydrides; f) formation of urethanes by reaction with isocyanates; and g) silylation.

Two simple to execute and easily scaled up reactions allow production of charged cellulose fibrils: derivatisation with GTMAC[17,27] or TEMPO-mediated oxidation[8,9,28] provide positively charged tetra-alkylammonium groups and potentially negatively charged carboxylate groups, respectively. Both modifications enhance the dispersibility of the functionalised CNF in water. For brevity these modified CNF are

henceforth referred to as cationic cellulose nanofibrils (CCNF) and oxidised cellulose nanofibrils (OCNF).

A wide range of techniques has been used to characterise the surface modification of these nanofibrils: infrared (IR) spectroscopy and zeta-potential measurements are commonly used to identify the new functional groups present and determine whether the surface charge has changed.[17,29–31] The degree of derivatisation (oxidation or substitution) is determined through an acid-base titration for oxidised cellulose and conductometric titration with $AgNO_3$ for cationic cellulose.[16,27,32] Recently, Kono & Kusumoto demonstrated that the degree of substitution (DS) on CCNFs could be calculated through quantitative ^{13}C solid-state NMR studies, thus supporting conductometric measurements.[33] Furthermore, small angle neutron scattering can be used to determine the cross-section shape and dimensions of the nanofibrils as well the structure of hydrogels.[12,34]

While the structure of OCNF and hydrogels formed from OCNF dispersions have been extensively probed,[8,9,20,28,35,36] CCNF based hydrogels are less well described. These would not be predicted to be interchangeable; CCNF bear fixed positive charges in the form of tetra-alkylammonium groups, while the carboxylate moieties on OCNF may be protonated, or coordinated with a range of metal ions. In spite of the body of research into the characterisation of cationic cellulose nanofibrils, *e.g.* quantifying DS and effect of DS on gelation and CCNF dimensions,[17,27,37] there is little understanding, at the molecular level, of CCNF surfaces and inter-nanofibril interactions. Herein we describe the influence of DS on physical interactions of CCNF probed using a combination of NMR spectroscopy, rheology and small angle neutron scattering to provide greater understanding of these nanoparticle surfaces and interactions.

5.4 Experimental Procedures

5.4.1 Materials and methods

α-Cellulose powder (C8002), sodium hydroxide pellets (≥98 %), glycidyltrimethylammonium chloride (≥90 %), 0.1 M $AgNO_3$ aqueous solution (≥95 %), and HCl (reagent grade) were purchased from Sigma-Aldrich UK and used as received. Aqueous solutions of $AgNO_3$, NaOH and HCl were made up to the required concentrations with deionised (DI) water. Sodium polyethylene sulfonate (1 mM, average M_w 9,000 – 11,000 g mol^{-1}) solution was supplied by Carisbrooke. Deuterium oxide (D_2O) was purchased from Goss Scientific.

5.4.2 Surface modification by derivitisation

Cationic cellulose: Following the semi-dry procedure described by Zaman,[17] α-cellulose was activated by mixing with 5 wt. % (relative to α-cellulose weight, corrected for residual moisture content, determined by thermogravimetric analysis (TGA) to be *ca.* 5 %) of powdered NaOH using a mortar and pestle for 5 min. The mixture was transferred to a polyethylene bag followed by addition of 36 wt. % DI water (relative to α-cellulose dry weight) and an appropriate measured quantity of GTMAC (α-cellulose:GTMAC molar ratios of 3:1, 2:1, 1:1, 1:2 and 1:3) was added drop-wise to the mixture, the paste was kneaded to homogenise the reactants and reacted at 65 °C for 75 min followed by purification by dialysis (Mw cut-off 12400 $gmol^{-1}$) against copious quantities of DI water (refreshed regularly) for 72 h. The product was concentrated by centrifugation, the supernatant discarded and a sample freeze dried and accurately weighed to determine solids content.

Conductometric titration: Two conductometric titration methods were used to determine DS, the molar percentage of tetra-alkylammonium chloride groups per anhydroglucose unit (AGU) in the bulk product: 1) titration of chloride ions with $AgNO_{3(aq)}$, as described previously[13] and 2) using a Mütek Particle Charge Detector (BTG) measuring the streaming potential of 0.25 wt. % cationic cellulose in DI water titrated against a 1 mM sodium polyethylene sulfonate solution, following a method previously described for poly(diallyldimethylammonium chloride),[38] repeated for volumes of 0.25, 0.50 and 1.0 cm^3 of the CCNF suspensions.

Titre volume (V_t), titrant concentration (C_t), molar mass of AGU (M_c = 162.15 g mol^{-1}), molar mass of substituent group (M_s = 151.63 g mol^{-1}), cationic cellulose

suspension volume (V_c), suspension concentration (C_c) from the Mütek titration and TGA water content values (T_w) were used to determine the DS of the sample. Substituent mole equivalent per g ($Seq\ g^{-1}$) was determined from plotting molar charge equivalent (*eq)* against weight of cellulose (*g)* with the gradient as $eq\ g^{-1}$. The degree of substitution can be calculated using Equation 1:

$$DS\ \% = \left[\frac{(Seq\ g^{-1} * M_c)}{(1 - Seq\ g^{-1} * M_s)}\right] \text{x}100 = \left[\frac{(mol.substituents)}{(mol.AGU)}\right] \text{x}100 \qquad \text{(Eq. 1)}$$

Characterisation: FTIR spectra for α-cellulose and CCNF (DS = 23.0(9) %) powders were obtained on a Perkin Elmer Spectrum 100 spectrometer with a universal ATR sampling accessory; ten scans were acquired in the range 4000 – 600 cm^{-1} (Figure. D.1, Appendix D). Prominent bands at 1440 cm^{-1} and 1483 cm^{-1} were attributed to the CH_2 bending mode and methyl groups of the moieties arising from GTMAC reaction in accordance with data previously published.[17]

Transmission electron microscope (TEM) images of CCNF were obtained on a JEOL JEM-2100Plus instrument with an operating voltage of 200 kV. Before image acquisition, samples were deposited on copper grid and negatively stained with uranyl acetate.

5.4.3 CCNF stabilised hydrogels

Hydrogel formation: Bulk, never-dried CCNF dispersion (6.40 wt. %, concentration accurately measured) was diluted with DI water to yield 4 wt. %, 2 wt. % and 1 wt. % dispersions which were homogenised using an IKAT18 basic Ultra-Turrax high speed homogeniser at 13,500 rpm for 15 min. Dispersion to form hydrogels was completed by sonication using a VibraCell ultrasonicator (Sonics and Materials) at a power output of 45 $W.cm^{-2}$ using 1 s on/off pulses for 2 min. Dispersions were stored at 4 °C until required.

Hydrogel rheology: Dynamic rheology of the CCNF hydrogels was studied using a Gemini Advanced Cone and Plate Rheometer (Bohlin Instruments); distance between cone and plate 150 µm and cone angle 4°. CCNF 2 wt. % suspensions with DS ranging between 10.6 – 23.0 % were analysed with gel samples placed on the 40 mm diameter plate and allowed to relax for 5 min prior to measurement. An oscillatory shear sweep (0.01 – 10 Hz) was used to determine the dynamic viscosity (η'), elastic storage modulus (*G*') and loss modulus (*G''*). A thixotropic loop was

performed by measuring the shear viscosity over a ramp of 0.01 – 150 s^{-1} followed by return to 0.01 s^{-1} with zero strain applied.

5.4.4 Cationic cellulose nanofibril characterisation

Nuclear Magnetic Resonance (NMR) spectroscopy: Solid-state NMR spectroscopy was used to detect the presence of functional groups on the CCNF. These experiments were conducted using a Bruker Avance III spectrometer equipped with a 4 mm wide bore probe and operating at ^{1}H and ^{13}C frequencies of 400.23 and 100.65 MHz, respectively. Hydrogels were transferred into Kel-F inserts using a needle and syringe. Lyophilised cationic and α-cellulose powders were packed directly into zirconia rotors. ^{1}H-^{13}C cross-polarisation magic angle spinning (CP/MAS) NMR experiments of hydrogels were performed using recycle delays of 20 s, 1094 scans and MAS rates of 5 kHz. ^{1}H-^{13}C CP/MAS NMR experiments of reference powders were performed using recycle delays of 20 s, 256 scans and MAS rates of 5 kHz (Figure D.5). CP kinetics curves were measured using contact times from 0.005 to 10 ms and were fitted to Equation 2:[39]

$$I(t) = I_0(1 - T_{IS}/T_{1\rho}^{I})^{-1}\left[exp\left(-\frac{t}{T_{1\rho}^{I}}\right) - exp\left(-\frac{t}{T_{IS}}\right)\right] \qquad \text{(Eq. 2)}$$

where *I(t)* is the peak intensity, I_0 is the absolute intensity, T_{IS} is the cross-polarisation time constant and $T^{I}_{1\rho}$ is the longitudinal relaxation time in the rotating frame. The degree of substitution was calculated using Equation 3, in accordance with the methodology published by Kono *et al*.[33]

$$Degree\ of\ Substitution = \frac{\frac{I_{C10}}{3}}{I_{C1}} \times 100 \qquad \text{(Eq. 3)}$$

where I_{C10} and I_{C1} are the ^{13}C peak intensities of signals due to the three methyl carbon atoms (C10) and AGU anomeric carbon atom (C1), respectively, from the fitted curves. All experiments were conducted at 25 °C except where otherwise stated. Hartmann-Hahn conditions were optimised using hexamethylbenzene and all spectra were referenced to external tetramethylsilane (TMS).

High-resolution magic angle spinning (HR-MAS) NMR experiments were conducted using a Bruker Avance III spectrometer operating at a ^{1}H frequency of 800.23 MHz equipped with a 4 mm probe, using Kel-F inserts as above. ^{1}H HR-MAS NMR spectra

were acquired using a recycle delay of 5 s and MAS rates ranging from 2 to 10 kHz. ^{1}H longitudinal relaxation times (T_1) experiments were performed using an inversion recovery pulse sequence with a recycle delay of 10 s. Sixteen points were recorded at variable time delays ranging from 0.1 to 20 s. ^{1}H T_1 times were calculated from fitting the evolution of intensities to the mono-exponential function, Equation 4:

$$\mathrm{M_z}(\tau) = \mathrm{M_0} * \left[1 - 2\mathrm{e}^{\left(\frac{-\tau}{T_1}\right)}\right] \qquad \text{(Eq.4)}$$

where M_z is the z-component of magnetisation, M_0 is the equilibrium magnetisation and τ is the time delay.

Solution-state NMR experiments were carried out using a Bruker Avance I spectrometer operating at a ^{1}H frequency of 499.69 MHz equipped with a 5 mm triple resonance probe. Samples of hydrogels (500 µL) were transferred into NMR tubes using a needle and syringe. Variable temperature experiments were carried out in the range between 5 and 45 ^{o}C. ^{1}H T_1 relaxation times were measured using an inversion recovery pulse sequence with a recycle delay of 10 s. Sixteen points were recorded at variable time delays ranging from 0.1 to 20 s.

Zeta-potential characterisation: A DTS1070 Zetasizer cell was filled with 0.5 mL of dilute CCNF dispersions, ~0.1 wt.% and placed in a Zetasizer Nanoseries. Electrophoresis was induced in the sample by applying an electric field across the suspension of CCNF. The electrophoretic mobility of the CCNF in the electric field was used to calculate the zeta-potential by applying the Henry Equation, 5:

$$U_E = \frac{2\varepsilon z f(K\alpha)}{3\eta} \qquad \text{(Eq.5)}$$

where z is zeta-potential, U_E is electrophoretic mobility, ε is the dielectric constant, η is viscosity and $f(K\alpha)$ is Henry's function. Electrophoretic determinations of zeta-potential are most commonly made in aqueous media and moderate electrolyte concentration, thus, $f(K\alpha)$ in this case is 1.5 (referred to as the Smoluchowski approximation). The cell temperature was set to 25 ^{o}C, the zeta-potential measured in triplicate (based on twenty measurements per sample) for each CCNF of specific DS and the average value reported.

Small angle neutron scattering (SANS): SANS measurements were carried out on the Sans2d beamline at the ISIS Neutron and Muon Source, Science and Technology

Facilities Council, Rutherford Appleton Laboratory, Didcot, UK.[40] Hydrogels were placed in a 1 mm thick, 1 cm wide quartz cell with Teflon stoppers, holding ~0.3 mL. The Q range measured was 0.0046 – 1.3634 Å. To probe the structure of CCNF gels, contrast matching SANS experiments were performed using CCNF/H_2O and CCNF/D_2O. Scattering patterns were reduced using routines in the Mantid software package to correct for the scattering of air and the sample holder (rendering the data instrument independent) and a background of H_2O/D_2O subtracted before the data was analysed using SaSview 2.1 fitting software. Various models were tested, beginning with a simple rigid cylinder, but the best fit was found to be a flexible, ellipsoidal cylinder model. The flexible, ellipsoidal cylinder model is described in full by Chen *et al.*[41] and Dreiss.[42] In short, this model is of a number of locally stiff, ellipsoidal cross-section rods, defined by the cross-section minor radius, r_a, the axis ratio, r_b/r_a, persistence length, lp, and the contour length, L (Figure 5.1). The Kuhn length, b = 2*lp, is a measure of stiffness. Scattering length densities (SLDs) were fixed (cellulose 1.76 x 10^{-6}, H_2O -5.62 x 10^{-7}, D_2O 6.34 x 10^{-6} $Å^{-2}$) and, as the aspect ratios of CNF are very large,[43] fibril length does not impact scattering patterns in the Q range accessed, thus L was fixed at 10,000 Å (full fitting parameters, Table D.1, Appendix D).

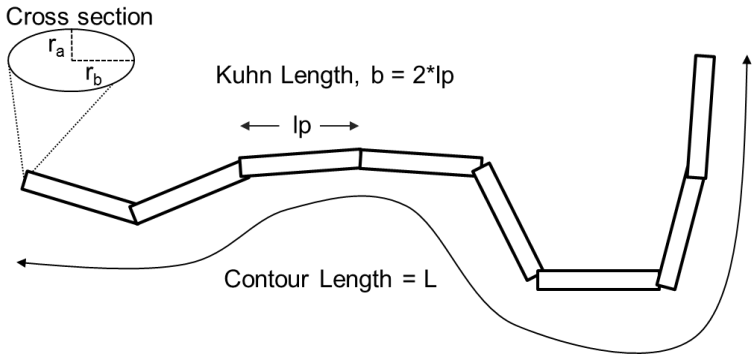

Figure 5.1 Schematic of the flexible, ellipsoidal cylinder model as applied to CCNF. The Kuhn length was used to describe the stiffness of the nanofibrils dispersed in the hydrogel.[44]

5.5 Results

5.5.1 Surface modification and characterisation

The nucleophilic substitution of alkali activated primary alcohol groups exposed on the cellulose surface with GTMAC resulted in cationisation of the nanofibrils, leading to a positive surface charge (Scheme 5.1, reaction d). Increasing molar ratio of GTMAC:AGU resulted in proportionally higher DS (from 10.6 % at 0.5 mole *eq* GTMAC to 23.0 % at 3 mole *eq* GTMAC). A yield of 88 %, based on cellulose dry mass, was achieved for the cationisation process at the highest DS. The degree of surface modification was controlled by modulating the quantity of GTMAC and the DS of cellulose nanofibrils assessed using FTIR and conductometric titration (Figure D.1-3, Appendix D). Solid-state NMR spectroscopy was used to confirm the presence of the $–N^{+}(CH_3)_3$ groups, introduced by reaction with GTMAC, on the surface of the nanofibrils (carbon C_{10} in Figure 5.2). Moreover, a very good agreement was found between the DS calculated from conductometric and NMR spectroscopy experiments (Figure 5.3). The CCNF zeta-potential increased upon cationisation from 38.8 to 50.3 mV as the $–N^{+}(CH_3)_3$ groups graft to the surface (Figure 5.3). Additionally, comparison of ^{13}C-NMR signals, arising from C4, in crystalline and amorphous forms, revealed no discernable change in crystallinity upon cationisation[45] (crystallinity index = 0.38) (Figure D.4).

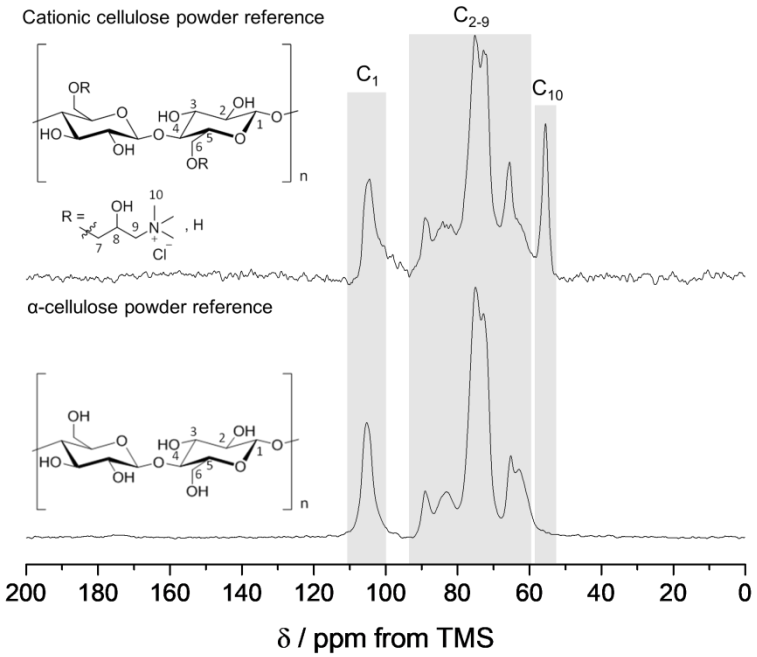

Figure 5.2 ^{1}H-^{13}C CP/MAS NMR spectra for α-cellulose and CCNF (DS 23.0%) powders, acquired using MAS rates of 10 kHz. The signal at 55.5 ppm is assigned to the methyl carbon resonances of the quaternary ammonium group and used to determine DS.

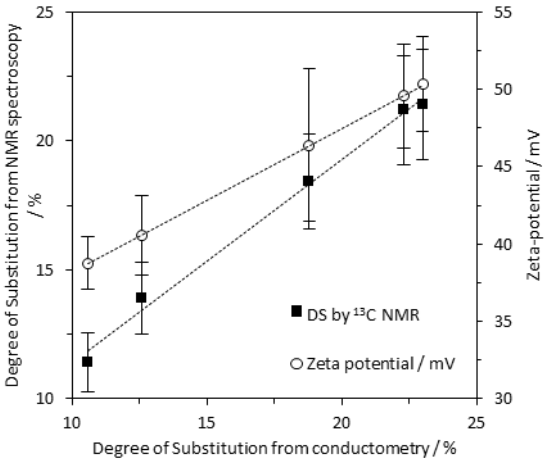

Figure 5.3 Black squares: DS determined from ^{13}C solid state NMR spectra according to equation 3 is in good agreement with the DS determined by conductometry (trend line R^2 = 0.99). White circles: zeta-potential for dispersed CCNF in DI H_2O as DS increases (trend line R^2 = 0.99 and gradient = 0.93).

5.5.2 Characterisation of functionalised nanofibrils

To compare the effect of DS of the CCNF on the structure of the dispersed CCNF gel, SANS with contrast matching was employed. This is a non-invasive technique used to obtain structural information from the samples *in situ*, based on SLD differences. For each CCNF hydrogel system, the H_2O/D_2O contrasts were plotted and the model simultaneously fitted to both sets of SANS data (Figure 5.4 and Figure D.6-9, Appendix D). The resultant ellipsoidal cross-section flexible cylinder model provided information pertaining to CCNF cross section and fibril stiffness, Table 5.1.

Table 5.1 Summary of fitted parameters for nanofibrils with increasing % DS derived from simultaneously fitting D_2O and H_2O contrasts to a flexible ellipsoidal cylinder model.[a]

DS / %	radius / Å	axis ratio	Kuhn length / Å
10.6(3)	14(1)	2.1(3)	175(8)
12.6(1)	11.6(8)	3.2(6)	230(14)
18.8(2)	6.7(8)	8.4(2)	303(22)
23.0(9)	6.3(8)	6.6(1)	296(21)

[a] Parameters held constant were: background, contour length (10,000 Å), sldCyl (1.75×10^{-6}) and sldSolv ($D_2O = 6.34 \times 10^{-6}$ and $H_2O = -5.61 \times 10^{-7}$)

The CCNF cross-section dimensions were observed to change with increasing DS. The minor radius, r_a, derived from the model changes from 1.4 nm to 0.6 nm and the axis ratio, r_b/r_a, from 2.1 to 6.6, giving fibril cross-section dimensions of 2.8 x 5.9 nm for CCNF with DS = 10.6 % and 1.2 x 8.3 nm for CCNF with DS = 23.0%. These dimensions are in broad agreement with previous reports[37] and the changes imply that the fibrils become wider and flatter as surface derivatisation increased. An increase in the Kuhn length from 18 to 30 nm (Table 5.1, Figure 5.5) was observed with increasing DS, ascribed to "stiffening" of the fibrils arising from charge repulsion as the density of surface $-N^+(CH_3)_3$ groups increased. We return to discussion of the implication of the apparent flattening discerned from SANS measurements later.

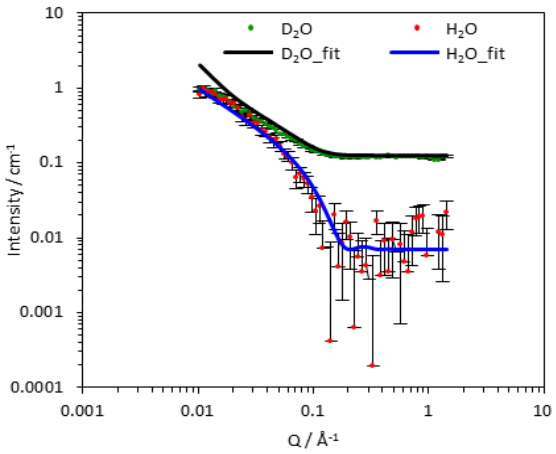

Figure 5.4 Experimental SANS spectra of cationic cellulose hydrogels (10.6 % DS) fitted to a flexible ellipsoidal cylinder model (scattered points are measured data and solid lines are the simultaneously fitted curves) in D_2O (green points, black line) and H_2O (red points, blue line). This model describes the CCNF particles as flexible fibrils.

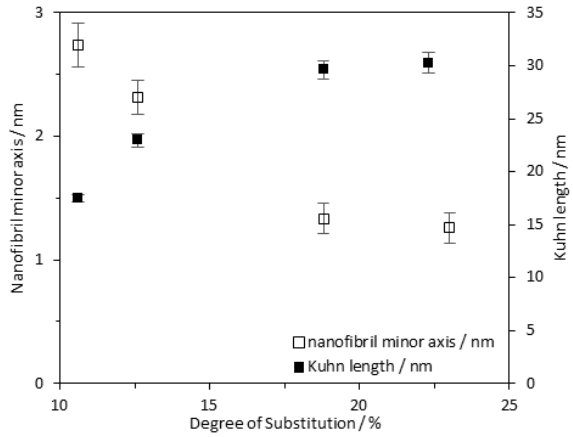

Figure 5.5 CCNF dimensions determined from the simultaneously fitted D_2O/H_2O data to the model nanofibril diameter and nanofibril Kuhn length.

5.5.3 CCNF hydrogel rheology

The rheological properties of the hydrogels formed by dispersion and sonication of CCNF in water were measured as a function of varying DS using both oscillatory sweep and thixotropic loop experiments. It was apparent that, as the CCNF DS increased, the hydrogels became stiffer (Figure 5.6a). Furthermore, a relationship between hydrogel elastic storage modulus and Kuhn length was observed, (Figure 5.6b), pointing to a change in the nature of the hydrogel associated with changes in shape and stiffness of the CCNF.

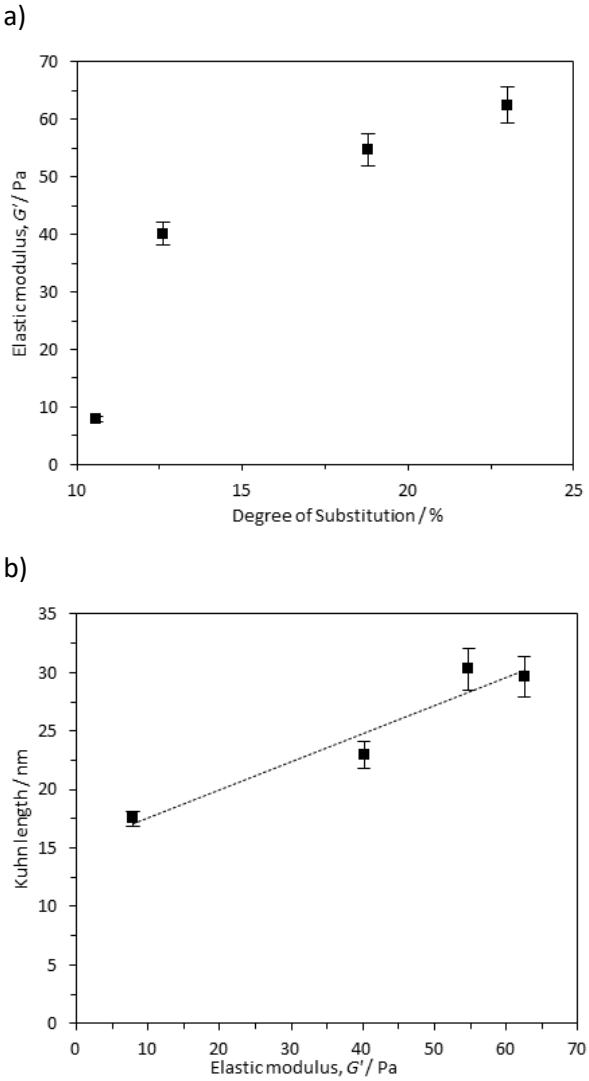

Figure 5.6 a) Influence of cationic cellulose nanofibril DS on the elastic storage modulus and b) Kuhn length of the 2 wt. % cationised cellulose hydrogels, R^2 = 0.9306.

Table 5.2 Summary of hydrogel rheology for cationised cellulose. DS values; complex (*G**), elastic (*G*') and viscous (*G*'') moduli; phase angles (δ); viscosities (η); and yield stresses (τ^0) of the aqueous gels obtained. Oscillatory rheological data were obtained for 2 wt. % hydrogels at 1.02 Hz and shear sweep data at shear rate 113.17 s^{-1}.

DS / %	*G** / Pa	δ / °	*G*' / Pa	*G*'' / Pa	η / Pas	τ^0 / Pa
10.6	8.3	18.6	7.9	2.7	0.1	3.8
12.6	40.8	10.1	40.4	7.2	0.3	38.1
18.8	55.3	7.4	54.8	7.1	0.3	49.5
23.0	63.4	9.5	62.5	10.5	0.4	53.3

Complex modulus increased for hydrogels formed from CCNF with greater DS, while phase angle decreased (Table 2, Figure. S10 – 13)), i.e. gels became more elastic.

5.5.4 Probing local mobility of surface functional groups using ^{1}H NMR relaxation measurements

^{1}H Longitudinal relaxation times (T_1) of the hydrogels formed were measured as a function of varying DS, using solution-state and HR-MAS NMR experiments. Signals arising from the ^{1}Hs of the $–N^+(CH_3)_3$ moiety were used for quantification as these were distinct, while other signals were overlapped (Figure D.14-16). Relaxation profiles of these ^{1}Hs are affected by molecular motions and are thus a suitable probe for the effect of DS on local viscosity. To investigate the dependence of ^{1}H longitudinal relaxation times on the mobility of the cationic groups, the hydrogel with a DS of 23.0 % was subjected to varying temperatures. In the temperature range employed, ^{1}H solution-state NMR T_1 times for the $–N^+(CH_3)_3$ and water protons increased with temperature (Table D.2), indicating that these hydrogels are in the "slow tumbling regime".[46] The slower relaxation profiles observed at higher temperatures reflected increased motional freedom. Comparing fibrils with variable DS: longer ^{1}H T_1 values were recorded in hydrogels with a lower DS (10.6 %) in comparison with hydrogels with higher DS (23.0 %) (Figure 5.7 & 8). Therefore, it was possible to conclude that the quaternary ammonium groups and water molecules were more mobile in hydrogels with lower DS, showing that the local mobility of the grafted quaternary ammonuim group depends on the DS.

Interestingly, an inverse relationship was found between DS and ^{1}H HR-MAS T_1 values of $–N^+(CH_3)_3$ and water acquired with different MAS rates (Figure 5.9 and

D.17). While the spectra did not change dramatically (Figure D.17), the ^{1}H T_1 times increased when all the samples were subjected to higher spinning speeds, possibly reflecting shear thinning behaviour in these CCNF hydrogels. This effect was more evident for hydrogels with lower DS (10.6 %). The shear force produced by the spinning rates used was significantly greater than that required to "break" the gels (as evidenced by the rheology data presented in Table 5.2 and Figure D.9-12), so it is hypothesised that there are multiple levels of CCNF interaction. When monitoring ^{1}H T_1 times of the $-N^{+}(CH_3)_3$ group we are only assessing the local mobility of the groups grafted onto the surface of the fibres. During rheology studies these local environments do not change significantly, as it is the macrostructure and mesostructure of the gel that are most affected by the external stress. The ^{1}H relaxation time measurements suggest that, along with the changes at mesoscale reflected by the rheological properties, local mobilities of both water and grafted $-N^{+}(CH_3)_3$ groups on the CCNF are reduced with increased strength of the hydrogels.

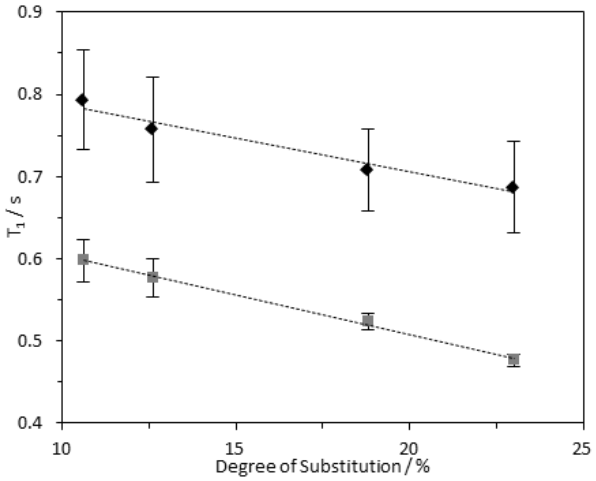

Figure 5.7 ^{1}H solution-state (grey square data series) and HR-MAS NMR (black diamond data series) T_1 times for $-N^{+}(CH_3)_3$ group ^{1}Hs in 4 wt. % CCNF hydrogels with DS 10.6 – 23.0 %, acquired at 25 °C. HR-MAS experiments were conducted with an MAS rate of 2 kHz

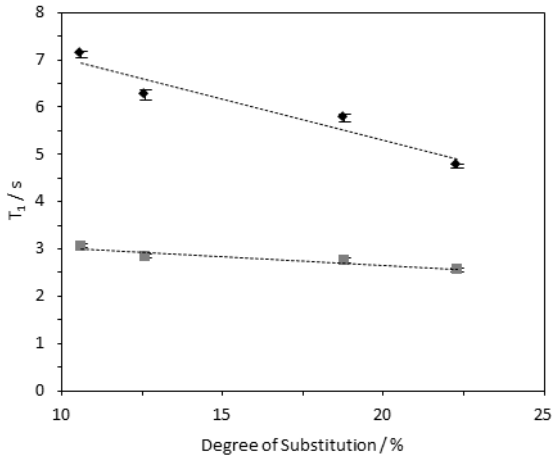

Figure 5.8 ^{1}H solution-state (grey square data series) and HR-MAS NMR (black diamond data series) T_1 times for water ^{1}Hs in 4 wt. % CCNF hydrogels with DS 10.6 – 23.0 %, acquired at 25 °C. HR-MAS experiments were conducted with an MAS rate of 2 kHz.

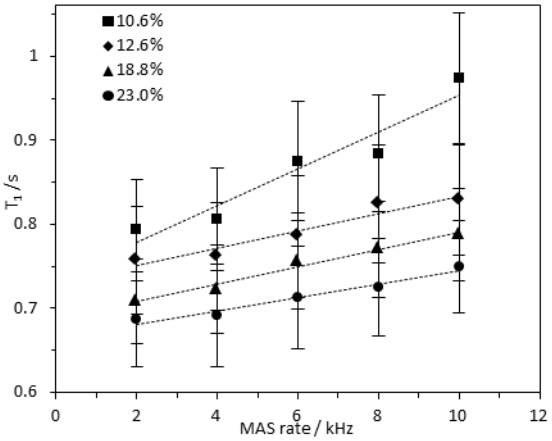

Figure 5.9 ^{1}H HRMAS T_1 times for $-N^+(CH_3)_3$ group ^{1}Hs in 4 wt. % CCNF hydrogels with increasing DS, acquired with MAS rates between 2 and 10 kHz.

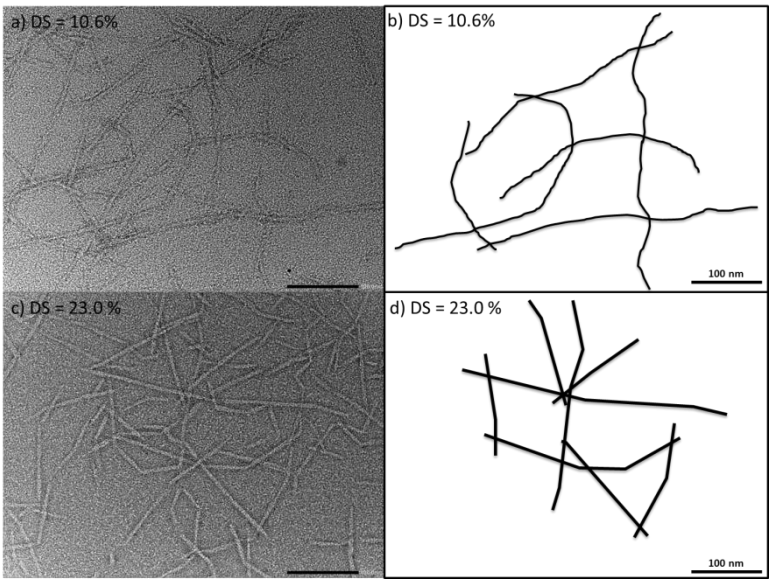

Figure 5.10 TEM images of CCNF after dispersion in water (a and c) and traces of selected fibrils (b and d). Fibril cross-section diameters are similar to those derived from SANS data fitting. a) Low DS = 10.6 %, scale bar = 100 nm, b) trace of low DS CCNF, c) High DS = 23.0 %, scale bar = 100 nm and d) trace of high DS CCNF. As DS increases, a change in the morphology of the CCNF is observed with low DS fibrils appearing more flexed and higher DS fibrils straighter. The traces are provided to highlight the change in morphology between the two CCNF.

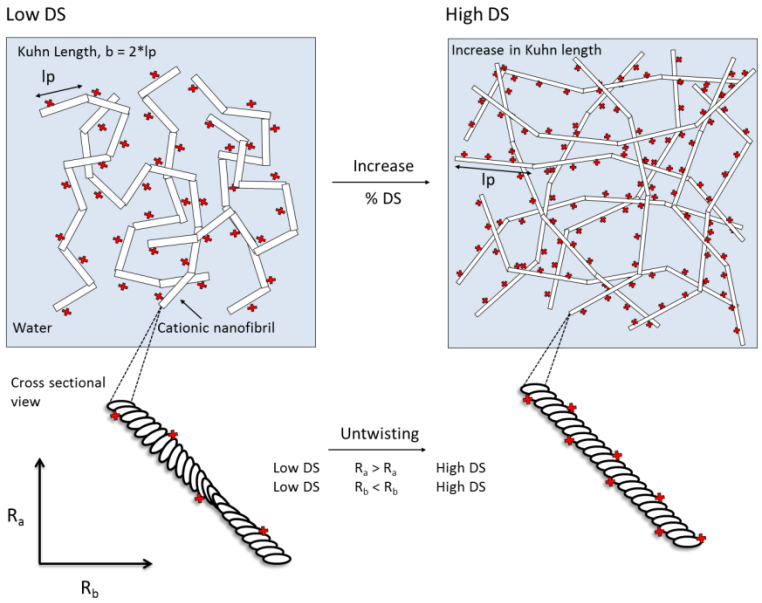

Figure 5.11 A schematic illustrating the postulated change in CCNF morphology as DS increases, reflecting SANS data fitting and TEM images. As the DS on the surface of the nanofibrils increases, so too does the Kuhn length, resulting in more rigid nanofibrils. The CCNF also untwist to form more flattened ribbon-like nanofibrils - stiffer, more elastic hydrogels result (lp = persistence length and 2*lp = Kuhn length).

5.6 Discussion

Stable hydrogels were formed upon the dispersion of cationically surface modified cellulose nanofibrils in water. The physical interactions of the surfaces of CCNF were investigated using NMR, SANS and rheology to reveal the fundamental form of the particles and structuring in the hydrogels.

The presence of tetra-alkylammonium moieties arising from grafting with GTMAC was confirmed by ^{1}H-^{13}C CP/MAS solid-state NMR (Figure 5.2), which revealed a peak at 55.5 ppm, corresponding to the three methyl group carbon atoms of the quaternary ammonium moiety. Very good agreement was obtained for the values of DS obtained from conductometric titration measurements (*versus* $AgNO_3$, or sodium polyethylene sulfonate solutions) and quantitative NMR analysis (Figure 5.3).

As previously reported,[37] the modified nanofibrils were much more dispersible in DI water than the α-cellulose precursor, but remained largely water insoluble (DS was limited to <25 % to minimise formation of soluble CCNF[47]). Moreover, while all CCNF prepared formed stable hydrogels in water following dispersion by sonication, nanofibrils with higher DS were more readily dispersed and formed stiffer and more elastic gels. The linear relationship, with gradient close to unity, between DS and zeta-potential (Figure 5.3) suggested that the etherification to install cationic groups was largely limited to the nanofibril surfaces. The maximum theoretical DS achievable for surface functionalisation, calculated following Habibi *et al.*,[35,16], was *ca* 32 %, thus the CCNF produced here may not reflect full nanofibrillar surface saturation. Further, the unchanging crystallinity index suggested that the bulk structure of the elemental nanofibril remained untouched by the modification (Figure D.4).

SANS was used to probe the CCNF cross-section and to elucidate the gel structure and nanofibril interactions. The reduced scattering data was fitted to a flexible ellipsoidal cylinder model, which describes the CCNF as a fibril with somewhat flattened cross-section and varying degrees of flexibility. Further, results suggest that charge repulsion between the positively charged nanofibril surfaces serve to facilitate defibrillation, producing individualised fibrils, which become stiffer with increasing DS, as evidenced by an increase in Kuhn length (Figure 5.5) and supported by TEM images (Figure 5.10), showing flexed fibrils in samples with low DS and distinctly straighter fibrils in high DS materials. As with oxidised cellulose nanofibrils,

the very high fibrillar aspect ratio[43] provides a particulate network, forming hydrogels. The nanofibrillar cross-section dimensions measured are consistent with values reported for cationic cellulose nanofibrils, determined by AFM and Cryo-TEM[37] and the theoretical range of unmodified cellulose crystallites of 1.5 – 2 nm by 3 – 5 nm, based on the 36-glucan-chain elementary model of the cellulose Iβ structure,[48] although the 24-glucan chain elementary fibril postulated by Fernandes *et al*.[49] could lead to thinner forms.

The level of surface modification present on the dispersed nanofibrils influenced the rheology of the resultant hydrogels. CCNF with higher DS formed stiffer hydrogels reflected in higher elastic storage moduli (Figure 5.6a, Table 5.2). As this change in rheological behaviour was also mirrored in the increased stiffness of the dispersed nanofibrils (Kuhn length) and a change in apparent cross-section, it is postulated that this change in hydrogel structure arises from:

1. Increased charge repulsion with increased DS leading to loss of flexibility and straightening and stiffening of fibrils along their length - reflected in longer Kuhn lengths and decreased mobility of surface $-N^{+}(CH_3)_3$ groups, and

2. Untwisting, or unravelling, of CCNF to form flatter, more ribbon-like structures at higher DS, reflected in changes in cross-section shape and diameter– surface charge repulsion caused CCNF to untwist into flattened ribbon-like fibrils as DS increased.

The changes in rheological behaviour of CCNF hydrogels with different DS can be correlated with the changes in local mobility of grafted quaternary ammonium groups and water molecules monitored by ^{1}H T_1 relaxation times. Thus, low DS CCNF gels result from entanglement of long twisted flexible fibrils, which become less twisted and more rigid as DS increases (Figure 5.10). Entanglement of these stiffer units leads to stiffer, more elastic hydrogels.

It is well documented that cellulose nanofibrils possess a twist along the AGU chain axis: computational modelling (molecular dynamics) has been used to demonstrate that cellulose nanofibrils adopt a half twist every 3 – 4 nm along the chain axis;[50,51,52] this twisting has also been observed by AFM and TEM analyses and is especially apparent in well-dispersed ribbon-shaped bacterial cellulose.[53,54] We suggest that

the introduction of a positive surface onto the cellulose causes nanofibrils to untwist due to charge repulsion along the surface (Figure 5.11). Furthermore the values for Kuhn length (18 – 30 nm) are similar to those previously reported for cellulose ~10 – 20 nm (using a similar model)[55] and ~50 – 60 nm for oxidised cellulose nanofibrils (determined from peak force quantitative nanomechanical mapping).[56]

This hypothesis for the apparent change in CCNF structure is supported by the rise in hydrogel elastic moduli of 7.9 – 62.5 Pa. These hydrogels are highly thixotropic as the viscosity decreases rapidly as the shear rate increases. Increasing the oscillation frequency gave increased complex modulus and decreased phase angle values, associated with increasing elastic behaviour with decreasing perturbation time. As the DS increased, both the elastic and viscous moduli values increased, but the elastic modulus, already much higher, increased to a greater extent, which is a good indication of structuring within the hydrogel.

5.7 Conclusion

Combining results from neutron scattering experiments, rheological measurements and analysis of ^{1}H NMR T_1 relaxation times of the water and grafted $–N^{+}(CH_3)_3$ groups, changes in the form of cationised cellulose nanofibrils and structuring in hydrogels formed therefrom is revealed.

With increased degree of reaction with GTMAC, the density of positively charged moieties on the surface of the CCNF increases, leading to charge repulsion and stiffening of the fibrils. Physical entanglement of these stiffer CCNF results in stiffer, but more fragile, gels. Changes in the apparent cross-section dimensions of the individualised fibrils, derived from fitting of SANS data, are postulated to reflect untwisting of the fibrils. Thus, low DS CCNF are characterised by fibrils that are twisted and flexed, and which entangle to form weak hydrogels, while higher DS CCNF fibrils are more rigid, flatter, ribbon-like structures that result in stiff, elastic viscous shear thinning hydrogels.

5.8 Acknowledgments

We acknowledge ISIS for the provision of beamtime for the SANS experiments (experiment number RB1520375) and Dr Richard K. Heenan for their assistance in setting up the SANS2D instrument during the experiment. S.M.R thanks the University of East Anglia for her postgraduate studentship. Y.Z.K., K.J.E. and J.L.S. acknowledge financial support from the EPRSC and Innovate UK - from the grants EP/N033337/1 and EP/N033310/1. TEM images were obtained at the Microscopy and Analysis Suite in Bath University with the assistance of Ursula Potter. J.C.C. thanks Vincenzo Calabrese for his assistance with rheology analysis. This research was partly supported by funding from the EPSRC Centre for Doctoral Training in Sustainable Chemical Technology (EP/L016354/1), in the form of a PhD studentship for J.C.C. Additional research data supporting this publication are available as electronic supplementary files at the DOI: 10.1039/c7sm02113e.

5.9 References

1. D. Klemm, F. Kramer, S. Moritz, T. Lindström, M. Ankerfors, D. Gray, and A. Dorris, *Angew. Chemie - Int. Ed.*, 2011, **50**, 5438–5466.

2. S. Kalia, S. Boufi, A. Celli, and S. Kango, *Colloid Polym. Sci.*, 2014, **292**, 5–31.

3. B. G. Rånby, *Discuss. Faraday Soc.*, 1951, **11**, 158–164.

4. F. Alloin, A. Dufresne, and M. A. S. A. Samir, *Biomacromolecules*, 2005, **6**, 612–626.

5. Y. Habibi, L. A. Lucia, and O. J. Rojas, *Chem. Rev.*, 2010, **110**, 3479–3500.

6. G. Siqueira, J. Bras, and A. Dufresne, *Polymers (Basel).*, 2010, **2**, 728–765.

7. R. J. Moon, A. Martini, J. Nairn, J. Simonsen, and J. Youngblood, *Chem Soc Rev*, 2011, **40**, 3941–3994.

8. T. Saito, S. Kimura, Y. Nishiyama, and A. Isogai, *Biomacromolecules*, 2007, **8**, 2485–91.

9. T. Saito, Y. Nishiyama, J. L. Putaux, M. Vignon, and A. Isogai, *Biomacromolecules*, 2006, **7**, 1687–1691.

10. T. Saito, T. Uematsu, S. Kimura, T. Enomae, and A. Isogai, *Soft Matter*, 2011, **7**, 8804.

11. X. Shen, J. L. Shamshina, P. Berton, G. Gurau, and R. D. Rogers, *Green Chem.*, 2015, **18**, 53–75.

12. R. J. Crawford, K. J. Edler, S. Lindhoud, J. L. Scott, and G. Unali, *Green Chem.*, 2012, **14**, 300–303.

13. J. C. Courtenay, M. A. Johns, F. Galembeck, C. Deneke, E. M. Lanzoni, C. A. Costa, J. L. Scott, and R. I. Sharma, *Cellulose*, 2017, **24**, 253–267.

14. J. You, J. Cao, Y. Zhao, L. Zhang, J. Zhou, and Y. Chen, *Biomacromolecules*, 2016, **17**, 2839–2848.

15. A. Pei, N. Butchosa, L. a. Berglund, and Q. Zhou, *Soft Matter*, 2013, **9**, 2047.

16. T. Saito and A. Isogai, *Biomacromolecules*, 2004, **5**, 1983–9.

17. M. Zaman, H. Xiao, F. Chibante, and Y. Ni, *Carbohydr. Polym.*, 2012, **89**, 163–70.

18. Y. Habibi, *Chem. Soc. Rev.*, 2014, **43**, 1519–1542.

19. C. Goussé, H. Chanzy, G. Excoffier, L. Soubeyrand, and E. Fleury, *Polymer (Guildf).*, 2002, **43**, 2645–2651.

20. J. F. Sassi and H. Chanzy, *Cellulose*, 1995, **2**, 111–127.

21. Y. Habibi, A.-L. Goffin, N. Schiltz, E. Duquesne, P. Dubois, and A. Dufresne, *J. Mater. Chem.*, 2008, **18**, 5002–5010.

22. J. K. Pandey, W. S. Chu, C. S. Kim, C. S. Lee, and S. H. Ahn, *Compos. Part B Eng.*, 2009, **40**, 676–680.

23. A. Junior de Menezes, G. Siqueira, A. A. S. Curvelo, and A. Dufresne, *Polymer (Guildf).*, 2009, **50**, 4552–4563.

24. G. Siaueira, J. Bras, and A. Dufresne, *Biomacromolecules*, 2009, **10**, 425–432.

25. S. P. Akhlaghi, R. C. Berry, and K. C. Tam, *Cellulose*, 2013, **20**, 1747–1764.

26. C. Chang and L. Zhang, *Carbohydr. Polym.*, 2011, **84**, 40–53.

27. M. Hasani, E. D. Cranston, G. Westman, and D. G. Gray, *Soft Matter*, 2008, **4**, 2238–2244.

28. A. Isogai, T. Saito, and H. Fukuzumi, *Nanoscale*, 2011, **3**, 71–85.

29. M. Hasani, E. D. Cranston, G. Westman, and D. G. Gray, *Soft Matter*, 2008, **4**, 2238–2244.

30. J. L. Ren, R. C. Sun, C. F. Liu, Z. Y. Chao, and W. Luo, *Polym. Degrad. Stab.*, 2006, **91**, 2579–2587.

31. A. Isogai, T. Saito, and H. Fukuzumi, *Nanoscale*, 2011, **3**, 71–85.

32. D. da Silva Perez, S. Montanari, and M. R. Vignon, *Biomacromolecules*, 2003, **4**, 1417–25.

33. H. Kono, K. Ogasawara, R. Kusumoto, K. Oshima, H. Hashimoto, and Y. Shimizu, *Carbohydr. Polym.*, 2016, **152**, 170–180.

34. K. Edler, D. Celebi, Y. Jin, and J. Scott, *Acta Crystallogr. Sect. A*, 2014, **70**, C1320.

35. Y. Habibi, H. Chanzy, and M. R. Vignon, *Cellulose*, 2006, **13**, 679–687.

36. N. Masruchin, B.-D. Park, V. Causin, and I. C. Um, *Cellulose*, 2015, **22**, 1993–2010.

37. A. Olszewska, P. Eronen, L.-S. Johansson, J.-M. Malho, M. Ankerfors, T. Lindström, J. Ruokolainen, J. Laine, and M. Österberg, *Cellulose*, 2011, **18**, 1213–1226.

38. R. Pelton, B. Cabane, Y. Cui, and H. Ketelson, *Anal. Chem.*, 2007, **79**, 8114–8117.

39. W. Kolodziejski and J. Klinowski, *Chem. Rev.*, 2002, **102**, 613–628.

40. R. K. Heenan, S. M. King, D. S. Turner, and J. R. Treadgold, in *17th Meeting of the International Collaboration on Advanced Neutron Sources*, 2005, pp. 1–6.

41. W. Chen, P. D. Butler, and L. J. Magid, *Langmuir*, 2006, **22**, 6539–6548.

42. C. A. Dreiss, *Soft Matter*, 2007, **3**, 956.

43. Q. Li and S. Renneckar, *Cellulose*, 2009, **16**, 1025–1032.

44. T. Strey, Description of the Model Functions, http://danse.chem.utk.edu/downloads/ModelfuncDocs.pdf, (accessed2006.

45. R. H. Newman, *Holzforschung*, 2004, 58, 91.

46. C. L. Cooper, T. Cosgrove, J. S. van Duijneveldt, M. Murray, and S. W. Prescott, *Soft Matter*, 2013, **9**, 7211–7228.

47. L. Yan, H. Tao, and P. R. Bangal, *Clean - Soil, Air, Water*, 2009, **37**, 39–44.

48. S.-Y. Ding and M. E. Himmel, *J Agric Food Chem*, 2006, **54**, 597–606.

49. A. N. Fernandes, L. H. Thomas, C. M. Altaner, P. Callow, V. T. Forsyth, D. C. Apperley, C. J. Kennedy, and M. C. Jarvis, *Proc. Natl. Acad. Sci. U. S. A.*, 2011, **108**, 1195–1203.

50. K. Conley, L. Godbout, M. A. Whitehead, and T. G. M. Van De Ven, *Carbohydr. Polym.*, 2016, **135**, 285–299.

51. S. Paavilainen, T. Róg, and I. Vattulainen, *J. Phys. Chem. B*, 2011, **115**, 3747–3755.

52. Z. Zhao, O. E. Shklyaev, A. Nili, M. Naseer, A. Mohamed, J. D. Kubicki, V. H. Crespi, and L. Zhong, *J. Phys. Chem. A*, 2013, **117**, 2580–2589.

53. S. Elazzouzi-hafraoui, Y. Nishiyama, L. Heux, F. Dubreuil, C. Rochas, and J. Putaux, *Biomacromolecules*, 2008, **9**, 57–65.

54. S. Hanley, J.-F. Revol, L. Godbout, and D. Gray, *Cellulose*, 1997, **4**, 209–220.

55. C. G. Lopez, S. E. Rogers, R. H. Colby, P. Graham, and J. T. Cabral, *J. Polym. Sci. Part B Polym. Phys.*, 2015, **53**, 492–501.

56. I. Usov, G. Nyström, J. Adamcik, S. Handschin, C. Schütz, A. Fall, L. Bergström, and R. Mezzenga, *Nat. Commun.*, 2015, **6**, 7564.

Chapter 6:

6 Paper 6: Mechanically robust cationic cellulose nanofibril scaffolds with tuneable biomimetic porosity for cell culture

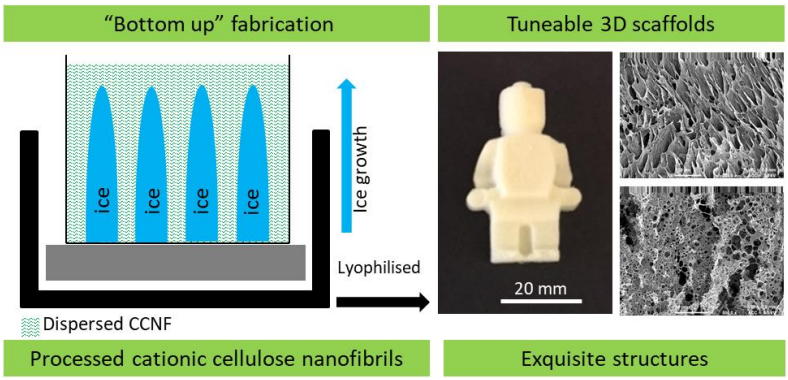

6.0 Publication Commentary

Thus far scaffolds studied in this thesis have been flat membrane or films with modified surfaces. In order to grow larger cell constructs 3D scaffolds needed to be developed. In the previous chapter the production of CCNF that disperse in H_2O to form stable hydrogels were described. These hydrogels could be used as a viscous medium to suspend non-adherent cell lines, or lyophilised, to yield 3D porous aerogel or "foam" structures. These are "bottom-up" approaches to the development 3D scaffolds. Decellularisation of plant tissue is an example of "top-down" production of cellulose based materials for cell scaffolds. The benefits and limitations of these approaches are discussed in the next chapter and the "bottom-up" approach was chosen for the generation of 3D materials, as this offers more flexibility in tuning the properties through chemical modifications, as well as in the preparation of complex forms, e.g. mimicking organs or organ parts.

Building on findings in the previous chapter, CCNF hydrogels were directionally frozen and lyophilised, leaving porous foams with aligned macro-channels as well as fine structures, to be investigated as 3D scaffolds. The remaining cationic cellulose network was delicate and it quickly became apparent that further modifications were required to obtain materials with suitable mechanical strength to withstand manual handling and hydration in cell culture media, whilst maintaining internal porosity. It was demonstrated that these foams could be reinforced using the glyoxalisation modification described previously.

It was deemed desirable to characterise the internal porosity of the materials, as porosity is beneficial for increasing the mass transfer of nutrients and O_2 to the cells as well as for the removal of waste products. There are several methods commonly used to probe pores within a solid including: small angle X-ray scattering, mercury porosimetry and gas adsorption. However, these techniques require the sample to be dehydrated and some can only measure accessible pores. Here a technique that could be used to probe the pore size in the hydrated form was required, as cellulose is known to swell when hydrated and this reflects the environment that the cells experience. To probe the internal porosity of hydrated samples at the meso- and macro-scale a combination of scanning electron microscopy, NMR cryoporometry and NMR relaxometry was used.

A major challenge faced was how to visualise and quantity the number of cells on the scaffolds. SEM was used to visualise cells attached to the surface of the scaffold, but this is a time intensive procedure, which can disrupt the cell cytoskeleton, and can only be used to assess the cells on the surface. Previously we have used the fluorescent dye, 4',6-diamidino-2-phenylindole (DAPI), to stain the nuclei of attached cells to calculate a percentage of cells attached. Confocal florescent microscopy was tested to try and image the cells throughout the scaffold using a z-stack. However, due to the opacity of the material we were unable to obtain suitable florescent images. Another method considered for identification of the cells within the scaffold was X-ray micro-tomography. This was investigated, but the scattering due to the cells was too similar to that of the cellulose scaffold to allow location of cells or determination of cell number.

Instead, a cell metabolic assay was used as a proxy for cell number. The MTT, 3-(4,5-dimethylthiazol-2-yl)-2,5-diphenyltetrazolium bromide, assay is a colorimetric assay for assessing cell metabolic activity. Soluble MTT is reduced enzymatically in the cell to form insoluble formazan crystals, which are purple in colour and can be dissolved in solvent and absorption intensity measured at 570 nm. There are several follow-up studies that could be conducted to compliment the metabolic assay including rezasurin or picogreen cell assays, which allow measurement of the cell metabolism or quantify DNA present respectively. Rezasurn is a blue non-destructive assay and the dye is reduced in the cell to form resorufin, which is pink and highly red fluorescent. The picogreen assay allows quantification of DNA from the cells on the scaffold, a value which can be calibrated to provide a cell number. These assays could provide further insight into the viability of cells on the modified cellulose 3D scaffolds..

6.1 Statement of Authorship

<table>
<tr><th colspan="10">This declaration concerns the article entitled:</th></tr>
<tr><td colspan="10">Mechanically robust cationic cellulose nanofibril scaffolds with tuneable biomimetic porosity for cell culture</td></tr>
<tr><td colspan="10">Publication status (tick one)</td></tr>
<tr><td>Draft manuscript</td><td></td><td>Submitted</td><td></td><td>In review</td><td></td><td>Accepted</td><td></td><td>Published</td><td>✓</td></tr>
<tr><td>Publication details (reference)</td><td colspan="9">Courtenay, J. C., Filgueirass, J. G., Riberio de Azevedo E., Jin, Y., Edler, K. J., Sharma, R. I. and Scott, J. L., (2018) J. Mater. Chem. B. Accepted Manuscript DOI:10.1039/C8TB02482K</td></tr>
<tr><td>Candidate's contribution to the paper (detailed, and also given as a percentage).</td><td colspan="9">Formulation of ideas:
This paper builds on the candidate's previous work using hydrogels of dispersed cationic cellulose nanofibrils to form a range of 3D scaffolds for tissue engineering. One of the methods to introduce aligned porosity, via freeze drying directionally frozen hydrogels, had been identified by YJ, KJS & JLS previously for oxidised cellulose hydrogels. Only a single point of concept experiment had been conducted by YJ.(JCC contribution 90%).The manuscript was written by JCC and editorial feedback was provided by supervisors. JGF and ERA gave technical input for NMR relaxometry analysis.

Design of methodology:
Experiments were discussed and planned with supervisors. NMR relaxometry studies were discussed with collaborators at IFSC, Brazil. (JCC contribution 90%).

Experimental work:
Most (80 %) of the experimental work was conducted and analysed by the candidate. NMR relaxometry studies were performed at IFSC, Brazil by JF & ERA after several telecom meetings taking place to plan the necessary experiments.

Presentation of data in journal format:
80% of figures were prepared by the candidate. The data for Figure 4 and Table 2 was acquired by JGF & ERA at IFSC and analysed in telecom meetings between collaborators.</td></tr>
<tr><td>Statement from candidate</td><td colspan="9">This paper reports on original research I conducted during the period of my Higher Degree by Research candidature</td></tr>
<tr><td>Signed</td><td colspan="6"></td><td>Date</td><td colspan="2"></td></tr>
</table>

6.2 Abstract

3D foam scaffolds were produced in a “bottom-up” approach from lyophilised cationic cellulose nanofibril (CCNF) dispersions and emulsions (CCNF degree of substitution 23.0 ±0.9 %), using a directional freezing /lyophilisation approach, producing internal architectures ranging from aligned smooth walled micro channels, mimicking vascularised tissue, to pumice-like wall textures, reminiscent of porous bone. The open, highly porous architecture of these biomimetic scaffolds included mesopores within the walls of the channels. A combination of SEM and NMR cryoporometry and relaxometry was used to determine the porosity at different length scales: CCNF foams with aligned channels had an average macropore (channel) size of 35 ±9 µm and a mesopore (wall) diameter of 26 ±2 nm, while CCNF foams produced from directional freezing and lyophilisation of Pickering emulsions had mesoporous walls (5 ±3 µm) in addition to channels (54 ±20 µm). Glyoxal crosslinking both enhanced robustness and stiffness, giving Young’s moduli of 0.45 to 50.75 MPa for CCNF foams with degrees of crosslinking from 0 to 3.04 mol. %. Porosity and channels are critical scaffold design elements for transport of nutrients and waste products, as well as O_2 / CO_2 exchange. The viability of MG-63 cells was enhanced on crosslinked, mechanically stiff scaffolds, indicating that these exquisitely structured, yet robust, foams could provide biomaterial scaffolds suitable for industrial applications requiring 3D cell culturing.

6.3 Introduction

Current demand for donor organs and tissues for transplantation vastly surpasses availability. For example, more than 100,000 US patients wait on the organ donor list in 2018 and, on average, 22 will die per day.[1] The goal of tissue engineering is to develop new cell constructs that can be implanted into a patient to restore function to the damaged organs.[2] This process requires a biocompatible scaffold to support the cells, often by mimicking the extracellular matrix (ECM), as these proliferate and grow into tissues.[3] Traditionally, adherent cells are cultured on a two-dimensional (2D) scaffold *in vitro*. Cells growing on 2D scaffolds tend to only be attached to the substrate at their periphery, which forces the cells into a monolayer culture, rather than promoting layering as would be found *in vivo*, as well as limiting the size of the cell population produced.[4] Once the cell layer has reached 100 % confluence (all available surface is covered), cell viability can decrease, and cell death can occur as mass transfer of nutrients and oxygen diffusion is limited to depths of 100-200 µm.[5] To retain cell viability beyond this depth, a vascularised network is required.[6–8] Furthermore, if primary keratinocytes are grown to 100 % confluence, the phenomenon of "terminal differentiation" can arise: cells receiving insufficient nutrients die and those that remain alive become senescent, limiting the size of the cell construct that can be grown on a 2D scaffold.

On the other hand, 3D scaffolds require internal porosity to mimic the vascular morphology of native tissue, facilitating transfer of nutrients and gases and allowing larger tissue fragments to be grown. Ideally, the scaffolds should be resorbed and replaced, over time, by the newly regenerated tissue at the site of implant.[9] A 3D arrangement of cells enables more complex cell-cell and cell-ECM interactions as cells are surrounded by ECM or scaffold, due to the greater surface area available for adhesion. Thus, cells cultured in a 3D scaffold more accurately mimic the response and behaviour of cells *in vivo*, beneficial for applications in both cell culturing for tissue engineering and as model tissues for drug development.[10]

Interconnecting porous networks can be used to promote cell growth, migration and mass transfer of nutrients.[11] Generally, a larger pore size is considered to be beneficial for improving both cell migration and nutrient flow, however, this decreases the specific surface area of the scaffold, in turn reducing the matrix ligand density available for cell binding. Instead of migrating into the bulk of the material,

cells tend to cluster around the edges of the scaffold. O'Brien *et al.*, demonstrated that increasing pore size from 96 to 151 µm increased nutrient permeability through scaffolds,[12] however, a pore size of between 20 and 120 µm was required for optimal balance between nutrient flow and ligand binding density.[11 12] Therefore, a compromise must be reached between the two factors, pore size and specific surface area, of a 3D scaffold.[13]

Decellularised tissue has been investigated as a "top-down" method of obtaining the complex tissue structure and ECM composition needed for tissue regeneration, whilst retaining the microvasculature (<10 µm in diameter) that cannot readily be fabricated by current techniques such as 3D printing.[14] Human donor or animal tissues can be used, but need to be sterilised and decellularised by enzymatic or detergent methods to remove the native cells and proteins. The remaining material is the ECM, which can vary in composition and structural properties, depending on the source.[8] It is important that the decellularising process does not disrupt the ECM or adversely affect the biological activity or mechanical integrity of the remaining structure.[15] The performance of the tissue can degrade with age and human tissue in particular, is in short supply.[16] Decellularised scaffolds based on plant tissue have been reported,[17] but, despite much of the vascularised structure being in place, scaffold shapes are limited to the shape of the plant tissue from which it was derived and further shape modulation is challenging.

Complementing the "top-down" approaches to the creation of porous 3D scaffolds, there are also a range of "bottom-up" methodologies to produce complex structures for cell culture, including: electrospinning polymer solutions to form 3D nanofiber meshes,[18,19,20] 3D printing of "bioinks" to fabricate complex scaffold architectures[21] and the lyophilisation of dispersions or solutions to produce open porous aerogels or foams.[22] Additive manufacturing approaches can reportedly give access to structures with minimum feature lengths of <100 µm,[21] while reverse templating can be used to achieve porosities of 50 – 85 % and interconnecting pores of 50 µm in size.[23,24]

There are several other "bottom-up" approaches to fabricate scaffolds suitable for applications in tissue engineering. For example, foam templating by generation of bubbles in solutions of polysaccharides containing surfactants,[25] followed by freeze drying and crosslinking with a carbodiimide cross-linker yields a porous structure

with pore diameters of 206 – 250 μm.[26] Foam templating routes have also been applied to poly(vinyl alcohol) solutions[27] and dextran-methacrylate solutions.[28] Scaffolds so produced present highly ordered pore arrays with uniform and tuneable pore sizes.[29] As pores are interconnected mass transfer of nutrients to cells within such scaffolds is enhanced.

Freeze drying, or lyophilisation, is a popular method to introduce porosity into the scaffold due to its low cost, simplicity and versatility.[22] In this process, ice crystals act as a porogen, leaving a porous structure post sublimation under vacuum.[30] The rate of cooling during the freezing step can affect the size and distribution of ice crystals formed and thus the size and form of the pores within in the resulting foam.[31] An advantage of using this technique is that water is commonly the solvent; hence impurities, such as surfactants, are not added during the lyophilisation stage, making it especially beneficial for biological applications. The introduction of emulsions, nanoparticles and dilute polymer solutions into the material can further modulate macro- and mesopore formation.[30] Ice crystals grown in a unidirectional fashion leave behind channels of aligned pores, mimicking the vascularity of native tissue[32] and can be applied to a range of scaffold materials, including: hydroxyapatite,[33] silk fibroin,[34] gelatin,[35] dextran[36], and, more recently, chitosan-alginate blends,[37] cellulose-chitosan blends,[38] and cellulose solutions.[39] The resultant scaffolds have the potential to expand the use of these materials from 2D films to 3D porous scaffolds and many authors suggest that the channels can promote vascularisation *in vivo*, although corroborating cell studies are only reported for some materials.

Scaffolds fabricated from cellulose, using both “top-down” and “bottom-up” approaches, have been tested in a range of cell culture applications.[40–43] Cellulose offers many beneficial attributes to tissue engineering, such as biocompatibility, versatile chemical and physical properties, and ease of processing. It is also a cost effective and sustainable material, which makes it suitable for industrial applications.[44–48] However, previous reports of directionally frozen/freeze dried cellulose hydrogels for scaffolds have largely focussed on the materials characterisation aspects – few reports of the growth of cells on these 3D scaffolds have appeared.[30, 31]

Previously, we have demonstrated that cellulose surfaces grafted with cationic moieties allow for attachment of MG-63 cells in the absence of matrix ligands.[49]

Here we use similarly modified nanofibrillar materials to develop novel porous 3D scaffolds that we suggest offer many advantages over “top-down” scaffolds such as those derived from decellularised plant tissue. In particular the use of a scalable method offering ease of manufacture, tuneable porosity and mechanical properties, to prepare materials that can be stored without special requirements, yet which mimic vascularised tissue, may provide supports beneficial for various cell culture applications.

6.4 Experimental Procedures

6.4.1 Materials and methods

Cellulose powder (C8002), sodium hydroxide pellets (≥98 %), glycidyl trimethylammonium chloride (GTMAC, ≥90 %), DMSO (≥99 %), 1-ethyl-3-methylimidazolium acetate (97 %), cyclohexane (99.5 %), absolute ethanol (≥99 %) and *N*,*N*-dimethylacetamide (DMAc) were purchased from Sigma-Aldrich and used as received (except DMAc, which was dried over 3Å molecular sieves prior to use). For crosslinking modifications, glyoxal 40 % w/w aqueous solution was purchased from Alfa Aesar and made up to required concentrations with deionised (DI) water. Mobile phases for HPLC were prepared from H_2SO_4 (99.99%) and sodium phosphate monobasic monohydrate, sodium phosphate dibasic and sodium azide powders purchased from Sigma Aldrich.

For cell studies, Dulbecco's Modified Eagle Medium (DMEM, GlutaMAX™), non-essential amino acids, sodium pyruvate, trypsin (0.05 %) and trypan blue (0.4 %) were purchased from Gibco and stored at 4 °C. Foetal bovine serum (FBS, non-USA origin), MG-63 human osteosarcoma cells, and methylthiazolyldiphenyltetrazolium bromide (MTT) powder were purchased from Sigma-Aldrich. Phosphate buffer solution (PBS, 0.1 µm sterile filtered) was purchased from HyClone and penicillin streptomycin from Life Technologies. For cell fixation, a glutaraldehyde solution (25 wt. % in H_2O), hexamethyl-disilazane (HMDS, >99 %), dry acetone and 1 wt. % osmium tetroxide solution were purchased from Sigma Aldrich.

6.4.2 Surface modification by derivitisation

Cationic cellulose: Cellulose modified with GTMAC was prepared as described in reference [50], using 3 mol equivalents of GTMAC relative to cellulose anhydroglucose units. The resultant "cationic cellulose nanofibrils" are henceforth abbreviated as CCNF.

Characterisation: Fourier Transform Infrared (FTIR) spectra were obtained on a Perkin Elmer Spectrum 100 spectrometer with a universal ATR sampling accessory; 10 scans were acquired in the range 4000 – 600 cm^{-1}. FTIR measurements, used to confirm the molecular identity of the grafted moieties, have been previously substantiated by ^{1}H-^{13}C cross polarization / magic angle spinning NMR spectroscopy.[49] The degree of substitution (DS) of cationic cellulose was determined

to be 23.0 ±0.9 %, by conductometric titration, as described in reference [49] (Fig. E.1 – 3 and ESI). The degree of crosslinking (DXL) was between 1.2 and 3.0 %, as determined by HPLC analysis following a method adapted from Schramm *et al*.[51] (Fig. E.4-6).

6.4.3 3D scaffold formation

Foams: CCNF dispersions, 1, 2 and 4 wt. %, were prepared by homogenising lyophilised CCNF powder in DI water using an IKAT18 Ultra-Turrax high speed homogeniser at 13,500 rpm for 15 min. Dispersion to form hydrogels was completed by sonication using a Sonic Dismembrator Ultrasonic Processor (Fisher Scientific) with a 3.2 mm tip at a power output of 45 W cm^{-2} as 1 s on/off pulses for 2 min. Dispersions were stored at 4 ^{o}C until required. To form the crosslinked hydrogels, stock glyoxal solutions were prepared at 5, 10 and 20 wt. % in DI water. These were added to appropriate quantities of a 2 wt. % CCNF dispersion to yield 1 wt. % CCNF aqueous dispersions containing 2.5, 5 or 10 wt. % glyoxal. To introduce macropores into the structure of the hydrogel, oil-in-water emulsions were prepared using oil: aqueous phase volume ratio of 30:70. Typically, 0.3 mL of cyclohexane was mixed with 0.7 mL of CCNF aqueous dispersion (1 wt. % prepared as described above) and sonicated (45 W cm^{-2} as 1 s on/off pulses for 30 sec) to effect emulsion formation.

Cast films were flash frozen in liquid nitrogen prior to lyophilisation. CCNF hydrogels and emulsions were subjected to directional freezing: 250 µL of the sample was placed into the well of a 48 tissue culture well plate, which was set atop a metal block partially submerged in a bath of liquid nitrogen, resulting in directional growth of ice-crystals from the bottom of the sample. Once fully frozen, samples were lyophilised to remove the ice crystals. More complex shaped foams were produced by freezing the CCNF hydrogels in silicon moulds (Fig. E.7). The lyophilised foams containing glyoxal were heated in an oven for 1 h at 125 ^{o}C to allow the crosslinking reaction to proceed.

Films: CCNF powder (of mass required to yield a 4 wt. % final solution) was added to DMSO, forming a slurry, which was dispersed using an overhead stirrer (900 rpm) with a PTFE stirrer head for 5 min at room temperature. Ionic liquid EMImOAc, was added to yield 30:70 w/w, EMImOAc:DMSO, and the mixture stirred for 1 h at room temperature, resulting in a 4 wt. % CC solution. For comparison, a solution of unmodified cellulose (UC) was prepared using the same procedure.

CC and UC films were formed by casting the solutions described above onto a clean glass sheet using an Elcometer 3700 reservoir and an Elcometer 4340 Automatic film applicator, with a gap of 0.8 mm between the blade and glass surface. The films were regenerated by immersion in an ethanol anti-solvent bath for 24 h. Residual EMImOAc and DMSO were removed by Soxhlet extraction with ethanol overnight. The films were washed twice with copious amounts of DI water to remove excess EtOH before being stored in 20 wt. % MeOH solution to inhibit bacterial growth.

6.4.4 Scaffold Characterisation

NMR Cryoporometry: Using a procedure adapted from Johns *et al.*,[52] foam and film samples were hydrated in PBS overnight, excess PBS was removed, the samples placed in individual NMR tubes and sealed using damp absorbent paper to maintain humidity. The ^{1}H NMR signal was recorded on a 400 MHz Bruker Avance spectrometer equipped with a 5 mm BBO probe, running with the boil-off from liquid nitrogen as cooling gas, and a BVT3200 temperature control unit with a precision of ±0.1 K. Actual *versus* recorded temperatures had previously been verified using methanol.[53] A simple spin echo sequence was used, with an echo time of 2.2 ms, to ensure minimal suppression of signal from liquid water and complete suppression of signals from both cellulose materials and frozen water.[54,55] Measurements were performed by decreasing the temperature to 218 K in order to completely freeze the sample, followed by stepwise temperature increase in 5 K increments up to 258K, then in 1 K increments to 267 K, 0.2 K increments to 271 K, and finally to bulk melting temperature using a temperature step of 0.1 K. At each increment signals were recorded after establishment of thermal equilibrium, achieved by a waiting time of 20 min (Fig. E.8 – 13).

The melting point depression, ΔT, is related to the pore radius, r, via bulk properties of the probe liquid, P, as described by the Gibbs-Thomson equation:

$$\Delta T \propto {}^{P}/_{(r-s)} \qquad (1)$$

where P is 25 nm for water and s represents the thickness of a pre-molten liquid-like layer on the surface of the substrate, here assumed constant over the temperature range at two monolayers thick, *i.e.* 0.6 nm.[56,57]

NMR T_2 relaxation: NMR Carr−Purcell Meiboom−Gill (CPMG) experiments were performed using a Bruker Minispec MQ-20 spectrometer operating with a magnetic field of 0.5 T (^{1}H Larmor frequency of 20 MHz); 50,000 echoes were acquired with echo time of 70 μs and recycle delay of 15 s. The CPMG decay curves were processed to obtain the T_2 distribution using a non-negative least square procedure known as a numerical Inverse Laplace Transform, ILT.[58,59] The obtained T_2 distributions were deconvoluted using log-gaussian functions to provide the contribution of each component in the pore structure. Fluid bound in a pore interacts with the pore surface, restricting the molecular mobility of the fluid. Such restriction is reflected by a decrease of the transverse relaxation time, T_2, and can be quantified, in the fast diffusion regime, by the relation:[60,61]

$$1/T_2 = \rho\,(S/V) = 2\rho/r, \qquad (2)$$

where ρ is the surface relaxivity, which depends on the particular porous media and is usually unknown, and S and V are the pore surface area and volume respectively. In a realistic scenario, the distribution of pore sizes and differences in the fluid mobility within the pores result in a multiexponential decay of the CPMG signal, i.e., a distribution of T_2 times.

To assess the pore structure of the cellulose foams, DMAc (HPLC grade) was used as a molecular probe, due to its weak interaction with the cellulose structure. DMAc does not significantly modify the cellulose pore structure, while water, often used as molecular probe for relaxometry experiments, alters the pore distributions in biomass samples.[62] Lyophilised modified cellulose foams and films were dried under reduced pressure (640 mmHg) for 24 h at 80 ^{o}C. Samples were soaked in DMAc and kept in a desiccator under a 600 mmHg vacuum for 36 h, following which excess DMAc was removed by centrifuge filtration at 600 g for 1 min (Corning Costar Spin-X, 0.45 um, nylon membrane filter). All measurements were carried out in duplicate and the CPMG decay of the mean used in the ILT procedure (Fig. E.14 – 16).

Scanning electron microscopy: Field Emission Scanning Electron Microscopy (FESEM) was used to characterise the internal morphology and porosity of the different CCNF foams. A JEOL FESEM 6301F was used to image the surface of the foams as well as the cross section and internal structure of the lyophilised CCNF foams at ultrahigh resolution. To prepare the samples for surface imaging, the foams

were carefully adhered to a metal stub with double sided carbon tape. To obtain a cross section, the dried foams were frozen in liquid nitrogen, fractured using a very sharp blade and attached to the stubs, prior to vacuum drying for 24 h. All samples were sputter coated with a 20 nm layer of chromium in an argon environment prior to imaging. A high sensitivity backscattered electron detector was used for computational imaging. The samples were imaged at an acceleration voltage of 5 kV at magnifications between 50x and 25,000x.

6.4.5 Mechanical properties

Foams: The Young's moduli of the CCNF foams were determined using an Instron 3343 electromechanical test machine. CCNF (23.0 ±0.9 % DS) crosslinked with 0, 2.5, 5, and 10 wt. % glyoxal solutions were tested. The dry foams were placed between steel plates and a 1000 N load cell was used to deliver a compressive load at a rate of 1 mm min^{-1} to the foams until deformation or failure occurred. Four samples were tested per crosslinked foam and an average reported. The Young's modulus of the foams was calculated using the equation:

$$E = \frac{Stress}{Strain} = \frac{F/A}{\Delta L/L} \qquad (3)$$

where *F* is the compressive load, *A* is the sample area, *ΔL* is the degree of sample compression and *L* is the original sample height.

Films: The bulk elastic moduli of the regenerated cellulose scaffolds were determined using a Dynamic Materials Analyser (DMA1 STAR^e System, Mettler Toledo). The samples used were films regenerated from 4 wt. % cellulose and CCNF (DS = 23.0 ±0.9 %) solutions, with a range of crosslinking in both sets (DXL 0 to 3 %). Both hydrated "never-dried" and dried films were cut into strips ≥1.50 cm in length by 0.50 cm width and the thickness recorded using a steel digital vernier micrometer calliper. The film strips were gripped between titanium tension clamp sample holders and a preload force of 1 N applied to the sample. An offset of 10 µm was set at a frequency of 1 Hz and the elastic moduli were determined over 5 min. Five samples were tested for each film and an average reported.

6.4.6 Cell studies

Cell culture: MG-63 cells were cultured in DMEM supplemented with 10 % FBS, 1 % v/v non-essential amino acids, 1 % v/v sodium pyruvate and 1 % v/v penicillin streptomycin at 37 ^{o}C in a humidified incubator with 5 % CO_2. When MG-63 cultures reached 80% confluence (3 – 4 days) the cells were passaged and reseeded in a T75 flask at a density of 5,000 cells / cm^2 with fresh media.

Cell viability: Lyophilised foams, placed in 48 well tissue culture plates and sterilised using a Hoefer™ UVC 500 crosslinker at 254 nm for 15 min prior to being rehydrated and soaked in three 0.5 mL aliquots of PBS, to remove any unreacted crosslinker. MG-63 cells were used to assess the viability of the CCNF foams as cell scaffolds. The scaffolds were seeded with a cell density of 10,000 cells cm^{-2} (corresponding to a total cell number of 9,500 cells per sample) in growth media and placed in an incubator at 37 ^{o}C in 5 % CO_2 to proliferate for a given time. Tissue culture plastic was used as a control "scaffold" for the MTT assay and material controls were performed for each sample. N=8 replicates per sample were measured.

A MTT stock solution of 50 mg mL^{-1} in PBS was prepared. After appropriate incubation time (1, 4 and 7 days), the growth medium was replaced with 250 µL of 5 mg mL^{-1} MTT in growth medium and incubated for a further 4 h. The culture medium was gently removed from the well plate and 200 µL of DMSO added to dissolve the formazan crystals generated in this assay. Well plates were placed on a plate shaker and gently agitated for 10 min. The DMSO-formazan crystal suspension was transferred to a 96 well plate and the absorption intensity recorded at 570 nm and 690 nm, using a Biotek® Synergy HT plate reader. To determine the activity the following equation was used:

$$MTT\ activity = (S_{\ 570\ nm}) - (MC_{570\ nm}) \qquad (4)$$

where *S* is the absorption of the sample and *MC* is the material control, i.e., absorption due to the sample material *sans* cells at the given wavelengths.

Cell visualisation: First, cells were grown on CCNF and CCNF crosslinked (XL) scaffolds for 24 h in growth medium. A fixative solution was prepared by adding 2 mL glutaraldehyde (GDA at 25 wt. %) to 10 mL double strength cell culture medium (*sans* serum) and diluted to 20 mL with DI H_2O. This gave a fixative solution of 2.5 wt. % GDA in normal strength culture medium.

The culture medium was very slowly removed from the scaffold keeping the pipette at the edge of the scaffold away from the cells. The samples were gently washed in 2 x 1 mL fresh medium (normal strength culture medium without serum) again keeping the pipette at edge of the scaffold. The wash medium was removed as above, replaced with the fixative solution and left for 2 h. The samples were rinsed three times with 1 mL wash medium. The cells were post-fixed in aqueous 1 wt. % osmium tetroxide for 1 h in a fume hood at ambient temperature, then washed in 1 mL DI H_2O three times at 15 min intervals.

The cells were dehydrated by sequential washing with solutions of acetone in H_2O gradually increasing in acetone content to 100 % dry acetone. Specifically solutions of 50, 70, 90, 95% and 100% acetone in H_2O were applied to the cells (on scaffold) for 15 min, repeated three times for each concentration. Acetone was replaced with 1:1 dry acetone:HMDS solution for 15 min, followed by three sequential treatments with 100 % HMDS for 30 min each. Excess HMDS was removed and the samples allowed to air dry in a fume hood for 2 h prior to mounting onto SEM stubs.

FBS absorption: A phosphate buffer solution (mobile phase) was prepared by adding a solution of 13.8 g sodium phosphate monobasic monohydrate in 500 mL DI H_2O to 14.2 g sodium phosphate dibasic in 500 mL DI H_2O until the pH was 6.8. The slightly acidic solution was made up to 1 L with DI H_2O, 0.2 g of sodium azide added and the solution degassed. A solution of 10 wt. % FBS in PBS was prepared, 250 µL of the FBS solution was added to each sample and the plate stored in an incubator for 24 h. The amount of FBS absorbed onto the scaffold surface was determined using an Agilent Technologies 1260 infinity HPLC. A range of FBS solutions with concentrations in the range 0.1 to 30 wt. % were prepared and a calibration curve constructed. HPLC analysis: size exclusion column (TSKgel G4000 PWXL, 7.8 mm, 10 x 30 mm, 50 °C), mobile phase phosphate buffer (0.7 L min^{-1}), and UV detector. The amount of FBS present was calculated by subtracting the concentration present in the solution from the initial concentration of 10 wt. %.

6.5 Results and Discussion

Application of directional freezing and lyophilisation to aqueous dispersions of CCNF and CCNF stabilised oil-in-water Pickering emulsions, led to preparation of 3D cationic cellulose scaffolds in the form of foams with exquisite tuneable structure. Unidirectional ice crystal formation resulted in channels in the tens of micron range, mimicking vascular structures, and preservation of spherical pores arising from emulsions, yielded pumice-like wall textures, reminiscent of porous bone (Fig. 6.1).

Crosslinking, previously shown to enhance cell spreading[63] (indicative of cell viability and scaffold compatibility), was used to render the delicate structures robust enough for handling and repeated immersion in cell growth media, as would be required for use in tissue engineering applications.

To illustrate their utility as tissue culture scaffolds, the attachment and viability of MG-63 cells was assessed using MTT assays and SEM analysis to discern how well cells became integrated into the bulk of the putative scaffold material and whether or not these cells began to proliferate.

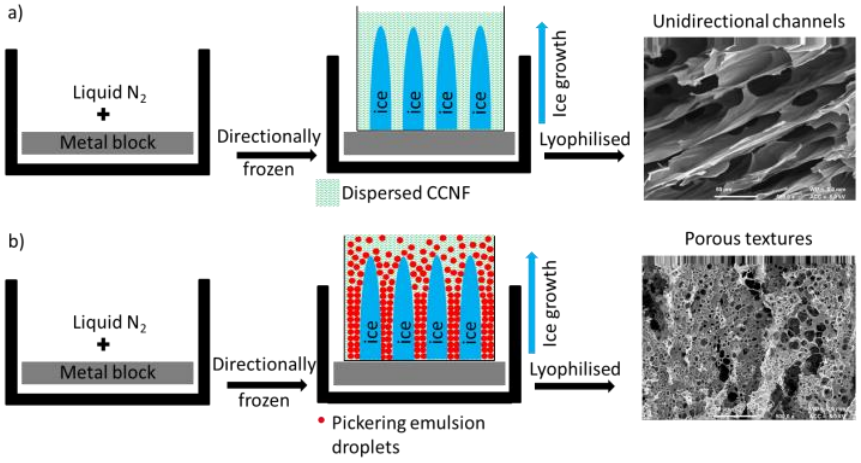

Figure 6.1 Directional freezing followed by lyophilisation process: a) CCNF dispersions b) CCNF stabilised oil-in-water Pickering emulsions

6.5.1 "Bottom-up" fabrication of vascularised 3D scaffolds

3D scaffolds, with variable form, internal architecture and robustness, were constructed using a "bottom-up" approach from "cationic cellulose", CC, bearing quaternary ammonium groups derived from glycidyl trimethylammonium chloride (GTMAC) grafting, either as CC nanofibrils, or dissolved and regenerated CC films.

To induce directional freezing, low weight % CCNF dispersions (weak hydrogels) were placed, in containers, on metal blocks immersed in liquid nitrogen. This resulted in exclusion of the CCNF into "walls" surrounding oriented ice crystals, which, upon lyophilisation, yielded aligned channels, reflecting the size of the ice crystals formed. Cyclohexane in water CCNF stabilised Pickering emulsions treated similarly resulted in both channel-like porosity and walls bearing much smaller pores, 3 – 5 μm in diameter, due to oil droplet templation of the hydrogel. These materials are designated "CCNF PE" henceforth.

Although the foams contained both aligned micro channels reflecting the longitudinal ice crystal growth, and pores, reflecting the emulsion structure, these were very delicate and easily compressed, or even dispersed. Even gentle agitation in cell culture medium caused the scaffolds to break apart, rendering these useless as scaffolds in cell culture applications. Hence, the foams were crosslinked to enhance robustness,[64] especially when hydrated, and to retain the complex internal architecture.

To reinforce these delicate porous materials, glyoxal, a crosslinker, was added to the CCNF dispersions and later reacted by heating, in order to fix the complex internal structure, through in situ glyoxalation – these materials are designated as "CCNF XL". In common with most reactive cross-linkers, unreacted glyoxal is cytotoxic, but once reacted to form acetal and hemiacetal linkages with cellulose, does not inhibit cell viability.[63] This modification served to support the delicate structures, maintaining the integrity of the vascularised or porous internal architecture, but it has also been shown previously that crosslinking further increases the spreading of attached MG-63 cells on cationised cellulose scaffolds.[63] Furthermore, modification of the mechanical properties of the scaffold can act as a stimulus to up-regulate physiological processes and signalling pathways within the cell cycle, thus promoting cell growth.[65,66] Thus, these materials could serve as very flexible scaffolds, allowing external shape/size, internal architecture, rigidity and robustness to be varied while also offering opportunities to modulate cell response, as described later.

6.5.2 Scaffold porosity

To determine the effect of lyophilisation and glyoxalisation on macroporosity, the CCNF, CCNF XL, and CCNF PE scaffolds were characterised using SEM and compared to regenerated lyophilised films (Fig. 6.2 and Fig. E.17 – 19). Structures accessible

ranged from unidirectional, vascularised materials with smooth walls (Fig. 6.2a), foamed walls (Fig. 6.2c) to more open pore structure materials (Fig. 6.2b), compared with regenerated cationic cellulose films (Fig. 6.2d). (For comparison, an SEM image and pore size distribution for unmodified cellulose films is included in the ESI (Fig E.19).) To determine the average pore size diameter SEM images were analysed using ImageJ software yielding the following average pore sizes: CCNF = 35 ±9 µm, CCNF XL = 60 ±20 µm, CCNF PE = 54 ±20 µm and 5±3 µm, and CC film = 20 ±10 µm. The presence of 5 wt. % glyoxal in the CCNF XL hydrogel appeared to reduce the alignment of ice-crystals formed during the freezing process, while emulsion templating introduced smaller pores, ~5 µm in diameter, into the walls of the lyophilised hydrogel structure. Film structures, while porous, appear to show less connectivity between pores and a dense "skin" layer.

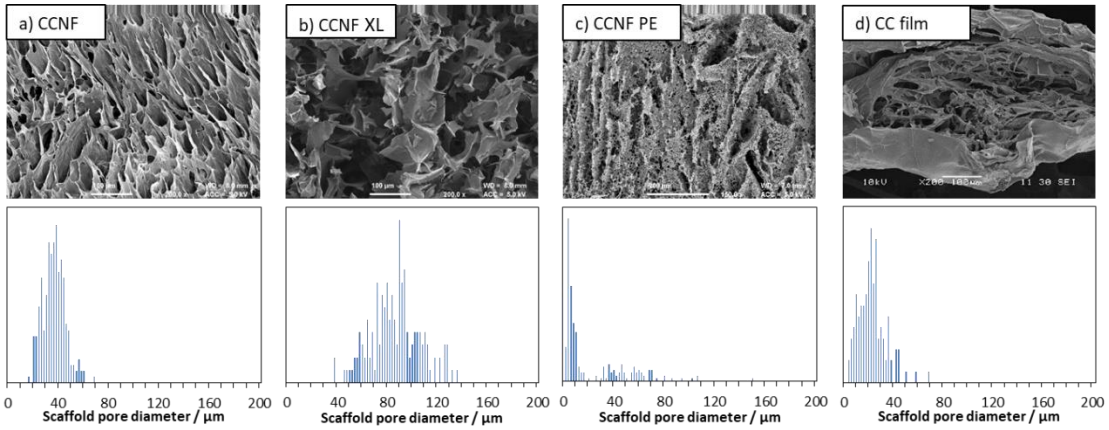

Figure 6.2 SEM images and pore size distributions of lyophilised foams a) 2 wt. % CCNF hydrogel, CCNF; b) 2 wt. % CCNF hydrogel + 5 wt. % glyoxal, CCNF XL; c) 1 wt. %. CCNF Pickering emulsion templated hydrogel, CCNF PE; and d) regenerated 4 wt. % cationic cellulose film, CC.

Along with the macroporous network, visible in SEM images, mesopores occur within the walls of the freeze dried foams. NMR cryoporometry was used to probe the permeability of the foam walls to PBS (Fig. 6.3 and Table 6.1). PBS was used to reflect typical cell culture media. Importantly, this technique allows the pore structure of hydrogels to be analysed in the hydrated materials, thus more accurately mimicking the microenvironment cells would experience in scaffolds. The smallest mesopore diameter, 20 ±2 nm, was observed in CCNF XL foams, where the pore size was found to be very similar to that in the control regenerated CC films, 18 ±2 nm. The wall pore modal diameter determined for CCNF foams was 25 ±2 nm and was not significantly affected by the concentration of initial CCNF dispersion used.

Crosslinking appeared to lead to a slight reduction in wall pore diameter to 20 ±2 nm. In contrast the CCNF PE foam does not allow for penetration of PBS solution into the walls, as reflected by a modal diameter matching that determined for the bulk PBS solution control. It is likely that this reflects the densification of CCNF at the oil/water interface in the Pickering emulsion,[67] yielding structures permeated by a plethora of pores arising from oil droplets, but with dense close-packed CCNF walls.

a)

b)

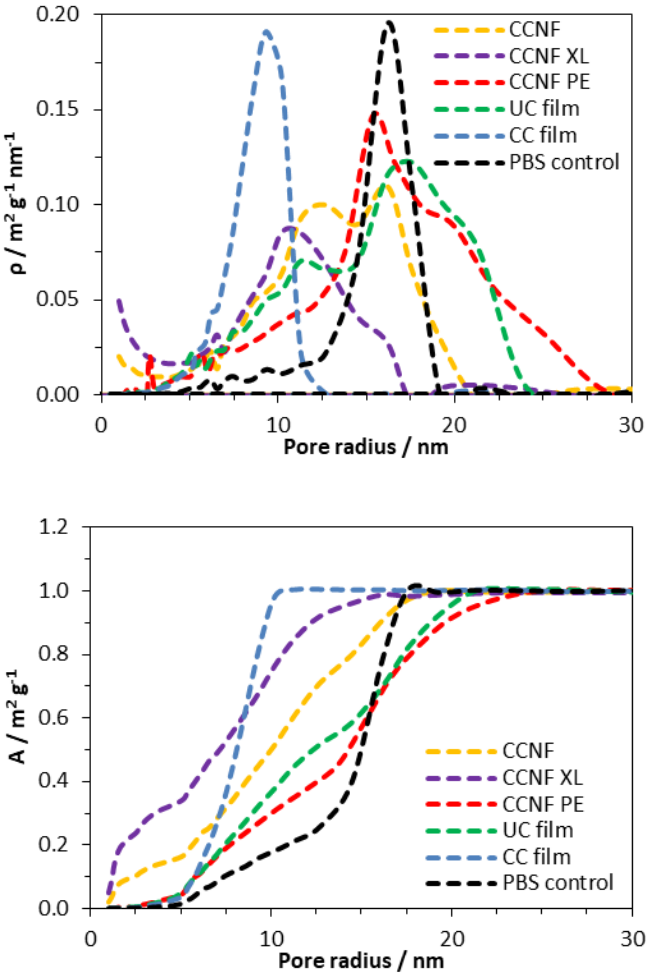

Figure 6.3 Size distribution of mesopores in hydrated CCNF foams from NMR cryoporometry measurements: a) specific pore surface area density, ρ, and b) specific cumulative pore surface area. The walls of the CCNF freeze dried foams are permeable to the PBS solution, with 1wt. % foams exhibiting the largest pores ascribed to the more open network formed by dispersed nanofibrils. Crosslinked foams have the smallest pores, at 20 nm compared to 25 nm for uncrosslinked foams. The CCNF PE material appears to have dense (albeit very thin – SEM) walls that do not allow for penetration of PBS as the modal diameter calculated is the same as that arising from a bulk PBS solution. This reflects dense packing of nanofibrillar walls formed from fibrils adsorbed at the oil/water interface in the emulsion.

These 3D scaffolds, formed from CCNF dispersions and emulsions, thus have porosity at three different scales: large pores or channels resulting from ice-crystal

templation; smaller pores arising from templation by oil droplets in Pickering emulsions; and nanoscale pores reflecting packing of the CCNF within the walls of the foamed structures. As this differing porosity could be beneficial for both penetration of cells into the scaffold and mass transfer of nutrients, gases and waste products to and from cells during cell growth, we sought to unify the porosity measurements to allow comparison of potential scaffold materials and thus to inform future selection of the form of templates.

NMR T_2 relaxometry experiments were used to probe the accessibility of DMAc to three different scales on the materials, given by each component in the T_2 distribution. Such scales are related to pores of a few nanometers, for T_2 values of about 10^{-3} s, mesopores of dozens of nanometers, for T_2 values ranging from 10^{-2} to 10^{-1} s and large pores of hundreds of nanometers up to one micrometer, for T_2 values above 10^{-1} s. The T_2 distributions for all scaffolds are shown in the Electronic Supplementary Information (Fig. E.14 – 16).

Table 6.1: Effect of CCNF surface modification and crosslinking on the mesopore modal diameter, determined by NMR cryoporometry, and macropore diameter, determined by analysis of SEM images.

Scaffold type	Sample	Mesopore diameter / nm	Macropore diameter / µm
a	CCNF 1 wt. %	25 ±2	
a	CCNF 2 wt. %	26 ±2	35 ±9
a	CCNF 4 wt. %	27 ±2	
a	CCNF XL 2 wt. %[d]	20 ±2	60 ±20
b	CCNF PE 1 wt. %	30 ±2	5 ±3[e], 54 ±20[f]
c	CC 4 wt. %	18 ±2	20 ±10
c	UC 4 wt. %	35 ±2	0.6 ±0.3
Control	PBS	32 ±2	n/a

a Directionally frozen dispersions, *b* directionally frozen Pickering emulsions; *c* cast regenerated films; *d* crosslinker concentration in solution = 5 wt. %; *e* macropore diameter - emulsion droplets; *f* macropore diameter - channels.

The proportion of DMAc accessing pores on each length scale can be estimated from the respective relative areas of the log-gaussian obtained from deconvolution (Fig. 6.4). The greater the accessibility, the more pores are filled with the fluid at a particular length scale. Thus, CCNF XL has a greater accessibility of pores on the

smallest scale in comparison to CCNF and CCNF PE, suggesting that crosslinking increases the number of accessible nanopores in the cell wall. This reflects the observation that crosslinked cellulose materials are less prone to hornification than uncrosslinked celluloses.

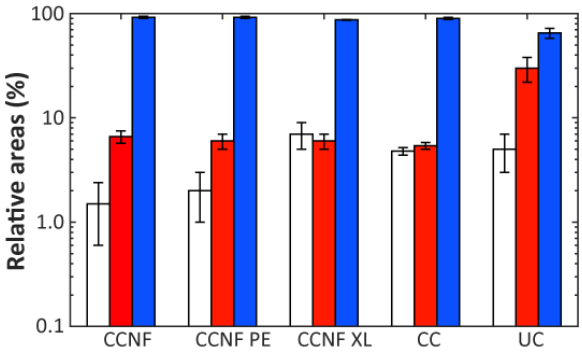

Figure 6.4 Relative areas of the log-gaussian obtained from deconvolution for CCNF, CCNF PE, and CCNF XL foams, compared to CC and unmodified cellulose (UC) films as controls. The left (white) bars indicate the nanopores, the centre (red) bars the mesopores and the right (blue) bars the large pores.

While the T_2 distributions do not give precise pore sizes due to the unknown surface relaxivity for each sample, if the (reasonable) assumption is made that the surface relaxivity is similar in the different pore categories, the linear relationship between the pore size and T_2 (Eq. 2) allows estimation of the ratio between the mean of the components seen in the T_2 distribution. There is a reasonable correlation between the cryoporometry data and the central T_2 values for the mesopore components (Fig. E.16). Thus, based on the average pore sizes determined by NMR cryoporometry results and the T_2 values for the mesopore components, it is possible to estimate the pore sizes in the hundreds of nm length scale, which is neither accessible by NMR cryoporometry nor by SEM. The pore sizes thus calculated are shown in Table 6.2.

Table 6.2: Mesopore sizes evaluated from NMR relaxometry and cryoporometry.

Scaffold type	Sample	T_2 / ms	Large pore diameter / nm
a	CCNF 2 wt. %	382 ±2	300 ± 30
a	CCNF XL 2 wt. %[d]	353 ±2	350 ± 40
b	CCNF PE 1 wt. %	209 ±1	320 ± 20
c	CC 4 wt. %	135 ±1	180 ± 20
c	UC 4 wt. %	117 ±5	70 ± 7

a Directionally frozen dispersions, *b* directionally frozen Pickering emulsions; *c* cast regenerated films; *d* crosslinker concentration in solution = 5 wt. %

6.5.3 Mechanical properties and robustness

As mentioned previously, uncrosslinked CCNF foams were very delicate, becoming broken up and dispersing readily in DI H_2O or buffer upon even very gentle agitation. Foams formed in moulds to create more complex 3D shapes, as may be required in the production of suitable tissue samples in *ex vivo* cultures, completely dispersed in cell culture medium (Fig. 6.5). Thus, in their native state, the foams were not compatible with the handling requirements for cell culture techniques.

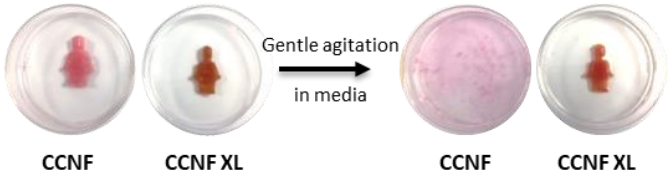

Figure 6.5 CCNF and CCNF XL foams soaked in DMEM cell culture medium. The CCNF foams swelled by 10% upon hydration in H_2O, whereas the CCNF XL foams retained their dry dimensions. After shaking in a centrifuge vial for 10 s CCNF foams broke up and dispersed in H_2O, whereas CCNF XL foams remained intact.

To avoid compromising the exquisite structures formed by sequential soaking in glyoxal solution and heating (as used previously[63]), glyoxalation was effected *in situ*: glyoxal solutions were added to the hydrogels prior to freezing and the curing step took place post lyophilisation on the now dehydrated foam. This simple procedure is attractive for manufacturing as it reduces the number of processing steps required in foam scaffold fabrication, making scaffold manufacture readily scalable. The dry foams thus produced had degrees of crosslinking from 1.18 to 3.04 mol. %, as determined by HPLC analysis (Fig. E.6), comparable with glyoxalation conducted on cellulose films.[63]

As the concentration of glyoxal crosslinker used increased from 2.5 to 10 wt. %, the crosslinked scaffolds became more robust with mechanical properties, such as Young's modulus and compressive strength, increasing accordingly (Fig. 6a and b). Compressive strength, in particular, was enhanced, with the Young's modulus, *E,* increasing from 0.1 MPa for uncrosslinked CCNF foams to 50.8 ±8 MPa at 10 wt. % glyoxal (Fig. 6.6a). It was apparent from the compressive load versus compressive extension profiles that compression was occurring in two stages; initial compression at lower loading was assigned to the collapse of the large porous network and a second stage, at much higher loads, reflected the bulk of the material under compression (Fig. 6.6b). *E* was determined from the stress/strain at 30 %

deformation. Although the highest *E* value occurred in the most crosslinked foams, these tended to fracture more quickly, reflecting a more brittle structure; hence foams up to 5 wt. % were used in cell culture studies (Figs. E.20 – 23).

a)

b)

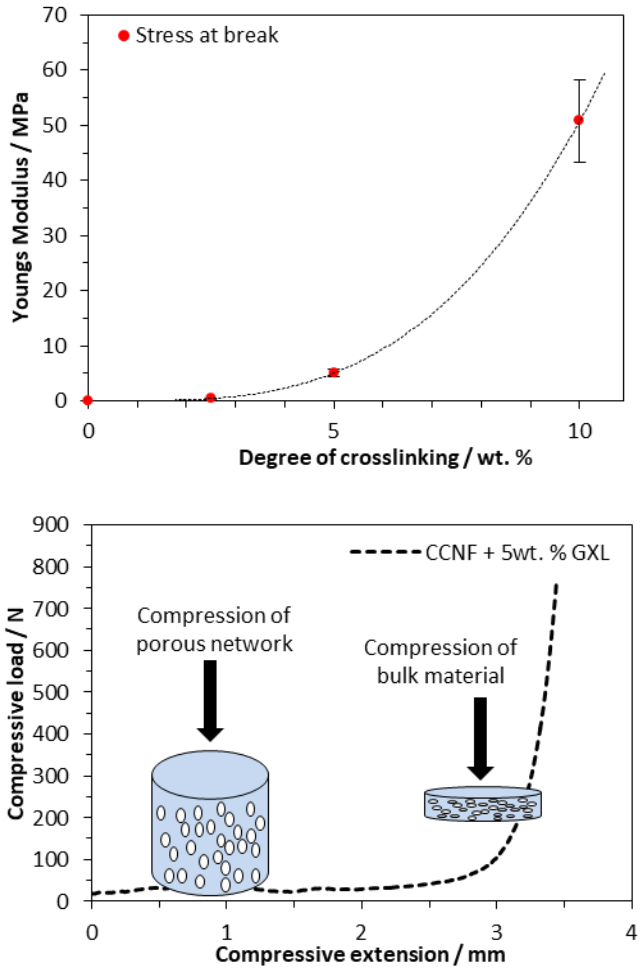

Figure 6.6 a) The Young's modulus, determined from the stress/strain at 30 % deformation, showed that crosslinking the CCNF foams had a significant influence on the robustness of the materials. b) Compressive load *versus* compressive extension graph showing the two phases of compression: first, compression of the porous network, followed by the greater load required to compress the bulk material (illustrated for CCNF XL).

Such foams represented a "sweet spot": materials were robust enough to handle and survive the manipulations required for cell studies (e.g., aspiration of media), yet were not rendered too brittle to be of utility: CCNF foams with a moderate level of crosslinking (exposed to 2.5 and 5 wt. % glyoxal, yielding DXL of 1.18 and 3.04 mol. %) remained intact in PBS and only disintegrated if subjected to very vigorous agitation. This enabled the foams to be handled without breaking during cell viability studies.

6.5.4 Cell response to 3D scaffolds

We have previously investigated the attachment of cells on the surface of CC films,[68] but here the presence of a "skin" on the surface of the regenerated CC films (Fig. E.17) rendered the porous internal structure beneath inaccessible to cells, so that cell studies were confined to the foamed scaffolds produced by directional freezing, lyophilisation and crosslinking.

The cell viability was determined by assessing cell metabolism using an MTT assay, which showed that MG-63 cells were viable on all 3D CCNF scaffolds after 7 days incubation at 37 ^{o}C in 5 % CO_2 (Fig. 6.7a).

We have reported previously that cell elongation can be promoted on crosslinked 2D CC scaffolds, an effect that was ascribed to increased elastic and shear moduli.[63] Thus, the enhanced level of cell viability on CCNF XL materials was expected. Nonetheless, to test whether or not the enhancement could be ascribed to enhanced sorption of proteins (present in FBS) to the cationic surface, protein adsorption studies were conducted. The quantity of protein (specifically bovine serum albumin, BSA) adsorbed to the scaffolds after incubation with cell culture medium for 24 h at 37 ^{o}C in 5 % CO_2 was quantified by HPLC analysis (Fig. 6.7b and Fig. E.24-26). While increased cationisation (increased DS) enhances protein absorption, there is no such correlation with crosslinking, suggesting that the enhanced cell viability on CCNF XL resulted from the structural properties of the scaffold (SEM images of growing cells on the 3D scaffolds are provided as Fig. S28). Not surprisingly, measured mechanical strength decreased on hydration of scaffolds, but there was no evidence of further degradation after 7 days incubation (Fig. S24 – 27).

It has been reported previously that the mechanical properties of a cell scaffold affect the mechanosensitive cell response, although this can be dependent on the cell type.[69] For example fibroblasts, smooth muscle cells and epithelial cells spread more and develop larger focal adhesions and actin stress fibres on stiffer scaffolds than on compliant ones.[70] Cells receive mechanical feedback from the substrate to which they adhere, even in the absence of externally applied forces,[71] as they attempt to deform the substrate. As cells elongate on stiff scaffolds they experience a higher stress than on softer more compliant scaffolds, which promotes the

assembly of the cytoskeleton into actin stress fibres and focal adhesions, and subsequently triggers signalling cascades that ultimately promote cell expansion.[72]

a)

b)

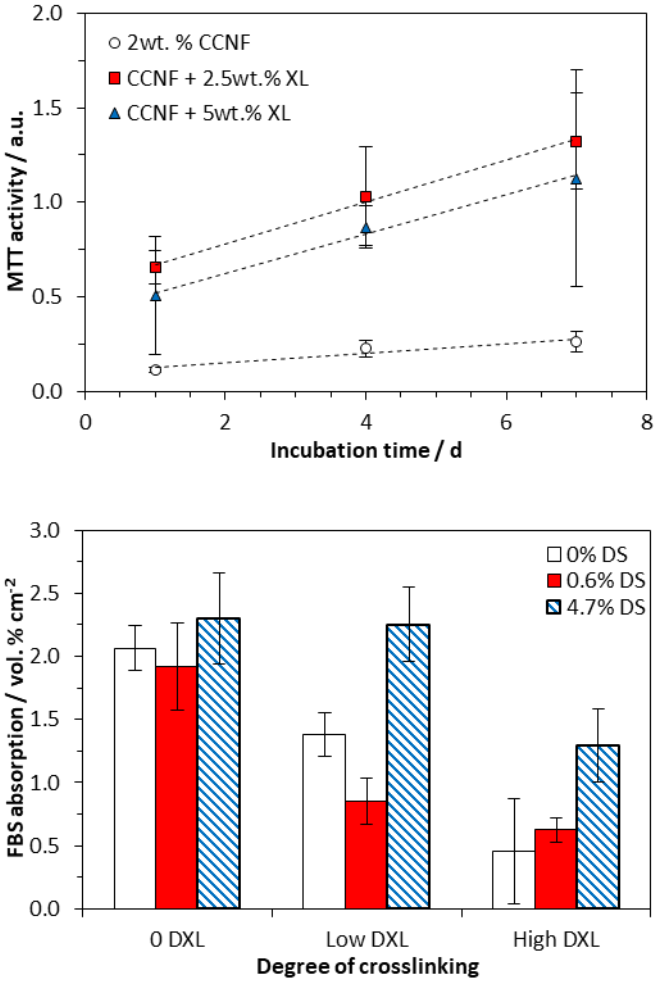

Figure 6.7 a) Cell viability on 2 wt. % CCNF 3D scaffolds after 1, 4 and 7 days incubation at 37 ^{o}C in 5 % CO_2. Tissue culture plastic was used as the control and the sample values have had the material control subtracted. It is evident that glyoxalation provides the foams with the structural support to use as 3D scaffolds as well as enhancing cell viability. b) HPLC analysis of the quantity of FBS, specifically bovine serum albumin (BSA), adsorbed onto the scaffold surface after 24 h incubation at 37 ^{o}C in 5 % CO_2. By comparison TCP bore 0.95 vol. % cm^{-2} BSA absorbed onto the surface.

Thus, we suggest that the cells adhered to the CCNF XL scaffolds due to the cationic surface charge, which promotes the initial phase of cell attachment, facilitating cell binding through electrostatic interactions and possibly aided by enhanced FBS sorption, particularly in the second phase of cell adhesion (Fig. 6.8). Once attached, the stiffer CCNF XL scaffolds provided the cells with a larger feedback force, promoting mechanotransduction signalling within by activating the Rho GTPase family to promote cell spreading and migration in the third phase of cell adhesion.[73]

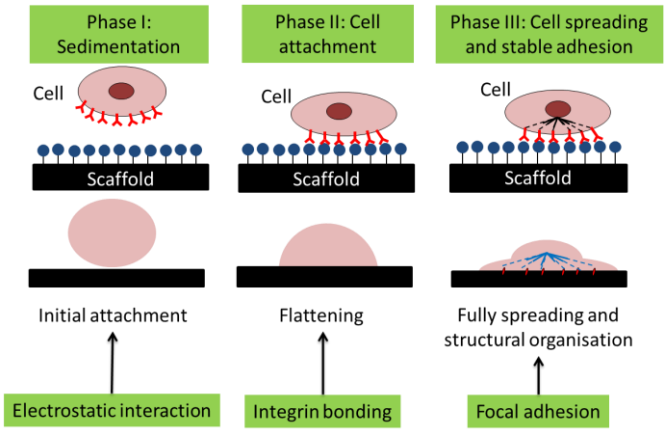

Figure 6.8 Schematic of the phases of passive *in vitro* cell adhesion. Phase I: Sedimentation of cells can be enhanced through electrostatic interactions, Phase II: Cell attachment is facilitated through the formation of integrin binding sites between the cell and scaffold and Phase III: Cell spreading occurs through focal adhesions the interactions with the force experienced by the cell actin cytoskeleton via mechanotransduction.[73]

These "bottom-up" scaffolds complement the current "top-down" decellularised plant tissue scaffolds available and offer a wide range of potential cell culture applications, potentially promoting the differentiation of tissue on the variable stiffness CCNF foams. Furthermore, the porosity and vascular structure of the foams facilitates mass transfer of O_2 and nutrients to the cells and the removal of waste products, required to maintain viable cultures, e.g. in and on larger 3D scaffolds shaped to mimic organs or to match specific damaged areas of tissue.

6.6 Conclusion

Robust 3D modified cellulose scaffolds with exquisite tuneable structure in the form of foams, with meso- and macro- scale pores were prepared by a "bottom-up" approach. Directionally freezing CCNF dispersions and emulsions, followed by lyophilisation, was used to produce a range of scaffolds with a variety of internal architectures from aligned micro channels with smooth walls, mimicking vascularised tissue, and pumice-like wall textures, reminiscent of porous bone. Directional freezing is a facile and low cost method to introduce porosity into tissue engineering scaffold materials and this process would be attractive for (relatively) large scale manufacturing as it has fewer steps than previous methodology.

To overcome the poor structural integrity of the CCNF foams, crosslinking by glyoxalisation was used. This also enhanced the Young's modulus and yielded scaffold materials suitable for cell culture as demonstrated by the improved viability of MG-63 grown on the scaffolds. It is postulated that the more porous structures arising, allowed for enhanced mass transfer of nutrients and gases into the scaffolds and removal of cell waste products, beneficial for cell growth. Porosity was characterised at all length scales by a combination of SEM image analysis, NMR cryoporometry and T_2 relaxation studies.

These scaffolds can complement the library of 3D porous materials derived from decellularised plant tissue, yet have the advantage over the "top-down" scaffolds, which usually require several treatments prior to application and can be limited in structure and shape, whereas, a variety of bulk 3D shapes can be prepared through process moulding the frozen hydrogel prior to lyophilisation and crosslinking.

These "bottom-up" scaffolds derived from dispersed CCNF require minimal modification, use known and scalable chemistries, and can be easily processed through the use of moulding techniques to create the desired 3D constructs, with modulated vascularity and wall porosity.

6.7 Acknowledgements

We gratefully acknowledge funding from the EPSRC Centre for Doctoral Training in Sustainable Chemical Technology (EP/L016354/1), in the form of a PhD studentship for JCC. SEM images were obtained at the Microscopy and Analysis Suite in Bath University with the assistance of Ursula Potter and the authors thank John Lowe for his assistance with NMR spectroscopy at the University of Bath.

6.8 References

1. J. Colaneri, *Am. J. Transplant.*, 2016, **16**, 8–10.
2. T. Dvir, B. P. Timko, D. S. Kohane, and R. Langer, *Nat. Nanotechnol.*, 2011, **6**, 13–22.
3. J. K. Kular, S. Basu, and R. I. Sharma, *J. Tissue Eng.*, 2014, **5**, 1–17.
4. D. Anton, H. Burckel, E. Josset, and G. Noel, *Int. J. Mol. Sci.*, 2015, **16**, 5517–5527.
5. W. Sekine, Y. Haraguchi, T. Shimizu, A. Umezawa, and T. Okano, *Biochips and Tissue chips*, 2011, **S1:007**, 1–9.
6. P. Carmeliet and R. K. Jain, *Nature*, 2000, **407**, 249–257.
7. J. Rouwkema, B. F. J. M. Koopman, C. A. V. Blitterswijk, W. J. A. Dhert, and J. Malda, *Biotechnol. Genet. Eng. Rev.*, 2009, **26**, 163–178.
8. J. R. Gershlak, S. Hernandez, G. Fontana, L. R. Perreault, K. J. Hansen, S. A. Larson, B. Y. K. Binder, D. M. Dolivo, T. Yang, T. Dominko, M. W. Rolle, P. J. Weathers, F. Medina-Bolivar, C. L. Cramer, W. L. Murphy, and G. R. Gaudette, *Biomaterials*, 2017, **125**, 13–22.
9. J. Mitra, G. Tripathi, A. Sharma, and B. Basu, *RSC Adv.*, 2013, **3**, 11073–11094.
10. F. A. Saleh and P. G. Genever, *Cytotherapy*, 2011, **13**, 903–912.
11. F. J. O'Brien, B. A. Harley, M. A. Waller, I. V Yannas, L. J. Gibson, and P. J. Prendergast, *Technol. Heal. Care*, 2007, **15**, 3–17.
12. F. J. O'Brien, B. A. Harley, I. V. Yannas, and L. J. Gibson, *Biomaterials*, 2005, **26**, 433–441.
13. Z. Ma, M. Kotaki, R. Inai, and S. Ramakrishna, *Tissue Eng.*, 2005, **11**, 101–109.
14. P. M. Crapo, T. W. Gilbert, and S. F. Badylak, *Biomaterials*, 2011, **32**, 3233–3243.
15. T. W. Gilbert, T. L. Sellaro, and S. F. Badylak, *Biomaterials*, 2006, **27**, 3675–3683.
16. J. J. Song and H. C. Ott, *Trends Mol. Med.*, 2011, **17**, 424–432.

17. D. J. Modulevsky, C. Lefebvre, K. Haase, Z. Al-Rekabi, and A. E. Pelling, *PLoS One*, 2014, **9**, e97835.

18. J. Doshi and D. H. Reneker, *J. Electrostat.*, 1995, **35**, 151–160.

19. H. S. Yoo, T. G. Kim, and T. G. Park, *Adv. Drug Deliv. Rev.*, 2009, **61**, 1033–1042.

20. H. W. Kim, H. S. Yu, and H. H. Lee, *J. Biomed. Mater. Res. - Part A*, 2008, **87**, 25–32.

21. B. Derby, *Science (80-.).*, 2012, **338**, 921–926.

22. K. R. Hixon, T. Lu, and S. A. Sell, *Acta Biomater.*, 2017, **62**, 29–41.

23. C. R. Almeida, T. Serra, M. I. Oliveira, J. A. Planell, M. A. Barbosa, and M. Navarro, *Acta Biomater.*, 2014, **10**, 613–622.

24. J. G. Torres-Rendon, T. Femmer, L. De Laporte, T. Tigges, K. Rahimi, F. Gremse, S. Zafarnia, W. Lederle, S. Ifuku, M. Wessling, J. G. Hardy, and A. Walther, *Adv. Mater.*, 2015, **27**, 2989–2995.

25. M. Costantini, C. Colosi, P. Mozetic, J. Jaroszewicz, A. Tosato, A. Rainer, M. Trombetta, W. Święszkowski, M. Dentini, and A. Barbetta, *Mater. Sci. Eng. C*, 2016, **62**, 668–677.

26. A. Barbetta, A. Carrino, M. Costantini, and M. Dentini, *Soft Matter*, 2010, **6**, 5213–5224.

27. C. Colosi, M. Costantini, A. Barbetta, R. Pecci, R. Bedini, and M. Dentini, *Langmuir*, 2013, **29**, 82–91.

28. M. Costantini, C. Colosi, J. Guzowski, A. Barbetta, J. Jaroszewicz, W. Święszkowski, M. Dentini, and P. Garstecki, *J. Mater. Chem. B*, 2014, **2**, 2290–2300.

29. M. Costantini, C. Colosi, J. Jaroszewicz, A. Tosato, W. Święszkowski, M. Dentini, P. Garstecki, and A. Barbetta, *ACS Appl. Mater. Interfaces*, 2015, **7**, 23660–23671.

30. L. Qian and H. Zhang, *J. Chem. Technol. Biotechnol.*, 2011, **86**, 172–184.

31. C. M. Murphy and F. J. O'Brien, *Cell Adhes. Migr.*, 2010, **4**, 377–381.

32. H. Zhang and A. I. Cooper, *Adv. Mater.*, 2007, **19**, 1529–1533.

33. S. Deville, E. Saiz, and A. P. Tomsia, *Biomaterials*, 2006, **27**, 5480–5489.

34. B. B. Mandal and S. C. Kundu, *Biomaterials*, 2009, **30**, 2956–2965.

35. X. Wu, Y. Liu, X. Li, P. Wen, Y. Zhang, Y. Long, X. Wang, Y. Guo, F. Xing, and J. Gao, *Acta Biomater.*, 2010, **6**, 1167–1177.

36. A. Autissier, C. Le Visage, C. Pouzet, F. Chaubet, and D. Letourneur, *Acta Biomater.*, 2010, **6**, 3640–3648.

37. S. Reed, G. Lau, B. Delattre, D. D. Lopez, A. P. Tomsia, and B. M. Wu,

Biofabrication, 2016, **8**, 015003.

38. G. Li, A. G. Nandgaonkar, Y. Habibi, W. E. Krause, Q. Wei, and L. A. Lucia, *RSC Adv.*, 2017, **7**, 13678–13688.

39. S. Flauder, T. Heinze, and F. A. Müller, *Cellulose*, 2014, **21**, 97–103.

40. M. Bhattacharya, M. M. Malinen, P. Lauren, Y.-R. Lou, S. W. Kuisma, L. Kanninen, M. Lille, A. Corlu, C. GuGuen-Guillouzo, O. Ikkala, A. Laukkanen, A. Urtti, and M. Yliperttula, *J. Control. Release*, 2012, **164**, 291–298.

41. B. Wang, X. Lv, S. Chen, Z. Li, J. Yao, X. Peng, C. Feng, Y. Xu, and H. Wang, *Carbohydr. Polym.*, 2018, **181**, 948–956.

42. E. Entcheva, H. Bien, L. Yin, C.-Y. Chung, M. Farrell, and Y. Kostov, *Biomaterials*, 2004, **25**, 5753–62.

43. M. Zaborowska, A. Bodin, H. Bäckdahl, J. Popp, A. Goldstein, and P. Gatenholm, *Acta Biomater.*, 2010, **6**, 2540–2547.

44. D. Klemm, B. Heublein, H.-P. P. Fink, and A. Bohn, *Angew. Chemie - Int. Ed.*, 2005, **44**, 3358–3393.

45. D. J. Modulevsky, C. M. Cuerrier, and A. E. Pelling, *PLoS One*, 2016, **11**, 1–19.

46. A. Sannino, C. Demitri, and M. Madaghiele, *Materials (Basel).*, 2009, **2**, 353–373.

47. A. Svensson, E. Nicklasson, T. Harrah, B. Panilaitis, D. L. Kaplan, M. Brittberg, and P. Gatenholm, *Biomaterials*, 2005, **26**, 419–31.

48. F. G. Torres, S. Commeaux, and O. P. Troncoso, *J. Funct. Biomater.*, 2012, **3**, 864–78.

49. J. C. Courtenay, M. A. Johns, F. Galembeck, C. Deneke, E. M. Lanzoni, C. A. Costa, J. L. Scott, and R. I. Sharma, *Cellulose*, 2017, **24**, 253–267.

50. J. C. Courtenay, S. M. Ramalhete, W. J. Skuze, R. Soni, Y. Z. Khimyak, K. J. Edler, and J. L. Scott, *Soft Matter*, 2018, **14**, 255–263.

51. C. Schramm and B. Rinderer, *Anal. Chem.*, 2000, **72**, 5829–5833.

52. M. A. Johns, A. Bernardes, E. R. De Azevêdo, F. E. G. Guimarães, J. P. Lowe, E. M. Gale, I. Polikarpov, J. L. Scott, and R. I. Sharma, *J. Mater. Chem. B*, 2017, **5**, 3879–3887.

53. S. Berger and S. Braun, *200 and more NMR experiments: A practical course*, Wiley-VCH Weinheim, Weinheim, 2004.

54. H. Y. Carr and E. M. Purcell, *Phys. Rev.*, 1954, **94**, 630–638.

55. S. Meiboom and D. Gill, *Rev. Sci. Instrum.*, 1958, **29**, 688–691.

56. Å. Östlund, A. Idström, C. Olsson, P. T. Larsson, and L. Nordstierna, *Cellulose*, 2013, **20**, 1657–1667.

57. C. Boissier, F. Feidt, and L. Nordstierna, *J. Pharm. Sci.*, 2012, **101**, 2512–2522.

58. G. C. Borgia, R. J. S. Brown, and P. Fantazzini, *J. Magn. Reson.*, 2000, **147**, 273–285.

59. S. W. Provencher, *Comput. Phys. Commun.*, 1982, **27**, 213–227.

60. K. R. Brownstein and C. E. Tarr, *Phys. Rev. A*, 1979, **19**, 2446–2453.

61. D. Capitani, V. Di Tullio, and N. Proietti, *Prog. Nucl. Magn. Reson. Spectrosc.*, 2012, **64**, 29–69.

62. C. Zhang, P. Li, Y. Zhang, F. Lu, W. Li, H. Kang, J. feng Xiang, Y. Huang, and R. Liu, *Polymer (Guildf).*, 2016, **98**, 237–243.

63. J. C. Courtenay, C. Deneke, E. M. Lanzoni, C. A. Costa, Y. Bae, J. L. Scott, and R. I. Sharma, *Cellulose*, 2018, **25**, 925–940.

64. F. Quero, M. Nogi, K. Y. Lee, G. Vanden Poel, A. Bismarck, A. Mantalaris, H. Yano, and S. J. Eichhorn, *ACS Appl. Mater. Interfaces*, 2011, **3**, 490–499.

65. R. G. Wells, *Hepatology*, 2008, **47**, 1394–1400.

66. E. A. Klein, L. Yin, D. Kothapalli, P. Castagnino, F. J. Byfield, T. Xu, I. Levental, E. Hawthorne, P. A. Janmey, and R. K. Assoian, *Curr. Biol.*, 2009, **19**, 1511–1518.

67. J. C. Courtenay, Y. Jin, J. Schmitt, K. J. Edler, and J. L. Scott, *Soft Matter*, 2018.

68. M. A. Johns, Y. Bae, F. E. G. Guimarães, E. M. Lanzoni, C. A. R. Costa, P. M. Murray, C. Deneke, F. Galembeck, J. L. Scott, and R. I. Sharma, *ACS Omega*, 2018, **3**, 937–945.

69. P. C. Georges and P. a Janmey, *J. Appl. Physiol.*, 2005, **98**, 1547–1553.

70. J. D. Humphrey, E. R. Dufresne, and M. A. Schwartz, *Nat. Rev. Mol. Cell Biol.*, 2014, **15**, 802–812.

71. R. G. M. Breuls, T. U. Jiya, and T. H. Smit, *Open Orthop. J.*, 2008, **2**, 103–109.

72. M. Tamada, M. P. Sheetz, and Y. Sawada, *Dev. Cell*, 2004, **7**, 709–718.

73. A. A. Khalili and M. R. Ahmad, *Int. J. Mol. Sci.*, 2015, **16**, 18149–18184.

Chapter 7

7 Concluding remarks

The aim of this PhD was to develop, through simple, robust and scalable chemical modifications, novel, decorated cellulose surfaces. These materials could be utilised to produce functional scaffolds, to facilitate cellular attachment and further tune, or regulate, cell response in tissue culture applications. The series of papers presented have shown that cationisation can be applied to cellulose materials, from nanofibrils to 2D surfaces, and used to produce complex 3D scaffolds. Initial cationisation of 2D surfaces enabled method development for degree of substitution (DS) to be quantified and for greater understanding of its influence on surface chemistry. Modified cellulose films provided good 2D models to investigate cell response and cell-scaffold interactions. This foundation of knowledge was transferred to cationisation of nanofibrils, unlocking a wide range of material to be produced. These CCNF and hydrogels were analysed and the interfibrillar molecular interactions characterised to provide understanding of interfibrillar interactions in these systems. The work described in the final paper in the narrative of this thesis took knowledge from all the previous papers to develop 3D modified cellulose scaffolds with the exquisite internal architectures required for more complex cell culturing on tuneable “bottom up” produced scaffolds.

The first two objectives were to identify a two-component system for cell attachment onto cellulose in the absence of FBS in cell growth media. Having reviewed types of modification in Chapter 1, in Chapter 2 the aim was achieved by grafting GTMAC onto the surface of cellulose, introducing a positive surface charge, and providing a material which showed significantly increased cell attachment compared to either unmodified, or oxidised (anionic), bacterial cellulose films.

Cationisation alone was shown to lead to similar levels of cell attachment to that obtained on tissue culture plastic. Methods to quantify the presence of quaternary ammonium groups on the cellulose surfaces were developed and surface zeta-potential measurements, used to confirm that the cationised scaffolds had a positive charge of 25 ±9 mV.

In Chapter 3 we developed the initial finding further by producing scaffolds with a wide range of DS (between 0 – 9.2 %) and combining this modification with glyoxalation (0.3 – 2.6 % degree of crosslinking) to obtain scaffolds with variable stiffness, with a shear moduli increasing from 76 to 448 kPa. To address the third objective, investigation into cell response identified that cationisation was vital for inducing FBS-free attachment, with as little as 1.4 % DS required, but that the shear modulus, governed by degree of crosslinking, was the more significant property for further regulating cell spreading. In Chapter 3 both the bulk and surface properties were characterised in detail and methods were optimised to enable this. Modulated crosslinking, with glyoxal, produced materials with variable (and tunable) surface shear moduli that resulted in differential cell spreading, suggesting a simple, but effective mechanism to control cell response. Thus, tuning properties was achieved using only two facile chemical modifications at varying levels, offers potential advantages in making production cost effective and enabling scale up of these two-component systems.

In Chapter 4 the focus moved from feasibility to scale-up of this technology to developing a method to scale-down the cationisation, in line with the fourth objective. This was achieved using GTMAC as a “reactive ink” and depositing droplets of reagent onto unmodified cellulose scaffolds using ink-jet printing. Cationic islands with average diameter of only 47 ±2 µm were achieved and directed attachment of cells localised to these modified regions was observed. A range of potential emergent applications for this technology were identified in Chapter 4 including: co-culturing cell lines; high throughput drug screening; and guiding cell orientation.

In chapter 5, to address the fifth objective, the established modification procedure was taken and applied to cellulose fibres, resulting in individualised CCNF, which dispersed in H_2O forming stable hydrogels. Combining results from neutron scattering experiments, rheological measurements and analysis of ^1H NMR T_1

relaxation times of the H_2O and grafted $–N^+(CH_3)_3$ groups, low DS CCNF were characterised as fibrils that are twisted and flexed, and which entangle to form weak hydrogels, while higher DS CCNF fibrils are more rigid, flatter, ribbon-like structures that result in stiff, elastic, viscous, shear thinning hydrogels. These hydrogels could now be investigated as 3D scaffolds.

The last objective was to produce 3D scaffolds from modified cellulose, as described in Chapter 6. This was achieved by turning the hydrogels made from dispersed CCNFs into porous foams, via directional freezing followed by lyophilisation, producing a range of scaffolds with a variety of internally architecture from aligned micro–channels, with smooth walls, mimicking vascularised tissue, and pumice-like wall textures, prepared from directionally freezing Pickering emulsions, reminiscent of porous bone. These possessed exquisite internal structure, with meso- and macro-pores which could be reinforced by glyoxalisation. A combination of NMR cryoporometry, NMR relaxometry and SEM were used to probe the pores at different length scales from a few nm to >100 μm. Glyoxalisation reinforced the scaffold structure and also enhanced metabolic activity of attached MG-63 cells. It was postulated that the crosslinked scaffolds provided a favourable microenvironment for cell growth as well as increased mass transfer of nutrients and waste product.

Developing robust scaffolds from dispersed CCNF is beneficial for industrial applications as they require minimal modification, using known and scalable chemistries, and can be easily processed through the use of mould and extrusion techniques to create the desired 3D constructs, with modulated vascularity and wall porosity. These “bottom-up” scaffolds can complement the library of 3D scaffold materials derived from decellularised plant tissue.

7.1 Further Development

7.1.1 Exploring cell response to tailored cellulose scaffolds

Much of the research conducted in this thesis focused on initial cell phenomena; cell attachment, morphology and viability on modified cellulose scaffolds. However, there are other important measures of the cellular response to a given substratum, these include: long term cell growth, cell proliferation and growth, to determine cell kinetics and doubling rate, which could be quantified by the assays such as resazurin. Probing signalling molecules expressed by adherent cell on the scaffolds using immune-staining and molecular biology techniques (RNA and Western Blott)

Several different cell lines could be screened on these scaffolds, such as primary cell lines, diseased cell lines and their healthy counterpart. Furthermore, stem cell differentiation can be guided by scaffold properties. For example the elastic moduli of the crosslinked scaffolds mimicked that of myocytes and osteogenic tissue, suggesting the potential to develop such materials into tailored scaffolds to produce musculoskeletal tissue from MSCs. Furthermore, cellulose composites can be produced with different properties.

7.1.2 Tuning scaffold properties to up-regulate cell cycle

Initial research investigating how scaffold properties influence the cell cycle took place at SUNY during the two month internship. The “cell cycle” describes the series of events leading to cell division and duplication and can be sectioned into phases that are controlled by a collection of proteins interacting with each other, the cyclins and cyclin-dependent kinases.[1] The main purpose of the cell cycle is to double the cell to replace damaged cells. The time it takes for a cell to double its genome is known as the interphase and each phase within the cycle is responsible for a specific role in the cell duplication process and occurs pre (S, G2) and post-mitotic (G1, G0) interphases. G1-phase follows directly after cell division whereby the cell starts to grow the necessary content for cell division, taking approximately 3 h. During the S-phase the process of DNA replication takes place and the cellular genome doubles, 7 h. Next the cells prepare to split occurs, G2, which takes 4 h and is referred to as the premitotic phase. Cell division finally occurs in the mitosis phase, M, where the

doubled DNA is organised in chromosomes and separates splitting the nucleus and rest of the cell, 30 – 60 min.

In normal proliferating tissue with cells undergoing constant division after mitosis then the next G1-phase occurs. G0 represents cells in their resting state, quiescence, such as specialised differentiated cells. Extracellular microenvironments and growth factor levels can also trigger cells to entre quiescence phase. Importantly this is a reversible and cells can re-enter the cell cycle upon given stimuli. Once a cell has entre the senescence process; however this is an irreversible series of steps that leads towards controlled cell death, apoptosis.

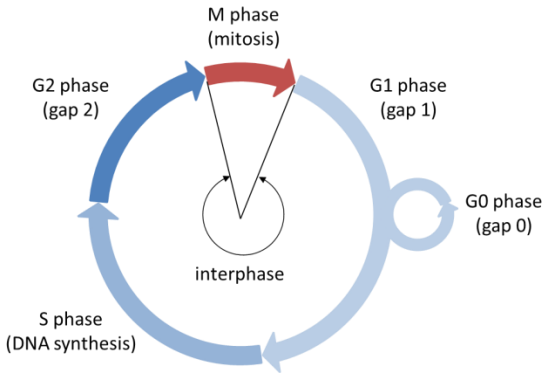

Figure 7.1 Schematic diagram of the cell cycle.

Understanding stimuli to re-initiate the cell cycle is important for treating disorders and promoting regeneration of differentiated cells such as neurons. On the other hand, a hallmark of cancerous tissue is the uncontrolled growth caused by constant triggering of the cell cycle. Thus understanding and regulating the cell cycle has many potential benefits in medicinal treatments.

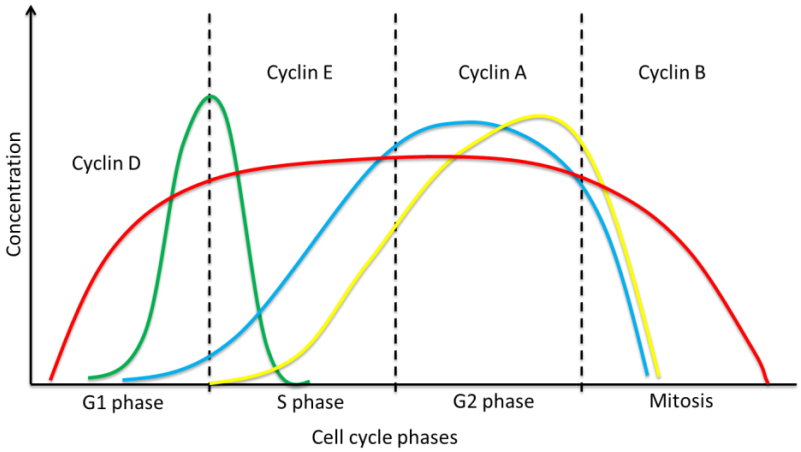

Figure 7.2 Relative Cyclin expression across cell cycle

Identifying the signalling proteins expressed by attached cells would provide information on whether the cell cycle is occurring or if the cells are in a quiescent state. Molecular biology techniques could be used to monitor the RNA expression such as reverse transcriptase quantitative polymerase chain reaction (RT-qPCR). This technique involves the reversion transcription of RNA to cDNA, followed by PCR amplifying the DNA, to quantitatively study gene expression. This technique offers an accurate way to investigate how scaffold properties influence cell proliferation through by measuring cyclin expression levels associated to specific phases.

7.1.3 Screening pathological state of cells: diseased versus healthy

The cancer osteosarcoma cell line MG-63 was used a model cell in this thesis. These cancerous cells are net negative due to elevated expression of anionic molecules in the cell membrane.[2] This difference in cell membrane between healthy and cancerous cell lines could be exploited to develop a screening technique. We would need to screen different non-cancerous cell lines to assess the ability of the modified cellulose scaffolds to support healthy cells. If there is a difference in how cell lines respond to the modified cellulose scaffolds, it is feasible the properties could be tuned to be selective to certain cell lines through ionic interactions. The selectivity of cancer cells could be developed into a cancer cell sensor to identify and isolate cancer cells from non-cancerous cells on micro-patterned scaffolds.

7.1.4 High throughput screening of pharmaceutical active ingredients

The use of inkjet printing could be expanded further to create more complex patterns like lines and gradients. These patterns could be used to control cell alignment and migration. The production of cell co-cultures with multiple cell types seeded onto the patterned scaffold, which better reflects natural tissue and provides for development of tissue functionality. Opportunities extend beyond the production of *ex vivo* tissues for clinical applications – for example, isolation of small groups of cells, or even individual cells, offers opportunities in screening of active agents, such as drugs, and selection of suitable patterning chemistries could lead to co-localisation of muscle and fat cells, of potential utility in clean meat production.

Other medical applications of cellulose scaffolds could include hydrogel membranes for wound healing, gradients of cationic cellulose could be used to promote the motility of fibroblast cells to the wound site. Also cellulose hydrogels could be

investigated as supports for non-adherent cell lines for potential use as injectable scaffolds for wound healing.

7.1.5 Edible scaffolds for cellular agriculture

The scaffolds in this thesis were developed for tissue engineering applications; however there is great potential to utilise these biomaterials for cellular agriculture. Essentially, cellular agriculture is the production of agricultural products from cell culture. The principles for culturing tissue for regenerative treatments can be applied to growing meat tissue. A potential advantage of using cellulose as the scaffold material is that it is edible and many of its modified forms are too. Viability of muscle cells such as C2C12 and primary cells would need to be conducted as proof of principle. This could be performed on both 2D and 3D scaffolds.

7.1.6 Scaling up cell culture

2D scaffolds are important in understanding the cellular response to substratum but that type of system has limited clinical application, apart from 2D wound dressing treatments. Therefore, they are a need to exploit the ability of cationic cellulose to support cell viability by developing 3D system. We have demonstrated methods of producing 3D scaffolds from lyophilised regenerated cellulose solutions and hydrogels. More complex shapes could be achieved using by 3D syringe printing the cellulose solution into an anti-solvent or electrospinning cellulose nanofibres. Potentially beneficial in complex 3D scaffold constructs designed to mimic a particular organ or biological component, such as bone or muscle.

In order to generate sufficient tissue either for tissue engineering or cellular agriculture applications, cell culturing would need to be performed in a bioreactor. There are many different such as hollow-fibre bioreactors, which offer much greater mass transfer of nutrient and oxygen to the cells as well was the removal of waste products. These systems are also a lot more efficient that standard 2D cell culture as the cell media can be recycled back into the bioreactor.

7.1.7 Formulated ingredients from modified cellulose nanofibrils

The structure and interactions of cationic cellulose nanofibrils was characterised within the thesis. There is a lot of potential to explore these nanofibrils further as ingredients in formulated products such as their ability to stabilise oil-in-water

Pickering emulsions by adsorbing to the interface acting as a physical barrier to coalesce. Moreover, the effect adding electrolytes and surfactants to cationic cellulose hydrogels can be investigated. The Hofmeister series of counter ions in coordinated with the quaternary ammonium moiety can be assessed. It would be interesting to probe how cationic nanofibrils interact with oxidised nanofibrils to determine whether stable hydrogels can still be obtained and if there properties differ. The two nanofibril modifications could be combined to form Zwitterionic nanofibrils and the structure and interactions characterised by SANS and rheology. From an application point of view there is scope to develop these nanofibrils as rheology modifiers and also assess their ability to be used in formulation, for example as stabilisers in topical gels and encapsulate active ingredients in Pickering emulsions.

7.1.8 3D Reference Interaction Site Model (RISM)of modified cellulose

To help interpret neutron scattering and NMR data, 3D Reference Interaction Site Model (RISM) is a computational technique used to model cellulose structures. It can model how a solvent hydrates and solvates the cellulose surface and calculate solvation energies, as well as the effect of electrolytes in the system. 3D RISM obtains a 3D-spatial distribution of atomic sites of water molecules around cellulose structures. Each peak in the spectrum indicates a binding position of an atomic site of the water molecule. It requires input of only the solute-solvent interaction potentials, a force field used in standard molecular simulation, and solvent thermodynamic conditions (temperature, density and composition).[3,4]

Preliminary investigations started in spring 2016, during a two-month internship with Prof Munir Skaf based at Centre for Computational Engineering & Sciences, Chemistry Institute at the University of Campinas in Brazil, as part of the Global Innovation Initiative. Several modified cellulose crystalline atomic structures were constructed and to input into RISM to model the hydration properties of cellulose and functionalized cellulose. By using this method, it could provide opportunities to compare experimental SANS results with the model to understand in greater depth the behaviour of dispersed modified cellulose nanofibrils systems. This collaboration is on-going and currently focusing on the interaction energies of modified cellulose surfaces as aggregation occurs.

7.2 References

1. C. Behl and Z. Christine, *Cell aging: molecular mechanisms and implications for disease*, Springer Science & Business Media, Heidelberg, 2013.

2. F. Schweizer, *Eur. J. Pharmacol.*, 2009, **625**, 190–194.

3. E. L. Ratkova, D. S. Palmer, and M. V. Fedorov, *Chem. Rev.*, 2015, **115**, 6312–6356.

4. T. Imai, A. Kovalenko, and F. Hirata, *Chem. Phys. Lett.*, 2004, **395**, 1–6.

Chapter 8

8 Appendix

A. Paper 2 Appendix: Surface Modified Cellulose Scaffolds for Tissue Engineering

A.1 Characterisation of modified cellulose

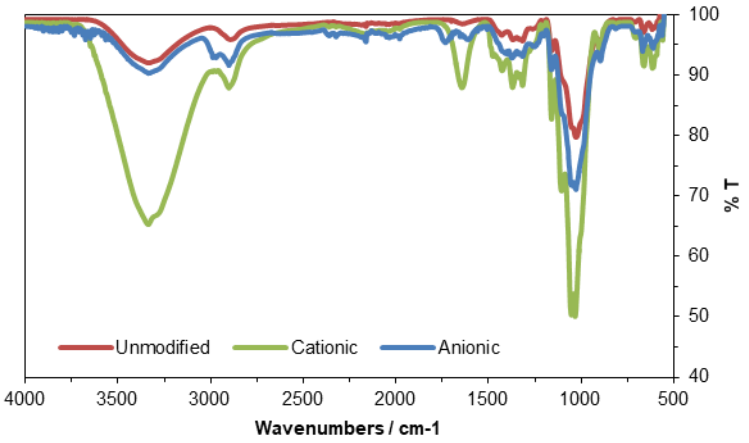

Figure A.1 FTIR spectra for unmodified, cationic (DS = 3.0 ±0.0 %) and anionic (DO = 7.6± 1.0 %) cellulose powders were obtained on a Perkin Elmer Spectrum 100 with a universal ATR sampling accessory; 10 scans were acquired in the range 4000 – 600 cm-1. FTIR: prominent bands at 1440 cm-3 and 1483 cm-3 were attributed to the CH2 bending mode and methyl groups of the cationic cellulose substituents in accordance with data published by (Zaman et al). The peak at 1754 cm-1 on the anionic cellulose spectrum is attributed to the carboxylic acid C=O stretch.

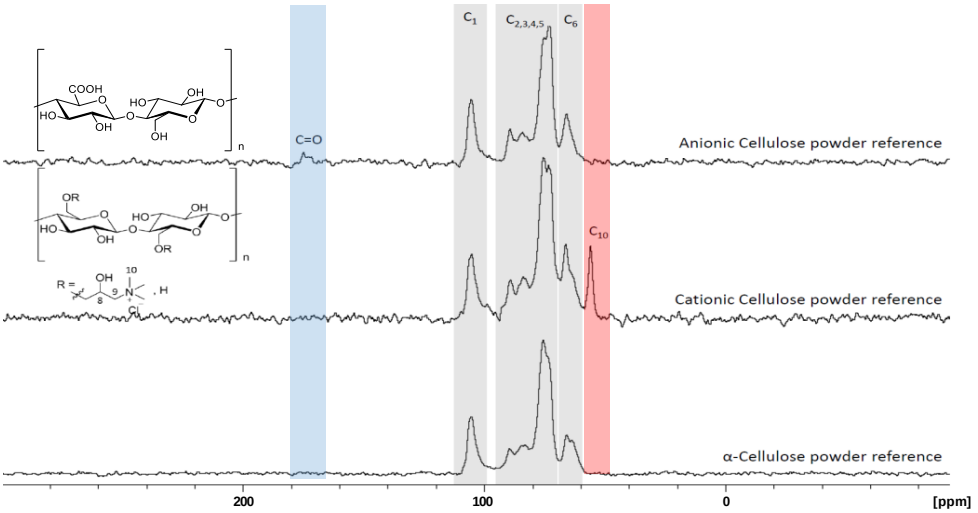

Figure A.2 ^{1}H-^{13}C CP/MAS NMR was performed on unmodified, cationic (DS = 3.0 ±0.0 %) and anionic (DO = 7.6± 1.0 %) cellulose powders (freeze dried). Spectra were acquired at 25 ^{o}C, an MAS rate of 10 kHz and a contact time of 2000 µs. ^{13}C solid-state NMR: signals between 66 ppm and 105 ppm referred to the anhydroglucose, while a signal at 175 ppm appeared upon oxidation, due to the carboxylic acid group (Saito et al. 2005), and a signal at 56 ppm due to the methyl groups on the quaternary ammonium was detected in the cationic cellulose sample (Chaker et al. 2015).

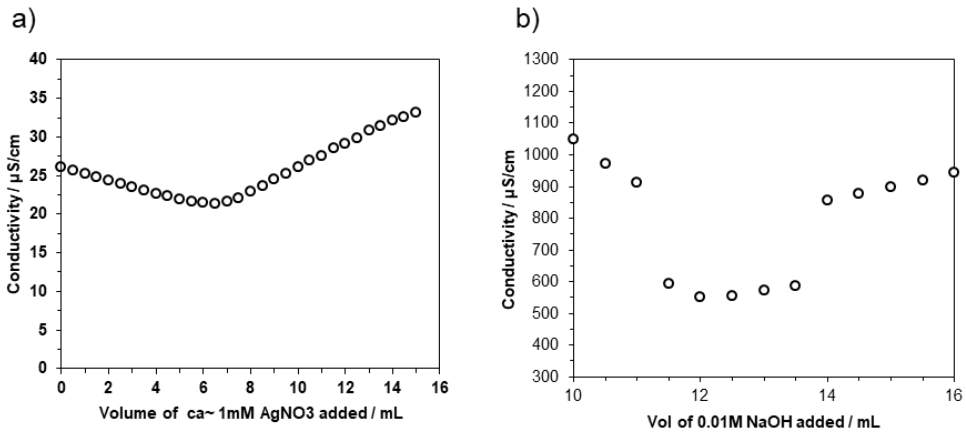

Figure A.3 a) Conductivity curve for cationic cellulose film in DI H2O titrated with ca ~ 1mM AgNO3 at 0.50 mL intervals. b) Conductivity curve following an acid/base titration for anionic cellulose film titrated with 0.01 mM NaOH at 0.5 mL intervals (bottom)

B. Paper 3 Appendix: Modulating cell response on cellulose surfaces; tunable attachment and scaffold mechanics

B.1 Characterisation of surface modified cellulose

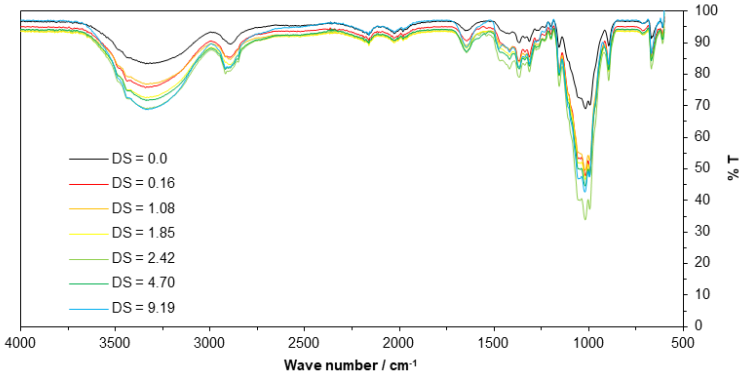

Figure B.1 FTIR spectra for unmodified, cationic (DS = 0 – 9 %) cellulose films were obtained on a Perkin Elmer Spectrum 100 with a universal ATR sampling accessory; 10 scans were acquired in the range 4000 – 600 cm^{-1}. FTIR: prominent bands at 1440 cm^{-3} and 1475 cm^{-3} were attributed to the CH_2 bending mode and methyl groups of the cationic cellulose substituents in accordance with data published by Zaman et al.[1]

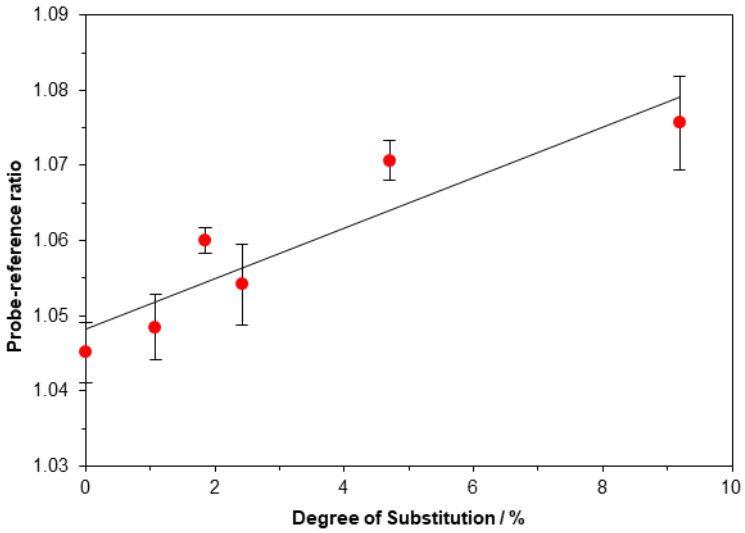

Figure B.2 The degree of substitution can be correlated to the relative intensity ratio between the peak at 1475 cm^{-1} (methyl groups of the cationic group) and 2920 cm^{-1} (CH reference signal).

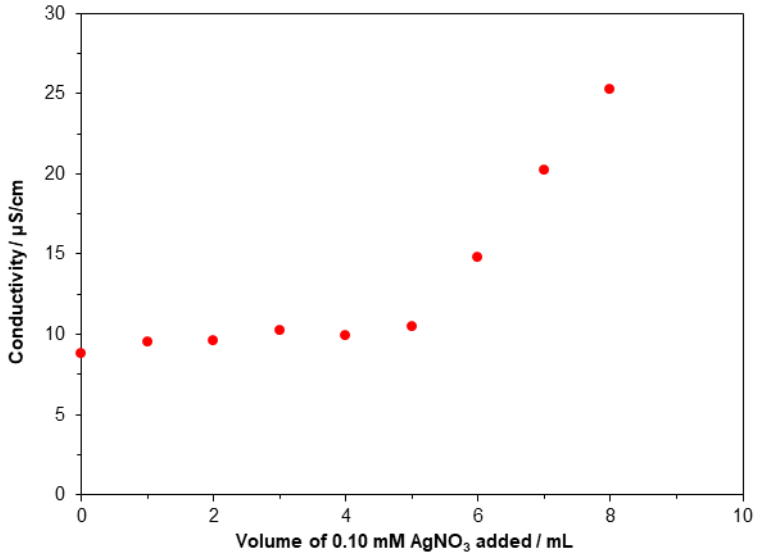

Figure B.3 Conductometric titration curve for a cationic cellulose film in DI H_2O titrated with 0.10 m*M* $AgNO_3$ in 0.50 mL aliquots. The DS for this sample is 2.4 %.

The degree of substitution is calculated using Eq. 1:

$$Degree\ of\ Substitution\ \% = \left[\frac{162.15 \times C \times V}{w - (151.63 \times C \times V)}\right] 100 \qquad \text{(Eq. 1)}$$

where C is the concentration of $AgNO_3$ solution (M), V is the volume of $AgNO_3$ solution (in dm^3), and w is the weight of the dried cationic cellulose sample (g), 162.15 is the M_w of the AGU and 151.63 is the difference in M_w between the AGU and cationised AGU bearing a trimethylammonium chloride group.

B.2 HPLC analysis of structural modification

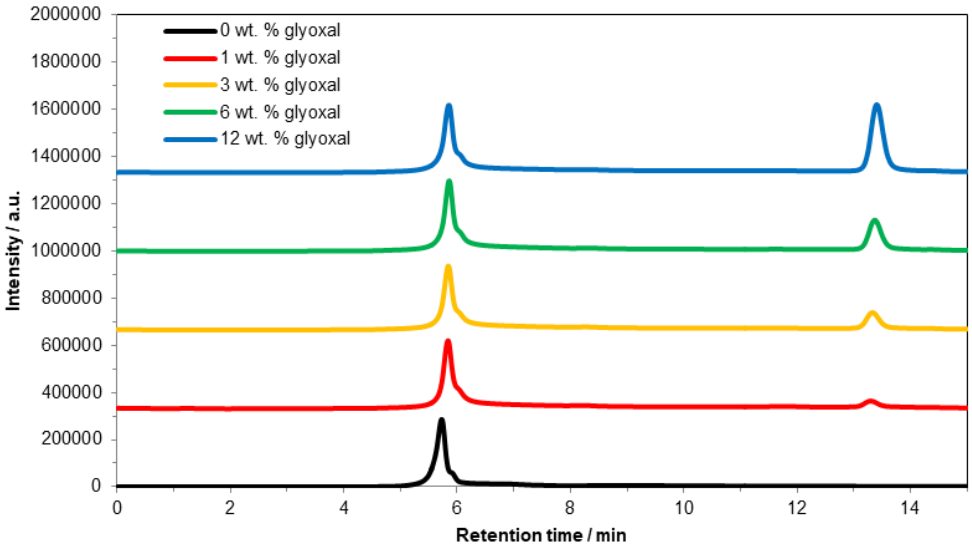

Figure B.4 Unmodified cellulose samples. Chromatograms of the hydrolysis solutions (NaOH c = 4 mol L^{-1}, 100 °C, 15 min): A-E hydrolysis solutions for cellulose films treated with 0, 1, 3, 6, 12 wt. % glyoxal. HPLC conditions; H_2SO_4 = 0.01 mol L^{-1}, BioRad Aminex HPX-87H; flow rate, 0.6 mL min^{-1}; column oven temperature, 50 °C; UV detector wavelength, 210 nm.

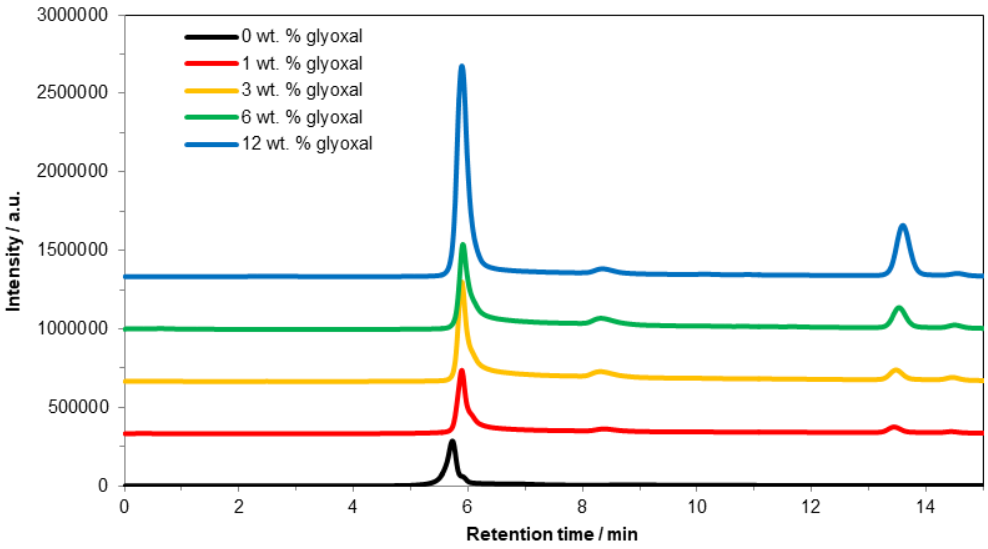

Figure B.5 Cationic cellulose samples. Chromatograms of the hydrolysis solutions (NaOH *c* = 4 mol L^{-1}, 100 °C, 15 min): A-E hydrolysis solutions for cationic cellulose films treated with 0, 1, 3, 6, 12 wt. % glyoxal. HPLC conditions; H_2SO_4 = 0.01 mol L^{-1}, BioRad Aminex HPX-87H; flow rate, 0.6 mL min^{-1}; column oven temperature, 50 °C; UV detector wavelength, 210 nm.

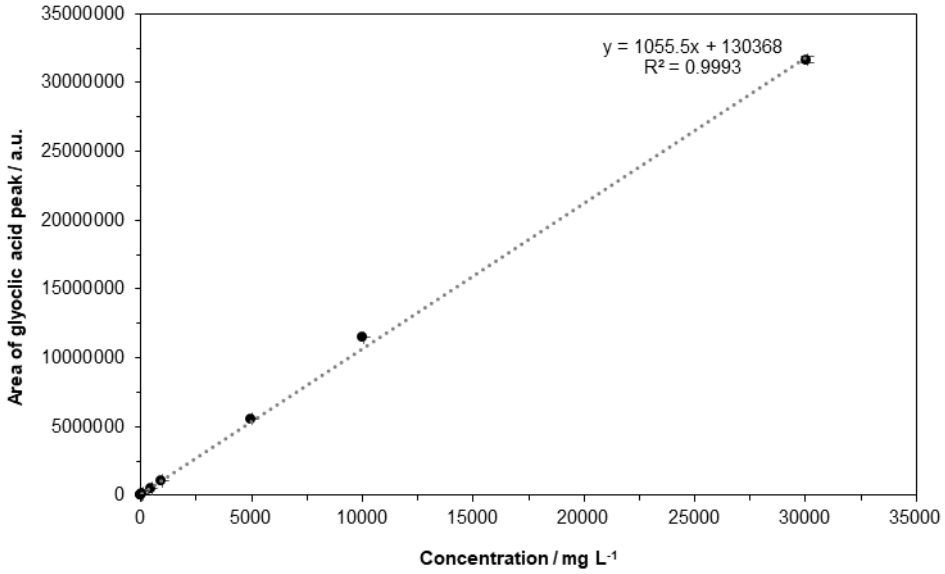

Figure B.6 Glycolic acid peak area for prepared standard solutions (20 – 30,000 mg L^{-1}). Calibration coefficient for glycolic acid was calculated from the gradient of the line to be 1055.5 a.u.^{2}/ mg L^{-1}. (n = 3, error bars = standard deviation)

B.3 Cell attachment studies

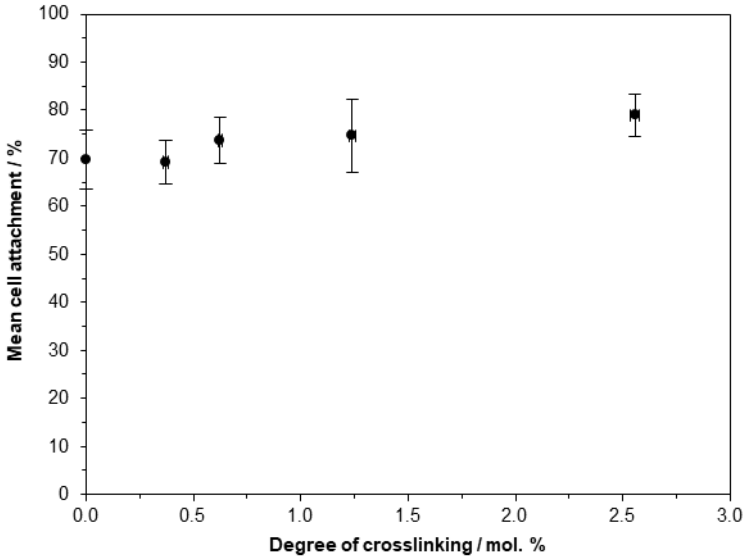

Figure B.7 The influence of glyoxal crosslinking on MG-63 cell attachment. Cells were incubated 1 h at 37 ^{o}C in 5 % CO_2 on cationically modified cellulose films (DS = 4.7 %) without FBS serum ligands adsorbed on the surface (n= 3; error bars show standard error). Cell attachment on cross-linked scaffolds were not significantly different from each other

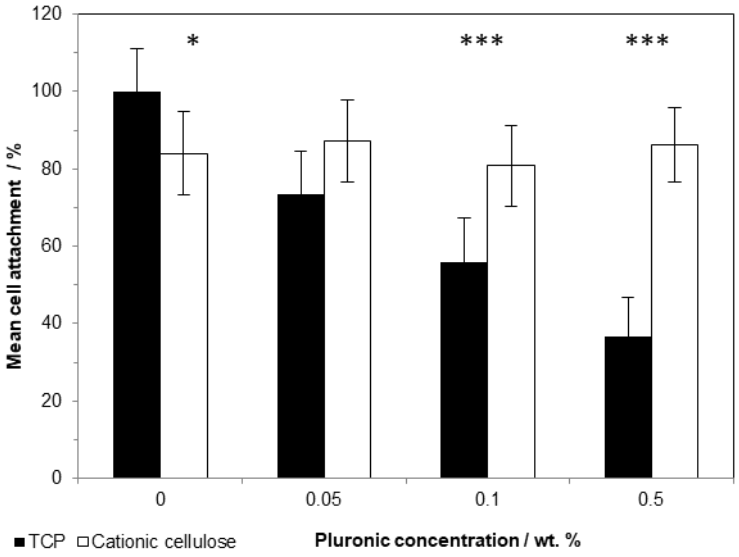

Figure B.8 The effect of Pluronic L127,which blocks non-specific cell binding sites, on MG-63 cell attachment (after 1 h incubation at 37 °C in 5 % CO_2) on tissue culture plastic and cationically modified cellulose films with no added ligands adsorbed on the surface (n=3; error bars show standard error).

B.4 Characterisation of scaffold properties

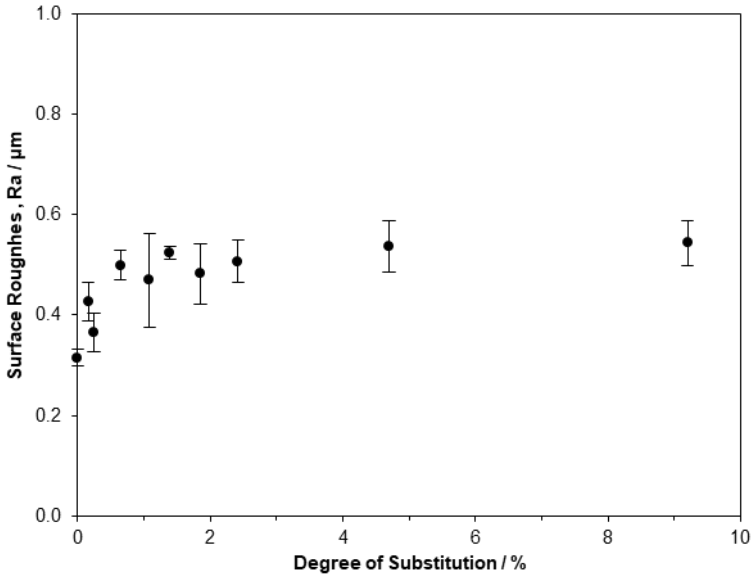

Figure B.9 Influence of DS on scaffold surface roughness. Minimal change in surface roughness was observed on the cationically modified scaffolds. AFM images processed and analysed with Gwyddion software. The surface roughness, R_a, was calculated using the "1D height analysis" function of the programme.

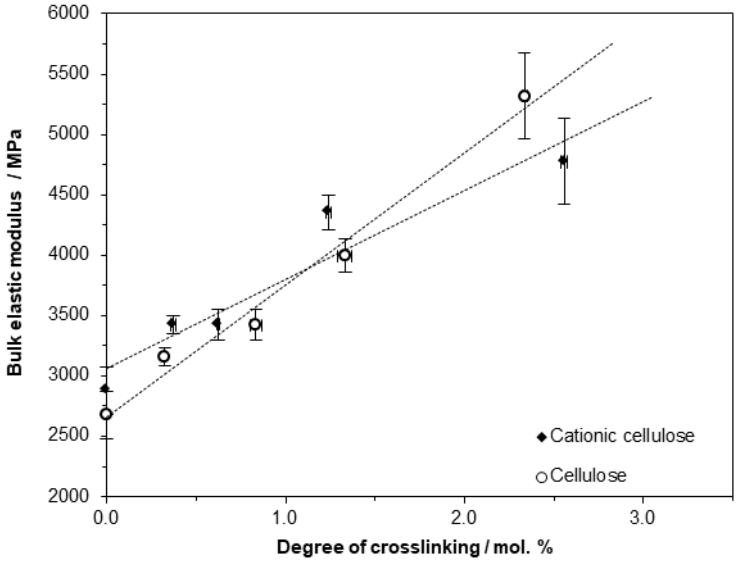

Figure B.10 The bulk elastic modulus of hydrated cellulose films increased upon crosslinking with glyoxal. The measurements were performed at 80 % relative humidity. (n=5; error bars show standard error). Cationic cellulose, $R^2 = 0.907$ & cellulose, $R^2 = 0.983$.

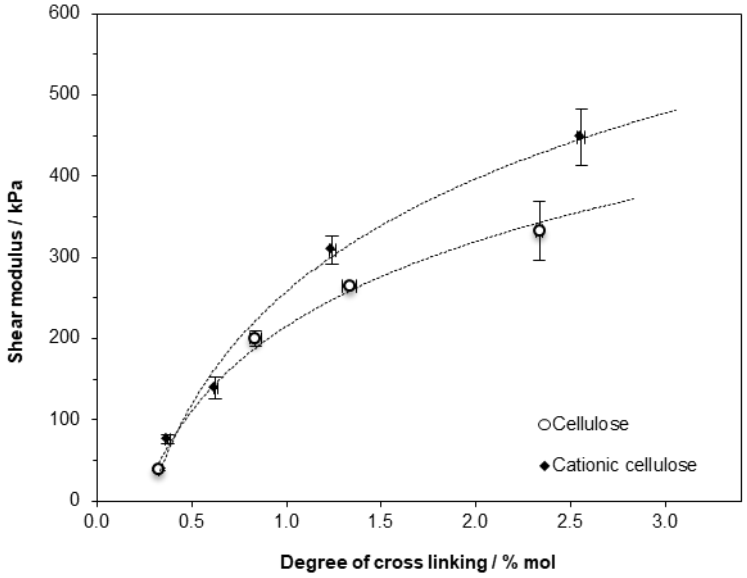

Figure B.11 The surface shear modulus of unmodified and cationic cellulose (4.7 % DS) films with increasing amounts of crosslinking by glyoxal. Data fitted to a logarithmic expression. (n=4; error bars show standard error). Cationic cellulose, $R^2 = 0.989$ & cellulose, $R^2 = 0.992$.

B.5 Cell spreading studies

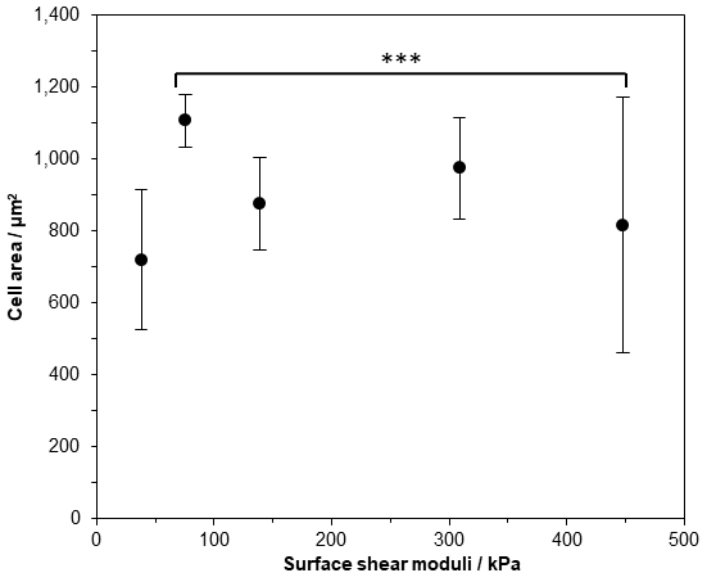

Figure B.12 Mean cell area after 24 h incubation at 37 °C in 5 % CO_2 on cationic cellulose scaffolds (DS = 4.7 % with increasing degrees of cross-linking (DXL = 0 – 2.6 %). Modulating the structural properties of the scaffolds through glyoxal crosslinking did influence cell area but the relationship was not a clear one. Cell area will initially increase once attached onto the surface as they flatten. However as cells elongate the projected area will not necessarily increase. This made distinguishing the influence on greater crosslinked scaffolds difficult. Hence aspect ratio was used as a clearer measure of cell spreading. (n= 51 – 116, error bars show standard error). MG-63 cells, incubated on tissue culture polystyrene, were used as the control: average cell area 1725 ±129 cm^2. *** were significantly different from non-crosslinked cationic cellulose with p value < 0.001.

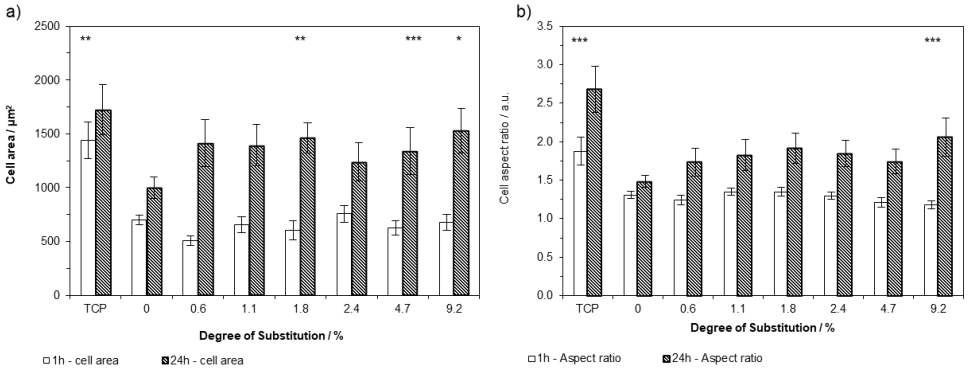

Figure B.13 a) The change in cell area; b) and aspect ratio after 24 h incubation at 37 ^{o}C in 5 % CO_2, (n= 24 - 435; error bars show standard error) demonstrated spreading of MG-63 occurred on the cationic cellulose scaffolds. The control scaffold was treated tissue culture plastic and cells on this surface exhibited an average area of 1725 ±129 µm^2 and an aspect ratio of 2.68 ±0.17. Samples marked ***, ** and * are significantly different from unmodified cellulose with $p < 0.001$, $p < 0.01$ and $p < 0.05$ respectively.

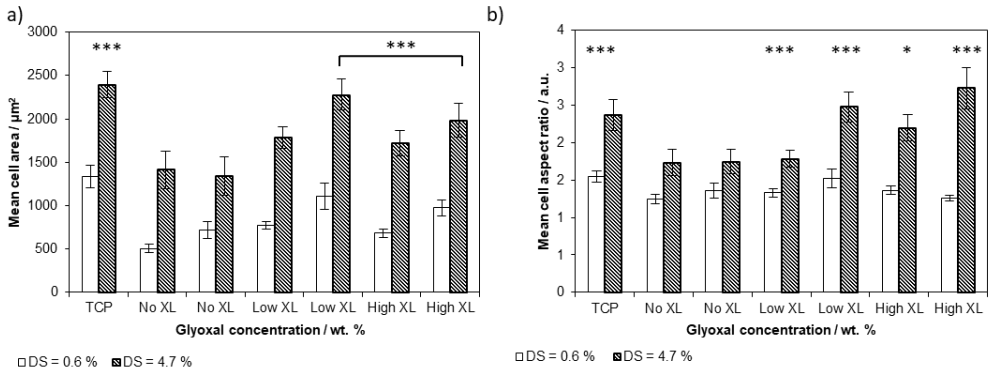

Figure B.14 Influence of DS and DXL on MG-63 morphology; cell area (a) and aspect ratio (b) on cationic cellulose scaffolds (DS 0.6 and 4.7 %) treated with varying glyoxal concentrations (0, 1, 6 wt. %) after 24 h incubation at 37 ^{o}C in 5 % CO_2, (n= 38 - 193; error bars show standard error). Cell images were analysed by ImageJ to calculate the average cell aspect ratio and area. Tissue culture plastic was used as a control, where cells had an area of 1725 ±129 cm^2 and an aspect ratio of 2.37. Samples marked ***, ** & * were significantly different from uncross-linked cationic cellulose with $p < 0.001$, $p < 0.01$ and $p < 0.05$ respectively.

C. Paper 4 Appendix: Simple to fabricate, micropatterned, 2D cellulose scaffolds for localised cell attachment

C.1 Interfacial Tension Of GTMAC 'Inks'

For an ink solution to jet effectively from the DIMATIX inkjet printer heads, the interfacial tension (IFT) needs to be in the range 32 – 42 dynes / cm, at jetting temperature. The IFT of GTMAC solutions was obtained by the pendent drop method on a SCA20 contact angle instrument. The droplet volume was set at 20 µL delivered from a 500 µL Hamilton syringe with a needle diameter of 1.27 mm diameter. Ten measurements were taken for each sample and the average reported.

C.2 Scanning probe microscopy

SPM was employed to obtain topography and capacitance gradient (*dC/dz*) images of unmodified, and cationic, cellulose films using a Park NX-10 Atomic Force Microscope.[2,3] Kelvin force and capacitance coupling measurements were conducted in parallel by applying an electric AC signal at 17 kHz to the metal-coated cantilever - the DC potential was applied to the cantilever to nullify the AC signal at 17 kHz to determine the electric potential of the sample. The capacitance gradient (*dC/dz*), or capacitance coupling, of the tip to the sample was proportional to the second harmonic of the AC signal (34 kHz). The AFM images were processed and analysed using Gwyddion software [4] and the "1D height analysis" function of the programme used to calculate the capacitance coupling signal distribution on the film.

C.3 NMR Analysis of GTMAC Hydrolysis

To test stability of GTMAC "inks" to hydrolysis when exposed to elevated temperatures during printing, the rate of hydrolysis of GTMAC in a basic aqueous solution was determined by using the relative integrated areas of well-defined signals in ^{1}H NMR spectra. GTMAC (100 mg, 0.66 mmol) was added to NaOD (40 wt. % aqueous solution, 67.6 mg) and 1000 mg of D_2O. The solutions were reacted at 25, 45 and 65 ^{o}C for 2 h and ^{1}H NMR spectra recorded every 5 min. ^{1}H NMR spectra were recorded on a Bruker Avance 500 NMR spectrometer at 500 MHz.

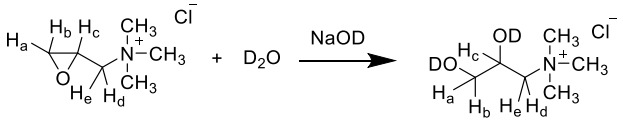

Scheme C.1 Hydrolysis of GMTAC by NaOD in D_2O

The rate of hydrolysis was determined from the change in integrated area for protons attached to the carbon atoms of the epoxide, H_a-H_e, over the 2 h reaction time. The half-life at each temperature was calculated from Equation 1:

$$t_{1/2} = \frac{\ln 2}{k} \quad \text{(Equation 1)}$$

Where *k* is the rate constant determined as the gradient of the plot ln (integral area) *vs*. time.

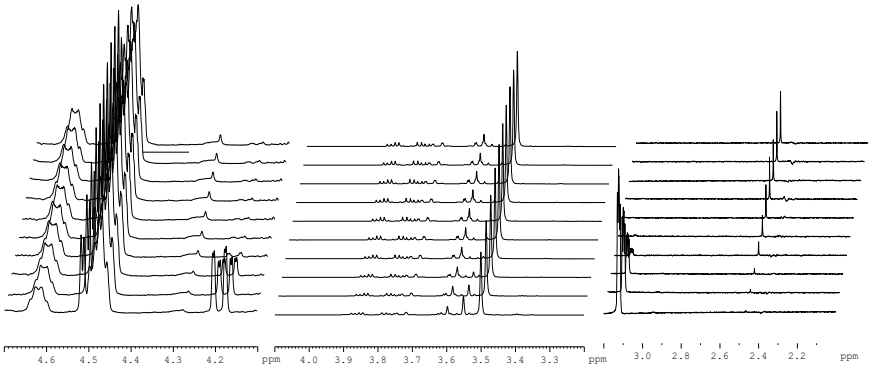

Figure C.1 Stacked ^{1}H NMR spectra for the hydrolysis of GTMAC in 1 mol g^{-1} solution of NaOD in D_2O at a reaction temperature of 65 ^{o}C. Spectra were acquired at 5 min intervals.

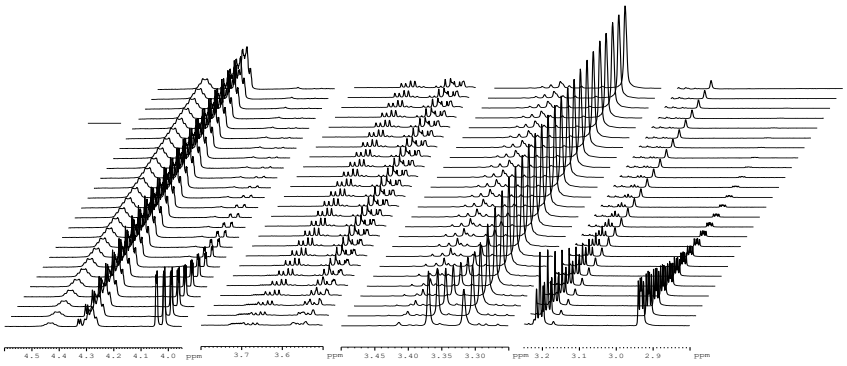

Figure C.2 Stacked ^{1}H NMR spectra for the hydrolysis of GTMAC in 1 mol g^{-1} solution of NaOD in D_2O at a reaction temperature of 45 ^{o}C. Spectra were acquired at 5 min intervals.

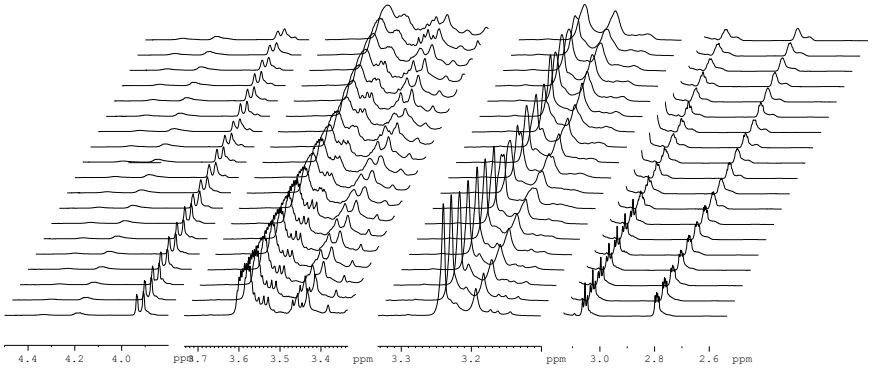

Figure C.3 Stacked ^{1}H NMR spectra for the hydrolysis of GTMAC in 1 mol g^{-1} solution of NaOD in D_2O at a reaction temperature of 25 ^{o}C. Spectra were acquired at 5 min intervals.

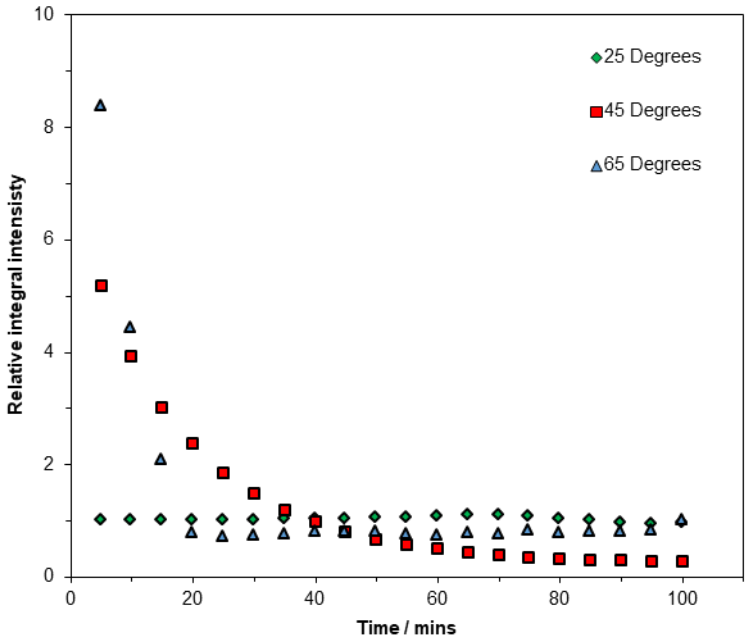

Figure C.4 Change in integrated area for the GTMAC resonance at 3.55 ppm (due to epoxide protons) at 25 ^{o}C (diamonds); 45 ^{o}C (squares); and 65 ^{o}C (triangles).

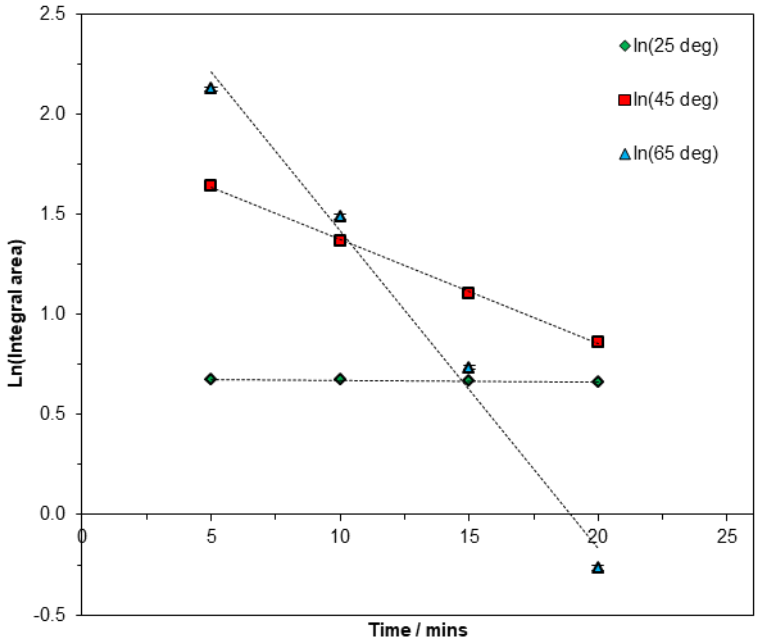

Figure C.5 1st order kinetic plots for base hydrolysis of GTMAC at 25 ^{o}C (diamonds); 45 ^{o}C (squares); and 65 ^{o}C (triangles). At 25 ^{o}C the epoxide was not hydrolysed within the two hour measurement period. 1st order rate constants were determined from the gradient of the plots of ln (integral area) *vs*. time: 25 ^{o}C = 0.001 min^{-1}; 45 ^{o}C = 0.052 min^{-1}; 65 ^{o}C = 0.159 min^{-1} (R^2 = 0.9362, 0.9991 and 0.9893 for fitted lines). Half-lives, $t_{½}$, for hydrolysis at 45 ^{o}C and 65 ^{o}C were calculated as 13 and 4 min respectively. Exposure of GTMAC to elevated temperatures in the heated nozzle of the printer was brief enough to avoid hydrolysis.

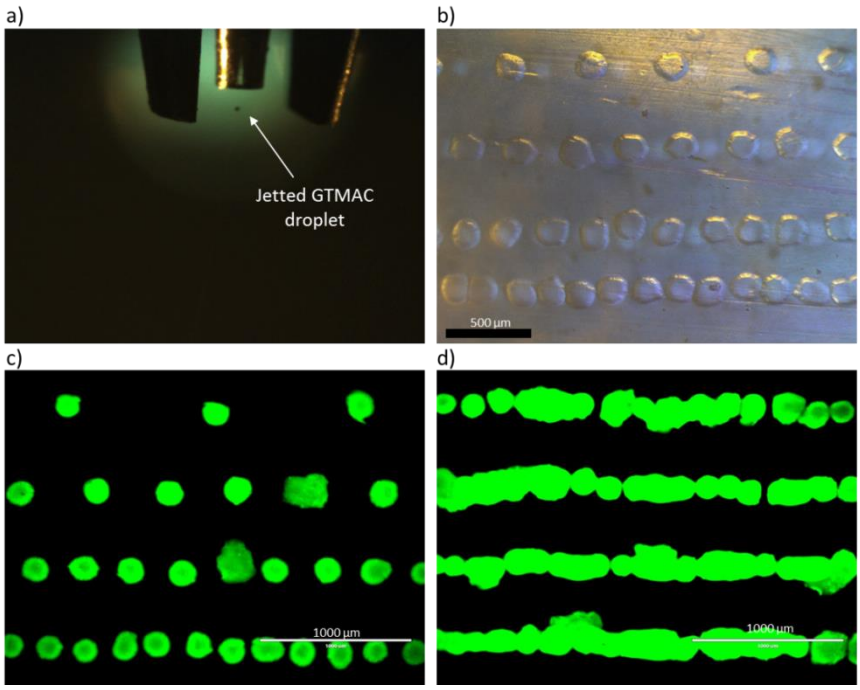

Figure C.6 a) Image of GTMAC droplet jetted from inkjet nozzle. b) Optical microscope image of GTMAC droplets on cellulose film at increasing density of droplets per mm, scale bar =500 µm. c & d) Fluorescent microscope images of 5(6)-carboxyfluorescien stained cationic islands printed in lines at increasing linear droplet density, scale bar =1000 µm.

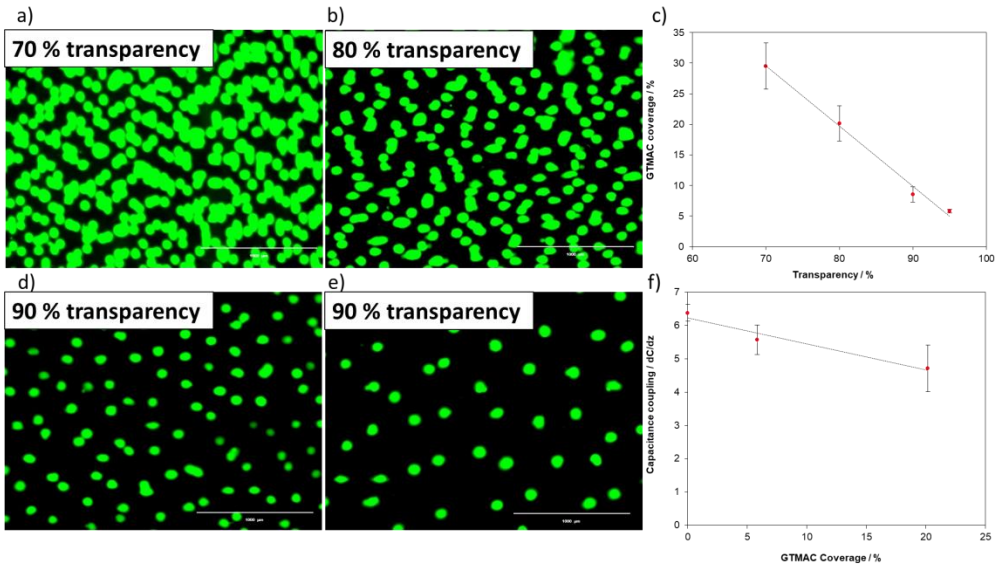

Figure C.7 Fluorescent microscope images of 5(6)-carboxyfluorescein stained cationic islands printed at different transparencies, scale bar =1000 µm: a) 70 % transparency, b) 80 % transparency, d) 90 % transparency, and e) 95 % transparency. c) Relationship between "transparency", or droplet density to percentage of GTMAC coverage across the film surface. f) A plot of capacitance coupling (from scanning probe microscopy) *vs*. GTMAC coverage shows how the increase in area of cationisation reduces the overall capacitance coupling of the film surface by counteracting to the negative charge of the bulk unmodified cellulose.

D. Paper 5 Appendix: Unravelling cationic cellulose nanofibril hydrogel structure: NMR spectroscopy and small angle neutron scattering analyses

D.1 Characterisation of modified cellulose

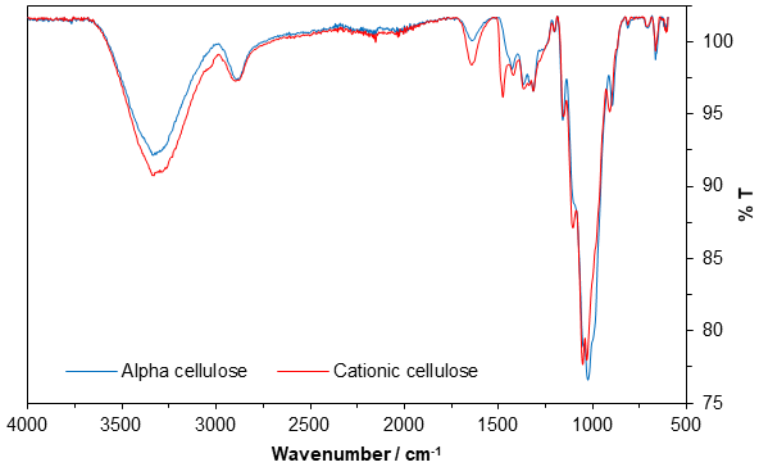

Figure D.1 FTIR spectra for unmodified α-cellulose and CCNF (DS = 23.0 ±0.9 %) powders were obtained on a Perkin Elmer Spectrum 100 with a universal ATR sampling accessory; 10 scans were acquired in the range 4000 – 600 cm^{-1}. FTIR: prominent bands at 1440 cm^{-1} and 1483 cm^{-1} were attributed to the CH_2 bending mode and methyl groups of the cationic cellulose substituents in accordance with data published by Zaman *et al*.[1].

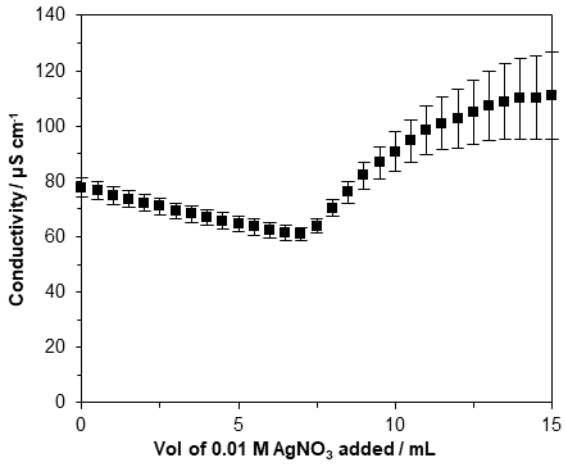

Figure D.2 Conductivity curve for CCNF in DI H_2O titrated with ca ~ 1 m*M* $AgNO_3$ at 0.50 mL intervals.

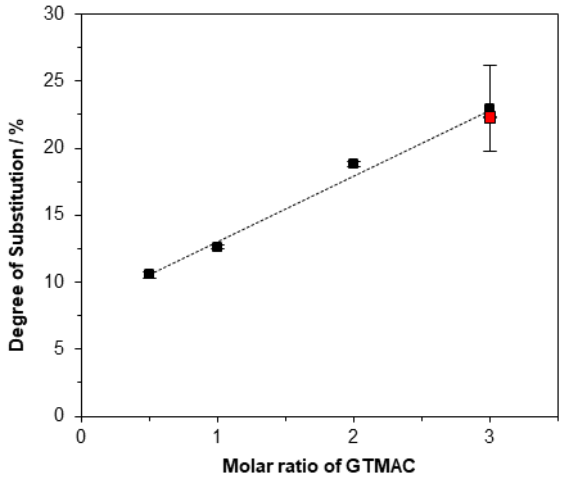

Figure D.3 a) DS of CCNF determined using a Mütek Particle Charge Detector (black points) and by conductometric titration (red point). The average of three values was reported with the standard error shown as error bars.

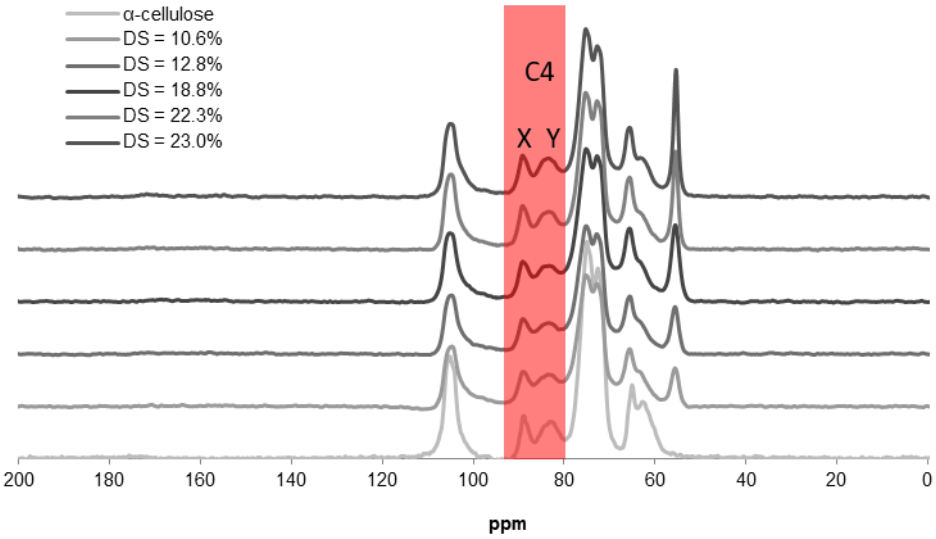

Figure D.4 Summary of ^{1}H-^{13}C CP/MAS NMR spectra for α-cellulose and CCNF (DS 10.6 - 23.0%) powders, acquired using MAS rates of 10 kHz. The signal at 55.5 ppm is assigned to the methyl carbon resonances of the quaternary ammonium group and used to determine DS. The crystallinity index was determined by separating the C4 region of the spectrum into crystalline and amorphous peaks, and calculated by dividing the area of the crystalline peak (87 – 93 ppm) by the total integrated area of the C4 peaks (80 to 93 ppm)

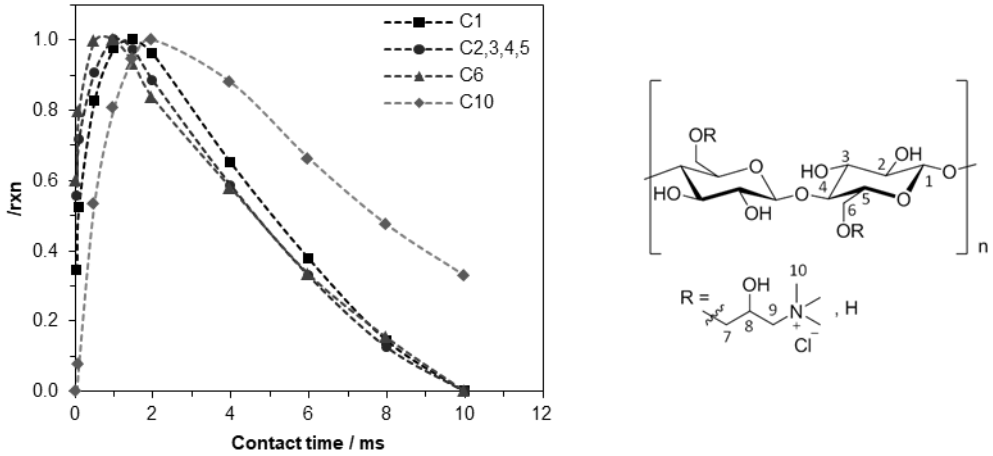

Figure D.5 ^{1}H-^{13}C Cross-polarisation kinetics curves for carbon peaks in CCNF powder (DS = 23.0 %). The experimental error associated with the measurement of peak intensities is below 10 %.

D.2 Small angle Neutron scattering

Table D.1 SANS fitting parameters for a flexible cylinder with elliptical cross-section model. The length was held at 1000 Å, sldCyl 1.75 x 10^{-6} and sldSolv: D_2O = 6.34 x 10^{-6}, H_2O = –5.61 x 10^{-7}.

Parameter	Description	Units
Scale	Volume Fraction	None
Background	Source background	cm^{-1}
Lengh	Length of the flexible cylinder	Å
Kuhn_length	Kuhn length of the flexible cylinder	Å
radius	Radius of the flexible cylinder	Å
Axis_ratio	Axis_ratio (major_radius/minor_radius	None
Sld	Cylinder scattering length density	10^{-6}Å
Sld_Solvent	Solvent scattering length density	10^{-6}Å

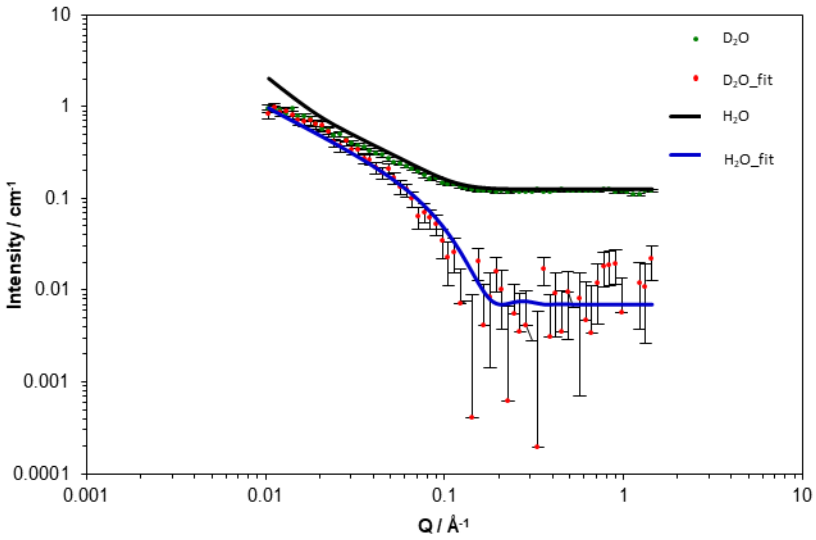

Figure D.6 Experimental SANS spectra of CCNF hydrogels (10.6 % DS) simultainiously fitted to a flexible ellipsoidal cylinder model (scattered points are data and solid lines are the fitted curves) in D_2O or H_2O.

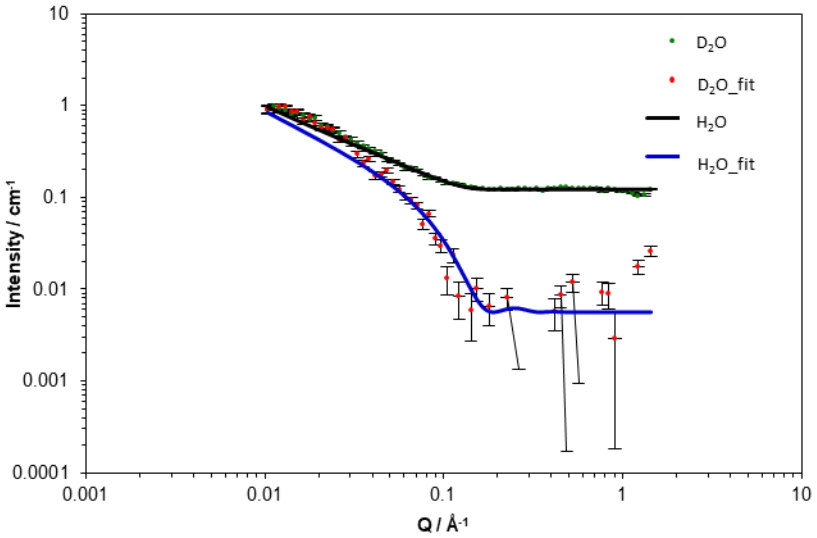

Figure D.7 Experimental SANS spectra of CCNF hydrogels (12.6 % DS) simultaneously fitted to a flexible ellipsoidal cylinder model (scattered points are data and solid lines are the fitted curves) in D_2O or H_2O.

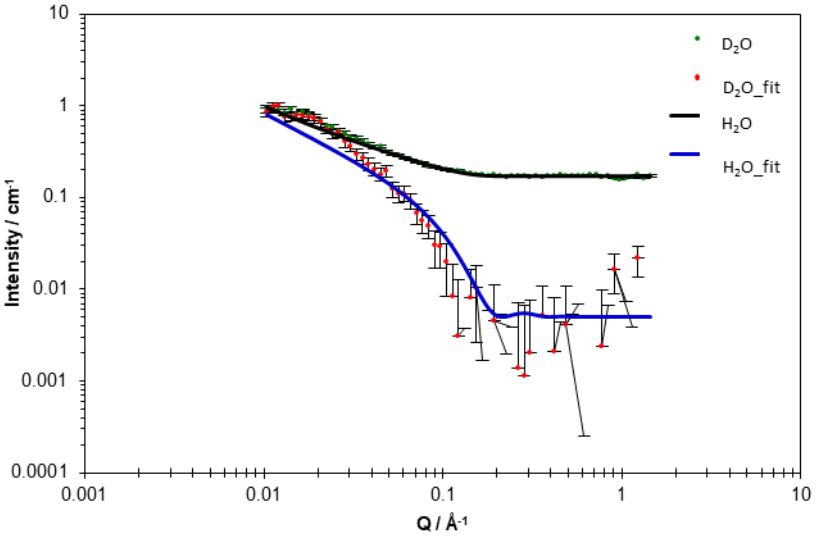

Figure D.8 Experimental SANS spectra of CCNF hydrogels (18.8 % DS) simultaneously fitted to a flexible ellipsoidal cylinder model (scattered points are data and solid lines are the fitted curves) in D_2O or H_2O.

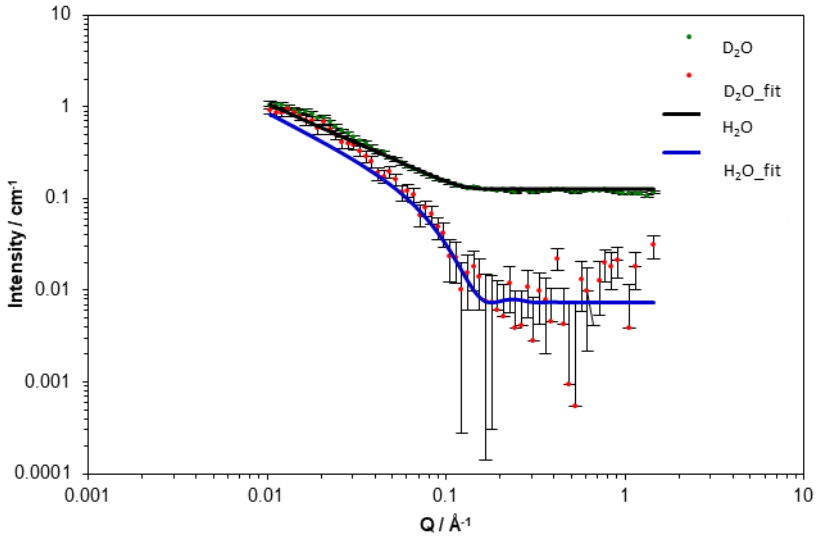

Figure D.9 Experimental SANS spectra of CCNF hydrogels (23.0 % DS) simultaneously fitted to a flexible ellipsoidal cylinder model (scattered points are data and solid lines are the fitted curves) in D_2O or H_2O.

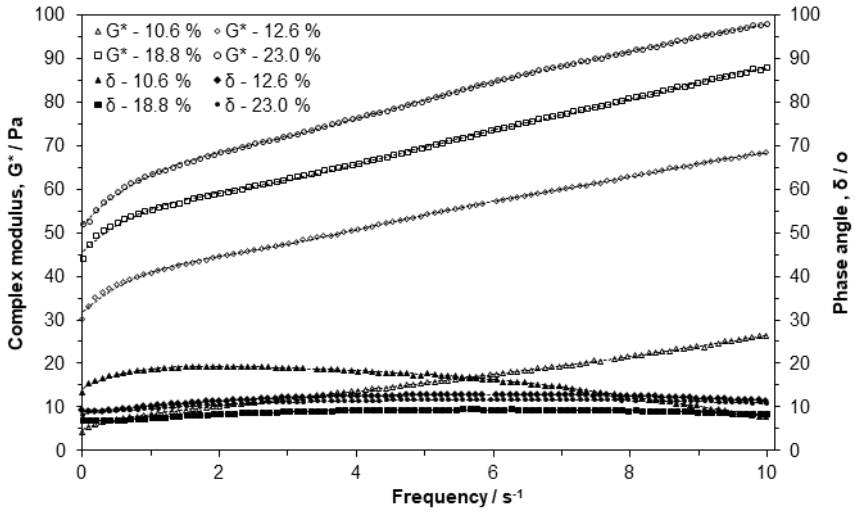

Figure D.10 Complex modulus (*G**) and phase angle (δ) *versus* frequency for 2 wt.% CCNF hydrogels with DS of 10.6, 12.6, 18.0 and 23.0 %. Values obtained at a frequency of 1.02 Hz. As the DS increased the complex modulus increased and the phase angle decreased, this is associated with increased elasticities.

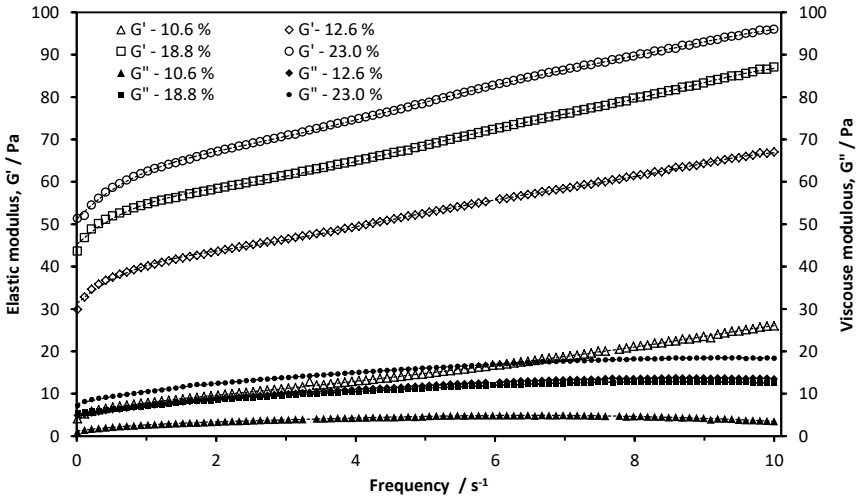

Figure D.11 Elastic (G') and viscous (G") modulus versus frequency for 2 wt.% CCNF hydrogels with DS of 10.6, 12.6, 18.0 and 23.0 %. Values obtained at a frequency of 1.02 Hz. As the DS increased both the elastic and viscous modulus values increased, but the elastic modulus is greater and increased more, which is a good indication of strong structuring within the gel.

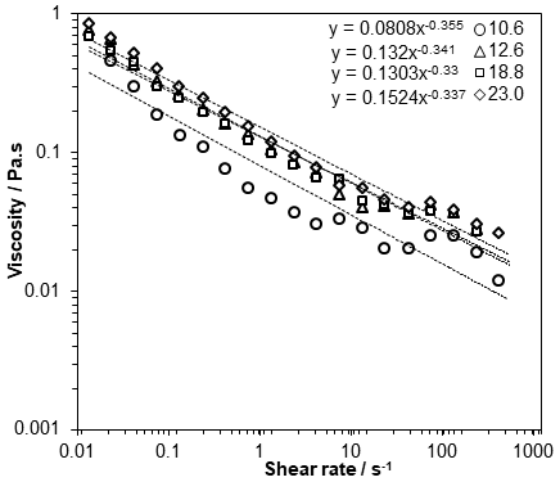

Figure D.12 Viscosity versus shear rate for 2 wt. % CCNF hydrogels with DS of 10.6, 12.6, 18.0 and 23.0 %. Values obtained at a shear sweap of 113.17 s^{-1}. Trend line fitted to a the expression $y = ax^{-b}$ to determine the degree of shear thinning of the hydrogels.

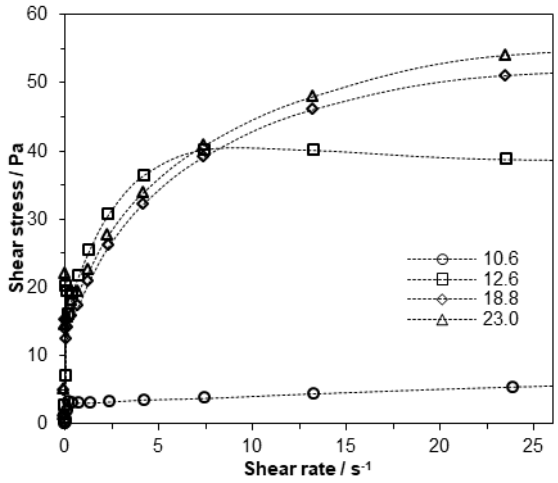

Figure D.13 Elastic (*G*') and viscous (*G*'') modulus versus frequency for 2 wt.% CCNF hydrogels with DS of 10.6, 12.6, 18.0 and 23.0 %. Values obtained at a frequency of 1.02 Hz. As the DS increased both the elastic and viscous modulus values increased, but the elastic modulus is greater and increased more, which is a good indication of strong structuring within the gel.

D.3 NMR Spectroscopy

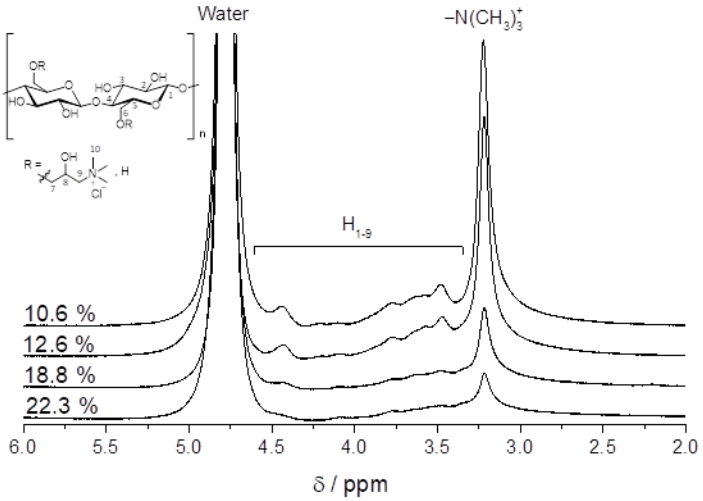

Figure D.14 ^{1}H solution-state NMR spectra of 4 wt. % CCNF hydrogels with DS between 10.6 – 23.0 %, acquired at 25 °C.

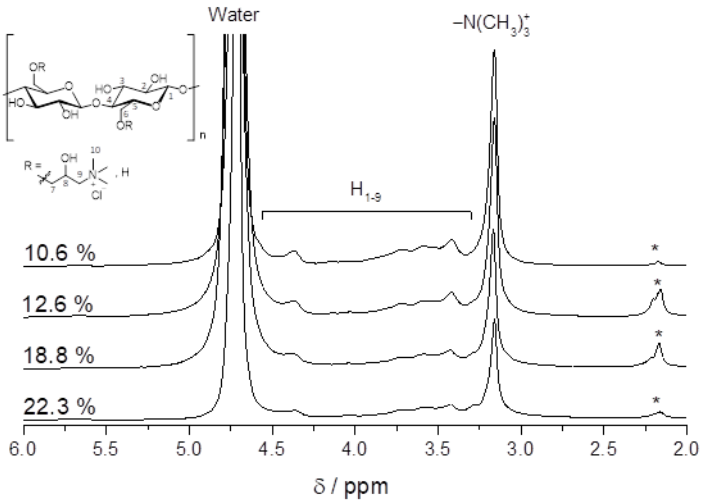

Figure D.15 ^{1}H HR-MAS NMR spectra of 4 wt. % CCNF hydrogels with DS between 10.6 – 23.0 %, acquired at 25 °C with a MAS rate of 2 kHz. Asterisks represent spinning sidebands.

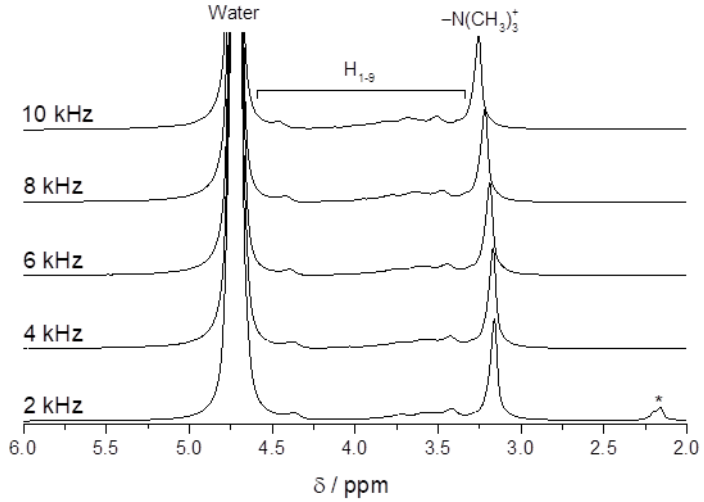

Figure D.16 ^{1}H HR-MAS NMR spectra of 4 wt. % CCNF hydrogels with MAS rates between 2 and 10 kHz, acquired at 25 °C. The asterisk represents spinning sidebands.

Table D.2 ^{1}H solution-state T_1 relaxation times for the trimethyl protons in 4 wt. % CCNF hydrogels with DS 23 %, acquired between 5 and 45 °C.

T / °C	T_1 / s	
	Trimethyl	Water
5	0.41 (± 0.009)	2.14 (± 0.036)
25	0.48 (± 0.008)	2.56 (± 0.041)
45	0.54 (± 0.014)	3.75 (± 0.026)
65	0.79 (± 0.009)	4.73 (± 0.043)

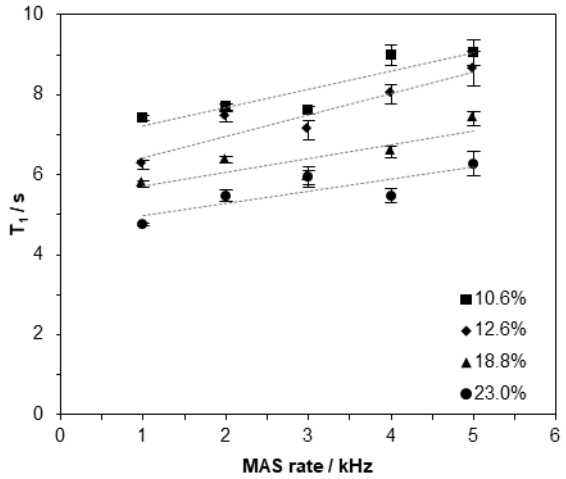

Figure D.17 ^{1}H HRMAS T_1 times for water protons in 4 wt. % CCNF hydrogels with increasing DS, acquired with MAS rates between 2 and 10 kHz.

The following equation was used by Asano *et al.* (2012) to calculate the pressure (*P*) exerted on styrene-butadiene rubber samples from the MAS rate (*k*), using the inner radius of the rotor (*r*) and the sample density (ε),[5]

$$P = \frac{4}{3}\pi^2 k^2 r^2 \varepsilon.$$

Even though the polymeric hydrogels under study are heterogeneous mixtures of liquid and solid components, the same expression can be used to roughly estimate the inner pressure. The pressure inside the rotor due to centrifugal forces was determined to be in the range of 30 to 3000 Pa for CCNF gels (for MAS rates between 2 and 10 kHz), values which are significantly greater than the yield stresses (τ^0 in the range of 3 to 54 Pa).

E. Paper 6 Appendix: Mechanically robust cationic cellulose nanofibril scaffold with tuneable biomimetic porosity for cell culture

E.1 Characterisation of modified cellulose

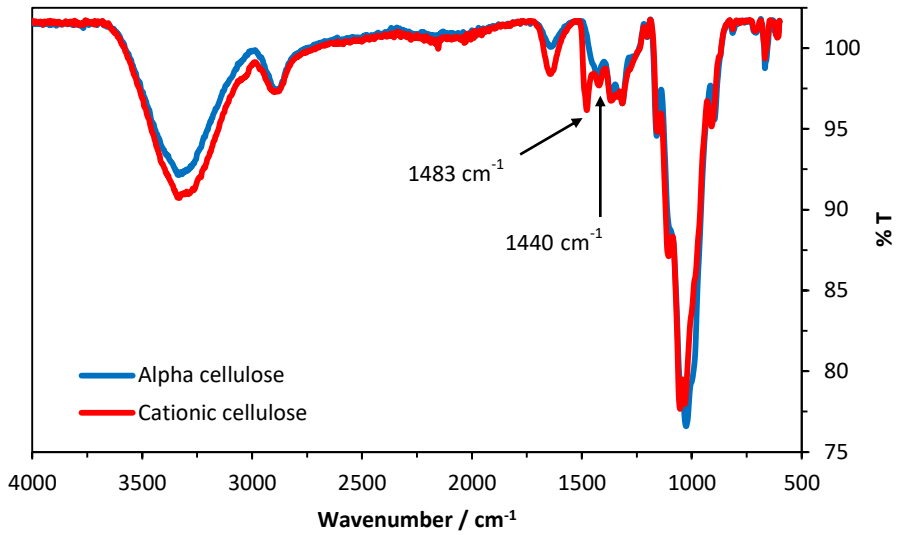

Figure E.1 FTIR spectra for unmodified α-cellulose and CCNF (DS = 23.0 ±0.9 %) powders were obtained on a Perkin Elmer Spectrum 100 with a universal ATR sampling accessory; 10 scans were acquired in the range 4000 – 600 cm^{-1}. FTIR: prominent bands at 1440 cm^{-1} and 1483 cm^{-1} were attributed to the CH_2 bending mode and methyl groups of the cationic cellulose substituents in accordance with data published by Zaman *et al.*[1].

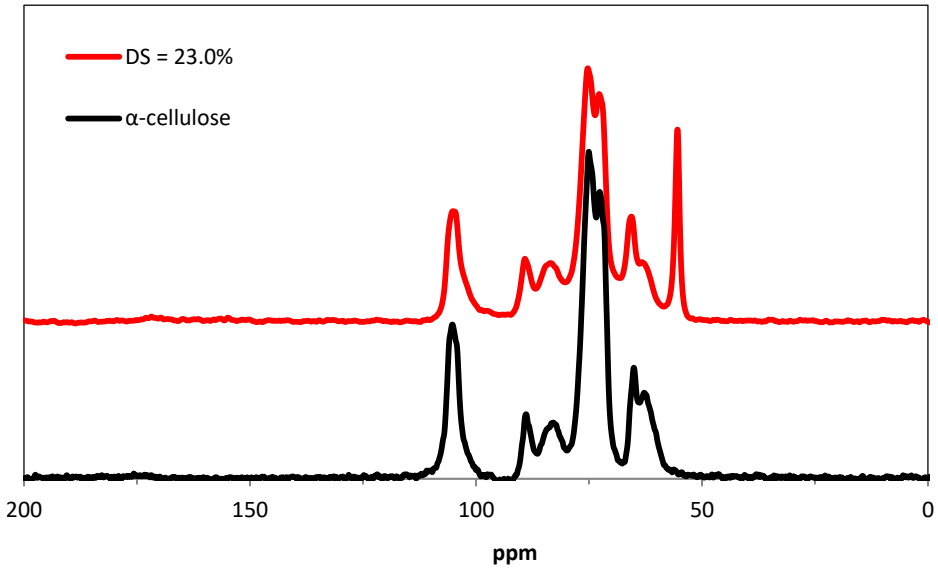

Figure E.2 ^{1}H-^{13}C CP/MAS NMR spectra for α-cellulose and CCNF (DS = 23.0%) powders, acquired using MAS rates of 10 kHz. The signal at 55.5 ppm is assigned to the methyl carbon resonances of the quaternary ammonium group and used to determine DS.

Conductometric analysis of degree of substitution

The degree of substitution of cationic cellulose was determined by conductometric titration of chloride ions (trimethylammonium chloride groups) with $AgNO3_{(aq)}$ as described previously.[6] The conductivity was monitored using a SevenMulti Mettler Toledo conductivity probe. The degree of substitution is calculated by:

$$Degree\ of\ Substitution\ \% = \left[\frac{162.15\times(C\times V)}{w-(151.63\times C\times V)}\right] 100 \qquad \text{(Eqn. 1)}$$

Where C is the concentration of $AgNO_3$ solution (*M*), V is the volume of $AgNO_3$ solution (in dm^3), and w is the weight of the dried cationised cellulose sample (g), 162.15 is the M_w of the anhydroglucose unit (AGU) and 151.63 is the difference in M_w between the AGU and cationised AGU bearing trimethylammonium chloride groups. Triplicate samples were analysed and an average reported.

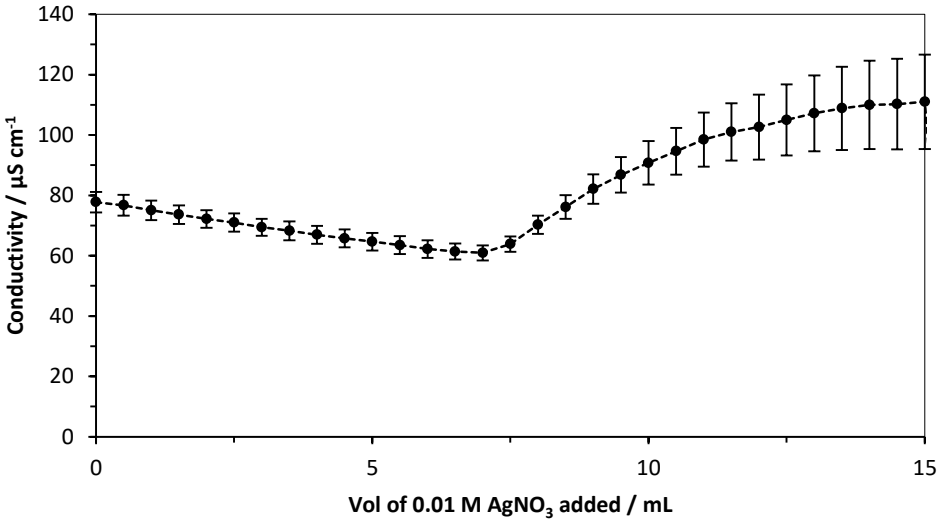

Figure E.3 Conductivity curve for CCNF in DI H_2O titrated with *ca* ~ 1 m*M* $AgNO_3$ in 0.50 mL aliquots.

Degree of crosslinking

The degree of crosslinking (DXL) was determined by HPLC analysis following a method adapted from Schramm *et al*.[7] Briefly, dry crosslinked cellulose films were hydrolysed, filtered, and the concentration of glycolic acid in each solution was determined by HPLC analysis. Once the mass of glyoxal present in the crosslinked films was determined (using a calibration curve) the DXL was calculated using the following equation:

$$Degree\ of\ Crosslinking\ \% = \left[\frac{162.15 \times Mol_{glyoxal}}{w - (58.04 \times Mol_{cellulose})}\right] 100 \qquad \text{(Eqn. 2)}$$

Where $Mol_{glyoxal}$ is the amount of glyoxal detected by HPCL (mol), $Mol_{cellulose}$ is the amount of cross linked cellulose present (mol) and *w* is the weight of the dried cross linked cellulose sample (g), 162.15 is the M_w of the AGU and 58.04 is the difference in M_w between the AGU and cross linked AGU bearing a glyoxal group. Triplicate samples were analysed for each material and an average reported.

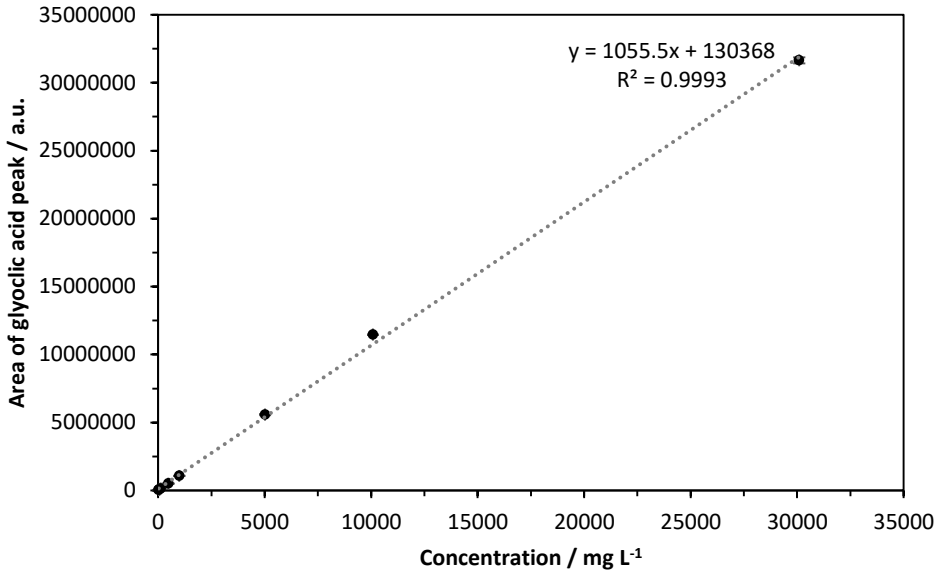

Figure E.4 Glycolic acid peak area for prepared standard solutions (20 – 30,000 mg L^{-1}). Calibration coefficient for glycolic acid was calculated from the gradient of the line to be 1055.5 a.u./ mg L^{-1}. (n = 3, error bars = standard deviation)

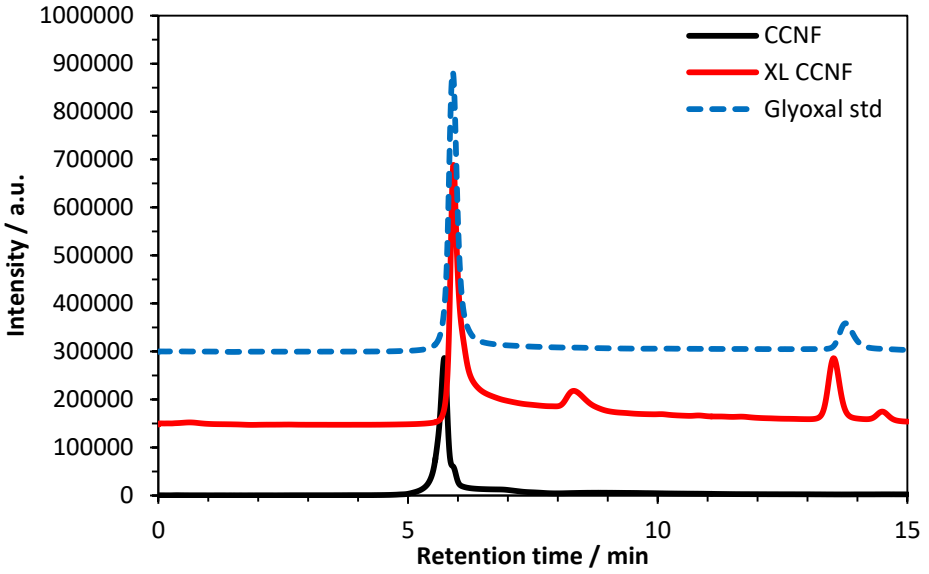

Figure E.5 HPLC analysis of glyoxylic acid present after the base hydrolysis of crosslinked cellulose foams. The large peak at 5.9 min refers to the solvent front and the peak for glyoxylic acid occurs at 13.7 min.

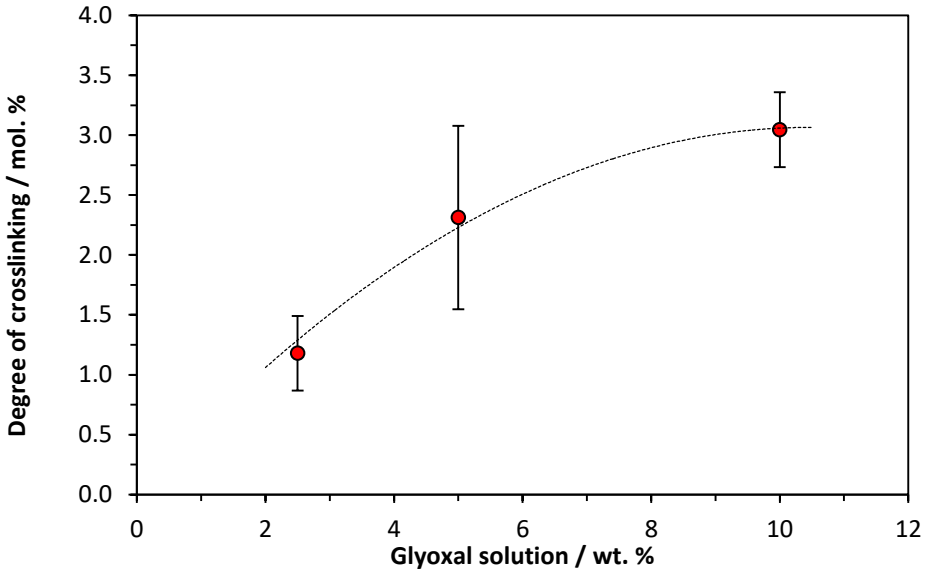

Figure E.6 The effect of glyoxal concentration on degree of crosslinking was calculated from the integrated area for the glyoxylic acid peak, which was proportional to the amount of glyoxal added to the CCNF dispersion (fitted line to guide the eye).

E.2 Formation of 3D scaffolds

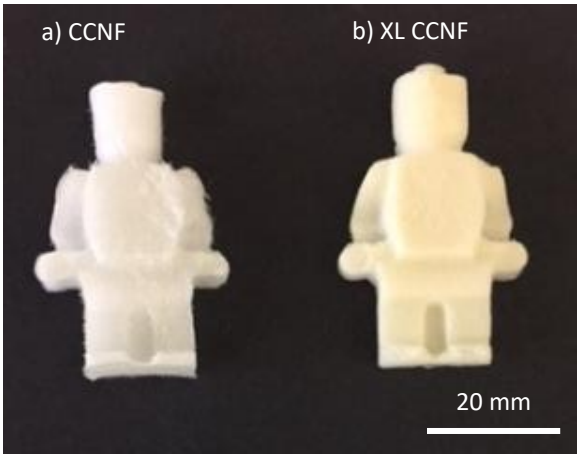

Figure E.7 Image of lyophilised 3D foam scaffolds produced from CCNF and CCNF XL hydrogels cast in moulds.

E.3 NMR Cryoporometry

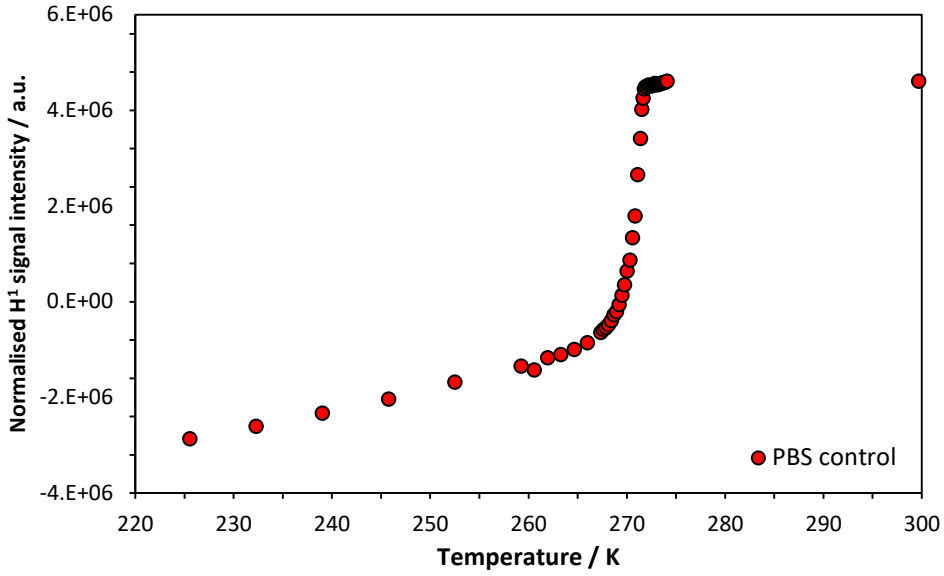

Figure E.8 H_2O signal peak intensity from H^1 NMR spectra from a PBS control in a temperature range from 218 K to 300 K.

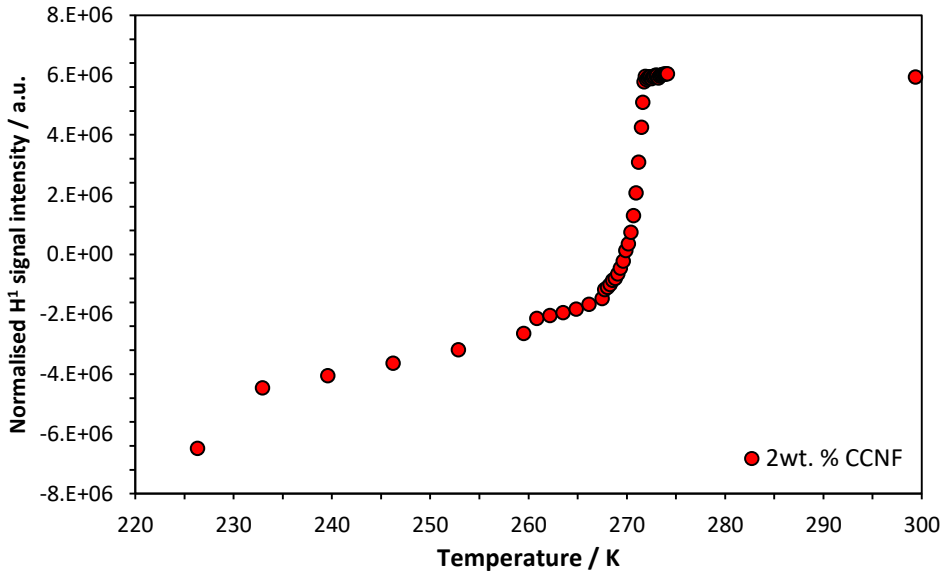

Figure E.9 H_2O signal peak intensity from H^1 NMR spectra from a hydrated CCNF sample in a temperature range from 218 K to 300 K.

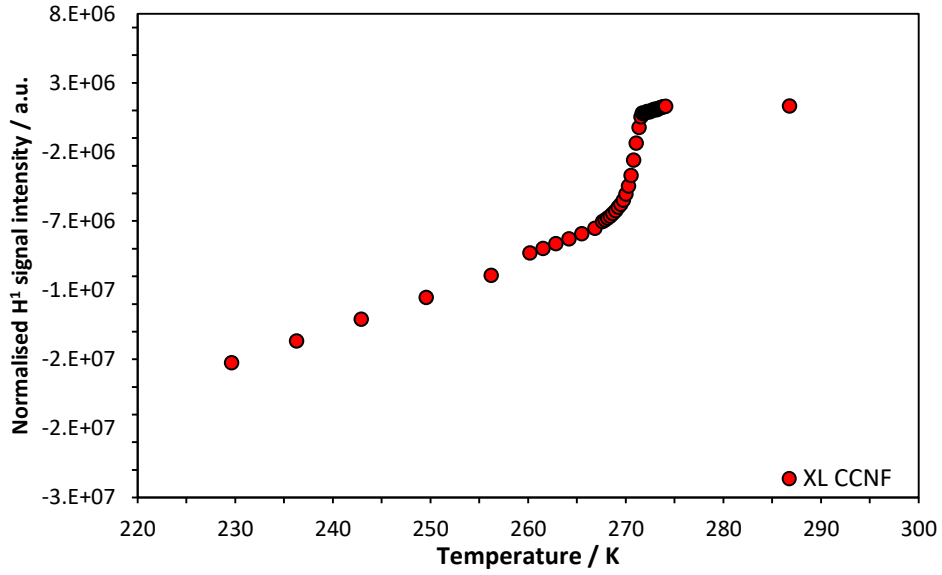

Figure E.10 H_2O signal peak intensity from H^1 NMR spectra from a hydrated CCNF XL sample in a temperature range from 218 K to 300 K.

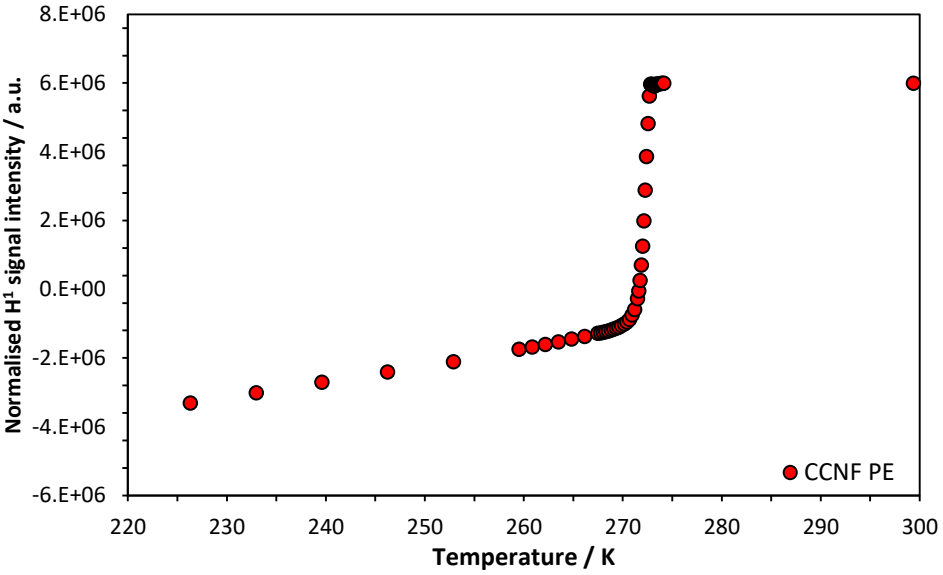

Figure E.11 H_2O signal peak intensity from H^1 NMR spectra from a hydrated CCNF PE sample in a temperature range from 218 K to 300 K.

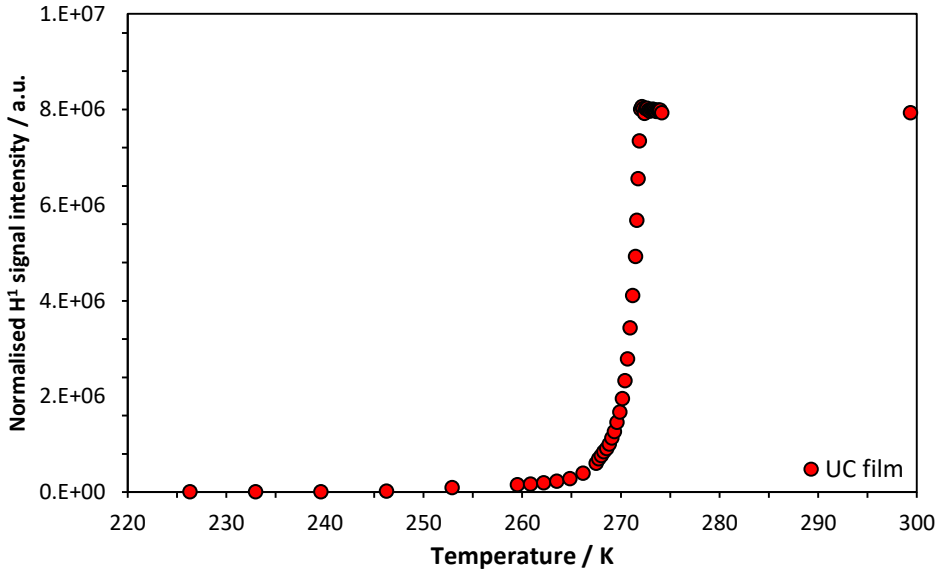

Figure E.12 H_2O signal peak intensity from H^1 NMR spectra from a hydrated UC film sample in a temperature range from 218 K to 300 K.

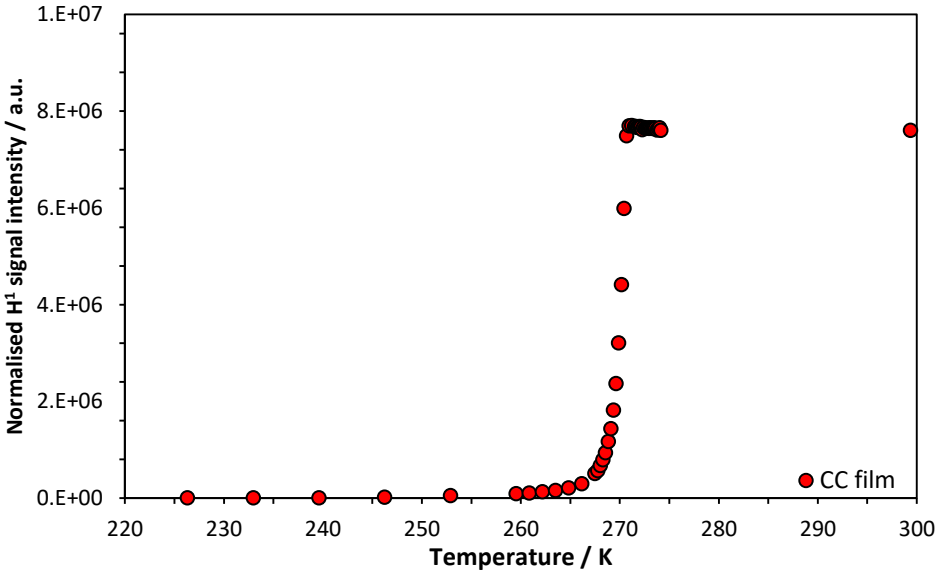

Figure E.13 H_2O signal peak intensity from H^1 NMR spectra from a hydrated CC film sample in a temperature range from 218 K to 300 K.

E.4 NMR T_2 relaxometry

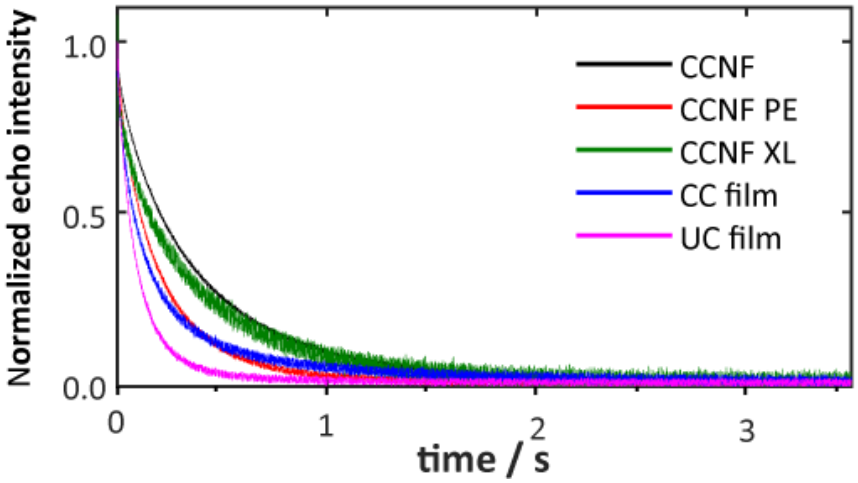

Figure E.14 Time decay of the echo intensities measured in Carr−Purcell Meiboom−Gill (CPMG) NMR experiments for all samples. The signal clearly shows different decay rates associated with distinct pore structures.

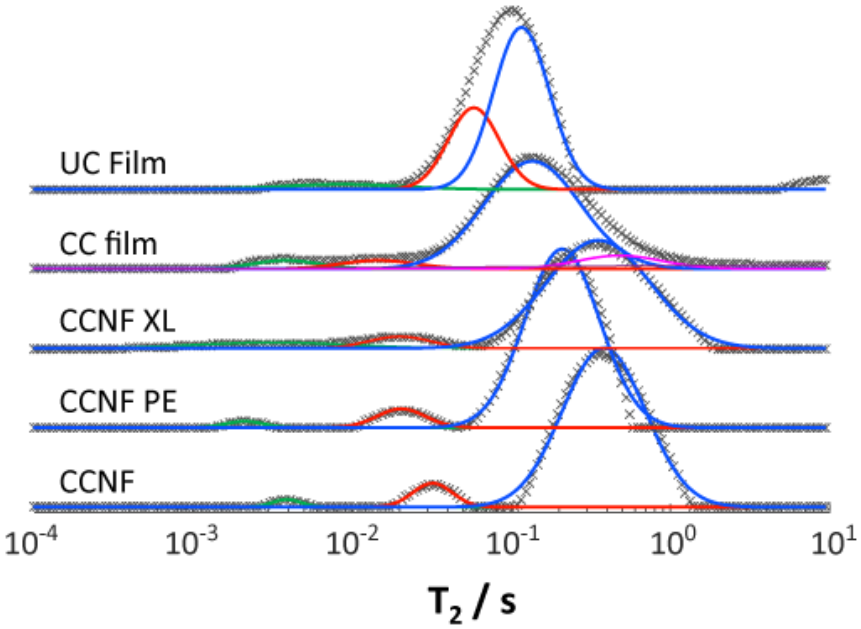

Figure E.15 The T_2 distributions for all samples, obtained from the ILT procedure[8,9] applied to the CPMG decays and normalized by area. Three length scales are observed on the distributions: nanopores, ranging from 10^{-3} to 10^{-2} s, mesopores, from 10^{-2} up to 10^{-1} s and large pores, for T_2 from 10^{-1}s. The asymmetry of the large pore component for the CC film is due to the presence of free solvent in the sample, and is not considered in the analysis. (Free solvent refers to fluid contained in pores that are large enough not to affect the transverse relaxation.[10,11])

Similar distributions for the three CCNF samples were observed with almost no overlap between the components. The UC and CC films have a significant difference on the mesopore scale, with a bigger relative area on the UC film. This means that

there are more DMAc molecules, in proportion, on this scale on the UC film than in the CC material.

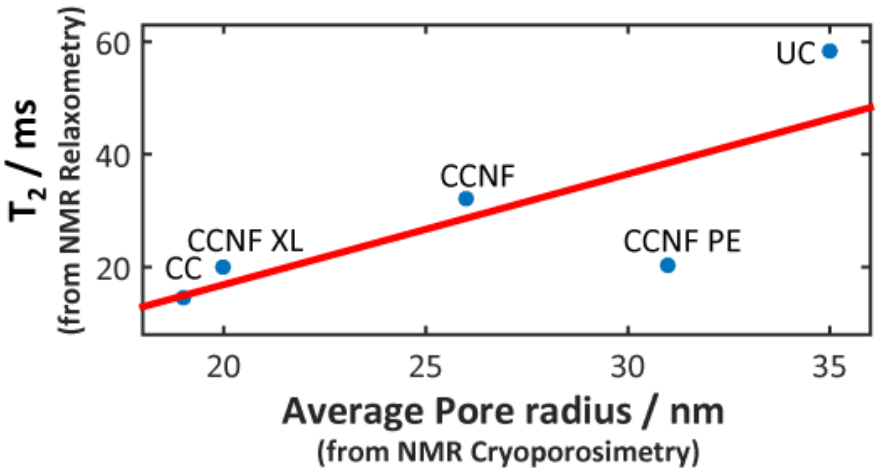

Figure E.16 Correlation between the mesopore components of the T_2 distributions above and the pore sizes estimated from cryoporometry measurements. The correlation coefficient between the two data sets is given by $R^2 = 0.77$.

Once this correlation was established, it provided the proportionally factor between T_2 and pore radius values, which allow estimation of the sizes of the larger pores (length scale of hundreds nanometers), from the NMR data, providing extra information about pore sizes on a length scale that that neither NMR cryoporometry nor SEM could be used to probe.

E.5 SEM analysis

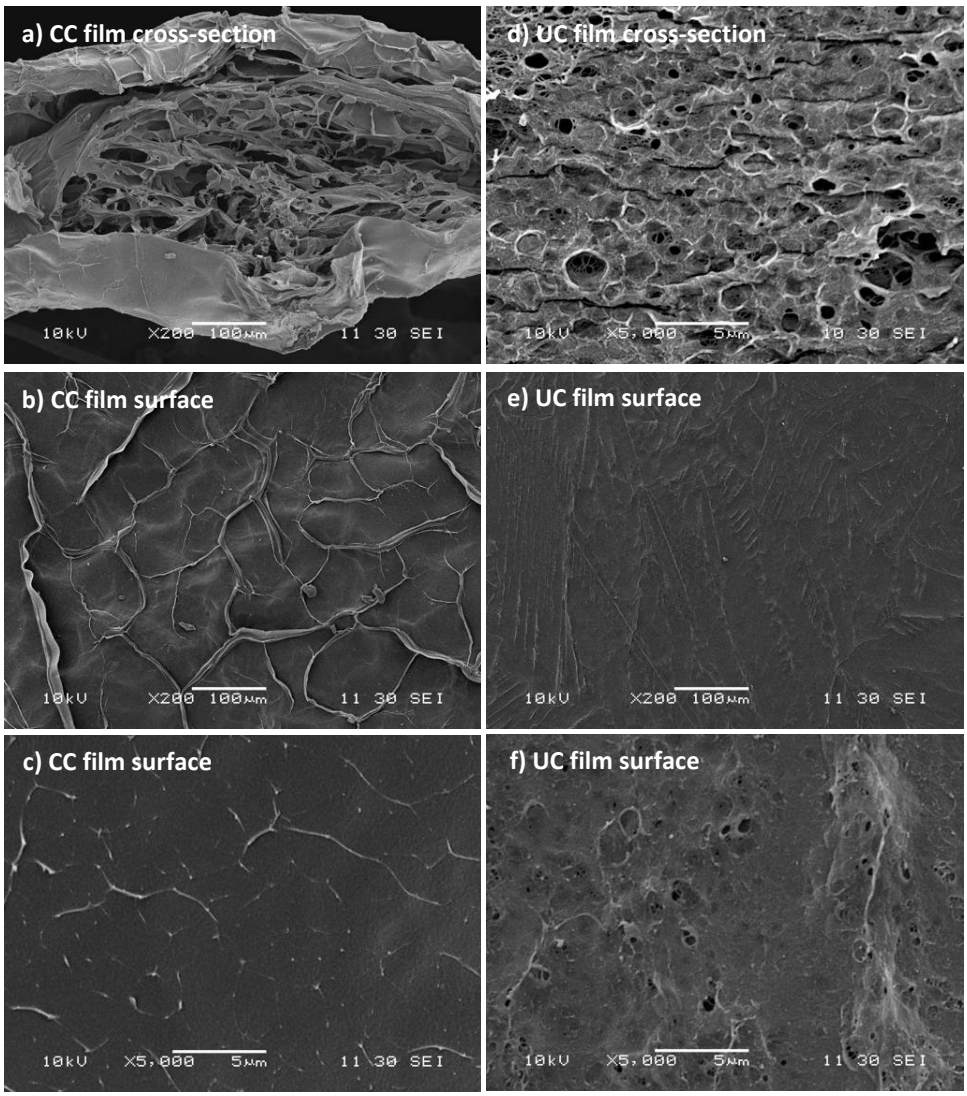

Figure E.17 SEM images of films: a, b and c) lyophilised, regenerated CC and d, e and f) unmodified cellulose. The porosity in the films is evident in the images of film cross-sections (a and d), but not at the surface. A "skin" on the surface of the films is due to the anti-solvent regeneration process.

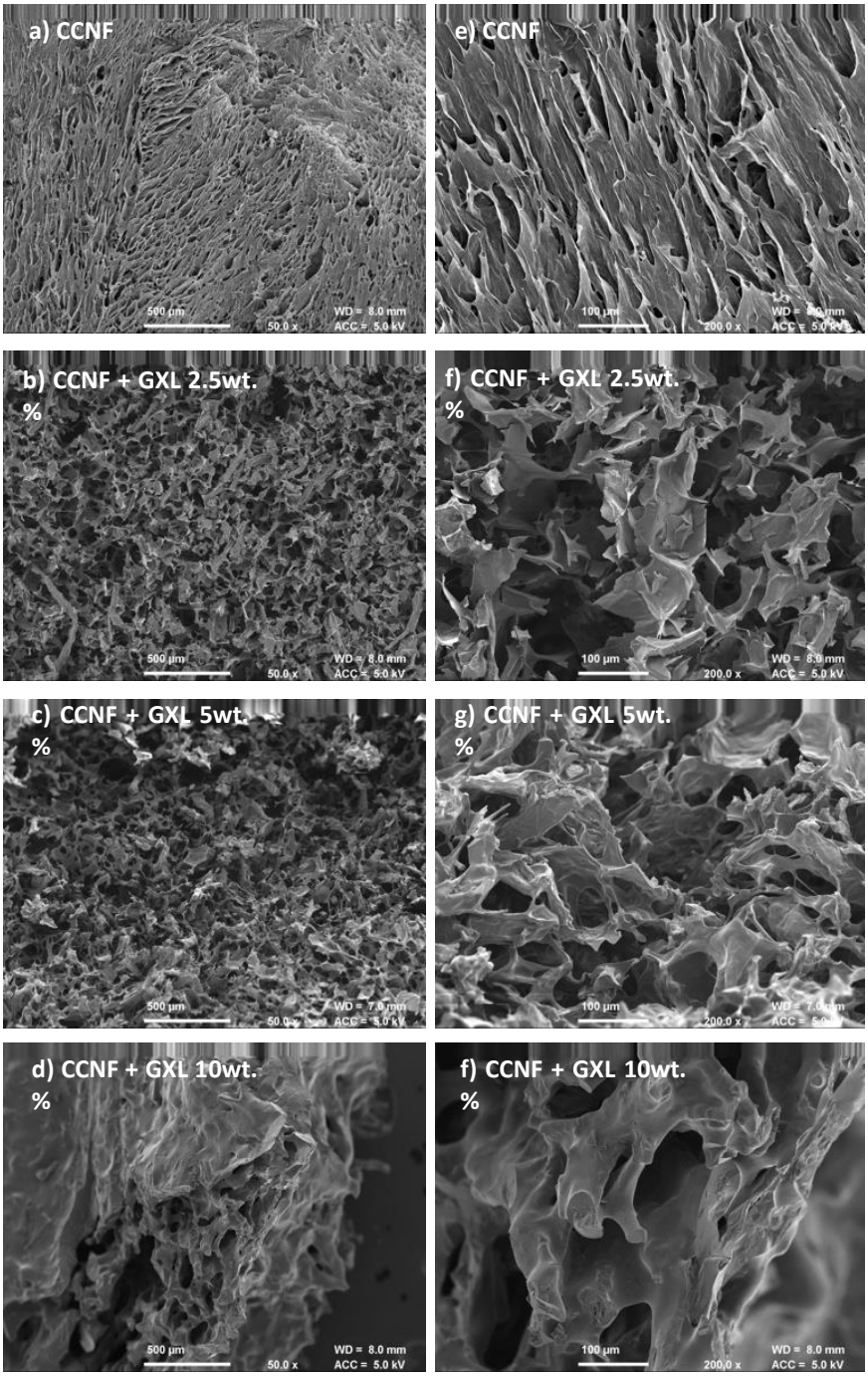

Figure E.18 SEM images of lyophilised CCNF foams; a) CCNF, b) CCNF + 2.5 wt. % glyoxal, c) CCNF 5 wt. % glyoxal and d) CCNF 10 wt. % glyoxal, and at higher magnification e) CCNF, f) CCNF + 2.5 wt. % glyoxal, g) CCNF 5 wt. % glyoxal and h) CCNF 10 wt. % glyoxal. ImageJ software was used to analyse the images to characterise porosity. It is apparent that the amount of glyoxal present in the hydrogel affected the pore size and morphology.

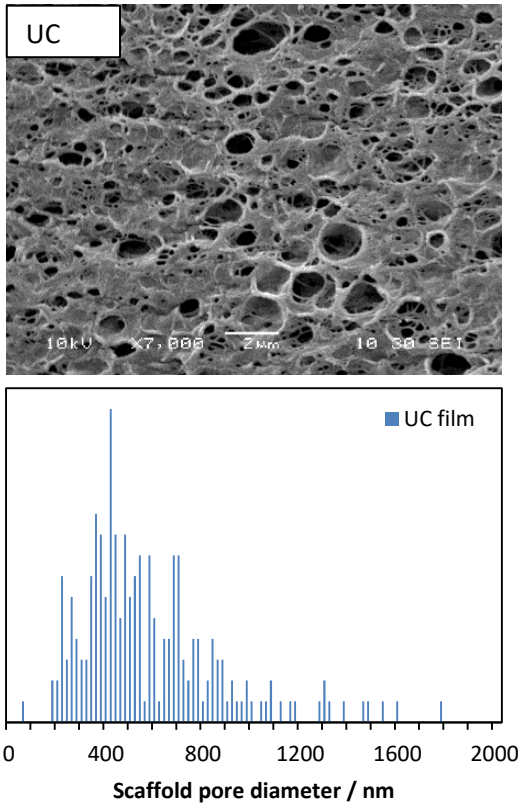

Figure E.19 SEM image of cast regenerated UC film (top). To determine the average pore size diameter SEM images were analysed using ImageJ software. Histogram of pore diameter for regenerated UC film (bottom).

E.6 Compressive load testing

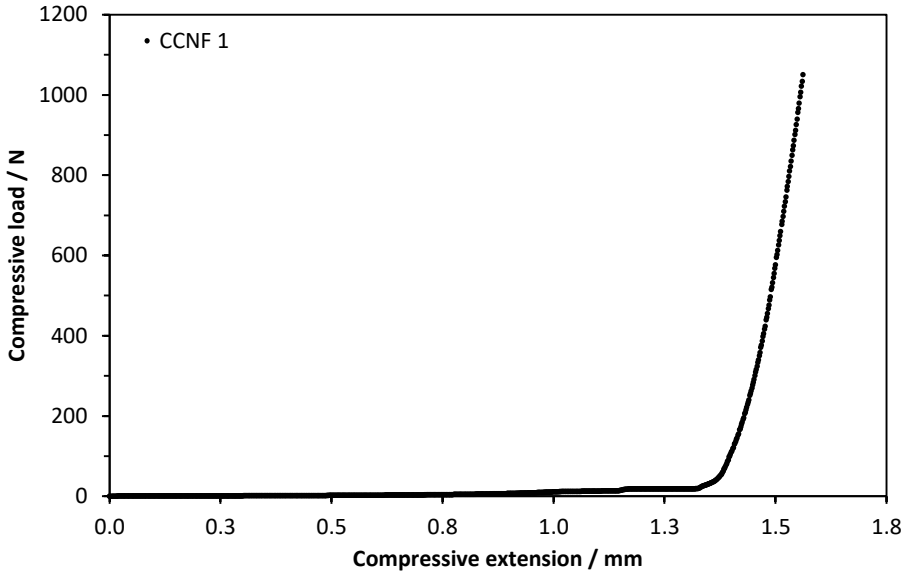

Figure E.20 CCNF lyophilised foam, compressive load *vs*. compressive extension graph, demonstrating the two phases of compression. The first phase represents the compression of the porous network, followed by the compressive load required to compress the bulk material.

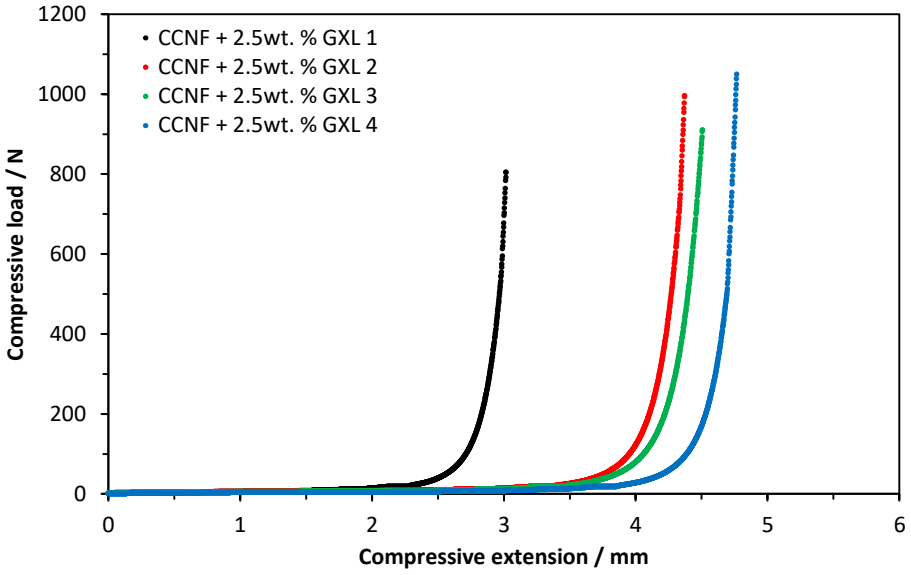

Figure E.21 CCNF + 2.5 wt. % glyoxal lyophilised foam, compressive load *vs*. compressive extension graph demonstrating the two phases of compression. The first phase represents the compression of the porous network, followed by the compressive load required to compress the bulk material.

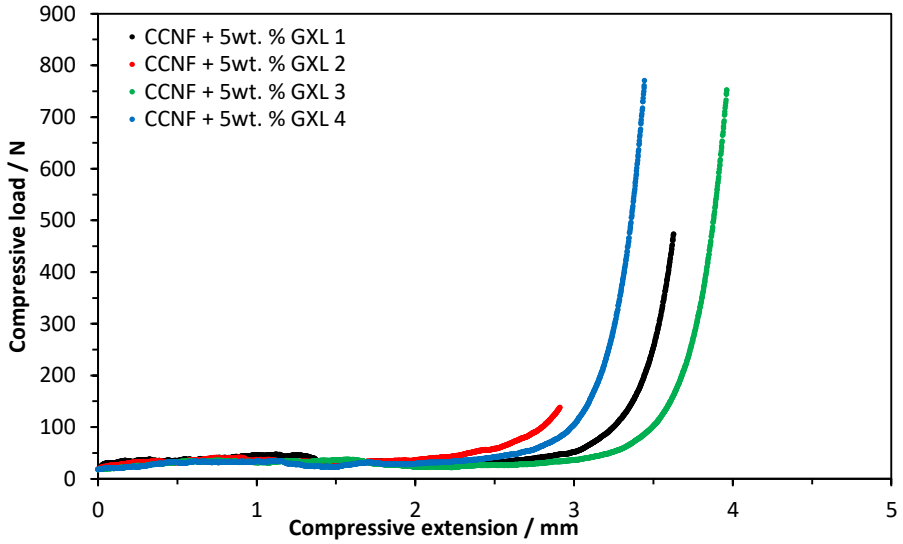

Figure E.22 CCNF + 5 wt. % glyoxal lyophilised foam, compressive load *vs*. compressive extension graph demonstrating the two phases of compression. The first phase represents the compression of the porous network, followed by the compressive load required to compress the bulk material.

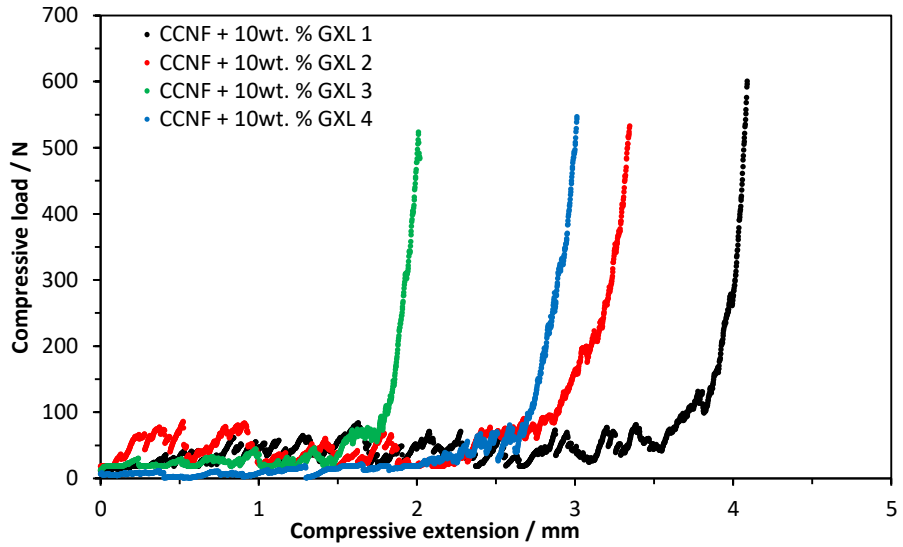

Figure E.23 CCNF + 10 wt. % glyoxal lyophilised foam, compressive load *vs*. compressive extension graph demonstrating the two phases of compression. The first phase represents the compression of the porous network, followed by the compressive load required to compress the bulk material.

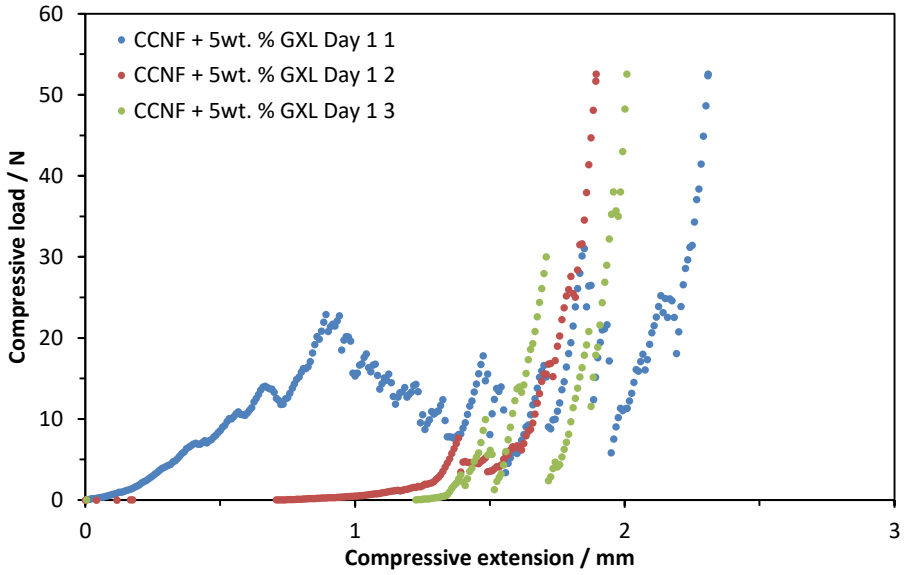

Figure E.24 CCNF + 5 wt. % glyoxal lyophilised foam, compressive load *vs*. compressive extension. Prior to testing samples were placed in PBS for 1 day to hydrate.

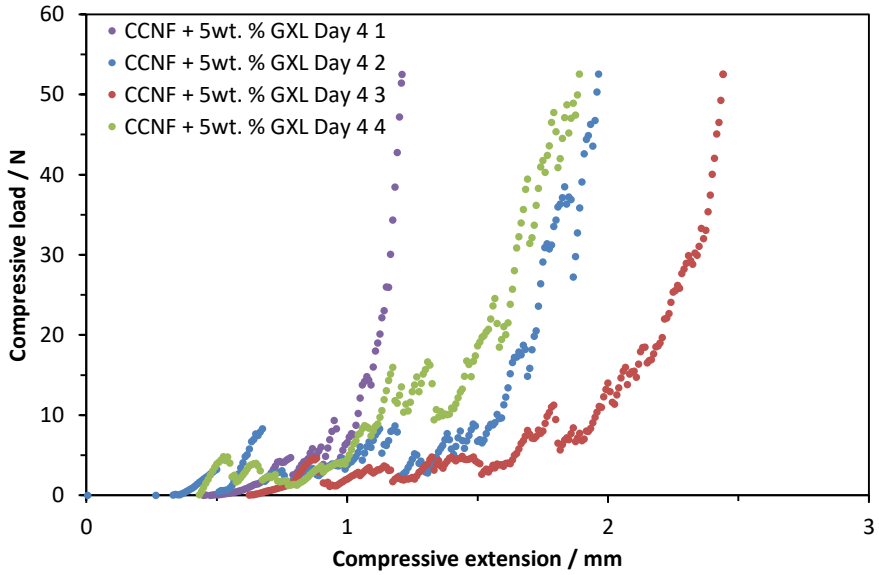

Figure E.25 CCNF + 5 wt. % glyoxal lyophilised foam, compressive load *vs*. compressive extension. Prior to testing samples were placed in PBS for 4 days to hydrate.

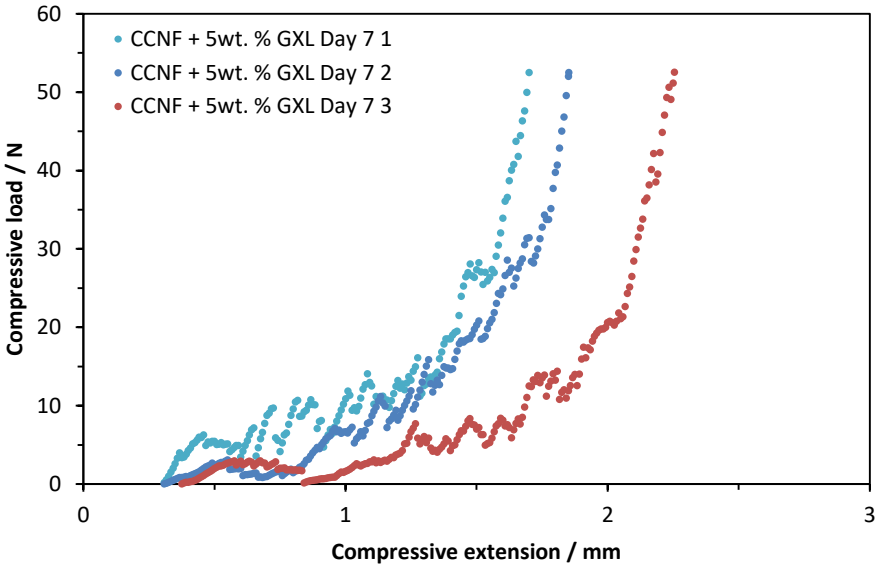

Figure E.26 CCNF + 5 wt. % glyoxal lyophilised foam, compressive load *vs*. compressive extension. Prior to testing samples were placed in PBS for 7 days to hydrate.

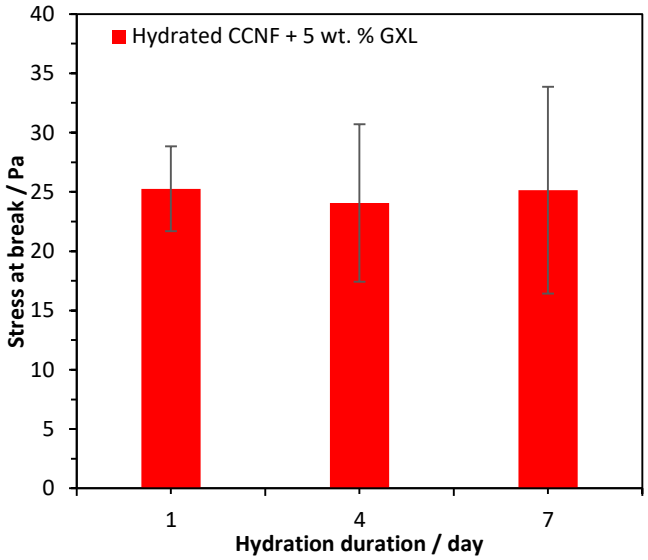

Figure E.27 Stress at break for samples of CCNF + 5 wt. % glyoxal lyophilised foam, hydrated for 1, 4 and 7 days prior to testing - stress calculated from the compressive load and cross sectional area of the sample. Hydrating the samples in PBS reduced the mechanical strength of the scaffolds, however, for CCNF XL foam (crosslinked with 5 wt. % glyoxal) there was no evidence of degradation of mechanical properties over 7 days. Conversely uncrosslinked CCNF foams collapsed to form hydrogels after only 1 day.

E.7 Cell visualisation

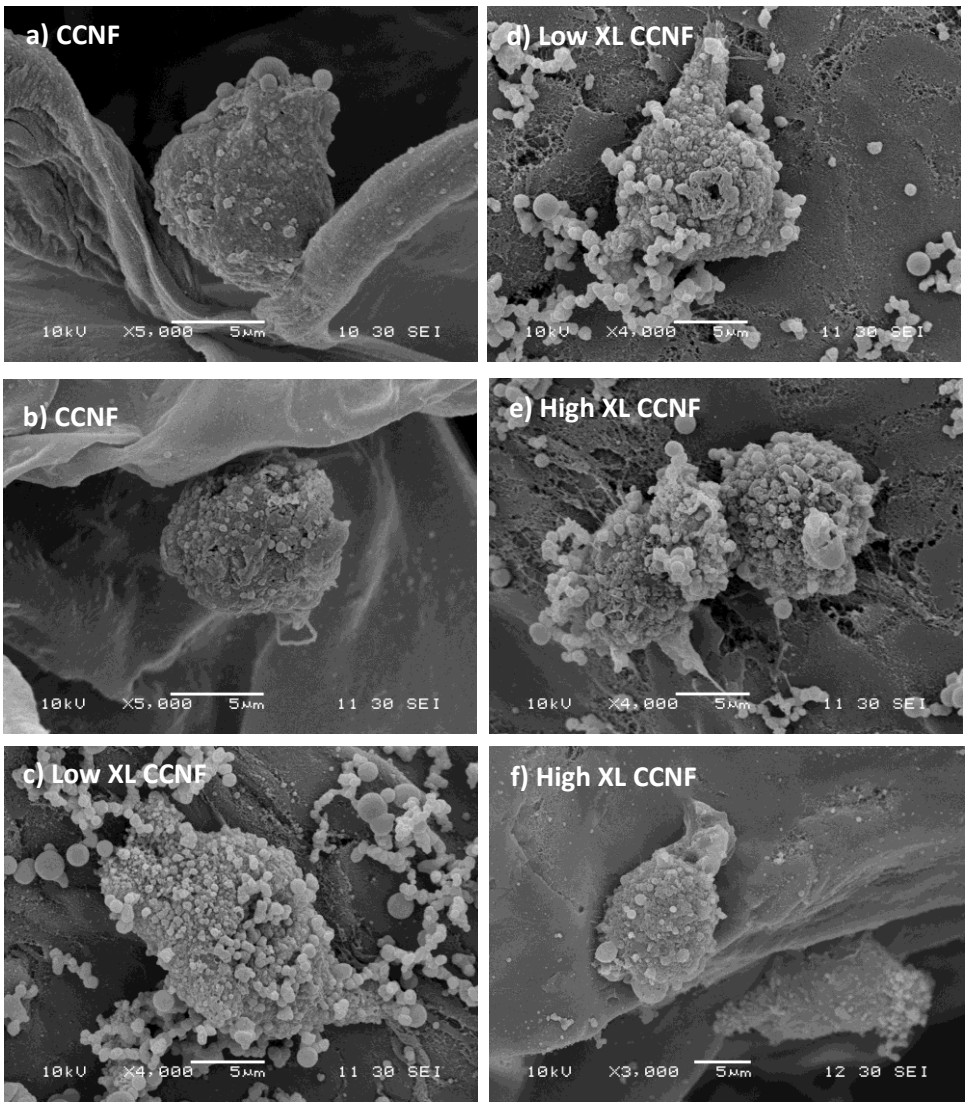

Figure E.28 SEM images of fixed MG-63 cells growing on the walls of 3D CCNF scaffolds. a-b) cationic cellulose c-d) Low XL cationic cellulose and e-f) High XL cationic cellulose 24 h incubation at 37 ^{o}C in 5 % CO_2. The attached cells appear to be more elongated on the XL cationic cellulose scaffolds, indicating spreading.

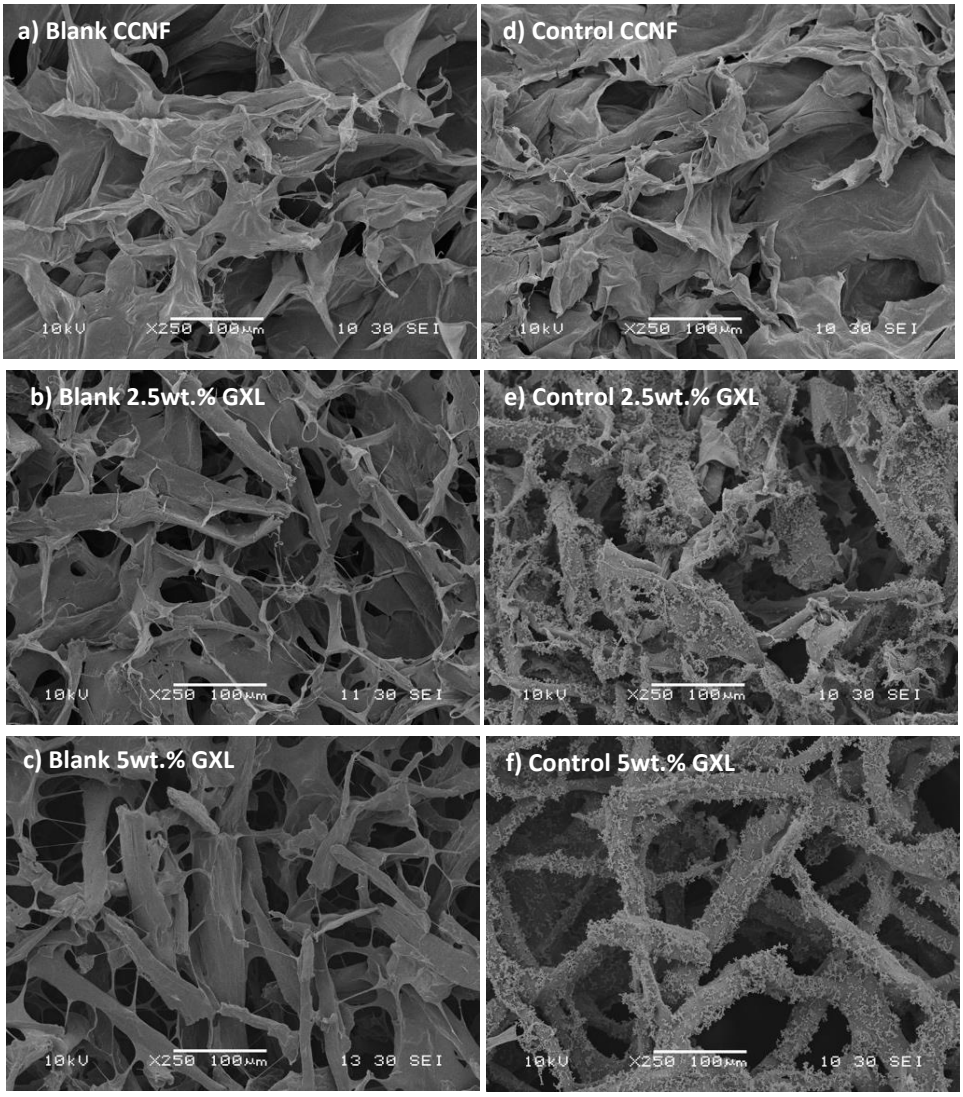

Figure E.29 SEM images of different lyophilised CCNF foams: a) – c) blank scaffolds, which were prepared using SEM following the methodology in the manuscript without being hydrated in cell culture media; d) – f) control scaffolds, which have been hydrated in FBS containing cell media without cells present. Some proteins within the media appear to be immobilised on the surface of XL CCNF scaffolds. The proteins could be fixed to the scaffold through the exposed aldehyde groups present in the XL surface.

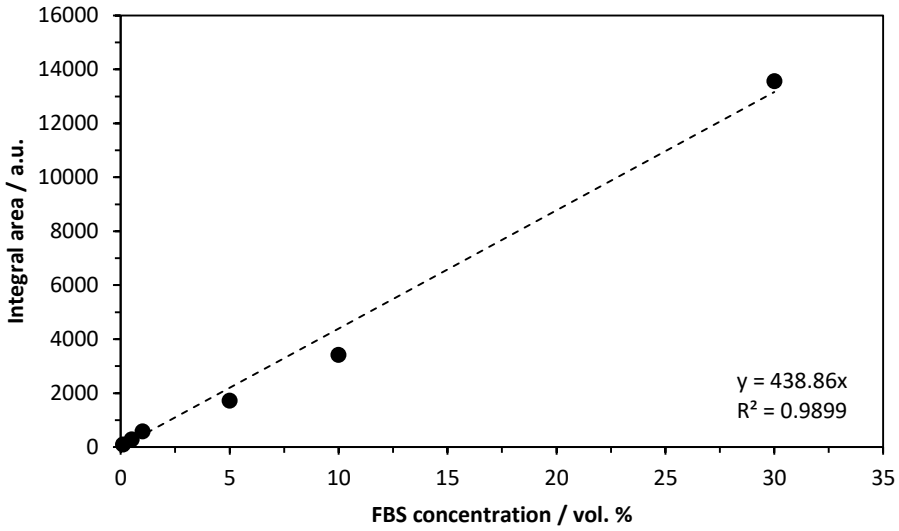

Figure E.30 FBS peak area for prepared standard solutions (0.1 – 30 vol. %). Calibration coefficient for glycolic acid was calculated from the gradient of the line to be 438.9 a.u./ vol. %. (n = 3, error bars = standard deviation)

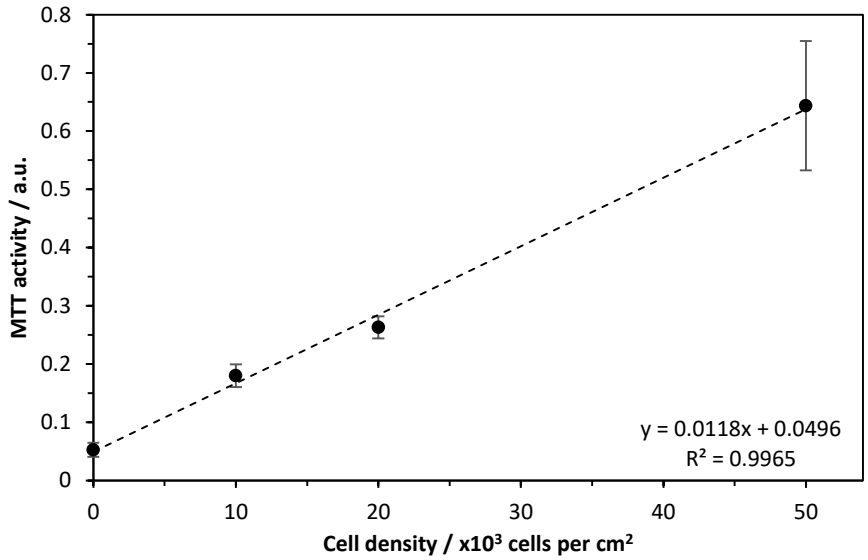

Figure E.31 Assay comparing the effect of cell seeding density on MTT expression after 4 h incubation at 37 ^{o}C in 5 % CO_2.MTT absorbance measured at 570nm. Calibration coefficient for MTT was calculated from the gradient of the line to be 0.0118 a.u./ cell density. (n = 6, error bars = standard deviation)

F. References

1. M. Zaman, H. Xiao, F. Chibante, and Y. Ni, *Carbohydr. Polym.*, 2012, **89**, 163–70.

2. R. F. Gouveia and F. Galembeck, *J. Am. Chem. Soc.*, 2009, **131**, 11381–11386.

3. E. S. Ferreira, E. M. Lanzoni, C. A. R. Costa, C. Deneke, J. S. Bernardes, and F. Galembeck, *ACS Appl. Mater. Interfaces*, 2015, **7**, 18750–18758.

4. D. Necas and P. Klapetek, *Cent. Eur. J. Physic*, 2012, **10**, 18–188.

5. A. Asano, S. Hori, M. Kitamura, C. T. Nakazawa, and T. Kurotsu, *Polym. J.*, 2012, **44**, 706–712.

6. J. C. Courtenay, M. A. Johns, F. Galembeck, C. Deneke, E. M. Lanzoni, C. A. Costa, J. L. Scott, and R. I. Sharma, *Cellulose*, 2017, **24**, 253–267.

7. C. Schramm and B. Rinderer, *Anal. Chem.*, 2000, **72**, 5829–5833.

8. S. W. Provencher, *Comput. Phys. Commun.*, 1982, **27**, 213–227.

9. G. C. Borgia, R. J. S. Brown, and P. Fantazzini, *J. Magn. Reson.*, 2000, **147**, 273–285.

10. K. R. Brownstein and C. E. Tarr, *Phys. Rev. A*, 1979, **19**, 2446–2453.

11. D. Capitani, V. Di Tullio, and N. Proietti, *Prog. Nucl. Magn. Reson. Spectrosc.*, 2012, **64**, 29–69.